

**MULTI DIRECTIONAL FORGING
OF ZINC ALUMINUM (ZA27) BASED COMPOSITES
REINFORCED WITH SiC AND Al₂O₃ PARTICLES**

Thesis

Submitted in partial fulfillment of the requirements for the degree of

DOCTOR OF PHILOSOPHY

By

ANJAN B N

(MT15F01)



**DEPARTMENT OF METALLURGICAL AND MATERIALS
ENGINEERING**

**NATIONAL INSTITUTE OF TECHNOLOGY KARNATAKA
SURATHKAL, MANGALURU-575025**

April - 2021

**MULTI DIRECTIONAL FORGING
OF ZINC ALUMINUM (ZA27) BASED COMPOSITES
REINFORCED WITH SiC AND Al₂O₃ PARTICLES**

Thesis

Submitted in partial fulfillment of the requirements for the degree of

DOCTOR OF PHILOSOPHY

by

ANJAN B N

(MT15F01)

Under the guidance of

Dr. Preetham Kumar G.V

Associate Professor



**DEPARTMENT OF METALLURGICAL AND MATERIALS
ENGINEERING**

**NATIONAL INSTITUTE OF TECHNOLOGY KARNATAKA
SURATHKAL, MANGALURU-575025**

April - 2021

DECLARATION

I hereby declare that the Research Thesis entitled **MULTI DIRECTIONAL FORGING OF ZINC ALUMINUM (ZA27) BASED COMPOSITES REINFORCED WITH SiC AND Al₂O₃ PARTICLES** Which is being submitted to the **National Institute of Technology Karnataka, Surathkal** in partial fulfilment of the requirements for the award of the Degree of **Doctor of Philosophy** in Department of Metallurgical and Materials Engineering is a bonafide report of the research work carried out by me. The material contained in this Research Thesis has not been submitted to any University or Institution for the award of any degree.

Register Number : 155058-MT15F01

Name of the Research Scholar : ANJAN B N

Signature of the Research Scholar:



Department of Metallurgical and Materials Engineering

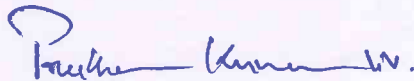
Place: NITK-Surathkal

Date: 14/08/2020

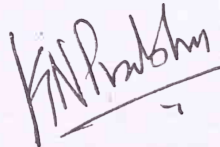
CERTIFICATE

This is to certify that the Research Thesis entitled **MULTI DIRECTIONAL FORGING OF ZINC ALUMINUM (ZA27) BASED COMPOSITES REINFORCED WITH SiC AND Al₂O₃ PARTICLES** submitted by **Mr. ANJAN B N** (Reg. No: 155058-MT15F01) as the record of the research work carried out by him, is accepted as the Research Thesis submission in partial fulfilment of the requirements for the award of degree of **Doctor of Philosophy**.

Research Guide



Dr. Preetham Kumar G.V
Associate Professor
Department of Metallurgical and Materials Engineering



Chairman - DRPC

Date:

ACKNOWLEDGMENT

I express my deep sense of gratitude and indebtedness to my supervisor **Dr. Preetham Kumar G.V**, Associate Professor, Department of Metallurgical and Materials engineering, National Institute of Technology Karnataka, Surathkal for providing precious guidance, inspiring discussions and constant supervision throughout the course of this work being carried out. His timely help, constructive criticism and conscientious efforts made it possible to present the work contained in this thesis.

I am grateful to **Dr. K Narayana Prabhu**, Professor and current Head of the Department of Metallurgical and Materials Engineering, NITK, Surathkal. I would also like to thank **Dr. Anandhan Srinivasan**, Professor **Dr. Udaya Bhat K**, Professor and **Dr. Jagannath Nayak**, Professor previous Head of the Department of Metallurgical and Materials Engineering for providing the laboratory facilities, necessary funding for the research work.

I express my sincere thanks to **Dr. Ramesh M R**, Associate Professor and **Dr. Narendranath S**, Professor, Former HoD, Department of Mechanical engineering, National Institute of Technology Karnataka, Surathkal for providing me the necessary facilities in the department.

I am grateful to the members of the Research Program Assessment Committee including **Dr. Saumen Mandal**, Assistant Professor, Department of Metallurgical and Materials Engineering and **Dr. Mrityunjay Doddamani**, Assistant Professor, Department of Mechanical Engineering, for their unbiased and critical evaluation during the progress of my research.

I am thankful to get constant encouragement and support from all the Teaching staff of the Department of Metallurgical and Materials Engineering, NITK, Surathkal, during the entire research work. I would like to express my sincere thanks and gratitude to Applied Mechanics Department staff for their kind help, encouragement for the successful completion of this research work.

I specially thank to our technical staff Mr. Dinesha, Mr. Sathish, Mr. Yashwanth, Mr. Ismail and Mr. Ramachandra. I extend my gratitude to Mrs. Rashmi Banjan for helping in taking SEM micrographs.

I express sincere thanks Mrs. Sharmila Dinesh for helping in necessary documentations for journal papers and thesis. I also thank to our office staff Mrs. Vinaya Shettigar, Mr. Sundara Shettigar, Mr. Lokesh Naik and Mr. Yogish for their kind support related to research work in the department.

I would like to thank my parents for their wise counsel and a sympathetic ear. You are always there for me. Finally, there are my friends. We were not only able to support each other by deliberating over our problems and findings, but also happy by talking about things other than our research papers.

ANJAN B N

ABSTRACT

Selection of materials with the expected characteristics is a very important for any industrial application. In the engineering and automotive industries, the current tendency is to use metal matrix composite for production of various components for high performance application. The aim of this study was to investigate the effect of SiC and Al₂O₃ (5 and 10 wt %) reinforcement in ZA27 matrix alloy. Further to investigate and develop the application of the MDF techniques, which may lead to an improvement in mechanical and tribological properties of these composite for industrial application. To analyse the influence of parameters such as applied load, sliding distance and sliding speed on dry sliding wear behavior of solutionized and MDF processed material using pin on disc test rig was conducted. In this study, the composite were prepared by stir casting technique followed by squeezing process. Multi directional forging (MDF) is one of the severe plastic deformation (SPD) techniques used to develop ultrafine-grained (UFG) materials. Multi directional forging technique was used to process the ZA27/SiC/Al₂O₃ /SiC + Al₂O₃ composites to produce refined microstructure in order to study the relationship between the microstructure and mechanical properties. The effects of the MDF processes have been studied on ZA27 based composite at 100 °C and 200 °C of processing temperature with a total equivalent strain of 0.54 and 1.08 respectively. Before MDF process, base alloy and prepared composites were homogenized at 365°C for 5 hours by using muffle furnace and quenched in water to room temperature. The standard metallographic technique was used to analyse the microstructural features of the ZA27 based composite. MDF processed composite were characterized by analyzing the X-Ray diffraction (XRD) profiles and studying microstructures using optical microscopy, scanning electron microscopy (SEM) attached with energy dispersive spectroscopy (EDS) and transmission electron microscopy (TEM). Density was measured using standard density measurement kit and both theoretical and experimental densities were compared. Mechanical properties such as hardness, tensile strength and ductility from tensile test and fracture surface morphologies of the tensile test samples of both MDF processed and unprocessed composites were studied. Wear behavior of composites before and after MDF process were studied with their wear mechanisms.

Results revealed that, density of ZA27 alloy decreased by incorporation of SiC and Al₂O₃ particles. Some Clusters and fair dispersion of SiC and Al₂O₃ particles in ZA27 matrix were observed in microstructure and confirmed by EDX. SiC reinforced composites performs better when compared with Al₂O₃ reinforced, mixture of SiC+Al₂O₃ particles reinforced and ZA27 base matrix material. As the percentage of reinforcement increased from 5 wt% to 10 wt% the properties of the material also increased. Porosity level decreased with an increase in the number of MDF passes when compared with unreinforced materials.

Composites reinforced with SiC particles in 5 and 10 wt % were MDF processed at different temperature. The average grain size was reduced from 25-30 µm to 0.2-0.35 µm, 0.45-0.5 µm respectively in the case of samples MDF processed at 100 °C up to three passes and for 200 °C up to six passes it shows 0.8-1.0 µm, 0.9-1.2 µm respectively. The initial lamellar Al-rich and Zn-rich phase was gradually refined to a spherical shape and distributed more uniformly with an increasing number of passes. Ultimate tensile strength of the composite material was increased with that addition of SiC particles and also by MDF process. The highest ductility was obtained when the sample forged at 100 °C 3 passes. Initial ascast condition showed a brittle type of fracture. Brittle mode of fracture was transformed into ductility mode by MDF processing. Wear results showed that samples tested with lower load and sliding distance were showing abrasive type of wear mechanism but as the applied load and sliding distance increased, mechanism changed to adhesion type. This is due to the rise in temperature between the interface of pin and disc, material detached from the pin as debris gets adhered to the surface of pin which influences the mode of mechanism to switch from abrasion to adhesion. MDF processed ZA27/SiCp for 3 passes at 100 °C showed better wear resistance with ultra-fine grains and higher hardness.

Composites reinforced with Al₂O₃ particles in 5 and 10 wt % were MDF processed at 100 °C up to three passes reduced the grain size from 20-30 µm to 0.4-0.45 µm, 0.5-0.6 µm respectively with the dual type of microstructure having both lamellar to the cellular structure. On further MDF processing at 200 °C upto 6 passes showed the grain size of 1.2-1.4, 1.5 µm with equiaxed grain structure. Small cracks were seen at the edges of the Al₂O₃ particle because of load applied during MDF process upto 3

passes at 100 °C and with a higher number of passes the Al₂O₃ particle broken into several pieces and forms a cluster of Al₂O₃ particle. Addition of Al₂O₃ particle increased the UTS and hardness values in both 5 and 10 wt % reinforced composites and further improvement in UTS and hardness value is due to MDF process upto three passes at 100 °C and upto six passes at 200 °C. The ductility of Al₂O₃ particle reinforced composites was low when compared with other composites. Wear rate of Al₂O₃ reinforced composite was more when compared with SiC reinforced ones. Results of wear test showed that Al₂O₃ reinforced composites MDF processed for 3 passes at 100 °C gives higher wear resistance, with abrasion type of wear mechanism.

For ZA27/SiC +Al₂O₃ composites with the average grain size reduced from 15-20 µm to 0.2-0.25 µm, 0.3-0.4 µm when processed at 100 °C upto three passes and 0.8-0.9 µm, 0.9-1.1 µm when processed at 200 °C upto Six passes. Hardness, ultimate tensile strength and ductility of the composites were improved by MDF processing. Substantial improvement in ductility of the present composites after several MDF passes can be attributed to the elimination of as-cast morphology as well as grain refinement, reduction in micro porosity (or micro-voids), redistribution of reinforcing particles, and also the change in the composition of the phases. In an overall, the results of wear test shows, SiC reinforced composite performed better as compared with Al₂O₃ reinforced and Mixture of SiC+Al₂O₃ reinforced material. Wear study of composites indicated that the specific wear rate was highly influenced by applied load and sliding distance. As an application, a Cylinder Roller Bearing is fabricated by best performing ZA27/SiC/ Al₂O₃/SiC+Al₂O₃ composite material.

Keywords: ZA27, Multi directional forging, Composite, Microstructure, Ductility and Strength, Wear, Grain refinement, Wear mechanisms.

CONTENTS

ACKNOWLEDGEMENT	i
ABSTRACT	iii
CONTENTS	vi
LIST OF FIGURES	ix
LIST OF TABLES	xix
NOMENCLATURE	xxi
1. INTRODUCTION	01
1.1 Objectives of the Present Work	07
1.2 Thesis Organization	08
2. LITERATURE REVIEW	11
2.1 Principle of Multi-Directional Forging (MDF)	12
2.2 Experimental Factors Influencing MDF	13
2.2.1 Strain imposed in MDF and number of passes	13
2.2.2 Pressing Speed	14
2.2.3 Pressing Temperature	14
2.2.4 Friction and Lubrication	14
2.3 Advantages and Disadvantages of MDF	14
2.4 Zinc-Aluminium Alloy (ZA ALLOY)	15
2.5 Casting Technique	19
2.6 Microstructure, Mechanical properties and Wear behavior of Zinc-Aluminum based composites reinforced with SiC, Al ₂ O ₃ and other different types of particles.	23
2.7 Wear	30
2.8 Microstructure and Mechanical properties of SPD Processed materials	39
2.9 Wear Behavior of SPD Processed Materials	43

3. EXPERIMENTAL TECHNIQUES AND MATERIALS USED	45
3.1 Research Methodology	45
3.2 Material	46
3.3 Casting Process	46
3.4 Heat Treatment	49
3.5 Multi Directional Forging	49
3.6 Physical Properties Evaluation	52
3.6.1 Density	52
3.7 Mechanical Properties Evaluation	53
3.7.1 Rockwell Hardness	53
3.7.2 Tensile Test	53
3.8 Wear Test	54
3.9 Microstructural Analysis	55
3.9.1 Optical Microscopy	55
3.9.2 Scanning Electron Microscopy	55
3.9.3 Transmission Electron Microscopy	56
3.9.4 X-Ray Diffractometry	56
4. RESULTS AND DISCUSSION	57
4.1 Base Material Properties Evaluating	57
4.1.1 Microstructure Evolution	57
4.2 MDF Processing Temperature	61
4.3 ZA27 Reinforced With SiC Composites Properties Evaluation	61
4.3.1 Density	61
4.3.2 Microstructure	62
4.3.3 XRD Analysis	71
4.3.4 Mechanical Properties Evaluation	72
4.3.5 Wear Properties Evaluation of SiC reinforced composites	79
4.4 ZA27 Reinforced With Al ₂ O ₃ Composites Properties Evaluation	84

4.4.1	Density	84
4.4.2	Microstructure	85
4.4.3	XRD Analysis	93
4.4.4	Mechanical Properties Evaluation	94
4.4.5	Wear Properties Evaluation of Al ₂ O ₃ reinforced composites	100
4.5	ZA27 Reinforced With SiC+Al ₂ O ₃ Composites Properties Evaluation	105
4.5.1	Density	105
4.5.2	Microstructure	105
4.5.3	XRD Analysis	111
4.5.4	Mechanical Properties Evaluation	113
4.5.5	Wear Properties Evaluation of SiC+Al ₂ O ₃ reinforced composites	120
5	APPLICATION	125
5.1	Application – ZA27/ SiC/ Al ₂ O ₃ / SiC+Al ₂ O ₃ Composite Material For Cylinder Roller Bearing	125
6.	CONCLUSIONS	129
6.1	Scope for future work	133
	REFERENCES	135
	APPENDIX I	155
	APPENDIX II	175
	APPENDIX III	176
	LIST OF PUBLICATIONS	183
	BIO-DATA	185

LIST OF FIGURES

Fig. No.	Contents	Page No.
2.1	Schematic diagram of MDF processing along with three directions.	12
2.2	Phase diagram of Zn-Al binary alloy system (Y. H. Zhu 2004).	16
3.1	Research Methodology	45
3.2	Schematic diagram of stir casting setup for the fabrication of MMC	47
3.3	Schematic three dimensional exploded view of the Squeeze casting split type die with plunger.	48
3.4	Photograph of Squeeze casting dies with plunger.	48
3.5	Photograph of the (a) 250 ton hydraulic press (b) Casted sample after squeezing.	49
3.6	Schematic three dimensional exploded view of the Multi directional forging split type die with plunger.	51
3.7	Photograph of Multi directional forging die with plunger	51
3.8	Photograph of the (a) 40 ton hydraulic press (b) MDF processed samples.	52
3.9	Tensile test specimen (All dimensions are in mm)	53
3.10	Schematic representation of pin on disc wear testing machine	54
4.1	SEM with Energy dispersive spectroscopy image showing ZA27 alloy composition.	57
4.2	Optical microscopy images (a) Ascast ZA27 alloy at lower magnification (b) Ascast ZA27 alloy at higher magnification.	58
4.3	SEM images (a) Ascast ZA27 alloy (b) Solutionized ZA27 alloy	58
4.4	XRD patterns of ascast and solutionized ZA27 alloy	58
4.5	Engineering stress versus engineering strain graph of tensile test for ascast ZA27 alloy and solutionized ZA27 alloy.	60
4.6	SEM images of the tensile fracture surfaces of ZA27 alloy (a,c) Ascast ZA27 alloy (b,d) ZA27 alloy in solutionized condition.	60
4.7	ZA27/SiC composite processed by MDF (a) At room temperature (b) Upto 3 passes at 100°C (c) Upto 6 passes at 200°C	61
4.8	Energy dispersive spectroscopy images for alloy composition and	62

	presence of SiC particles confirmation	
4.9	Optical microscopy images (a) Ascast ZA27/SiC 5% composite (b) Solutionized ZA27/SiC 5% composite (c) ZA27/SiC 5% MDF processed at 100°C for 3 passes (d) ZA27/SiC 5% MDF processed at 200°C for 6 passes (e) Ascast ZA27/SiC 10% composite (f) Solutionized ZA27/SiC 10% composite (g) ZA27/SiC 10% MDF processed at 100°C for 3 passes (h) ZA27/SiC 10% MDF processed at 200°C for 6 passes.	63
4.10	SEM images (a) Ascast ZA27/SiC 5% composite (b) Solutionized ZA27/SiC 5% composite (c, d) SiC Particle distribution in ZA27/SiC 5% composite (e1) ZA27/SiC 5% - MDF processed at 100°C for 3 passes (e2) ZA27/SiC 5% - MDF processed at 100°C for 3 passes (higher magnification x10,000) (f) ZA27/SiC 5% MDF processed at 200°C for 6 passes showing cellular type of grains (g) ZA27/SiC 5% MDF processed at 200°C for 6 passes showing mixture of cellular and lamellar type of grains structure.	65
4.11	SEM images (a) Ascast ZA27/SiC 10% composite (b) Solutionized ZA27/SiC 10% composite (c, d) SiC Particle distribution in ZA27/SiC 10% composite (e) ZA27/SiC 10% - MDF processed at 100°C for 3 passes (f) ZA27/SiC 10% - MDF processed at 100°C for 3 passes (higher magnification x5,000) (g,h) ZA27/SiC 10% MDF processed at 200°C for 6 passes showing cellular type of grain structure	66
4.12	Grain size distribution curve a) Solutionized ZA27/SiC 5% composite b) ZA27/SiC 5% - MDF processed at 100°C for 3 passes c) ZA27/SiC 5% - MDF processed at 200°C for 6 passes	67
4.13	Grain size distribution curve a) Solutionized ZA27/SiC 10% composite b) ZA27/SiC 10% - MDF processed at 100°C for 3 passes c) ZA27/SiC 10% - MDF processed at 200°C for 6 passes	67
4.14	Bright-field TEM micrograph a) ZA27/SiC 5% MDF processed at 100 °C for three passes b) ZA27/SiC 5% MDF processed at 200 °C for six passes c) ZA27/SiC 10% MDF at 100 °C for three passes reveals a large number of dislocations d) ZA27/SiC 10% MDF processed at 200 °C for six passes.	69
4.15	EDS analysis of the TEM image of ZA27/SiC 10% MDF at 100 °C upto three passes for the identification of Al-rich phase	70
4.16	EDS analysis of the TEM image of ZA27/SiC 10% MDF at 100 °C upto three passes for the identification of Zn rich phase	70

4.17	XRD patterns of ZA27 /SiC 5% ascast, solutionized and MDF processed at different temperature.	71
4.18	XRD patterns of ZA27 /SiC 10% ascast, solutionized and MDF processed at different temperature.	72
4.19	Rockwell hardness values of ascast and solutionized ZA27 alloy and ZA27/SiC composites MDF processed up to three passes at 100°C and up to six passes at 200°C. a) ZA27/SiC 5% b) ZA27/SiC 10%	73
4.20	Engineering stress versus engineering strain for the tensile test of ZA27 ascast alloy and ZA27/SiC 5% composite after solutionized, MDF processed up to three passes at 100°C and up to six passes 200°C	74
4.21	Engineering stress versus engineering strain for the tensile test of ZA27 ascast alloy and ZA27/SiC 10% composite after solutionized, MDF processed up to three passes at 100°C and up to six passes 200°C	74
4.22	SEM images of the fracture surfaces of after tensile tests of ZA27/SiC 5% composite in macroscopic scale (a) Ascast ZA27/SiC 5% (b) Solutionized ZA27/SiC 5% (b) ZA27/SiC 5% MDF at 100 °C up to 3 passes (d) ZA27/SiC 5% MDF at 200 °C up to 6 passes	75
4.23	SEM images of the fracture surfaces of after tensile tests of ZA27/SiC 5% composite (a) Ascast ZA27/SiC 5% (b) Solutionized ZA27/SiC 5% (b) ZA27/SiC 5% MDF at 100 °C up to 3 passes (d) ZA27/SiC 5% MDF at 200 °C up to 6 passes	75
4.24	Dimple size distribution curve a) ZA27/SiC 5% - MDF processed at 100°C for 3 passes b) ZA27/SiC 5% - MDF processed at 200°C for 6 passes	76
4.25	SEM images of the fracture surfaces of after tensile tests of ZA27/SiC 10 % composites in macroscopic scale (a) Ascast ZA27/SiC 10 % (b) Solutionized ZA27/SiC 10% (b) ZA27/SiC 10% MDF at 100 °C up to 3 passes (d) ZA27/SiC 10% MDF at 200 °C up to 6 passes.	77
4.26	SEM images of the fracture surfaces of after tensile tests of ZA27/SiC 10 % composite (a) Ascast ZA27/SiC 10 % (b) Solutionized ZA27/SiC 10% (b) ZA27/SiC 10% MDF at 100 °C up to 3 passes (d) ZA27/SiC 10% MDF at 200 °C up to 6 passes	78
4.27	Dimple size distribution curve a) ZA27/SiC 10% - MDF processed at 100°C for 3 passes b) ZA27/SiC 10% - MDF processed at 200°C for 6 passes	78

4.28	Wear rate of ZA27/ SiC 5 wt% composite in different condition (a) For 2000m of sliding distance (b) For 4000m of sliding distance.	80
4.29	Wear Resistance of ZA27/ SiC 5wt% composite in different condition	80
4.30	Wear rate of ZA27/ SiC 10 wt% composite in different conditions (a) For 2000m of sliding distance (b) For 4000m of sliding distance.	81
4.31	Wear Resistance of ZA27/SiC 10wt% composite in different conditions.	81
4.32	EDS analysis of the worn surfaces of composite material (ZA27/SiC 5% ascast - 39.24N - 2000m SEM micrographs of the worn surfaces of ZA27/SiC in 5 & 10 wt%. (a) ZA27/SiC 5% sol - 39.24N - 2000m (b) ZA27/SiC 5% -MDF 3 Pass 49.05N - 2000m (c) ZA27/SiC 5%-MDF 6 pass 58.86N -	82
4.33	2000m (d) ZA27/SiC 5% sol-39.24N - 4000m (e) ZA27/SiC 5%-MDF 3 pass- 49.05N - 4000m (f) ZA27/SiC 5%- MDF 6 Pass- 58.86N - 4000m (g) ZA27/SiC 10%- ascact 39.24N – 2000 (h) ZA27/SiC 10%- MDF 3 pass- 49.05N - 4000m	83
4.34	Energy dispersive spectroscopy images for alloy composition and presence of particles confirmation Optical microscopy images (a) Ascast ZA27/Al ₂ O ₃ 5% composite (b) Solutionized ZA27/Al ₂ O ₃ 5% composite (c) ZA27/Al ₂ O ₃ 5% MDF processed at 100°C for 3 passes (d) ZA27/Al ₂ O ₃ 5% MDF processed	85
4.35	at 200°C for 6 passes (e) Ascast ZA27/Al ₂ O ₃ 10% composite (f) Solutionized ZA27/Al ₂ O ₃ 10% composite (g) ZA27/Al ₂ O ₃ 10% MDF processed at 100°C for 3 passes (h) ZA27/Al ₂ O ₃ 10% MDF processed at 200°C for 6 passes SEM images (a) Ascast ZA27/Al ₂ O ₃ 5% composite (b) Solutionized ZA27/ Al ₂ O ₃ 5% composite (c, d) Al ₂ O ₃ Particle distribution in ZA27/ Al ₂ O ₃ 5% composite (e1) ZA27/ Al ₂ O ₃ 5% - MDF processed	86
4.36	at 100°C for 3 passes (e2) ZA27/ Al ₂ O ₃ 5% - MDF processed at 100°C for 3 passes (higher magnification x 5,000) (f1) ZA27/ Al ₂ O ₃ 5% MDF processed at 200°C for 6 passes showing cellular type of grains (f2) ZA27/ Al ₂ O ₃ 5% MDF processed at 200°C for 6 passes (higher magnification x 5,000)	87
4.37	SEM images (a) Ascast ZA27/Al ₂ O ₃ 10% composite (b) Solutionized ZA27/ Al ₂ O ₃ 10% composite (c, d) Al ₂ O ₃ Particle distribution in ZA27/ Al ₂ O ₃ 10% composite (e1) ZA27/ Al ₂ O ₃ 10% - MDF processed at 100°C for 3 passes (e2) ZA27/ Al ₂ O ₃ 10% - MDF	88

	processed at 100°C for 3 passes (higher magnification x 5,000) (f1) ZA27/ Al ₂ O ₃ 10% MDF processed at 200°C for 6 passes showing cellular type of grains (f2) ZA27/ Al ₂ O ₃ 10% MDF processed at 200°C for 6 passes (higher magnification x 5,000.	
4.38	Grain size distribution curve a) Solutionized ZA27/ Al ₂ O ₃ 5% composite b) ZA27/ Al ₂ O ₃ 5% - MDF processed at 100°C for 3 passes c) ZA27/ Al ₂ O ₃ 5% - MDF processed at 200°C for 6 passes	89
4.39	Grain size distribution curve a) Solutionized ZA27/ Al ₂ O ₃ 10% composite b) ZA27/ Al ₂ O ₃ 10% - MDF processed at 100°C for 3 passes c) ZA27/ Al ₂ O ₃ 10% - MDF processed at 200°C for 6 passes	89
4.40	Bright-field TEM micrograph a) ZA27/Al ₂ O ₃ 5% MDF processed at 100 °C for three passes showing lamellar structure b) ZA27/ Al ₂ O ₃ 5% MDF processed at 200 °C for six passes showing equiaxed structure c) ZA27/ Al ₂ O ₃ 10% MDF at 100 °C for three passes d) ZA27/ Al ₂ O ₃ 10% MDF processed at 100 °C for three passes showing dislocation.	91
4.41	EDS analysis of the TEM image of ZA27/ Al ₂ O ₃ 5% MDF processed at 200 °C for six passes for identification nano-crystalline particles inside the α phase	92
4.42	XRD patterns of ZA27 /Al ₂ O ₃ 5% ascast, solutionized and MDF processed at different temperature.	93
4.43	XRD patterns of ZA27/Al ₂ O ₃ 10% ascast, solutionized and MDF processed at different temperature.	93
4.44	Rockwell hardness values of ascast and solutionized ZA27 alloy and ZA27/Al ₂ O ₃ composites MDF processed up to three passes at 100°C and up to six passes at 200°C. a) ZA27/ Al ₂ O ₃ 5% b) ZA27/ Al ₂ O ₃ 10 %.	94
4.45	Engineering stress versus engineering strain for the tensile test of ZA27 ascast alloy and ZA27/Al ₂ O ₃ 5% composite after solutionized, MDF processed up to three passes at 100°C and up to six passes 200°C.	95
4.46	Engineering stress versus engineering strain for the tensile test of ZA27 ascast alloy and ZA27/Al ₂ O ₃ 10% composite after solutionized, MDF processed up to three passes at 100°C and up to six passes 200°C.	95
4.47	SEM images of the fracture surfaces of after tensile tests of ZA27/Al ₂ O ₃ 5% composites in macroscopic scale (a) Ascast ZA27/Al ₂ O ₃ 5% (b) Solutionized ZA27/Al ₂ O ₃ 5% (b) ZA27/Al ₂ O ₃	97

	5% MDF at 100 °C up to 3 passes (d) ZA27/Al ₂ O ₃ 5% MDF at 200 °C up to 6 passes	
4.48	SEM images of the fracture surfaces of after tensile tests of ZA27/Al ₂ O ₃ 5% composite (a) Ascast ZA27/Al ₂ O ₃ 5% (b) Solutionized ZA27/Al ₂ O ₃ 5% (b) ZA27/Al ₂ O ₃ 5% MDF at 100 °C up to 3 passes (d) ZA27/Al ₂ O ₃ 5% MDF at 200 °C up to 6 passes	98
4.49	SEM images of the fracture surfaces of after tensile tests of ZA27/Al ₂ O ₃ 10% composites in macroscopic scale (a) Ascast ZA27/Al ₂ O ₃ 10% (b) Solutionized ZA27/Al ₂ O ₃ 10% (b) ZA27/Al ₂ O ₃ 10% MDF at 100 °C up to 3 passes (d) ZA27/Al ₂ O ₃ 10% MDF at 200 °C up to 6 passes	98
4.50	SEM images of the fracture surfaces of after tensile tests of ZA27/Al ₂ O ₃ 10% composite (a) Ascast ZA27/Al ₂ O ₃ 10% (b) Solutionized ZA27/Al ₂ O ₃ 10% (b) ZA27/Al ₂ O ₃ 10% MDF at 100 °C up to 3 passes (d) ZA27/Al ₂ O ₃ 10% MDF at 200 °C up to 6 passes	99
4.51	Wear rate of ZA27/ Al ₂ O ₃ 5 wt% composite in different conditions (a) For 2000m of sliding distance (b) For 4000m of sliding distance.	100
4.52	Wear Resistance of ZA27/Al ₂ O ₃ 5wt% composite in different conditions	100
4.53	Wear rate of ZA27/ Al ₂ O ₃ 10 wt% composite in different conditions (a) For 2000m of sliding distance (b) For 4000m of sliding distance.	101
4.54	Wear Resistance of ZA27/Al ₂ O ₃ 10 wt% composite in different condition	102
4.55	SEM micrographs of the worn surfaces of ZA27/Al ₂ O ₃ in 5 & 10 wt%. (a) ZA27/Al ₂ O ₃ 5% ascast - 39.24N - 2000m (b) ZA27/Al ₂ O ₃ 5% - MDF 6 Pass - 49.05N - 2000m (c) ZA27/Al ₂ O ₃ 5% - MDF 3 pass - 58.86N - 2000m (d) ZA27/Al ₂ O ₃ 5% MDF 6 Pass – 58.86N - 4000m (e) ZA27/Al ₂ O ₃ 5% - ascast -- 39.24N - 4000m (f) ZA27/Al ₂ O ₃ 5% - MDF 3 Pass - 58.86N - 4000m (g) ZA27/Al ₂ O ₃ 10% - MDF 3 Pass 49.05N – 2000m (h) ZA27/Al ₂ O ₃ 10%- MDF 6 pass- 58.86N - 4000m.	103
4.56	EDS analysis of the worn surfaces of composite material (ZA27/Al ₂ O ₃ 10% - MDF 3 Pass 49.05N)	104
4.57	Optical microscopy images (a) Ascast ZA27/SiC+Al ₂ O ₃ 5% composite (b) Solutionized ZA27/SiC+Al ₂ O ₃ 5% composite (c) ZA27/SiC+Al ₂ O ₃ 5% MDF processed at 100°C for 3 passes (d) ZA27/SiC+Al ₂ O ₃ 5% MDF processed at 200°C for 6 passes (e)	107

- Ascast ZA27/SiC+Al₂O₃ 10% composite (f) Solutionized ZA27/SiC+Al₂O₃ 10% composite (g) ZA27/SiC+Al₂O₃ 10% MDF processed at 100°C for 3 passes (h) ZA27/SiC+Al₂O₃ 10% MDF processed at 200°C for 6 passes.
- SEM images (a) Ascast ZA27/SiC+Al₂O₃ 5% composite (b) Solutionized ZA27/ SiC+Al₂O₃ 5% composite (c, d) SiC+Al₂O₃ Particle distribution in ZA27/SiC+Al₂O₃ 5% composite (e1) ZA27/SiC+Al₂O₃ 5% - MDF processed at 100°C for 3 passes (e2) 4.58 ZA27/ SiC+Al₂O₃ 5% - MDF processed at 100°C for 3 passes (higher magnification x 10,000) (f1) ZA27/ SiC+Al₂O₃ 5% MDF processed at 200°C for 6 passes (f2) ZA27/ SiC+Al₂O₃ 5% MDF processed at 200°C for 6 passes (higher magnification x 10,000) showing cellular type of grains. 108
- SEM images (a) Ascast ZA27/SiC+Al₂O₃ 10% composite (b) Solutionized ZA27/ SiC+Al₂O₃ 10% composite (c, d) SiC+Al₂O₃ Particle distribution in ZA27/Al₂O₃ 10% composite (e1) ZA27/SiC+Al₂O₃ 10% - MDF processed at 100°C for 3 passes (e2) 4.59 ZA27/ ZA27/SiC+Al₂O₃ 10% - MDF processed at 100°C for 3 passes (higher magnification x 10,000) (f1) ZA27/ SiC+Al₂O₃ 10% MDF processed at 200°C for 6 passes (f2) ZA27/ SiC+Al₂O₃ 10% MDF processed at 200°C for 6 passes (higher magnification x 10,000) showing cellular type of grains 109
- Grain size distribution curve a) Solutionized ZA27/SiC+Al₂O₃ 5% composite b) ZA27/SiC+Al₂O₃ 5% - MDF processed at 100°C for 3 passes c) ZA27/SiC+ Al₂O₃ 5% - MDF processed at 200°C for 6 passes. 4.60 110
- Grain size distribution curve a) Solutionized ZA27/SiC+Al₂O₃ 10% composite b) ZA27/SiC+Al₂O₃ 10% - MDF processed at 100°C for 3 passes c) ZA27/SiC+ Al₂O₃ 10% - MDF processed at 200°C for 6 passes. 4.61 110
- Bright-field TEM micrograph a) ZA27/SiC+Al₂O₃ 5% MDF processed at 100 °C for three passes showing lamellar boundaries b) ZA27/SiC+Al₂O₃ 5% MDF processed at 100 °C for three passes showing equiaxed structure or broken lamellar structure c) ZA27/ 4.62 SiC+Al₂O₃ 10% MDF at 100 °C for three passes d) ZA27/ SiC+Al₂O₃ 5% MDF processed at 100 °C for three passes showing dislocation. 111
- 4.63 XRD patterns of ZA27 /SiC + Al₂O₃ 5% ascast, solutionized and 112

	MDF processed at different temperature.	
4.64	XRD patterns of ZA27 /SiC + Al ₂ O ₃ 10% ascast, solutionized and MDF processed at different temperature.	112
4.65	Rockwell hardness values of ascast and solutionized ZA27 alloy and ZA27/SiC+Al ₂ O ₃ composites MDF processed up to three passes at 100°C and up to six passes at 200°C. a) ZA27/ SiC + Al ₂ O ₃ 5% b) ZA27/ SiC + Al ₂ O ₃ 10 %.	113
4.66	Engineering stress versus engineering strain for the tensile test of ZA27 ascast alloy and ZA27/SiC+Al ₂ O ₃ 5% composite after solutionized, MDF processed up to three passes at 100°C and up to six passes 200°C.	114
4.67	Engineering stress versus engineering strain for the tensile test of ZA27 as-cast alloy and ZA27/SiC+Al ₂ O ₃ 10% composite after solutionized, MDF processed up to three passes at 100°C and up to six passes 200°C.	114
4.68	SEM images of the fracture surfaces of after tensile tests of ZA27/SiC+Al ₂ O ₃ 5% composites in macroscopic scale (a) Ascast ZA27/SiC+Al ₂ O ₃ 5% (b) Solutionized ZA27/SiC+Al ₂ O ₃ 5% (b) ZA27/SiC+Al ₂ O ₃ 5% MDF at 100 °C up to 3 passes (d) ZA27/SiC+Al ₂ O ₃ 5% MDF at 200 °C up to 6 passes.	117
4.69	SEM images of the fracture surfaces of after tensile tests of ZA27/SiC+Al ₂ O ₃ 5% composite (a) Ascast ZA27/SiC+Al ₂ O ₃ 5% (b) Solutionized ZA27/SiC+Al ₂ O ₃ 5% (b) ZA27/SiC+Al ₂ O ₃ 5% MDF at 100 °C up to 3 passes (d) ZA27/SiC+Al ₂ O ₃ 5% MDF at 200 °C up to 6 passes	117
4.70	Dimple size distribution curve a) ZA27/SiC+Al ₂ O ₃ 5% - MDF processed at 100°C for 3 passes b) ZA27/SiC+Al ₂ O ₃ 5% - MDF processed at 200°C for 6 passes	118
4.71	SEM images of the fracture surfaces of after tensile tests of ZA27/SiC+Al ₂ O ₃ 10% composites in macroscopic scale (a) Ascast ZA27/SiC+Al ₂ O ₃ 10% (b) Solutionized ZA27/SiC+Al ₂ O ₃ 10% zed ZA27/SiC+Al ₂ O ₃ 10% (b) ZA27/SiC+Al ₂ O ₃ 10% MDF at 100 °C up to 3 passes (d) MDF at 200 °C up to 6 passes.	119
4.72	SEM images of the fracture surfaces of after tensile tests of ZA27/SiC+Al ₂ O ₃ 10% composite (a) Ascast ZA27/SiC+Al ₂ O ₃ 10% (b) Solutionized ZA27/SiC+Al ₂ O ₃ 10% zed ZA27/SiC+Al ₂ O ₃ 10% (b) ZA27/SiC+Al ₂ O ₃ 10% MDF at 100 °C up to 3 passes (d) MDF	119

at 200 °C up to 6 passes.

4.73	Dimple size distribution curve a) ZA27/SiC+Al ₂ O ₃ 10% - MDF processed at 100°C for 3 passes b) ZA27/SiC+Al ₂ O ₃ 10% - MDF processed at 200°C for 6 passes.	120
4.74	Wear rate of ZA27/SiC+Al ₂ O ₃ 5 wt% composite in different conditions (a) For 2000m of sliding distance (b) For 4000m of sliding distance.	121
4.75	Wear Resistance of ZA27/SiC+Al ₂ O ₃ 5 wt% composite in different conditions	121
4.76	Wear rate of ZA27/ SiC+Al ₂ O ₃ 10 wt% composite in different conditions (a) For 2000m of sliding distance (b) For 4000m of sliding distance.	122
4.77	Wear Resistance of ZA27/SiC+Al ₂ O ₃ 10 wt% composite in different condition	122
4.78	SEM micrographs of the worn surfaces of ZA27/ SiC+Al ₂ O ₃ in 5 & 10 wt%.(a) ZA27/ SiC+Al ₂ O ₃ 5% ascast - 39.24N - 2000m (b) ZA27/ SiC+Al ₂ O ₃ 5% - sol - 49.05N - 2000m (c) ZA27/ SiC+Al ₂ O ₃ 5% - MDF 3 pass - 58.86N - 2000m (d) ZA27/ SiC+Al ₂ O ₃ 5% - MDF 6 Pass - 58.86N - 4000m (e) ZA27/ SiC+Al ₂ O ₃ 5% - ascast- 39.24 - 2000m (f) ZA27/ SiC+Al ₂ O ₃ 5% - sol- 58.86N - 4000m (g) ZA27/ SiC+Al ₂ O ₃ 10% - Ascact 39.24N – 4000m (h) ZA27/ SiC+Al ₂ O ₃ 10%- MDF 6 pass- 49.05N - 4000m.	123
5.1	Representation of cylinder Roller Bearing Parts	126
5.2	CAD model for different parts of Cylinder Roller Bearing a) Inner Ring b) Outer Ring c) Rollers d) Cage	127
5.3	Schematic diagram of cylinder roller bearing design	128
5.4	Photograph of Cylinder Roller Bearing	128
AI-1.1	Two dimensional representations of Squeeze casting Die (a) Plunger (b) Top view assembled (c) Right side view assembled (d) Front view assembled	155
AI-1.2	Two dimensional representations of MDF Procssing die (a) Plunger and Base plate (b) Main body part one (c) Main body part two (d) Assembled main body	157
AI-1.3	XRD patterns of ZA27/SiC 10% and SiC powder.	158
AI-1.4	Standard stick file XRD patterns for Silicon Carbide (00-019-0628)	159

AI-1.5	Standard stick file XRD patterns for Silicon Carbide (00-031-1232)	160
AI-1.6	Standard stick file XRD patterns for Silicon Carbide (00-037-0922)	161
AI-1.7	Showing two theta values for ZA27 based composites reinforced with 10wt % Al ₂ O ₃ particles	163
AI-1.8	Standard stick file XRD patterns for Alumina (00-010-0173)	165
AI-1.9	Standard stick file XRD patterns for Aluminum Oxide (00-023-1009)	167
AI-1.10	Standard stick file XRD patterns for Aluminum Oxide (00-026-0031)	168
AI-1.11	Standard stick file XRD patterns for Aluminum Oxide (00-050-1496)	169
AI-1.12	Comparison bar chart for UTS and % Elongation of SiC 5 wt% reinforced composites under various material condition	170
AI-1.13	Comparison bar chart for UTS and % Elongation of SiC 10 wt% reinforced composites under various material condition	170
AI-1.14	Comparison bar chart for UTS and % Elongation of Al ₂ O ₃ 5 wt% reinforced composites under various material condition	171
AI-1.15	Comparison bar chart for UTS and % Elongation of Al ₂ O ₃ 10 wt% reinforced composites under various material condition	171
AI-1.16	Comparison bar chart for UTS and % Elongation of SiC+Al ₂ O ₃ 5 weight% reinforced composites under various material condition	172
AI-1.17	Comparison bar chart for UTS and % Elongation of SiC+Al ₂ O ₃ 10 wt% reinforced composites under various material condition	173

LIST OF TABLES

Table No.	Contents	Page No.
1.1	Types of reinforcing particles in MMC	04
3.1	Materials used for the fabrication of composites	46
3.2	Chemical composition (wt. %) of the zinc-aluminum alloy	50
4.1	Chemical composition of ZA-27 matrix alloy	57
4.2	Density and Hardness values of ZA27 alloy	59
4.3	Experimental and Theoretical density with porosity percentage of ZA27/SiC 5% and 10%	62
4.4	Experimental and Theoretical density with porosity percentage of ZA27/Al ₂ O ₃ 5% and 10%	84
4.5	Experimental and Theoretical density with porosity percentage of ZA27/SiC+Al ₂ O ₃ 5% and 10%	105
5.1	Bearing Weight and Cost Estimation (B1, B2, B3)	126
AI-1.1	Showing two theta values for ZA27 based composites reinforced with 10wt %/ SiC particles	160
AI-1.2	Showing 2 theta value for SiC powder	160
AI-1.3	Showing 'hkl' and 2 theta value for Silicon Carbide (00-019-0628)	162
AI-1.4	Showing 'hkl' and 2 theta value for Silicon Carbide (00-031-1232)	162
AI-1.5	Showing 'hkl' and 2 theta value for Silicon Carbide (00-037-0922)	163
AI- 1.6	Showing two theta values for ZA27 based composites reinforced with 10wt %/ Al ₂ O ₃ particles	165
AI- 1.7	Showing two theta value for Al ₂ O ₃ powder	166

AI- 1.8	Showing ‘hkl’ and 2 theta value for Alumina (00-010-0173)	167
AI- 1.9	Showing ‘hkl’ and 2 theta value for Aluminum Oxide (00-023-1009)	169
AI- 1.10	Showing ‘hkl’ and 2 theta value for Alumina (00-026-0031)	170
AI- 1.11	Showing ‘hkl’ and 2 theta value for Aluminum Oxide (00-050-1496)	171
AII- 1.1	Mechanical properties and Grain size measurement values	175
AIV-1.1	Wear results calculation for pin on disc wear test of MDF processed ZA27/SiC 5 wt% composites.	176
AIV-1.2	Wear results calculation for pin on disc wear test of MDF processed ZA27/SiC 10 wt% composites.	177
AIV-1.3	Wear results calculation for pin on disc wear test of MDF processed ZA27/ Al ₂ O ₃ 5 wt% composites.	178
AIV-1.4	Wear results calculation for pin on disc wear test of MDF processed ZA27/ Al ₂ O ₃ 5 wt% composites.	179
AIV-1.5	Wear results calculation for pin on disc wear test of MDF processed ZA27/ SiC+Al ₂ O ₃ 5 wt% composites.	180
AIV-1.6	Wear results calculation for pin on disc wear test of MDF processed ZA27/ SiC+Al ₂ O ₃ 10 wt% composites.	181
	List of publication based on PhD Research Work	183

NOMENCLATURE

UFG	Ultrafine grains
CG	Coarse grains
MMC	Metal matrix composite
MDF	Multi Directional Forging
SPD	Severe Plastic Deformation
HCP	Hexagonal Close Packed
ECAP	Equal Channel Angular Pressing
ARB	Accumulative Roll Bonding
HPT	High Pressure Torsion
CEC	Cyclic extrusion and compression
RCS	Repetitive corrugation and straightening
CGP	Constrained groove pressing
EDAX	Energy Dispersive X-Ray
Φ	Channel angle
Ψ	Outer arc of curvature
Zn	Zinc
Al	Aluminum
Cu	Copper
Fe	Iron
Mg	Magnesium
ZA	Zinc-Aluminium

SiC	Silicon Carbide
Al ₂ O ₃	Alumina
α	Al rich FCC phase
η	Zn rich HCP phase
ε	CuZn ₄ HCP phase
β	Zn rich FCC phase
τ'	Distorted BCC structure (Zn ₁₀ Al ₃₅ Cu ₅₅)
n	Strain hardening exponent
K	Strength coefficient
XRD	X-Ray Diffractometry
OM	Optical Microscopy
SEM	Scanning Electron Microscopy
TEM	Transmission Electron Microscopy
HRB	Hardness Rockwell B
HRC	Hardness Rockwell C
HV	Vickers Microhardness
UTS	Ultimate Tensile Strength
T _m	Melting temperature
μm	Micrometer
nm	Nanometer
YS	Yield strength
UTS	Ultimate tensile strength

CHAPTER 1

INTRODUCTION

In the last few decades, severe plastic deformation (SPD) has emerged as the most successful technique in producing ultra-fine grained (UFG) materials in bulk quantity. Where grain size plays a prominent role in deciding the unusual properties of a material like strength, hardness, ductility, fatigue resistance, corrosion, and low-temperature superplasticity. A fine-grained material is harder and stronger than that of coarse-grained materials because the former has a greater total grain boundary area to obstruct the dislocation motion. For many materials, the yield strength σ_y varies with grain size according to

$$\sigma_y = \sigma_0 + k_y d^{-\frac{1}{2}} \quad \text{Equation - 1.1}$$

this expression is termed as Hall–Petch equation (Hall 1951) (Petch 1953), where d is the average grain diameter, and σ_0 (yield stress) and k_y (strengthening coefficient) is constants for a particular material. Ultrafine-grained (UFG) materials are defined as polycrystals with small grains, which lie in the range of sub micro meter (100~1000 nm) and nano meter (less than 100 nm) (Chengpeng et al. 2012). Conventional metal forming techniques like extrusion or rolling, are restricted in their ability to produce UFG structures for two reasons. First, there is a limitation on the overall strains that may be imposed using these techniques because for a large strain to develop using these techniques there will be a corresponding reduction in cross-section of work pieces. Second, the strains imposed in these techniques are limited and insufficient to give rise to UFG structures because of the generally low workability of metallic alloys at ambient temperatures. As a consequence of these limitations, there is a shift in the synthesis approach for nanoscale materials and alternative processing techniques have been developed. The severe plastic deformation (SPD) technique is one of such processes. Where submicron and even nanocrystalline metals and alloys can be easily

produced as compared to other available techniques to manufacture nanocrystalline materials. With increasing severity of deformation, the microstructure of material undergoes a substantial refinement and finally reaching a steady state ultrafine-grained (UFG) microstructure. Several SPD processes such as equal channel angular extrusion (ECAE), accumulative roll bonding (ARB) and torsion under high pressure (HPT), multi-axial forging (MAF) or multi directional forging (MDF), have been used as fine-grained materials producing techniques by many researches according to their requirement (Valiev et al. 2006).

In general, the present industries are more concern with large size work pieces, which can be easily processed by multi-axial forging or multi directional forging process. Any method of metal forming under an extensive hydrostatic pressure that may be used to impose a very high strain on a bulk solid without the introduction of any significant change in the overall dimensions of the sample and having the ability to produce exceptional grain refinement is known to be “SPD” process (Bansal and Sharma 2015). (Fethma et al. 2020) Compared to all other processes, MDF is a simple method because in this process a conventional forging machine is sufficient to deform in simple compression, so for the present study on the MDF process is focused. In order to convert a coarse-grained solid into a material with ultrafine grains, an exceptionally high strain is imposed in order to introduce a high density of dislocations which, in turn, re-arrange to form an array of grain boundaries with an increase in strain. High specific properties of the material are critical for many structural applications in automotive and aerospace design, so composites are one of the most advanced and adaptable engineering materials known to many researchers (Madhu et al. 2020). Progress in the field of materials science and technology have given birth to these fascinating and wonderful materials (Kai-bo et al. 2020). Composites are heterogeneous in nature (Lubin 1982). Since from last few decades, there is a technological breakthrough in composite fields. Many of our modern technologies require materials with unusual combinations of properties that cannot be met by conventional metal alloys (Jayashree et al. 2013). But now the designers have the freedom to choose materials suitable for the specific property needs of their end products and materials for a variety of applications ranging from opt electronics to space vehicles.

A composite material is a material composed of two or more constituents. The constituents are combined at a microscopic level and are distinct both physically and chemically and arranged or distributed in a suitable manner. Generally, a composite material could be described as comprising of reinforcement (fibres, particles/particulates, flakes and/or fillers) embedded in a matrix (metals, polymers, and ceramics). The desired shape is formed as the matrix holds the reinforcement. The reinforcement or additive constituents used for composite materials usually carry most of the load and provide the desired properties. The matrix will hold the reinforcement phase and under an applied force it deforms and distributes the stress to the reinforcement uniformly. The most commonly utilized matrix materials are either polymers or metals. However, although polymeric matrices are relatively cheap, more widely used and available in more varieties, metallic matrices offer greater strength and stiffness, especially at elevated temperatures. Furthermore, MMCs have superior fracture toughness, offer less pronounced anisotropy and have greater thermal resistance in oxidizing environments than their polymeric counterparts. New manufacturing routes, such as powder metallurgy processing, low-pressure plasma co-spraying, low-pressure liquid metal infiltration and squeeze casting, make the production of MMCs possible in a wide variety of grades and forms. These methods are currently competing to produce the lowest cost material with the most desirable mechanical properties.

In addition to automotive applications, MMCs are of considerable interest to the aerospace industry because of their potential for the production of lightweight, structurally efficient components used in virtually every sector of the aerospace industry. To take the most benefits of properties of the metal matrices and enhance them with proper reinforcements, the selection of a matrix should follow three basic requirements.

- a. The low melting point in order to permit liquid-phase fabrication processes without impairing the reinforcement properties.
- b. Sufficient ductility to provide strain accommodation around the brittle reinforcements.
- c. Low density to achieve high specific properties.

Considering the above criteria's, for the present study Zinc Aluminum Alloy (ZA-27) is selected as a matrix material. Zinc-based alloys are used mainly in the form of the die castings. The important features of such alloys are low cost, excellent castability, ability to use cheap carbon steel dies for processing. Zn-Al based alloys have been commercially accepted for many years since the first casting alloy was developed at the New Jersey Zinc Company in 1922. Only 0.25 % - 1.25 % of Al was being used in die casting technique for many years. The attractiveness of die casting has been further advanced by the recent development of a series of Zinc base alloys with a relatively large addition of Al, up to 30% with other alloying metals. A new family of Zn-Al based alloys with high aluminum and copper contents was developed based on the ZAMAK alloys in North America and China in the 1970s (Hua 2004). Zinc-aluminum based alloys were developed in a number of grades like ZA-8 (Zn-8 wt.% Al), ZA-12 (Zn-12 wt. % Al) and ZA-27 (Zn-27 wt.% Al) (Ismail et al. 2004). Due to the unique combination of properties, these alloys are also increasingly used to replace traditional alloys such as aluminum, bronze, brass and cast iron in many industrial and automotive applications.

Metal-matrix composite reinforcements can be generally divided into five major categories: a) Continuous fibres b) Short fibres c) Whiskers d) Wires e) Particulates.

The reinforcement does not always serve a purely structural task but also used to change the various properties such as wear resistance, friction coefficient and thermal conductivity. The reinforcement can be either continuous or discontinuous. Discontinuous MMCs are nearly isotropic and material worked with standard metal working techniques, such as extrusion, forging or rolling.

Table 1.1: Types of the reinforcing particles in MMC

Oxides:	MgO	SiO ₂	ZrO ₂	HfO ₂	TiO ₂	CeO ₂	Cr ₂ O ₃	Al ₂ O ₃	MoS ₂
Carbides:	SiC	ZrC	B ₄ C	Al ₄ C ₃	Cr ₃ C ₂	TaC	MoC	NbC	TiC
Nitrides:	TiN	ZrN	Si ₃ N ₄	Al ₂ N ₂	BN				
Borides:	ZrB ₂	SiB ₃	TaB ₂	MoB	NbB	TiB ₂			
Aluminides:	FeAl	Ni ₃ Al	Fe ₃ Al	NiAl					

Reinforcements are generally ceramics. Typically, these ceramics are oxides, carbides, and nitrides, which are used because of their excellent combinations of

specific strength and stiffness at both ambient temperature and at elevated temperatures. Typical reinforcing particles used in metal-matrix composites are listed in Table 1.1. Silicon carbide, boron carbide, and aluminum oxide are the key particulate reinforcements and can be obtained in varying levels of purity and size distribution. Furthermore, the use of discontinuous reinforcements minimizes problems associated with fabrication of continuously reinforced metal-matrix composites such as fibre damage, micro-structural heterogeneity, and fibre mismatch. For applications subjected to severe loads or extreme thermal fluctuations such as in automotive components, discontinuously-reinforced metal matrix composites have been used. Ceramics have become the most suitable materials for MMC reinforcements due to their special characteristics not found in traditional metal alloys. Silicon carbide (SiC), alumina (Al_2O_3) and boron carbide (B_4C) are more commonly used ceramics for many MMCs (Sastry et al. 2001) (Xu et al. 2003) (Orhadahwe et al. 2020). Among these ceramics, SiC and Al_2O_3 have been selected as the reinforcing materials for the present research work.

Particles of silicon carbide possess hardness value of approximately 2700 HV and are commonly used as grinding abrasives. SiC becomes more attractive as a reinforcing material due to its substantially lower cost. Combining SiC particles in a matrix material results in a composite that has better mechanical and physical properties than the unreinforced one, its strength, thermal conductivity, abrasion resistance and creep resistance are all superior to those of the base metal (Modi et al. 2007). The amount of SiC particulate added into the matrix alloy can be varied from 2 to 30 vol%, depending on applications. The unique Al_2O_3 microsphere-reinforced MMC has been developed by Comalco Aluminium Limited, Australia, using a proprietary liquid metallurgy technique. MMCs may be reinforced with Al_2O_3 in the form of either fibres, whiskers or even particulate, shows a better mechanical and tribological properties in different testing condition (Jovanovic et al. 2003). There are several fabrication techniques available to manufacture the MMC materials; there is no unique route in this respect. Due to the choice of material and types of reinforcement, the fabrication techniques can vary considerably. Different fabricating techniques are powder blending, diffusion bonding of foils, stir casting, squeeze casting, spray deposition, rheocasting, and physical vapor deposition. Since the present research

work deals with the stir casting technique followed by the squeezing process, the literature survey for stir casting is reported in detail.

Normally the liquid-phase fabrication method is more efficient than the solid-phase fabrication method because solid-phase processing requires a longer time. Stir casting involves the addition of particulate reinforcement into semisolid metal (SSM) by means of agitation. The advantage of stir casting lies in a lower processing temperature leading to a longer die life and high production cycle time. Defects that may occur if process parameters are not adequately controlled include the fact that non-homogeneous particle distribution results in sedimentation and segregation. Although stir casting is generally accepted as a commercial route for the production of MMCs by many types of research, however, some technical challenges were associated with producing a homogeneous, high-density composite. Effectiveness with which mechanical stirring can incorporate and distribute the particles throughout the melt depends on the constituent materials, the stirrer geometry and position, the speed of stirring, and the mixture temperature. (Prabu et al. 2006). For the betterment of properties, we have adopted squeeze casting or pressure die casting technique as it has many advantages over gravity casting like lower levels of porosity, good surface texture, fine micro-structures with higher strength components (Kurnaz et al. 2005). Researchers have found that materials with fcc and hcp crystal structures can be processed by MDF for obtaining ultrafine grains (Sakai et al. 2014). The zinc-aluminum based alloys were developed in a number of grades like ZA8 (Zn-8 wt. % Al), ZA12 (Zn-12 wt. % Al), ZA22 (Zn-22 wt. % Al) and ZA27 (Zn-27 wt. % Al). These alloys exhibit excellent castability and wear resistance, making it widely used one in general engineering applications like bearings. These materials are candidate materials for replacement of their conventional counterparts like aluminum cast alloys, copper based alloys and cast iron (Prasad 1998). The zinc-aluminum alloys have the typical dendritic structure in as-cast conditions, wherein the dendritic size and inter-dendritic spacing depend on the casting process parameters. The dendritic structure exhibits lower ductility and high heterogeneity in the mechanical properties of the cast alloy (Babic et al. 2010). Copper is added in the range of one to three weight percentages to improve the strength of Zn-Al alloys (Swati et al. 2020). This

would lead to the formation of ϵ (CuZn_4) phase during the solidification which imparts dimensional stability to the material.

Against this background, the present research work is undertaken to study the effects of SiC and Al_2O_3 reinforced particulate in ZA27 alloy. Further to investigate and develop the application of the MDF techniques, which may lead to an improvement in mechanical and tribological properties of advanced MMCs for industrial application. For potential use of fine-grained materials in industrial use particularly as bearing materials, wear property is a significant factor that needs to be considered. Therefore, it is important to study the tribological properties of MDF processed ZA27 based composites reinforced with SiC and Al_2O_3 particles. To analyse the influence of parameters such as applied load, sliding distance and sliding speed on dry sliding wear behavior of solutionized and MDF processed material using pin on disc test rig was conducted.

1.1 Objectives of Present Work

The objectives of the present work are stated below:

1. Fabrication of ZA27 based composites reinforced with SiC and Al_2O_3 by squeeze casting technique.
2. To process ZA27 alloy reinforced with SiC and Al_2O_3 composites by Multidirectional Forging technique.
3. To characterize the ZA27 based composite material with varying reinforcement content in weight percentage using optical microscope, SEM, TEM and XRD for both MDF processed and unprocessed samples.
4. To evaluate the effect of reinforcement in varying weight percentage, on the mechanical properties of both processed and unprocessed ZA27 based composites.
5. To study the wear properties of MDF processed ZA27 based composites with different wear parameters.

1.2 THESIS ORGANISATION

In the present work, multidirectional forging process is carried out to refine the grains of ZA27/SiC/Al₂O₃/SiC+Al₂O₃ composite materials. Microstructural evaluation of the MDF processed specimens is studied and the results are correlated with the observed mechanical, tribological properties. The present work consists of six chapters and is summarized as follows:

CHAPTER 1

In this chapter, the introduction of composite materials, fabrication technique and their applications, the background of Zinc aluminum alloys and multidirectional process have been described. The objectives of the present research work are prescribed through the literature review gap.

CHAPTER 2

This chapter outlines some of the recent research work published on composites with special emphasis on grain refinement and improvements in mechanical and wear behavior of various particulate reinforced metal matrix composites. A detailed description of MDF principle and experimental factor influencing the MDF process.

CHAPTER 3

The chapter describes the details of material selection, fabrication of composites by casting process, MDF process setup and explains the experimental procedure for multiple passes at different temperatures, methodology of present research, experimental and characterization techniques used in the present investigation in order to achieve the objectives.

CHAPTER 4

This chapter reports, results and discussion of the experiments carried out and states the effect of addition of different reinforcement and their composition in terms of weight percentage and also gives a detailed information regarding effect of MDF processing of ZA27/SiC/Al₂O₃/SiC+Al₂O₃ composite materials. Furthermore

microstructural characterization of the composite materials were also stated. Investigation on the effects of MDF process on the material properties such as density, grain size, ultimate tensile strength, ductility, fracture topography and wear behaviour of both processed and unprocessed ZA27 based composites.

CHAPTER 5

This chapter give the details regarding application of ZA27 based composites related to present research work - ZA27/SiC-Al₂O₃ - Cylinder Roller Bearing.

CHAPTER 6

This chapter presents the conclusions of various investigations carried out through this research work and also deals with future scope of work. The references and appendices are presented at the end of the thesis.

CHAPTER 2

LITERATURE SURVEY

In view of the high cost of currently used bearing materials, the automotive and machine tool sectors are in immediate need of materials having improved mechanical and tribological properties with low material cost compared to conventional bearing materials. This chapter outlines some of the recent research work published on composites with special emphasis on grain refinement and improvements in mechanical properties and wear behavior of various particulate reinforced metal matrix composites. Literature survey indicates that despite the increase in the production and use of zinc-aluminum cast alloys reinforced with ceramic material in recent times, only limited data are available on their casting characteristics, mechanical properties, microstructure, and wear behavior. Hence the literature survey of previous investigations on the usage of zinc-aluminum alloys has been reported in order to establish a base for the present study and also to have an overview of the production techniques, mechanical and tribological properties, and microstructure of zinc-aluminum alloys based composites that can be used as a bearing material.

Metal matrix composites have many advantages over monolithic metals like higher specific modulus, higher specific strength, better properties at elevated temperatures and a lower coefficient of thermal expansion. Because of these attributes metal matrix composites are under consideration for a wide range of applications. Metal matrix composites (MMCs) have recently become candidates for critical structural applications because of a combination of superior mechanical properties such as better elastic modulus, tensile strength, high-temperature stability and wear resistance in comparison with many alloys. The present-day trend is towards safe usage of the MMC parts in the automobile section, which work particularly at high temperature and pressure environments (Mishra & Satapathy 2014).

Severe plastic deformation processes like multi directional forging (MDF), equal channel angular pressing (ECAP), accumulative roll bonding (ARB), high pressure torsion (HPT), and friction stir processing (FSP) alter the properties by changing the grain size and structure to nano crystalline or sub-microcrystalline structures in various metals and alloys. For obtaining desired properties, ultrafine-grained structures with high angle grain boundaries and uniform grain structure across the entire volume of the sample are required (Valiev 2000) (Yida et al. 2017). The technique of MDF on composite materials has received little attention when compared with other severe plastic deformation processes like ECAP, ARB, and HPT.

2.1 Principle of Multi-Directional Forging (MDF)

MDF method was developed by Salishchev. The process of multiple forging is associated with dynamic recrystallization. Multiple forging is the simple process in which the free forging is repeated in three orthogonal directions, setting drawing with the change of the axis of the applied strain load. MDF is an advanced metal forming process capable of producing plastic deformation in a variety of materials. It is the simplest method to achieve larger strains with minimum dimensional change and allows processing of bulk products (Kaibyshev 2001).

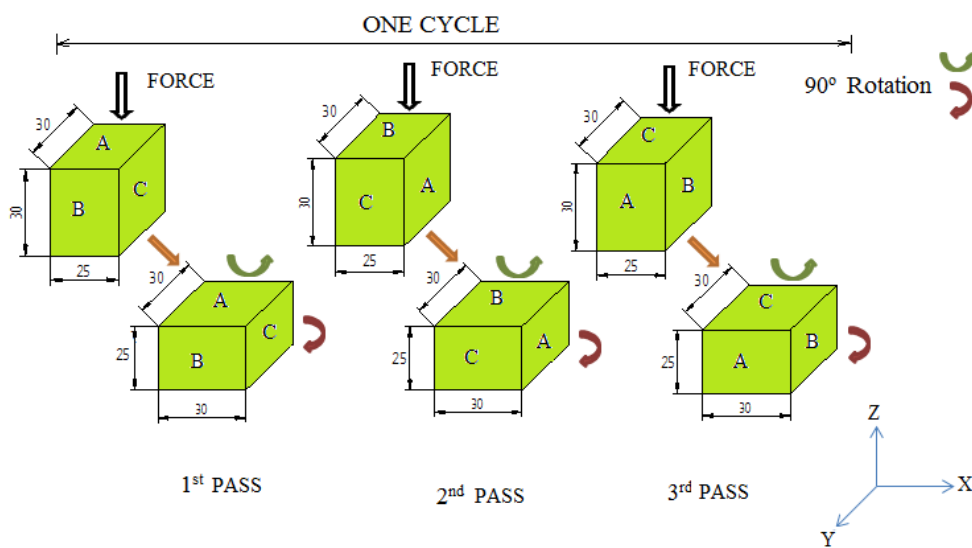


Figure 2.1: Schematic diagram of MDF processing along with three directions.

MDF involves plane strain deformation condition that is achieved by compressing the work piece through a split type die. In this technique the sample is pressed in die to a fixed strain, removed and rotated by 90° in two different directions, reinserted in the die and pressed to the same strain as shown in fig. 2.1. Along with deformation strain, deformation temperature also plays a critical role in refining the grain structure (Miura et al. 2012). The presence of high hydrostatic pressure in combination with large amount strain is essential for producing high densities of crystal lattice defects, particularly dislocations, which can result in significant refining of the grains. Grain refinement in SPD processes occurs by a multistep process (Mishra et al. 2007):

- a. Dislocations, which are initially distributed throughout the grains, rearrange and group together into dislocation "cells" to reduce the total strain energy.
- b. As deformation continues and more dislocations are generated, mis-orientation develops between the cells, forming "sub-grains".
- c. The process repeats within the sub-grains until the size becomes sufficiently small such that the sub-grains can rotate.
- d. Additional deformation causes the sub-grains to rotate into high angle grain boundaries, typically with an equiaxed shape.

2.2 Experimental Factors Influencing MDF

MDF processed material properties is influence by many factors like (a) Strain imposed, (b) Pressing speed, (c) Pressing temperature and (d) Friction and lubrication.

2.2.1 Strain imposed in MDF and number of passes

Expression for total effective strain (ϵ_{eff}) imparted on the MDF sample and it is given by Estrin and Vinogradov (2013).

$$\epsilon_{\text{eff}} = N * \ln\left(\frac{x}{y}\right) \quad \text{Equation - 2.1}$$

Where N = the number of processing steps and x, y are the initial height and width of the specimen.

2.2.2 Pressing Speed

Equilibrium structure in processed materials can be obtained by adopting slow pressing speed during the MDF process. Since the pressing speed is directly related to the strain rate imposed on the material, it is reasonable to expect a more equilibrium structure at a slow speed due to longer time available for the recovery process. Watanabe et al. (2017) in his investigation on AZ61Mg specimens shows strain rate sensitivity m is dependent of grain size (strain-rate sensitivity m became larger as grain size decreased). Miura et al. (2016) MDF was carried in the range of 3×10^{-3} to $3 \times 10^{-1} \text{ s}^{-1}$ under the same temperature. Less homogeneous microstructure was evolved for a strain rate of $3 \times 10^{-1} \text{ s}^{-1}$ as compared to $3 \times 10^{-3} \text{ s}^{-1}$.

2.2.3 Pressing Temperature

In general, it is easier to press specimens at a higher temperature but the pressing should be performed at the lowest possible temperature without the introduction of any significant cracking in the specimen. Maintaining a low pressing temperature ensures the potential for achieving both the smallest possible equilibrium grain size and the highest fraction of high-angle boundaries (Valiev et al. 2000). Cu based alloys were MDF processed under cryogenic temperature (Ramesh et al. 2019) which resulted in formation of micro-shear band.

2.2.4 Friction and Lubrication

In the MDF process, lubrication reduces the friction between the dies and the work piece. Subsequently, the amount of redundant shear strain is reduced and plane strain compression conditions are expected throughout the sample. Lubricate should be non-abrasive and non-corrosive and we can use different types of lubricate like Graphite, Glass, Nickel, Oils, Molybdenum Disulphide, Boron Nitride, Wax and Grease (Ujjwal et al. 2014).

2.3 Advantages and Disadvantages of MDF

Multi directional forging has a number of important technical characteristics, uniqueness, and benefits in comparison with conventional metal working processes.

2.3.1 Advantages of MDF

The multi-directional forging process is the simplest plastic deformation process for the following reasons.

- a. Multi directional forging can be processed on large-size work piece using a conventional forging machine.
- b. Multi directional forging can be applied to material in different temperature ie under cold, warm and hot working conditions.
- c. MDF can be applied to different metals, alloys and metal matrix composites like brittle materials including high strength.
- d. MDF is simply repeated compression type, hence one can carry out the same using any conventional testing machine.
- e. Potential to reach the requirement for industrial application.

2.3.2 Disadvantages of MDF

MDF is non-continuous process and it is time consuming as compared to other SPD processes like ECAP, HPT, and ARB.

2.4 Zinc-Aluminium Alloy (ZA ALLOY)

A Zn-Al based alloy was developed at the New Jersey Zinc company in 1922. A new family of hyper-eutectoid Zn-Al based alloys with high aluminum and copper contents was developed based on the ZAMAK alloys in North America and China in the 1970s. The major advancement in the zinc industry over the past years has been the development of zinc alloys to supplement the well-established alloys used in pressure die-casting. The copper content was up to 3 weight % and aluminum content was selected as about 8, 12 and 27 weight % (El-khair et al. 2004). The mechanical and physical properties of these alloys are much improved than the binary Zn-Al alloy. Due to the possession of a property like high wear resistance, these alloys are also increasingly used to replace traditional alloys such as aluminum, bronze, brass and cast iron in many industries for bearing applications and many structural materials. They can also be considered as competing materials for cast iron and even

for steels when being applied for operation under conditions of high mechanical loads and moderate operating temperatures. Interest for extending the application for these alloys is grounded by tribological, economic and ecological reasons. These alloys are relatively cheap and can be processed efficiently with low energy consumption, without causing damage to the environment. Zinc-aluminium cast alloys by virtue of their excellent castability, strength, stiffness and good mechanical properties such as ultimate tensile strength, hardness coupled with ductility and impact resistance, have found significant industrial usage during the past few years.

Addition of iron, copper, silicon have been highly interesting for engineering because addition of these alloying elements enhances the wear resistance, elastic modulus, yield strength and corrosion resistance under the service conditions of stress and temperature without having much detrimental effect on the superplastic behavior during production of components (Villegas et al. 2014).

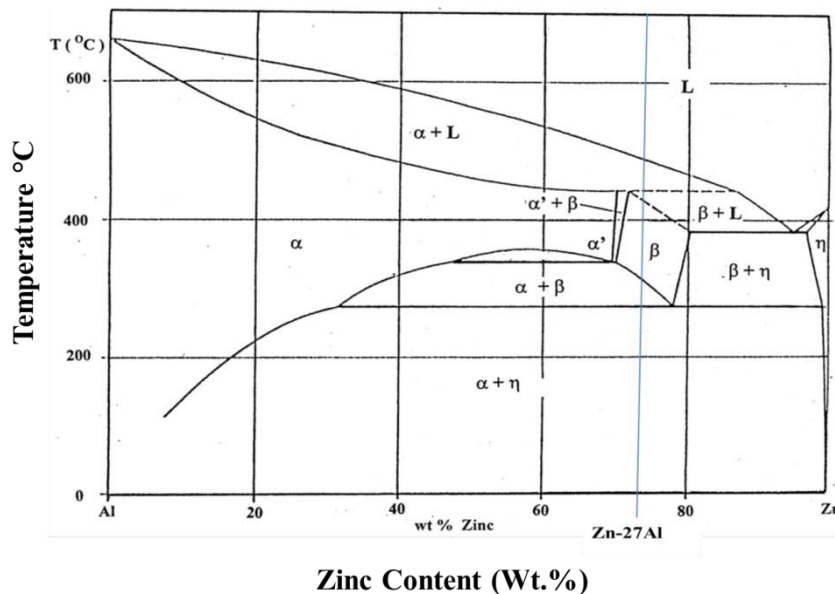


Figure 2.2: Phase diagram of Zn-Al binary alloy system (Zhu 2004).

Figure 2.2 shows the binary phase diagram of Zn-Al alloy by Presnyakov et al. which is modified by Goldal and Parr where α is Al-rich fcc phase, β is Zn rich fcc phase, η is Zn rich hcp phase, α' is supersaturated Al-rich fcc-phase (Y Hua Zhu 2004).

Microstructure of binary Zn-15Al alloy showed the pro-eutectic β dendrites and a mixture of α and η phases. By eutectoid reaction on cooling after solidification the formation of lamellar structure was seen this is due to the transformation of β phase in to α and η phases. Incorporation of Cu content above 2 % leads to the formation of ϵ phase in the inter dendritic region. By the addition of Cu and Si contents the increase in hardness value were also observed (Temel et al. 2014). Ductility of the ZA-15Al-3 Cu and Zn-15Al-3Cu-1Si alloy was not affected by the heat treatment but improvement was observed in hardness and tensile strength of the alloy. Shuqing et al. (2010) investigated the influence of different Al contents on microstructure, mechanical and wear properties of zinc based alloy. Results showed that hardness of alloy increased with increase in Al content. Highest ultimate tensile strength and elongation percent at room and elevated temperature was achieved for alloy with 27 % of Al content. Chen et al. (2002) studied the microstructural evolution and phase transformation of mechanically stirred non dendritic ZA27 alloy during partial re-melting. In his studies partial re-melting temperature was 460 °C and which is lower than the stirring temperature of 465 °C, so microstructure with globular grains needed for semi solid forming cannot be obtained. Starting primary non dendritic grains change in turn to connect non dendritic grains, long chain like structures and finally to coarsen connect grains. However the small near equiaxed grains between the primary non dendritic grains are evolved into small globular grains gradually some of which are also attached to the primary non dendritic grains during the subsequent heating process. Extruded zinc aluminum based alloys could take the material to potential applications for instead of brass and cast iron, due to their favourable characteristics (Torres et al. 1998). To obtain anneal hardening phenomenon in extruded Zn-Al alloy, the Al content should be in the range of 5-25 wt% and heating temperature should be above 280 °C. This can also enhance the electrical conductivity after annealing process (Yang ming et al. 2013).

Hector et al. (2005) studied the coarsening process of τ' precipitates during the isothermal aging of the zinc-22wt% aluminum-2 wt% Copper. In this study the initial microstructure consisted of a lamellar constituent of the α and η phases and isolated regions of the ϵ phase, after solution treatment at 350 °C for 5 days and then furnace

cooled annealing. τ' phase was formed by four phase reaction and the fast coarsening rate promoted a high decrease in hardness. External stresses accelerate the decomposition of metastable phases in Zn-Al based alloys was investigated by Zhu et al. 2004. The phases transformation and microstructure revealed the facts, a) decomposition of the supersaturated β_p Phase : $\beta_s' - \alpha' + \varepsilon + \eta$ b) decomposition of the metastable $\eta' \tau$ phase: $\eta' \tau - \eta + \alpha + \tau'$ c) Decomposition of the metastable ε phase: $\alpha + \varepsilon - \tau' + \eta$ d) precipitation of η phase in α phase: The high density of defects like dislocation and vacancies are introduced when the sample were deformed, which enhance the diffusion and accelerate the decomposition. Yang et al. (2012) worked on the heat treatment to know the effect of heat treatment on microstructure and mechanical properties of ZA27 alloy. Due to heat treatment process α and η phase dissolved, and the microstructure is mainly composed of supersaturated β phases. In the initial stage of aging the supersaturated β phase decomposed into irregularly cellular structure, which was developed along grain boundaries. In addition to that the supersaturated β phase transformed into the lamellar structure, which was developed within the grain. Mechanical properties like hardness and tensile strength both decreased with increase in aging time. Aashuri et al. (2004) investigated to obtain globular structure of ZA27 alloy by thermo-mechanical and semi-solid treatment. They observed that the dendritic structure of the cast ZA27 alloy can be transformed into a globular structure by holding the alloy at the temperature below and above the peritectic reaction. Cold working and recrystallization are required prior to semisolid holding. Semi solid processing such as isothermal holding and thixo-forming of the ZA27 alloy for a long period of time must be performed at above the peritectic temperature, as below the peritectic temperature the liquid is diffused into the solid particles in a short period of time and poor rheological behavior is achieved.

Chih et al. (2009) experimented on two alloy (Zn-22Al and Zn-22 Al-0.3 Cu) and studied work softening and anneal hardening behaviour were explored and compared in fine grained materials. Results showed that work softening behaviour is improved by a decrease in grain size and an increase in the relative amount of high angle boundaries. Prasad et al. (1998) investigated the tensile properties of some zinc based

alloys comprising 27.5% Al by varying material composition where copper was replaced by nickel, silicon and nickel + silicon materials. Tensile strength of the alloy increased with strain rate while test temperature produced a reverse effect and elongation of the specimen were improved as the strain rate/ test temperatures became higher. Due to the presence of thermally stable phases the modified alloys could become less temperature sensitive material. Mykura et al. (2002) studied the solid state reaction in Zn-Al based alloys. From their results it is observed that the transformation of metastable phases in ascast and heat treated alloy gives raise to irreversible dimensional changes on ageing. Amount of copper addition significantly affects the dimensional stability of Zn-Al alloys after casting but Zn-Al alloy where copper is replaced by silicon may form the basis for a family of dimensionally stable alloy system. They concluded that in sand and permanent moulded casting the volume changes may be reduced by a long term stabilising heat treatment before machining it to final product. Sixteen different types of zinc aluminum copper alloy were investigated to know the effect of phase transformations on mechanical properties by melting pure Zn-Al-Cu elements. The homogenization treatment was done on the ascast material at 350 °C for 180 hours. Results showed that the hardness value of homogenized alloys was low when compared with ascast alloys due to elimination of the dendritic structure and homogenization treatment caused the formation of most of the equilibrium phases. By the increase in Cu and Al volume fraction in the alloy increase the hardness value for both ascast and homogenized alloys, this is due to increase in volume fraction of the Cu containing θ and τ' phases (Jose et al. 2014).

2.5 Casting Technique

In general stir casting of MMC involves producing a melt of selected matrix material followed by the introduction of reinforcement material into the melt and the dispersion of the reinforcing material through stirring. Stirring is carried out vigorously to form a vortex, where the reinforcing particles are introduced through the side of the vortex. The formation of the vortex will drag not only the reinforcement particles into the melt but also all impurities which are formed on the surface of the melt. There are many factors which directly affect the properties of stir cast composite. Factors such as stirrer geometry including blade angle, stirring time,

stirring speed, pouring rate, the temperature of the melt, etc., must be optimized to achieve a better bunch of properties in the composite.

Achieving a homogeneous dispersion of reinforcement within the matrix is one such challenge which effects straight on the properties of composites. Hashim et al. (2002) part I- in MMCs the distribution of the reinforcement in the matrix alloy is influenced by numerous factors during casting process. Which contains rheological behaviour of the melt, the reinforcement addition method, interactions of the reinforcement and the matrix before, during and after mixing, and the changing particle distribution during solidification. The large differences in bulk properties between particles and matrix materials play a significant role, as do the surface properties of the reinforcement powders were discussed. Outcome of his review was particle density, size and volume fraction will affect the reinforcement settling rate. The surface properties of reinforcement will affect the wetting process. Various gases entrapment during particle addition will lead to poor dispersion of reinforcement with this porosity level will also increase. Usually reinforcement particles will occupy inter dendritic or between the secondary dendrite arm spacing; therefore the finer the spacing or the finer the matrix grain size, the better the particle distribution. Hashmi et al. (2002) Part II – in this he has explained the stirring parameters such as stirring speed, and impeller position in the crucible have a significant effect on the flow behaviour of the fluid. These parameters interact, with various combinations generating suitable conditions for composite mixing. The model was applied to the case of the more viscous glycerol fluid, and the results from this were compared with experimental results. The model was validated using a visualisation experiment which indicates that, despite some limitations arising from the simplification of the physical situation, the model is a useful tool in specifying process parameter in the production of MMCs. Satish et al. (2015) discussed the importance of different casting routes on microstructure and mechanical properties of metal matrix composites. In his review of available literature shows that processing techniques can be classified as stir casting, squeeze casting, compo-casting, solid state processing (powder metallurgy) and semi-solid processing (spray deposition). Stir casting process is widely used because of its simplicity, flexibility and low cost for the fabrication of large size components but at the cost of porosity formed. However, composites produced by squeeze casting,

compo-casting and powder metallurgy exhibit lower porosity. Spray forming technique, though advantageous in producing an exact shape product, but limited to small sized components. Microstructural evaluation showed the fair dispersion of zircon particles in the matrix, sound bonding between the particle and matrix at the interface. Hardness, abrasive wear resistance, elastic modulus and tensile strength were enhanced with the dispersions of zircon particles. Li Run et al. (2010) explained the effect of specific pressure applied during squeeze casting process on microstructure and mechanical properties of ZA27 alloy. Due to squeeze process the improvement in mechanical properties were observed. This improvement is attributed to elimination of micro pores in the alloy, microstructure refining as the applied pressure is increased and also it enhances the solubility of solute atom such as Mg, Cu and Al. Finally homogeneous mixture of Al and Cu in ZA27 alloy was achieved. Plasticity and strength of ZA27 alloy was increased by ϵ phase which is homogeneously distributed and the same can effectively block the movement of dislocation. Influence of stirring speed and stirring time on distribution of particles in cast MMC were investigated by Balasivanandha et al. (2006). Results revealed that during lower speed and lower stirring time reinforcement clustering occurred in few regions and in some regions recognized without SiC inclusion in aluminum matrix but after increasing the stirring speed and time of stirring better homogeneous distribution was achieved. Different casting parameters such as stirring speed, holding temperature and position of the stirrer in the molten melt are the deciding factors which influence the mechanical properties of cast metal matrix composite materials. In addition to that there are some other factor also, like reinforcement material, size and shape of reinforcement, percentage of reinforcement that can be incorporated in matrix which effect the various properties of the composites directly or indirectly. Altinkok et al. (2013) investigated on dry sliding wear behaviour of alumina/silicon carbide particles added to Al based metal matrix composite fabricated by stir casting technique. His investigation showed that wear result of alumina reinforced material differed from that of SiC reinforced material. By the increase in particle size the hardness value decreased but weight loss in wear and coefficient of friction showed better results with increase in particle size. This is due to, fine particle size MMCs were particles easily pulled out whole from the matrix during the test

when compared with coarse particle size MMCs. Jyothi et al. (2015) carried out a centrifugal casting on ZA27/Al₂O₃ Composites to know the wear characteristics. In this investigation the authors have considered different parameter such as particle size, location, melting temperature, sliding speed and normal load on wear characteristics of the composite material. Results revealed that for minimum wear rate one should optimise the centrifugal casting parameter and wear parameters i.e., considering the results of wear test – particle size of 40 µm, location of 30mm from centre, temperature of 600 °C, with a wt% of 20 and at sliding speed, normal load (100 rpm, 10N) gives best results. Fatih et al. (2005) have discussed the tensile and fatigue behaviour of ZA27 alloy fabricated by gravity casting and squeeze casting process. This work revealed that material produced by gravity and squeeze casting of ZA-8 alloy shows two distinct morphologies by β particles decomposition (fine lamellar and fine granular mixture). Small and very tight morphology can be achieved by squeeze casting with respect to gravity casting technique. Squeeze casted material performed better when compared with gravity cast materials. Importance of temperature on mechanical properties showed the decrease in strength by increasing the temperature value. ZA27 alloy is of specific interest due to its higher values of tensile strength of about 450 MPa at room temperature when fabricated in pressure die-cast root (Murphy et al. 1987). But the material limits its application below 100 °C because of its low creep strength (Durman et al. 1991), regrettably it suffers a sharp drop in strength with increased temperature. Even though ZA27 is thermodynamically unstable at ambient temperature, the existence of fine dispersion of metastable ε particles in the η matrix was observed even after 5 years of ageing, and the same is responsible for most of the improvement in mechanical properties by incorporation of Cu to Zn-Al based alloys (Durman et al. 1997).

Uniform distribution of particles was observed in microstructures of composites reinforced with SiC, ZrO₂ and C in ZA27 matrix. Homogeneous distribution of particulate reinforcement was achieved by stir casting technique followed by squeezing process. Accelerated response was seen in age hardening process because of presence of SiC, ZrO₂ and C particle in squeezed ZA27 composite but UTS and ductility were remarkably low, this is due to cracks initiated at particle matrix interface, propagate through the matrix and link up with other cracks which leads to

failure (Abou et al. 2011). Microstructure and mechanical properties of zinc aluminum based composites reinforced with rice husk ash, SiC and Graphite particles has been investigated by Kenneth Kanayo Alaneme et al. (2015). Microstructure results shows that the distributions of various particles were uniform and this is achieved by following unique step during stir cast technique. Mechanical properties like fracture toughness was improved by the addition of mixture of rice husk ash, SiC and Graphite particles. Chen et al. (2014) investigated the effect of casting parameters on microstructure and dendrite morphology of ZA27 zinc based alloy. Feathery grains can be achieved from normal equiaxed dendrites by changing the primary phase of ZA27 alloy. This type of observation can be seen during rising pouring temperature, solidifying in the mould with large chilling ability.

2.6 Microstructure, Mechanical properties and Wear behavior of Zinc-Aluminum based composites reinforced with SiC, Al₂O₃ and other different types of Particles.

Some of the research works and recent reports published in literature related to Zinc-aluminum alloy and its composite studies are discussed below.

Zhong liang et al. (1997) investigated the structure control of in-situ silicon particle reinforced in ZA27 composite materials. He observed that the morphology of silicon phases having a direct effect on various properties. Silicon and ZA27 alloy form an interface product which is in two different types, one is seen to be lamellar from eutectoid reaction and whilst the other is a precipitated divorce eutectic product at last solidification. Well distributed silicon with a size of 10~15 μm were observed in ZA27 alloy which in turn improved the wear resistance of the material. Appearance of Si precipitates in plate like shape in the dendrites or grain was observed in Auras and Schvezov (2002) research. The concentrations of these precipitates were high in interdendritic region. Here addition of SiC particle improved the wear resistance of the material and presence of SiC particle reduced the grain size in microstructure as the volume fraction of particle content increases. Mitrovic et al. (2012) investigated the wear behaviour of hybrid of ZA27/SiC/Graphite composites under dry sliding conditions. The results showed that, the addition of particle had improved the wear resistance of the material when compared with base ZA27 alloy. Further upon

increasing the normal load and sliding speed the wear scar width also increased. Enhanced wear properties of the material led to propose the materials application related to tribo technical system. Pruthviraj et al. (2011) worked on synthesis and testing of zinc aluminium based metal matrix composites reinforced with SiC particles cast in sand moulds containing metallic copper, steel and cast iron chills respectively. They observed that bonding between matrix and dispersoid was good with no agglomeration. It was also found that these properties increase with an increase with an increase in the dispersoid content up to 9 wt%. Copper end chill was found to be more effective when compared to the other type of chill blocks. Wear resistance of the metal matrix composite developed improved as the dispersoid content increases and copper chill was found to have a major effect on wear because of its high volumetric heat capacity. Bearing in machinery serve a vital role as load carrying element and it is subject to intense tribological environment, where any damage results in loss of productivity and financial aspects. To enhance the tribological properties of ZA27 alloy for bearing application, Amar Patnaik et al. (2015) investigates friction and wears behaviour of CaO particulate reinforced ZA27 alloy composites. The results of TGA plot shows diminishing order of thermal stability from 10 % to 0 %. Damping capacity shows improvement in comparisons with neat alloy except for 2.5 wt % filler content. Steady state specific wear rate of the composite shows increasing trend with sliding velocity and normal load irrespective of filler content. Damping behaviour of aluminate particulate reinforced ZA27 alloy metal matrix composites at varying temperature was investigated by Shanta sastry et al. (2001). The results revealed that damping capacity of the materials was increase with increase in temperature whereas the dynamic modulus was found to decrease with the increase in temperature. Low temperature damping capacity was attributed to coefficient of thermal expansion mismatch induced dislocations and intrinsic damping of the matrix. High temperature damping capacity was due to matrix reinforcement interface and thermo elastic damping. Khan Hasib Kaisa et al. (2011) have evaluated the characterization of SiC_p reinforced zinc aluminum metal matrix composites for bearing materials. Results indicate that the SiC reinforced composite exhibit better wear resistance with increase in SiC content. Hardness value of composite improved with increased SiC particle content at the cost of compressive

yield strength. Srimant et al. (2014) investigated the erosion wear behavior, processing and characterization of SiC particle reinforced ZA27 MMCs. It was found that mechanical properties like tensile strength, microhardness and impact strength were improved by addition of reinforcement but at the cost of flexural strength and composites possess very low amount of porosity. During erosion test impact velocity and filler content are found to be most significant factors among all other factors. Mainly with an increase in impact velocity, deeper wear grooves, micro cracks and fragmented dispersed phase were observed in SEM micrographs of eroded surfaces. Babic et al. (2007) investigated the tribological properties of composites with substrate made of ZA27 alloy reinforced by the graphite particles of size 20, 35, 100 microns in different quantities. From the results it was reported that composites showed highest wear resistance when compared with base substrate. Composite material with 100 micros size of graphite particles reinforced in the amount of 3 mass % exhibits lower wear rate under lubrication condition and wear scar width was decreased upto 60 % with respect to base material. Jelena et al. (2016) studied the influence of corrosion on surface appearance and microstructure of compo cast ZA27/Silicon carbide composites in NaCl solution. Microstructure observation showed that micro cracks was noticed close to the SiC particles in the composites, the process of corrosion occurred preferentially in the η phase and in the region of the $\alpha + \eta$ phase mixture. Regions rich in zinc are susceptible to the corrosion attack, while the aluminum rich areas are much more resistant. Finally in sodium chloride solution, zinc aluminum based silicon carbide reinforced composite with a higher content of SiC particles showed lower corrosion resistance compared with the composites with a minor content of particulate reinforcement.

Alicia E. Ares and Carlos E. Schvezov (2013) focused on the study of the directional heat extraction on the SiC distribution in ZA metal matrix composites. Here in his study the influence of solidification on microstructure of MMC were also analysed with the help of cooling rate, temperature gradients and interphase velocities measurements. It was observed from the microstructure that addition of particles produces a finer structure than in the columnar zone and the equiaxed grain size is never larger than the columnar width and results revealed that increase in cooling

velocity in the liquid was found to increase the columnar zone length. Presence of ceramic particles in ZA27 alloys affects the thermodynamic local condition and the kinetics of nucleation, producing a finer microstructure. Biljana et al. (2009) have evaluated the microstructure and mechanical properties of Zn25Al3Cu based composites with large Al₂O₃ particles at room and elevated temperatures. Compo casting technique was used to fabricate the composite by the incorporation of 3, 8, 16 wt % of Al₂O₃ particles in semisolid metal matrix. Results indicate that the composites exhibit high hardness with increase in Al₂O₃ content. At room temperature the composites shows highest compressive strength when compared with base material. In the temperature range from 70 to 170 °C compressive yield strength of all materials decreases, but the rate of decrease is different for the matrix alloy and composites. Due to thermal stress present in the material leads to cracks in large Al₂O₃ particles as there is a large mismatch between thermal co-efficient during cooling. Particles which have low thermal expansion coefficient will sustain a tensile stress and may crack during cooling. Yasin et al. (2009) have studied the microstructure, mechanical and tribological properties of a binary zinc aluminum alloy and five ternary zinc aluminum alloys with different Cu content in as-cast state and results were compared with those of SAE65 bearing bronze. Hardness of the ternary alloys increased with increasing Cu content, but their UTS decreased above 3% copper. Friction coefficient and temperature of the material and bronze increased in the early period of run and reached nearly constant levels after a sliding distance of roughly 400 km. The wear rate of ternary alloys was found to be much lower than that of SAE65 bronze. Adhesion was found to be the most effective wear mechanism for the Al-40Zn-Cu alloys, but both abrasion and adhesion operated considerably to cause the wear of the SAE65 bronze.

Kiran et al. (2013) investigated the mechanical properties of as cast ZA27/Gr/SiC hybrid composite for the application of journal bearing. It was found that uniform distribution of fine particles with α dendrites surrounded by $\alpha+\eta$ eutectoid, residual η phase and metastable ϵ phase in interdendritic regions were observed. By the addition of SiC particles the mechanical properties like ultimate tensile strength and hardness was improved but at the cost of ductility. Prasad et al. (2001) studied the abrasive

wear characteristics of a Zn based alloy and Zn /SiC composites. The influence of various processing parameters on the abrasive wear response was examined. It was noticed that at low applied load the composites attained superior wear resistance when compared with matrix material and at higher load the trend seen to be reversed. Micro cracks and ploughing was also observed as an wear mechanisms and the abrasive medium grieved from capping, clogging attrition and shelling while the SiC particles experienced fracturing in due course of abrasion. Mehmet et al. (2007) have investigated the effect of Mn as an alloying element on the microstructure and mechanical properties of cast zinc aluminum alloy. Results showed that the hardness and creep resistance of the material increased continuously with increasing manganese content and yield strength, UTS as no effect on addition of Mn. Additionally, the impact strength of the material improved with increasing initially and then decreased gradually. Incorporation of Mn resulted in microstructural changes of the alloy having the development of complex intermetallic compound (MnAl₆). Increase in creep resistance and decrease in tensile and impact strength were thought to have been caused by the changing morphology and amount of intermetallic. Optimum mechanical properties were achieved by addition of 0.045 wt. % to 0.063 wt. % Mn. Mitrovic et al (2010) have evaluated the influence of heat treatment on the sliding wear behavior of a ZA-27 alloy. Dry and lubricated sliding wear tests were conducted on as-cast and heat-treated ZA-27 samples over a wide range of applied loads and sliding speed. The tribological results were related to the microstructure and mechanical properties. Reduction in the hardness and tensile strength was observed due to heat treatment, but increase in elongation was also seen in the same samples. The heat-treated samples as well as the reinforced samples attained significantly improved tribological behavior over the as-cast ones, both from the aspects of friction and wear. The worn surfaces of the samples were examined by scanning electron microscope in order to determine the wear mechanisms. Dominant wear mechanisms for tested alloys were abrasion and adhesion. However, under conditions of higher applied load delamination has considerable role in wear process of as-cast alloy. Due to that, difference in wear behavior of heat-treated vs. as-cast alloy is amplified in the area of higher loads. Martinez et al. (2003) have investigated the structure and properties of Zinc aluminum copper alloy reinforced with Al₂O₃

particles by the means of powder metallurgy technique. It was observed that decrease of 30% in density is achieved from the 27 vol % alumina composite compared with the base matrix material. Composites with 7 vol% alumina un-sintered also showed changes in its mechanical deformation as a function of strain rate, at low strain rate it behaves in a ductile manner, and for values of strain rate higher than 10^{-3} s^{-1} behaves as a brittle material. Prasad et al. (1995) have investigated the abrasive wear characteristics of Zn-37.2Al-3.5Cu-0.2Mg alloy dispersed with SiC particles. The wear response of the samples was discussed in terms of specific features of their micro constituents like silicon carbide and the predominant material removal mechanism in a given set of experimental conditions. The observation showed that the composites performs lower wear rates than that of matrix alloy when abrade with fine abrasive particles while a reverse trend was observed in the case of the coarser abrasive and increased brittleness of the composite led to fine debris formation and reduced thickness of the deformed subsurface layers and lesser entrapment of the debris in between the abrasive particles in this case as compared to those of the matrix alloy. Modi et al. (2006) has made an attempt to assess the contribution of various parameters on the dry sliding abrasive wear response on ZA alloy under the conditions of varying applied loads and sliding distances. The factors whose contribution has been examined include dispersion of alumina particle, cracking tendency, role played by the alumina particles, lubricating, load bearing, deformability characteristics and thermal stability of the various micro constituents. The study suggests that the mentioned factors contribute to a varying degree towards controlling the abrasive wear behaviour of the specimens. The microstructural observation showed that fairly uniform distribution of the dispersoid alumina particles with reasonably sound dispersoid/matrix interfacial bonding is achieved. Addition of alumina particles in the matrix alloy significantly increased the hardness while density and tensile properties are in reverse condition. Wear rate got increased with applied pressures and sliding velocity. Predominating effect of micro cracking tendency was observed which was caused by alumina reinforcing particles. Adhesion was the main wear mechanism at low speed and micro cracking and abrasion also contributed to material loss in the other cases. Shivakumar et al. (2017) have reported a study on mechanical properties and dry sliding wear behaviour of molybdenum disulphide

reinforced zinc aluminium alloy. From the results it is observed that the mechanical properties like hardness, ultimate tensile strength and yield strength increased with 0.5 wt% MoS₂ reinforcement in ZA27 matrix and further decreased with increase in filler content. Percentage elongation of the composite decreased with increase in the MoS₂ reinforcement content. Applied load played a major role as influencing parameter wear rate followed by filler content, sliding distance and sliding velocity. Li Zi quan et al. (2006) have investigated the aging microstructural characteristics of zinc aluminum alloy and zinc aluminum/SiC composites. Continuous changes were observed in structure, morphology and size of sub grain in primary dendrite during aging process. The lamella decomposition of β phase beside SiC is evidently more rapid than that of the alloy. SiC particles strongly accelerate neighbouring β phase decomposition in aging process. SiC presence in the ZA27 matrix facilitates Zn and Cu diffusion and makes SiC neighbored matrix transformation easier, either eutectic or peritectic β phase transformed into lamellar of α and η phases in style of cellular decomposition. Aggregated Zn and Cu as well as oxides in the composites result in less amount of β phase and form spherical precipitates of CuZn. Bobic et al. (2011) have investigated the microstructure and mechanical properties of ZA27-Al₂O₃ composites obtained by powder metallurgy process. Atomization process was used to achieve homogeneous structure with dendrite morphology. The yield strength and elastic of the ZA27- Al₂O₃ composite decreases with an increasing temperature, but not as strong as in the ZA27 alloy. Seah et al. (2003) have described the mechanical properties and fracture mechanism of ZA27/TiO₂ particulate metal matrix composites with a primary objective of understanding the influence of the particulate reinforcement on various properties. The results revealed improvements in young's modulus, UTS compressive strength yield strength and hardness of the composites as the titanium dioxide content was increased, but at the expense of ductility and impact strength. The fracture behaviour of the composites was also significantly influenced by the addition of TiO₂ particles. Segregation of reinforcing particles and cracking of individual particles present in the microstructure are responsible for the initiation of fracture in the composites. Incidence of the particle cracking increases with the reinforcement

content in the matrix. Final fracture of the composites is due to the propagation of cracks through the matrix as well as through the particles. Sandhyarani biswas et al. (2012) studied the erosion wear analysis of Al_2O_3 particles reinforced ZA27 alloy metal matrix composite using ANN method. Here in her studies the predominately influential parameters affecting the wear rate are identified. A prediction model based on artificial neural network is used to predetermine the erosion rate at different training and testing of large number of independent variables. The results showed that erosion wear resistance of the material improved with the reinforcement of Al_2O_3 particles and this improvement is proportional to the Al_2O_3 content in the composites. Impact velocity is the most significant factor followed by the filler content while others have comparatively less significance on the erosion wear rate of the material.

2.7 Wear

Wear is characterized as a procedure of losing material from surfaces that have been rubbed against one another. Relative movement between machine surfaces practically prompts an adjustment in these surfaces and it leads to some type of mass loss from the surface. Wear resistance is an important property for UFG materials in order to evaluate their potential for use as structural wear components. The wear of sliding surfaces can occur by one or more wear mechanisms, including adhesion, abrasion, fatigue wear, corrosion wear and fretting. In addition, the wear properties of engineering materials have significant effect on the serviceability and durability of components. Hence, the wear properties must be taken into account in the design of engineering parts and this becomes especially important for the practical use of UFG materials. Wear relies on material properties like hardness, quality, pliability, work solidifying and so forth. Wear can be classified as:

- a) Adhesion
- b) Abrasive
- c) Erosion
- d) Fatigue
- e) Chemical Wear

Sliding wear results from the adhesive contact between two surfaces. There are basically two types of sliding wear Scoring and galling. Scoring occurs when there is a lubricated contact between surfaces while Galling occurs with dry friction of low sliding speed. The main theory for sliding wear of metals is based on the assumption

that contact between two surfaces occurs where asperities contact and the local deformation is plastic. Sliding wear occurs due to two or three different mechanisms. In first the oxide control of the sliding wear along with low wear rates are experienced at high temperatures because oxide growth takes place at high temperatures. Sometimes oxide debris leads to abrasive wear of the surface along with sliding wear which leads to new types of wear known as Fretting wear. The second mechanism occurs due to high contact stresses which breaks the oxide films and there is actual metal to metal contact which leads to cold welding and when there is relative movement between surfaces which results in fracture of small pieces from the surface. Wear caused by this mechanism leads to galling. The third mechanism occurs due to cyclic stresses generated by the pressing of one surface on the other surface.

The enormous number of research has been done on wear behavior of different zinc aluminum based materials with respect to tribological application and some of their results are stated below.

Temel savaskan et al. (2015) explained the tribological properties of Zn-25Al-3Cu-1Si alloy using block on disc type of wear test machine and the obtained results were also compared with SAE660 bearing bronze. Wear resistance, hardness, tensile and compressive strength was increased by T6 heat treatment process. Frictional coefficient of the material decreased by increasing the pressure, in addition to this it also increased the working temperature and wear volume. Effect of pressure on the wear volume of the alloys varies according to their hardness and strength. As the hardness and strength of the alloys increase they become less sensitive to pressure as far as their wear volume is concerned. Sharma et al. (1998) have evaluated the bearing characteristics of cast ZA-27/Graphite composite under lubricated, semidry and dry conditions. The bearing tests were conducted using a computer interfaced bearing test rig. It was found that in the tests conducted, the bearing fabricated from the composite revealed lower friction in comparison with the unreinforced ZA-27 alloy. Comparison in terms of friction and performance was also made between graphite reinforced and unreinforced bearing for semidry and dry condition. Girish et al. (1999) reported a study on un-lubricated sliding wear behaviour of zircon particles reinforced ZA27 alloy composite materials. The results indicated that wear rate of the composites were

lesser than that of the ZA27 alloy. The increase in applied load increased the wear severity by changing the wear mechanism from abrasion to particle creaking induced delamination wear. Temel et al. (2004) has made an investigation on effect of copper content on the mechanical and sliding wear properties of monotectoid based zinc aluminium copper alloys. It was observed that the hardness of the alloy increased gradually with increasing copper content upto 5 percent. The Wear rate, tensile strength and microhardness increased initially upto 2 % addition of copper but on further addition it leads to decrease in tensile strength. The friction co-efficient and temperature due to frictional heating were generally less for the copper containing alloys than the one without the element. Smearing and scratches were observed on the worn surface of the monotectoid based zinc aluminum copper alloy. Mario et al. (2010) have aimed their study to improve the wear resistance of ZA alloys. In his studies majorly three region were observed: columnar, equiaxed and columnar to equiaxed grain transition. For the obtained results one can understand that for the same wear conditions the equiaxed structure has a wear rate lower than the columnar and transition structure. By increasing the aluminum concentration the wear rate decreased with equiaxed structure but in columnar structure it is independent of aluminum content. For transition zone has an intermediate resistance between the columnar and the equiaxed structure for similar grain size. Savaskan et al. (2002) have studied the lubricated sliding wear behaviour of cast zinc based alloy bearing under static and dynamic loading condition. The results showed that among the Zn-Al alloys the wear resistance of the monotectoid based alloys was superior to those based on near eutectoid composition. Under dynamic loading condition, it increased with increasing copper content upto 2%, but declined thereafter. It also showed that loading condition have a strong influence on the wear rate. The wear resistance strongly correlates with the tensile strength. Under static loading conditions, as cast Zn-Al alloys showed higher wear resistance than the equivalent heat treated alloys, but this behaviour was reversed for dynamic loading. Adhesion and smearing is the main mechanism for wear in zinc based alloys, while abrasive wear dominates for the commercial SAE 660 bronze. Jeong-Lian et al. (2009) optimized the die casting condition for wear properties of alloy ZA91D components using the taguchi method and design of experiments analysis. This hybrid approach tries to strike the balance

amongst low costs, high efficiencies and good accuracy, the validation process via experimental data further ensures the quality of work. The results of optimal parameter combination for the die casting process was 21 MPa fusion slurry pressure, 47 m/s fusion slurry velocity and at the mould temperature of 234 °C. The regression model for wear losses yields reasonable results with less than 3 % errors between predicted and experimental data. Miroslav et al. (2010) have investigated the influence of solutionizing heat treatment for a period of 3 to 5 hour followed by quenching in water, on the sliding wear behaviour of a ZA27 alloys. Dendritic structure broken during the heat treatment more over uniformity of distribution of various micro constituents as well as their fineness increased with the duration of the solutionizing treatment. The solutionizing duration contributes to the tensile strength decrease and the elongation increase. The improved wear behavior of the heat treated alloys in spite of reduced hardness could be attributed to finer and more uniform distributed micro constituents and reduced cracking tendency. Both abrasion and adhesion wear mechanism were dominant. Alev et al. (2003) has investigated the effect of silicon content on the mechanical and tribological properties of montectoid based zinc aluminium silicon alloys. In his work he has fabricated eight ternary zinc aluminum silicon alloys and one binary Zn-Al based alloy by permanent mould casting. Microstructural observation revealed that the size and distribution of silicon particles were found to be dependent on the silicon content of the alloy, dendritic structure was removed by solution heat treatment process resulting fine grain structure, but had no significant effect on silicon particles. Mechanical properties like hardness and tensile strength increase with increasing silicon content upto 2 %, further decreased as the silicon content increased. The quench ageing treatment improved the mechanical properties but reduced their wear resistance. Adhesion, smearing and scratching were found to be the main characteristics of the wear surfaces of alloy. As the silicon content increased the scratches and pits/craters become deeper and larger on the wear surfaces. Zhu, Lee et al. (2003) have carried out the microstructure and ageing characteristics of a ZnAl₇Cu₃ alloy were studied using X-Ray diffraction, electron scanning microscopy and back-scattered diffraction techniques. Two stages of phase transformation were detected during ageing. Electron back-scattered diffraction technique was applied in distinguishing both zinc rich η and ϵ phases. Wear

behaviour, microstructure and dimensional stability of as cast zinc aluminum/ SiC metal matrix composites was investigated by R. Auras and C. Schvezov. Hardness, dimensional stability and wear tests were performed on five different alloy samples. Final effect of adding particles on the microstructure was to reduce the grain size as the volume fraction of the particle content increases. Dimensional stability tests showed that all the samples were stable during 1000 hour test, with changes in the dimension of less than 0.25 %. After the 1000 hour test, no change in the dimension was observed. The wear results indicated that the wear rate of Za alloy is strongly dependent on applied load in a non-linear manner and that the addition of SiC particles improves the wear properties of the matrix alloys. Zulkuf Balalan and Mehmet Kaplan (2007) have evaluated the microstructural and tribological properties of zinc aluminum cast alloys. Microstructure of the alloy shows that the incorporation of copper and Silicon led to the development of CuZn5 phase and Si+Zn phases in main matrix. The results revealed that the incorporation of copper and silicon caused increase in the tensile strength and hardness. This is due to the presence of aluminium higher wear resistance was obtained from the alloys containing higher percentage of aluminium and silicon. Deep pits/craters and continuous scratches were detected on the wear surfaces of samples. Ahmet Turk et al. (2006) have aimed their study to compare the wear properties of modified zinc aluminum alloy and conventional bearing bronze at the sliding speeds of 0.5 m/s, 1 m/s, 1.3 m/s, 1.7 m/s and 2m/s using two different applied load. The standard ZA-8 alloy was modified with 1% Pb, 1% Sn and 1% Cd alloys. The results have shown that the ZA-8 alloy and modified with Pb, Sn and Cd alloys revealed higher wear resistance when compared with bearing bronze. Degenerated microstructure were observed with decreased volume fraction of eutectic matrix and EDX analysis showed that each element was in the form of pure state after addition of Pb, Sn and Cd elements. The addition of Pb and Cd increased wear resistance of the alloy for all of the sliding speeds. But Sn alloying element caused worse wear resistance. Up to 1.7 m/s sliding speed the wear resistance of ZA alloy increased but it decreased with further increasing the sliding speed. The friction coefficients of ZA alloys are higher than that of the bronze bearing. G.

Ranganath et al. (2001) have investigated the dry sliding wear behavior of zinc aluminium-27 composites reinforced with garnet particles. Liquid metallurgy technique was used to fabricate the composites. Results showed that the garnet reinforced composites reveal lower wear rates when compared with matrix alloy. Further addition of garnet content decreased the properties of the composites. Increase in the applied load increased the wear severity by changing the wear mechanism from abrasion to particle cracking induced delamination wear. The composites exhibited abrasion wear at low loads while at high loads delamination wear was dominant. Worn surfaces and subsurface of the composites have been analysed using scanning electron microscope. On the basis of the above experimental observation, the sequence of micro-mechanical events, which lead to the generation of wear debris, has been summarized. Jovanovic et al. (2007) have investigated the effect of heat treatment on microstructure and sliding wear behaviour of ZA-27 during lubricated and dry sliding conditions. Annealing and subsequent heat treatment through the effect of cooling rate from the β phase region significantly change the previous as cast cored dendrite structure. Heat treatment markedly improved the elongation, while the strength was maintained high. Fracture surface of quenched sample consists of dimples indicating a ductile fractures. Slow cooling creates a mixed mode of fracture consisting of transgranular and intergranular fractures. The wear rate increases with load, and under dry sliding conditions the wear rate is approximately two times higher than under lubricated conditions. Adhesive wear was the major mechanism during both dry and lubricated condition. Modi et al. (2004) have evaluated the high-stress abrasive wear behaviour of zinc-based alloy composite containing Silicon carbide particle reinforcement. Zinc-based matrix alloy and cast iron was also investigated on similar lines for comparison purposes. Results showed that the zinc-based matrix alloy attained maximum wear rate and frictional heating, while those for the composite were the least, the response of the cast iron was intermediate between the two in general. Wear rate, friction coefficient and frictional heating increased with track radius and applied load. B.K. Prasad et al. (2001) have discussed the sliding wear response of a zinc based alloy in mixed lubrication condition at different sliding pressure and speeds. The obtained results were compared with SAE 660 bearing bronze. Speed and pressure are the major influencing factor on wear behaviour of the

material, zinc based alloys performed better when compared to bearing bronze. Incorporation of small amount of oil during testing has greatly improved the wear behaviour of the material than that of dry sliding condition. Yegneswaran et al. (2007) evaluated the wear behaviour of ZA based alloys as influenced by alloy composition, nature of the slurry and traversal distance. The results indicated that initially the wear rate increased with distance and decreased thereafter at longer traversal distance. In the liquid medium the wear loss was maximum and the addition of sand particles reduced the severity and extent of damaging effects lead to decreased wear rate. Silicon added alloy showed the better wear resistance than that of base material. Corrosion was predominant mechanism of material loss, erosion and abrasion playing secondary role in liquid medium. Purcek et al. (2002) have investigated the dry sliding friction and wear properties of zinc based alloys in comparison with SAE 660 bronze. Lower coefficient of friction and higher wear resistance of zinc based alloys was observed during the wear test. Wear resistance increased strongly with hardness and tensile strength but decreased with friction coefficient. The worn surface morphology showed that abrasive wear dominated in the case of 660 SAE bronze but adhesion and smearing was the main wear mechanism for zinc based alloys. Reason for lower wear rate in zinc based alloys can be attributed to smearing and embedding of oxidised layer formation in Zn-Al alloys. Babic et al. (2009) have investigated the effect of heat treatment and addition of graphite as reinforcing material on tribological improvement under dry and lubricating condition for Zinc aluminum alloys. The results showed that reduced coefficient of friction and lower wear rate of heat treated samples were observed for all applied load, lubricated and dry sliding conditions, this improvement can be attributed to finer and more uniform distribution of micro constituents and reduced cracking tendency. Heat treated alloys revealed ductile mode of fracture in comparison with ascast alloy. Addition of graphite particle has improved the wear properties by the formation graphite film on the surface of material which reduced the friction level. Dominant wear mechanisms for wear tested alloys were abrasion and adhesion type. Chen et al. (2014) has studied the microstructure, mechanical and wear properties of Zn-Al-Cu-TiB₂ in situ composites. The microstructure of the composites showed fine and uniform distribution of TiB₂ particles throughout the matrix and presence of this TiB₂

particle have improved the mechanical properties like hardness and tensile strength but a reduction in elongation of the composites is also observed. Frictional coefficient and wear rate decreased dramatically with the increase in TiB₂ content. Incorporation of 5% TiB₂ reduces the wear rate of the composite from 5.9×10^{-3} to $1.3 \times 10^{-3} \text{ mm}^3 \text{ m}^{-1}$. Influence of different Al contents on microstructure, tensile and wear behaviour of Zinc based alloy was investigated by Shuqing yan et al. (2010). Highest ultimate tensile strength and elongation percentage at room temperature and elevated temperature were seen in 27% Al content sample, it also exhibits the higher wear resistance at low load. When compared with base material the improvement in mechanical properties was observed in 30 % and 48% Al content materials, however UTS and elongation of the alloy still lower than that of ZA27 alloys this is due to the increase in segregation and void with increasing Al content. Hesham Elzanaty (2014) also investigated the influence of Al content on tribological properties of zinc based alloys. In his research zinc based alloys showed a reduction in strength and increase in ductility with increasing temperature. Higher hardness is obtained by increasing the Al weight percentage from 8 to 48 wt%. ZA27 exhibits the higher wear resistance at low load, this is due to better tightness of ZA27 alloy. S Baskar and G Sriram (2014) have carried out a systematic investigation on friction and wear behavior of journal bearing materials using pin on disc wear tester with three different lubricating oils. Results showed that the wear and friction of the material changed according to the sliding conditions of lubricating oils (synthetic lubricating oil, chemically modified rapeseed oil (CMRO) and CMRO with nano CuO. Among these three lubricating oils, one can contain nano CuO can be preferred for the lubrication purpose in journal bearing application because of its best performance. Aleksandar venci et al. (2014) have made an attempt to study the effect of addition of Si and Sr in Zn25Al alloys on structure, mechanical and tribological characterization. In spite of having good properties ZA alloys are rarely used because of its dimensional instability but this can be overcome by replacing the alloying element Cu by Si. Hardness values of Si added materials has no major changes when compared with Cu added ones but the alloy with 3% Si and 0.03 wt % strontium has the hardness

even higher than that of ZA27 alloy. Wear resistant of the alloy with Si was five times higher than ZA27 alloy, modification with Sr improved their wear resistance additionally with a slight increase in the coefficient of friction. Fatima et al. (2010) have focused the attention on effect of Al_2O_3 particle reinforcement on the wear behavior of ZA27 based composites using block on disc tribometer. Results showed that the composite showed better wear resistance than the matrix alloy. Enhancement in wear resistance can be attributed to the changes in the wear mechanism induced by the present of Al_2O_3 particle. Babic et al. (2009) have investigated the effect of heat treatment on the microstructure, hardness, tensile properties and tribological behaviour of ZA27 alloy. Microstructure of heat treated samples showed refined and uniform distribution of micro constituents. Hardness and tensile strength values were reduced with heat treatment and at longer solutionizing duration the hardness become practically constant. Applied load and sliding speed was the major influencing factor for wear rate. Frictional coefficient and wear volume loss increase with applied load and decrease with the sliding velocity. Ductile mode of fracture was observed in heat treated alloys, relatively smooth with shallow grooves and smearing of transferred material was seen in worn surfaces of heat treated material. Shu-qing Yan et al. (2009) has reported the observations pertaining to the friction and sliding wear characteristics of a ZA48 alloy under varying testing conditions. Composition segregation has a huge effect on wear resistance of the zinc aluminum alloy. Higher wear resistance was due to the combined effect of α and η phase. During wear test the soft η phase was acting as natural lubricant in sliding wear situation. Iron transferred from the steel ring to block and forced to the recess continuously during sliding wear, which forms a thin protective film at the contact surface, its load bearing capability would be improved. Geng Haoran et al. (2001) have investigated the effect of heat treatment and melting technique on antifriction and wear behaviour of ZAS35 zinc alloy and also compared with SAE 660 bronze and ZA27 alloy. ZAS35 alloy was superior to SAE660 bronze and ZA27 alloy in wear resistance and load bearing capacity, further improvement was observed by heat treatment process. For lower

sliding rate the ZAS35 performed better and TRT technique can reduce the friction coefficient and temperature.

2.8 Microstructure and Mechanical properties of SPD Processed materials

Materials processed by severe plastic deformation for mechanical properties improvement have growing interest among the specialists in material science. Therefore some of the severe plastic deformation process such as equal channel angular pressing, high pressure torsion, multidirectional forging and accumulative roll bonding have been developed in the recent years and some of their outcome are list in the below section.

Purcek et al. (2010) studied equal channel angular extrusion (ECAE) on Zn-Al alloy at the temperature of about 75 °C by using route B_c, which resulted in improvement of mechanical properties like ultimate tensile strength and ductility. They concluded that it was because of refined microstructure and high dislocation density occurred as a result of the ECAP processing. He also observed that tensile strength and maximum pressing load shows the similar trend. Sanjay et al. (2014) evaluated the mechanical properties, microstructure and wear of high leaded tin bronze after multidirectional forging process with a total equivalent strain of 0.75. The results indicated that improvement of ultimate tensile strength, hardness, yield strength and wear rate along with maintained ductility with the increase in the number of multidirectional forging passes. Grain size was reduced to 37nm from 120nm along with this fine dispersion of alloy particles were observed with the increase in MDF passes. Formation of lead lubricating layer on the surface of sample reduced the wear rate of the material, this due to the temperature generated near the pin surface at higher speed. Shengli et al. (2012) investigated the characterization of hot deformation behaviour of Zn-10.2Al-2.1Cu alloy using processing maps. The resulted showed that the maximum stress decreases with decreasing strain rate and increasing temperature with an activation energy of about 141.895kJ/mol. Microstructure observations shows that the partial dynamic recrystallization of the Zn rich phase occurs in the first stage (218-270 °C of temperature with a peak efficiency of 0.53) and full dynamic recrystallization occurs in the second stage (290-330°C of temperature and with a peak efficiency of 0.58).

Dendritic structure is partially fragmented and elongated within the eutectic matrix and some initial lamellar Al-rich is transformed into a spherical shape. Mohamed et al. (2015) investigated the influence of ECAP as grain refinement technique on microstructure evolution, mechanical properties and corrosion behavior of the pure aluminum material. The finest grain size observed was 0.3 μm after 10 number of ECAP passes, this reduction of grain size lead to increase in microhardness, tensile strength while the elongation decreased with the increase of ECAP number of passes. Corrosion resistance of the materials was also increase with number of ECAP passes this is due to the production of ultrafine grains with high disorientation angle upto 78 %. Gencaga et al. (2004) have studied the processing of eutectic zinc 5% aluminum alloy by equal channel angular pressing process. The analysis was carried out by considering route A method without giving rotation to the sample, route C method, here the sample is rotated by 180 °C after each pass. The study revealed that the equiaxed grain structure of the as received alloy was completely disappeared and instead a banded structure was formed by the ECAP process. It was observed that hardness and maximum load required for ECAP process showing similar trend with number of passes irrespective of route chosen. Gencaga Purcek (2005) improved the mechanical properties of zinc aluminum alloys using equal channel angular pressing technique. Here in his experiment he has used route B_c method, where the sample is rotated by 90° after every pass. The results showed that both strength and ductility of material increased with ECAP number of pass this is due to refined microstructure and high density of dislocation generated during the ECAP process. Minimum possible pressing temperature was taken to avoid macroscopic and microscopic shear cracking. Purcek et al. (2010) investigated the effect of equal channel angular extrusion on the mechanical and tribological properties of as cast Zn-40Al-2Cu-2Si alloy for four passes following route B_c. Tensile elongation to fracture was increased due to the number of ECAP pass that to without decreasing the strength. After ECAP processing the brittle mode as to converted to ductile mode. The improvement in various properties attributed to the breaking and refinement of large dendritic microstructure and the fragmentation of silicon and ϵ phase particles. The enhanced wear resistance was due to improved ductility and toughness of the material after ECAP process. Wear resistance of a material is usually determined by both its

strength and ductility, as described by the empirical Archard equation $W = K \frac{P}{H}$ where W is the wear rate, P is the applied pressure, H is the material's hardness or strength, and K is the wear coefficient related to the material's ductility. To improve mechanical properties several studies focused on grain refinement and microstructural evolution of ZK60 magnesium alloy prepared by multi axial forging during partial re-melting by Tao Jian-quan et al. (2012). Re-melting temperature and holding time effect on microstructure was remarkable. During MAF process with increasing the equivalent strain, the coarse grains are refined. Grain coarsening was observed in partial re-melting because of prolonged holding time and spheroidal semisolid microstructures were obtained with increasing reheating temperature. Maximum yield strength of 202 MPa and tensile strength of 315 MPa was achieved for thixoformed ZK60 magnesium alloy at 574 °C of temperature. Chou et al. (2007) studied the effect of cross-channel extrusion of zinc–22 wt. % aluminum eutectoid alloy. Results showed that grain refinement takes place after processing at 100 °C and 200 °C for 10 passes. Microstructure comprises lamellar structure in the annealed state was changed into spherical shape after deformation. Average grain size of the processed material was found to be in the range of 0.3 to 1 µm. The tensile strength of the sample decreased as the extrusion passes increased and it decreased with processing temperature. Chang et al. (2002) investigated the microstructural features on the deformability of zinc based alloys. They conducted the study in two types of microstructure viz., a) lamellar structure b) fine grained structure, and results showed the softening phenomenon in the lamellar structured alloy. Lamellar structure undergoes recovery or recrystallization at the early stages as compared to the fine grained structure at elevated temperature. They concluded that fine grained alloy owns excellent deformability than the lamellar structure. Kovosi et al. (2014) worked on modelling of dislocation density and strength on rehoforged A356 alloy during multi directional forging. They observed that the model predicts that dislocation density of cell interiors was increased with high rate during starting passes of multi direction forging process and with low rate in the further passes. The predicted model was in good agreement with experimental data and less sensitive to variation of Si particles aspect ratios. Sharath et al. (2016) studied the effect of multi directional

forging on the microstructure and mechanical properties of zinc 24 wt % of aluminum and 2 wt % of copper alloy material. Here the experiments were carried out at 100 and 200 °C upto a total strain of 0.6 and 1.2 respectively. They observed that the initial grain size was 30 µm and reduced to 2 µm when forged at 100 °C upto three passes and 1 µm of grain size when forged at 200 °C upto six passes. The results showed that as the number of passes increased the lamellar structure of Al and Zn rich phase was refined to spherical shape and distributed more uniformly. Improvement in the mechanical properties was observed with increase in number of MDF passes and after MDF process which changed the brittle mode of fracture to ductile mode of fracture. Hong et al. (2014) worked on ductility enhancement of EW 75 alloy by MDF process. His research showed that highest ductility can be achieved by multidirectional forging process on Mg-7Gd-5Y-1Nd-0.5Zr alloy and he also systematically evaluated the microstructure, texture and mechanical properties of the alloy. They observed that grain size was refined from 292 µm to 58 µm after MDF processing at 500 °C. Decrease in forging temperature leads to fine particles precipitation in large amount which in turn restricts the grain growth. The texture changes during MDF process which results in high schmid factor for basal slip. Large ductility was due to its fine recrystallization grains and weak texture. Wei Guo et al. (2013) enhanced the microstructure homogeneity and mechanical properties of ZA31 Si composites by cyclic closed die forging process. Results showed that increase in yield strength was observed with increase in Si content at room temperature but at the cost of UTS and elongation. During processing the dendritic and Chinese script structure of Mg₂Si was broken a transformed into smaller particles because of high amount of induced shear stress. Microstructural observation showed that fine grains and more uniform distribution of Mg₂Si particles were contributing to the enhancement of both strength and ductility of the material with increasing number of forging passes. The grain size of material increased with increase in processing temperature (7.9 µm to 13.6 µm when processed at 350 and 450 °C).

2.9 Wear Behavior of SPD Processed Materials

The enormous number of research has been done on wear behaviour of different UFG materials and metal matrix composites with respect to the tribological application.

Severe plastic deformed (SPD) materials have much strength than their coarse grain counterparts due to their UFG size and strain hardening, it is expected that they will have improved wear resistance. However, current research on the wear behavior of severe plastic deformation of materials shows some conflicting results.

Chuan Ting Wang et al. (2011) has made an attempt to characterize the wear behaviour of an aluminum alloy processed by equal channel angular pressing. Refined microstructure with increased hardness was observed after the ECAP process. But decrease in the wear resistance leads to an increase in mass loss with increasing numbers of ECAP passes, this is due to characteristics of grain refinement in the ECAP procedure and the inherent loss of a strain hardening capability. The wear properties of Equal channel angular pressed Al-2, 3 and 5 % Cu alloys under wear conditions using different sliding distances and loads were investigated (Aal et al. 2010). This study revealed an increase in the micro-hardness with increase in the number of equal channel angular pressing passes accompanied by fine dispersion of Cu content due to the decreased grain size. Sliding distance and applied load are the major factors influencing the mass loss of the material. (Ortiz et al. 2011) also showed an improvement in wear resistance was observed by increasing the number of equal channel angular pressing passes for an Al-Mg-Si alloy. The coefficient of friction and wear rate of the ECAP processed aluminum bronze material (Cu-10Al-4Fe) was investigated by Gao et al. (2008). Large uniform dispersion of second phase particles was observed by them after six number of passes. The coefficient of friction of the alloy decreased considerably with increasing number of ECAP passes. Conversely, some of the investigation results show adverse effect on wear behavior for equal channel angular press processed materials. Wear tests of the Al 1050 alloy were conducted on both the as-received alloy and the alloy after processing by equal channel angular pressing (Wang et al. 2011). The grain size of the alloy was reduced from 44 μm in the as-received condition to 1.3 μm after eight equal channel angular pressing passes. Though the hardness values increased significantly after processing, ECAP-processed samples had a similar coefficient of friction and higher mass loss than the as-received sample. The other study of the wear behavior of the as-cast and ECAP-processed Al-12%Si alloys showed that the mass loss increased with

increasing applied load (Kucukomeroglu 2010). Compared with the as-cast alloy, the wear resistance of the alloy decreased after six ECAP passes, especially for long sliding distances and high applied pressures. Thick oxide layer was identified by SEM and XRD analysis on ascast and processed alloy.

From the literature studies on Zn-Al alloy systems, it is observed that the mechanical and tribological properties of the material can be altered by changing the grain structure through the process of severe plastic deformation (SPD). Against to this background, the present research work has been undertaken with an objective to explore the potential of ZA alloy based composites as a bearing material and to investigate the effect of various particles on the mechanical and tribological behavior of the ZA-27 alloy based composites. Zinc and aluminum are lowest cost raw bearing materials compared to conventional bearing material and this work is an attempt to find a possible use of such economical materials which might gainfully be employed as low cost, high strength and wear resistant composites materials.

CHAPTER 3

EXPERIMENTAL TECHNIQUES AND MATERIALS USED

This chapter describes the details of the fabrication and processing method of composites and experimental techniques used in the present investigation in order to achieve the objectives.

3.1 Methodology of Research Work

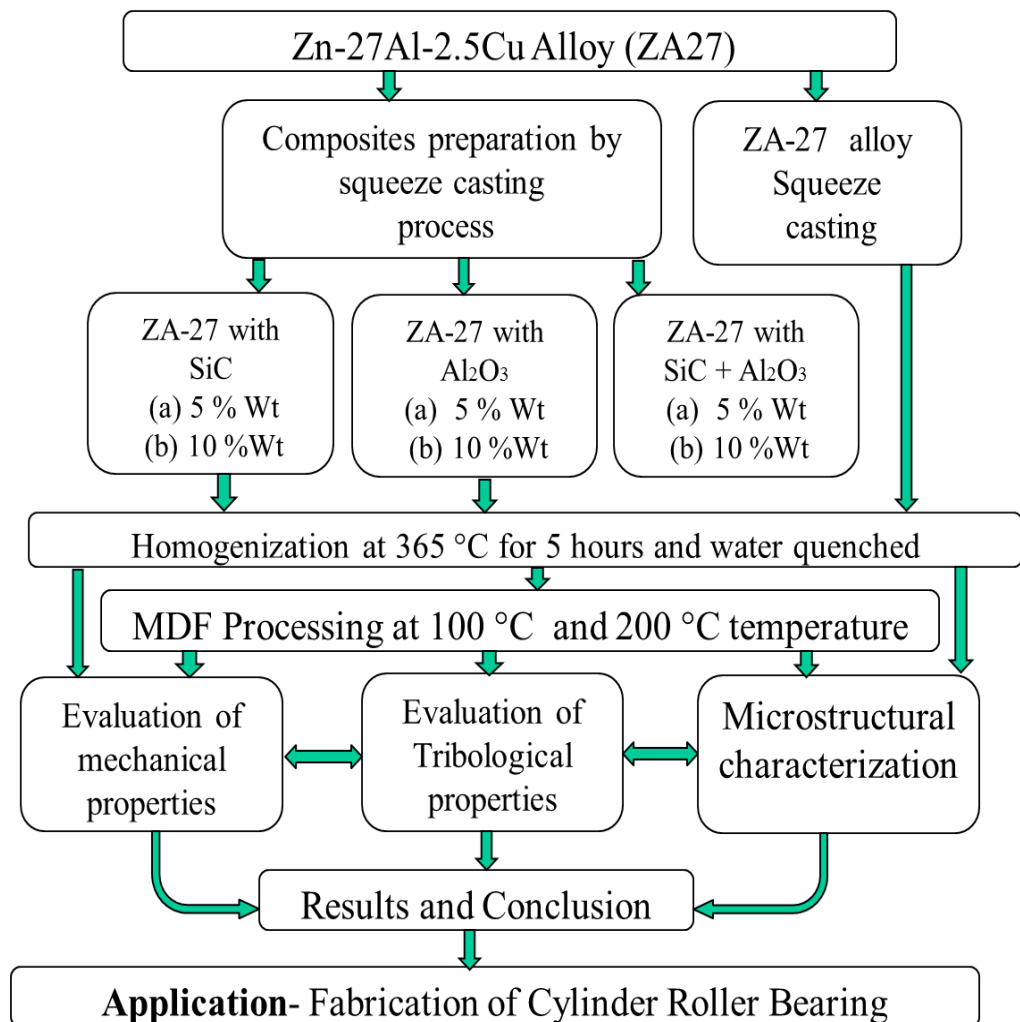


Figure 3.1: Research Methodology

3.2 Materials

The matrix and reinforcing materials used in the present work are represented in table 3.1

Table 3.1: Materials used for the fabrication of composites

1	Matrix component	Zinc- 27Aluminum- 2.5 copper (ZA-27)
2	Reinforcement	Micro sized (20 - 50 μm) (a) Alumina - (Al_2O_3) (b) Silicon Carbide - (SiC) (c) Mixture of Alumina and Silicon Carbide - ($\text{Al}_2\text{O}_3 + \text{SiC}$)
3	Wetting agent	Pure magnesium

3.3 Casting Process

Liquid state fabrication of metal matrix composites involves incorporation of dispersed phase into a molten matrix metal, followed by its solidification. In order to achieve better mechanical properties of the composite, good interfacial bonding (wetting) between the dispersed phase and the liquid matrix should be ensured. The simplest and most cost effective method of liquid state fabrication is stir casting. Stir casting is a liquid state method of composite materials fabrication, in which a dispersed phase (ceramic particles, short fibres) is mixed with a molten matrix metal by means of mechanical stirring (Kumar et al. 2015). The only problem associated with this process is the non-uniform distribution of the particles due to poor wettability and gravity regulated segregation. Figure 3.2 shows the schematic diagram of stir casting setup used for the fabrication of composites.

A weighted quantity of matrix alloy was taken in a graphite crucible and melted in a resistance furnace. The temperature was slowly raised to 550 °C. This molten metal was stirred using a stainless steel impeller at a speed 600 rpm to create the vortex. The impeller blades were designed in such way that it creates vortex to achieve the sound particle mixing. The reinforcement is preheated at a temperature of 450 °C to drive off the moisture. After the formation of vortex in the melt, the reinforcing particle was added with a separate pouring attachment at the rate of 15–20 g/min into the melt with stirring.

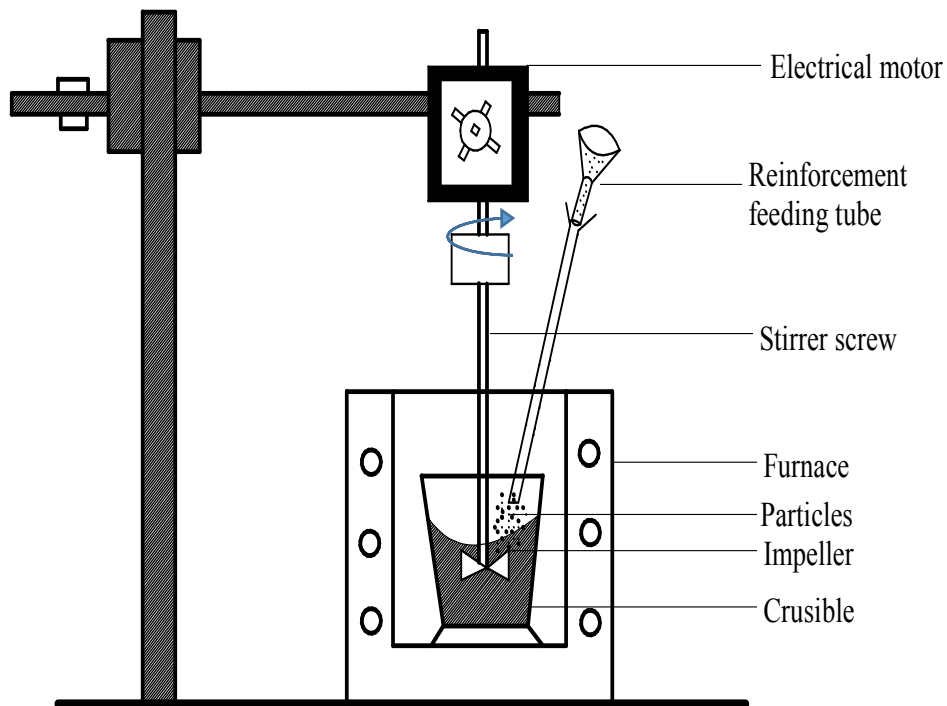


Figure 3.2: Schematic diagram of stir casting setup for the fabrication of MMC

The stirring was continued for another 2 minutes even after the completion of particle feeding for homogeneous distribution of the reinforcing particles. The mixture was poured into the preheated metal die and squeezed at 120 MPa pressure and allowed to solidify at room temperature. Figure AI- 1.1 shows two dimensional representations of Squeeze casting die design in all different view (a) Plunger (b) Top view assembled (c) Right side view assembled (d) Front view assembled. During stir casting, the amount of charge materials, stirring duration and position of the stirrer in the crucible were kept constant to minimize the contribution of variables related to stirring on distribution of reinforcing particles. Three dimensional exploded view of the Squeeze casting split type die with plunger is shown in fig. 3.3 and photograph of Squeeze casting dies with plunger is shown in fig. 3.4. The dimension of casted ingot is 60 x 50 x 60 mm (fig. 3.5) and machined to the dimension of 30 x 25 x 30 mm for further MDF processing.

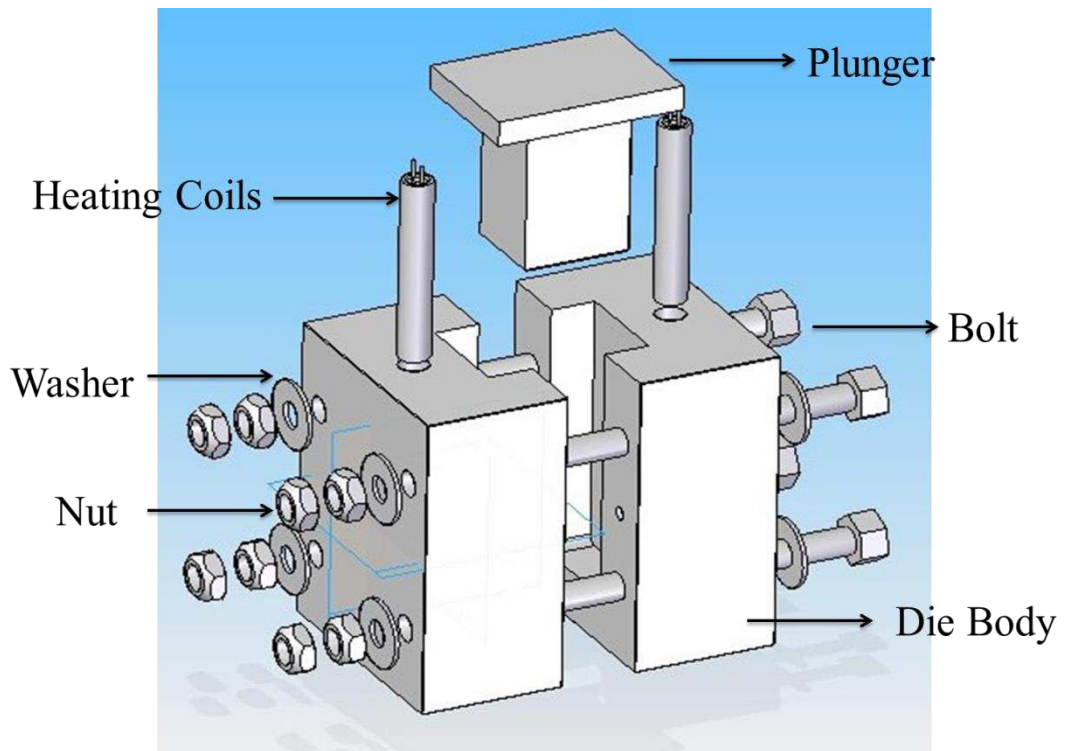


Figure 3.3: Three dimensional exploded view of the Squeeze casting split type die with plunger.

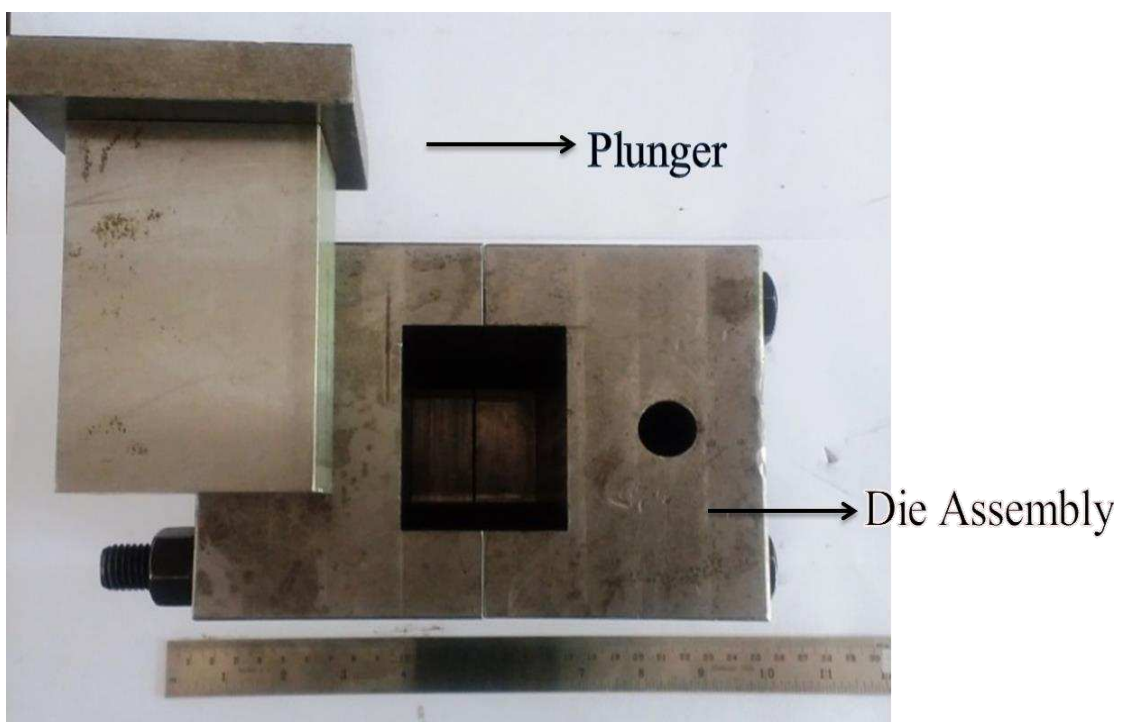


Figure 3.4: Photograph of Squeeze casting dies with plunger.

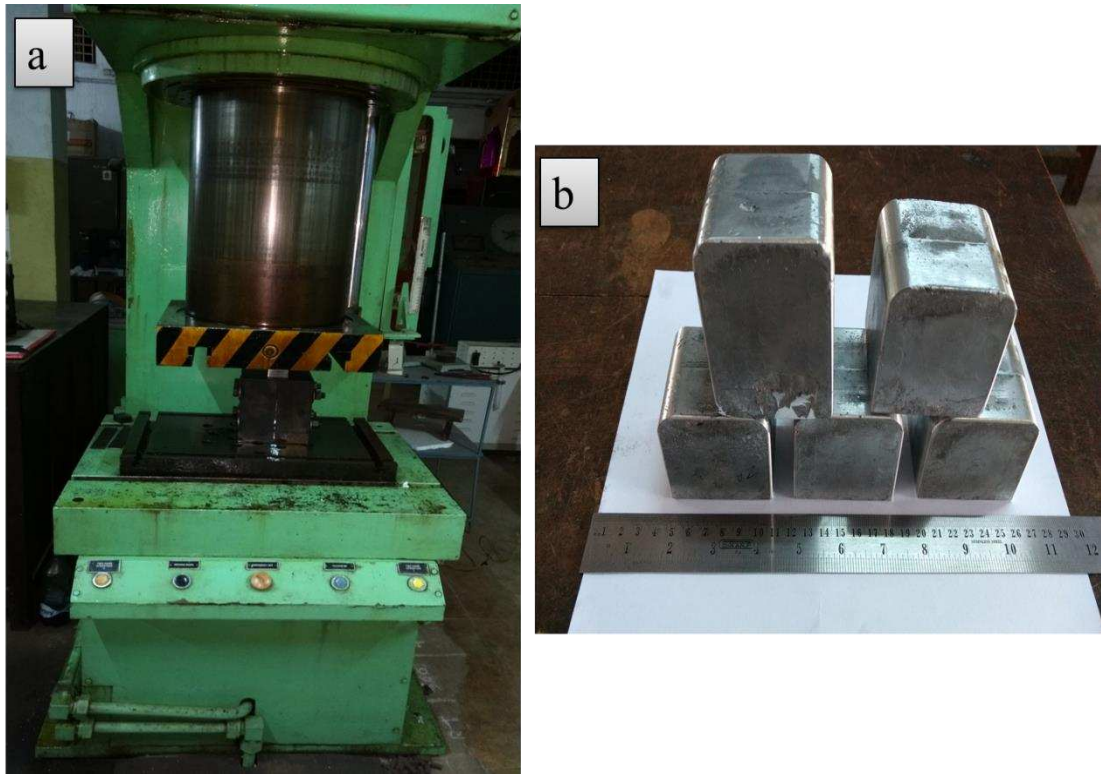


Figure 3.5: Photograph of the (a) 250 ton hydraulic press (b) Casted sample after squeezing.

3.4 Heat Treatment

Homogenization: During solidification of an ingot in casting process, micro segregation occurs, resulting in local compositional variations that are often removed by heat treatment. It is frequently necessary to homogenize the part before usage to promote uniformity of chemical composition and microstructure. Alloy ingots are normally homogenized by placing them in Muffle furnace at elevated temperatures for rather long times. Homogenization was carried out at 365 °C for 5 hours and quenched in water to room temperature.

3.5 Multi Directional Forging (MDF) Process

The experimental material was as-cast zinc - 27 wt. % aluminum - 2.2 wt. % copper (ZA27) alloy procured from the Asppice Engineering, Coimbatore and the alloy is reinforced with SiC, Al₂O₃ and SiC+Al₂O₃ separately to prepare MMC composites. The chemical composition of this material is shown in table 3.2.

Table 3.2: Chemical composition (wt. %) of the zinc-aluminum alloy

Material	Al	Cu	Fe	Cd	Mg	Sn	Zn
Weight %	25.0-28.0	2.0-2.5	0.06-0.07	0.005-0.006	0.01-0.02	0.002-0.003	69.3-72.9

Before MDF the base alloy and prepared composites were homogenized at 365°C for 5 hours by using muffle furnace and quenched in water at room temperature. Homogenization temperature was selected from binary phase diagram of Zn-Al alloy. In the binary system, a single phase supersaturated by Al exists at 365°C. The rectangular specimen of dimension 30 mm x 25 mm x 30 mm is machined from the as-quenched composites and subjected to MDF by using split type die as shown in fig. 3.7 for the different number of passes. Split type die is used for MDF technique with identical cross sections (fig.3.6), by the application of load using a punch the work piece is pressed in such a way that entire volume of work piece is confined within the die. Work piece is plastically deformed in nearly the same way of plane strain condition. Figure AI-1.2 shows the two dimensional representations of MDF Procressing die design (a) Plunger and Base plate (b) Main body part one (c) Main body part two (d) Assembled main body MDF. Material used for MDF die was hot tool steel, ie., H-13 which as chromium, molybdenum, vanadium and characterized by high hardenability and excellent toughness. The molybdenum and vanadium act as strengthening agents in addition to that chromium content assists H-13 to resist softening when used at high temperatures. The MDF technique applied to different passes to obtain consistently forged structure at constant pressing speed of 0.5 mm/m by using 40 ton hydraulic press (fig. 3.8 (a)). The forging operation will be conducted at 100°C ($\pm 5^\circ\text{C}$). The testing temperature was determined by conducting compression test at room temperature, 60°C, 80°C, 100°C and 120°C. It shows that the lowest possible temperature is 80°C ($\pm 5^\circ\text{C}$), without macroscopic and/or microscopic crack occurring in the samples during the MDF processing. The lowest possible temperature is desired during compression to control grain growth. The ram speed of the hydraulic press machine is 2 mm/min and Molybdenum disulfide (MoS_2) paste was used as lubricant. Final multi directional forged samples is shown in fig. 3.8 (b).

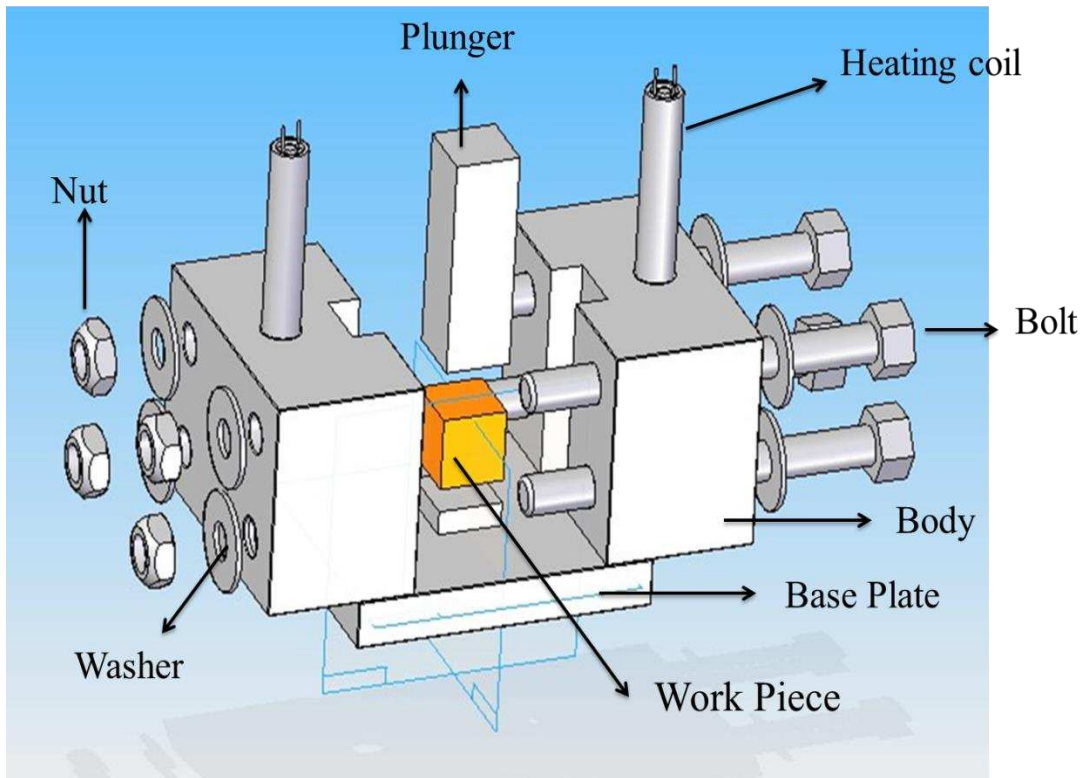


Figure 3.6: Three dimensional exploded view of the Multi directional forging split type die with plunger.

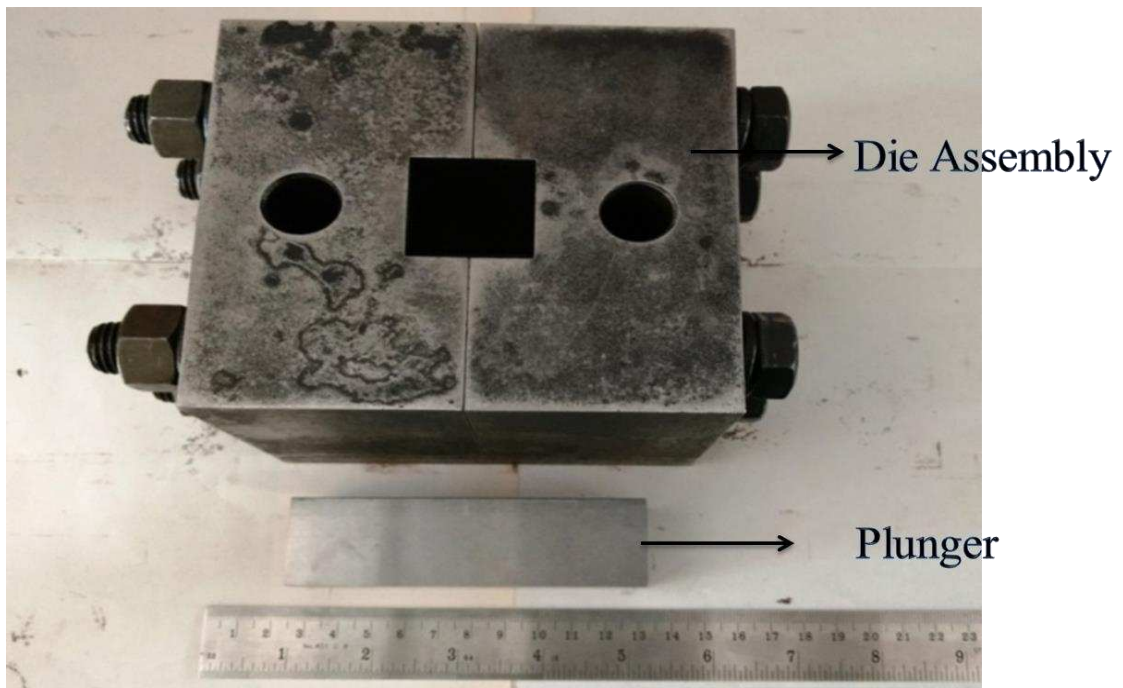


Figure 3.7: Photograph of Multi directional forging die with plunger.

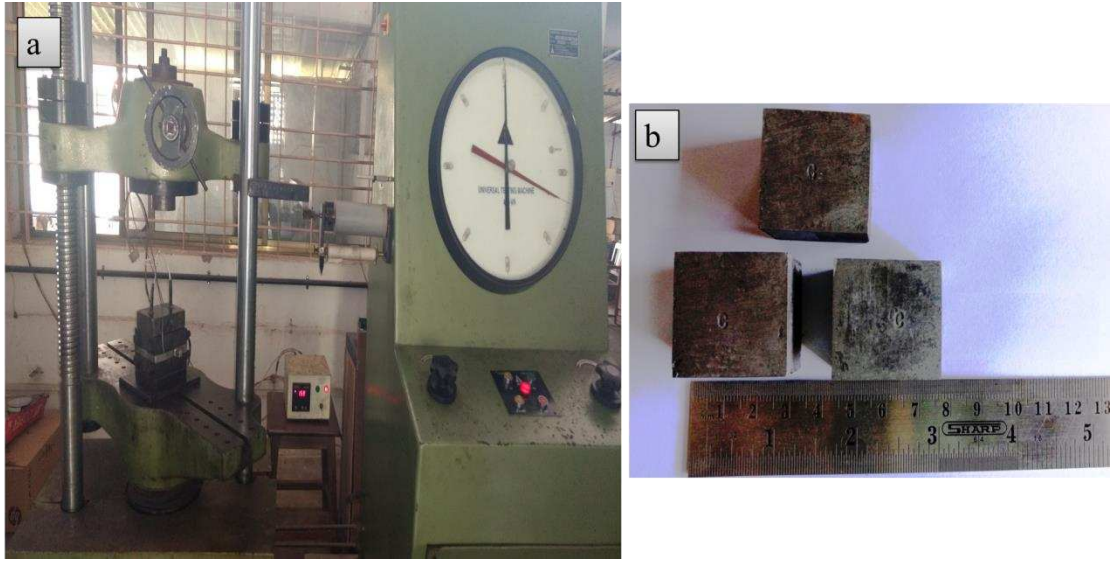


Figure 3.8: Photograph of the (a) 40 ton hydraulic press (b) MDF processed samples.

3.6 Physical Properties Evaluation

3.6.1 Density

Theoretical and experimental densities of the ZA27/SiC 5 wt% reinforced composites were compared with MDF processed samples. Experimental density was determined by density measurement kit (Contech-CAS-44) assisted with accurate weighing balance machine. Experimental density is calculated using equation (3.1) and theoretical density was evaluated by the rule of mixtures concept. Percent porosity of composites was calculated from equation (3.2) (Dora shiva prasad et al. 2014).

$$\rho^{\text{Expt}} = \frac{D}{D-I} \quad \text{Equation - 3.1}$$

Where, ρ^{Expt} =Experimental density (g/cm^3), D =Dry weight of the sample, I =Immersed weight of sample in water.

$$\% \text{ porosity} = \{(\rho^{\text{Theo}} - \rho^{\text{Expt}}) \div \rho^{\text{Theo}}\} \times 100 \quad \text{Equation - 3.2}$$

Where, ρ^{Theo} = Theoretical density (g/cm^3), ρ^{Expt} = Experimental density (g/cm^3).

3.7 Mechanical Properties Evaluation

3.7.1 Rockwell hardness

Rockwell hardness values are expressed as a combination of a hardness number and a scale symbol representing the indenter and the minor and major loads. The hardness number is expressed by the symbol HR and the scale designation. For soft materials such as copper alloys, soft steel, and aluminum alloys a 1/16" diameter steel ball is used with a 100-kilogram load and the hardness is read on the "B" scale. In testing harder materials, hard cast iron and many steel alloys, a 120 degrees diamond cone are used with up to a 150-kilogram load and the hardness is read on the "C" scale. The four important factors should be considered for scale selection i.e., Type of material, specimen thickness, test location, and scale limitations. The resulting Rockwell number represents the difference in depth from the zero reference position as a result of the application of the major load.

3.7.2 Tensile test

The specimens of composite material after the MDF process was machined into tensile samples as per the ASTM E-8M-04 standards as shown in fig. 3.9. Tensile testing was conducted on both processed and unprocessed specimens and a result of three tests is considered for each condition. Ultimate tensile strength and percentage of elongation will be evaluated using a Shimadzu universal testing machine. The UTS was determined from the load-displacement graphs recorded during the testing. The difference in gauge length before and after fracture was measured by using digital vernier caliper and the percent elongation to failure was measured.

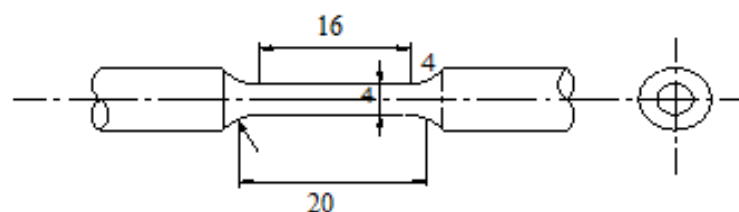


Figure 3.9: Tensile test specimen (All dimensions are in mm)

3.8 WEAR TEST

Wear rate of the material is measured by using pin-on-disk apparatus and it also helps in determining the coefficient of friction. The schematic diagram of the pin-on-disk apparatus is shown in the fig 3.10.

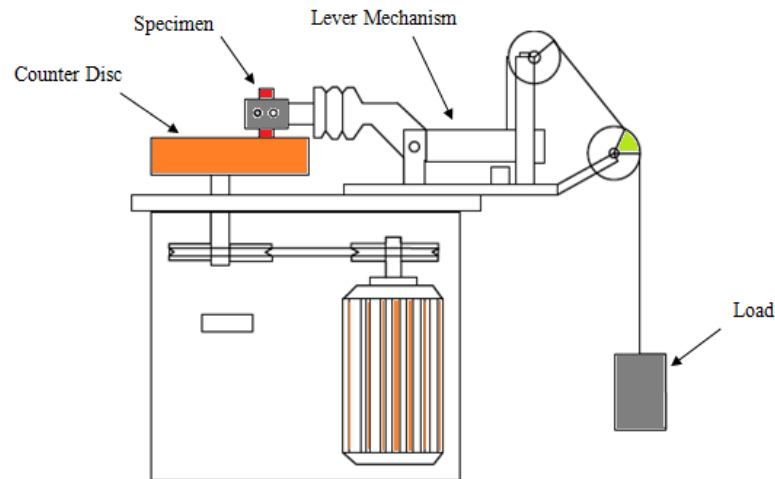


Figure 3.10: Schematic representation of pin on disc wear testing machine.

Sliding wear experiments were conducted using a computer aided pin on disc wear testing machine, (DUCOM) made pin on disc tribometer (TR-20LE-PHM 400-CHM 600). The polished pin samples with flat surfaces in the contact region and cleaned with acetone to remove dust or grease from the surfaces. EN 31 grade steel having hardness of 64 BHN was used as counterface (disk). The wear tests were conducted at room temperature in accordance with ASTM G99 standard having specimen diameter of pin 6 mm and 28 mm length. After wear testing, weight loss experienced by the pin was measured with the help of three digit accuracy weighing machine. By using the following formula wear rate is obtained (ASTM G99).

Wear rate:

$$W = \frac{m}{(\rho \times D)} \text{ in mm}^3/\text{m} \quad \text{Equation – 3.3}$$

Where m = mass loss in grams,

ρ = density, g/mm³

D = sliding distance in meters.

Co-efficient of friction:

$$\mu = \frac{\text{Frictional force}}{\text{Applied load}} \quad \text{Equation 3.4}$$

3.9 MICROSTRUCTURE ANALYSIS

3.9.1 Optical microscopy

The microstructural images of composites material before and after MDF processing were taken by using a Carl-Zeiss metallurgical microscope for investigation of uniformity of particles and grain size identification. The specimens prepared from the MDF processed samples are perpendicular to the directional of load applied for processing. Metallographic techniques were used to prepare the specimens and these specimens are mounted and mechanically polished on a series of silicon carbide (SiC) abrasive papers of increasingly finer grit size, and alumina paste was used on polishing cloth. Specimens were etched using nital reagent (2.5 % of Nitric acid + 97% of Alcohol/Methanol/Ethanol/Methylated spirit) and its formula is listed in ASTM E 407 as formula number 74 “Nital”.

3.9.2 Scanning electron microscopy with energy dispersive spectroscopy

The microstructures of all processed and unprocessed samples were analyzed by using a JEOL JSM-6380LA scanning electron microscope using the secondary electron (SE) and backscattered imaging modes. The EDS analysis of the samples was conducted for the elemental analysis of micro and macro constituents. EDS mapping analysis was done to study the distribution of the elemental components of each phase.

3.9.3 Transmission electron microscopy

Grain size measurement of fine grains and microstructural study was conducted using TEM for specimens before MDF and after MDF process. Thin disc specimens of 3 mm diameter were punched from the thinned samples. The punched disc is further thinned down to 80 μm by disc polishing. The samples were then dimpled up to 20 μm . Ion milling of the dimpled samples was carried out at 6° beam angle with beam energy of 5 keV till perforation, it is followed by further milling at 2.5 keV with beam angle of 3°. The ion milled samples were studied under transmission electron microscope (Make JEOL, Model- JEM-2100) to reveal the microstructure of the material. The measurements of the grain sizes were made directly from TEM micrographs.

3.9.4 X-Ray diffraction analysis for phase identification

Samples were subjected to X-ray diffraction studies to identify the phases present in it. The samples were characterized by using X-ray diffractometer, (operated with Cu-K α radiation at 30 kV and 20 mA). The 2θ range was selected between 30° to 90°. In the present work the same range is selected because one can expect the phases of major intense peaks. The diffracted data was analyzed with the help of JCPDF data files to identify the peaks corresponding to different constituent phases.

CHAPTER 4

RESULTS AND DISCUSSION

4.1 Base Material Properties Evaluating

The ZA-27 alloy used in the present research is obtained in the form of commercial ingots having the chemical composition as per ASTM B 669-82 ingot specification as shown in table 4.1. The presence of the constituents of ZA 27 alloys has been confirmed by SEM / EDS spectra, which is as shown in fig. 4.1.

Table 4.1: Chemical composition of ZA-27 matrix alloy.

Elements	Aluminum	Copper	Iron	Zinc
Percentage (%)	25-28	2.0-2.5	0.03-0.04	Balance

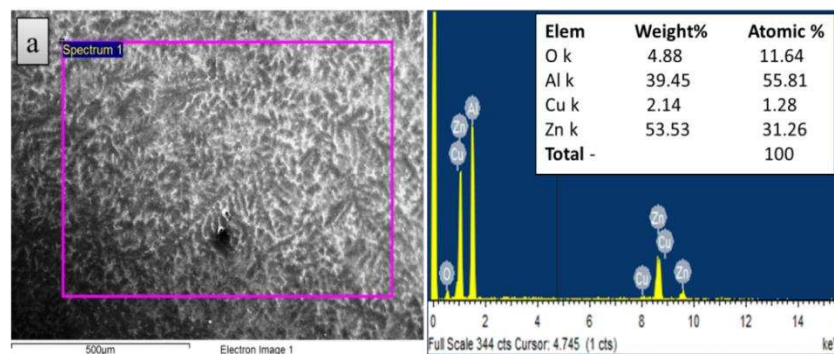


Figure 4.1: SEM with Energy dispersive spectroscopy image showing ZA27 alloy composition.

4.1.1 Microstructure Evolution

The optical and SEM images of ascast and solutionized alloy are shown in fig. 4.2 and 4.3 respectively. The main micro constituents in the alloy can be seen more clearly in fig. 4.2 (b). The microstructure of ZA27 alloy consists of a dendritic structure with α aluminum-rich dendrites, zinc rich eutectoid $\alpha+\eta$ phase in inter-dendritic regions along with metastable ϵ (Cu-rich) phases (Chen et al. 2004). Non-metallic inclusions,

for example, oxides of Al, Cu, Zn, Mg or intermetallic compounds (CuZn_4 , AlCu , Al_4Cu , AlMg , $\text{Mg}_2\text{Zn}_{11}$, and FeAl_3) may be present in the microstructure of the ZA27 alloy (Choudhary et al. 2005).

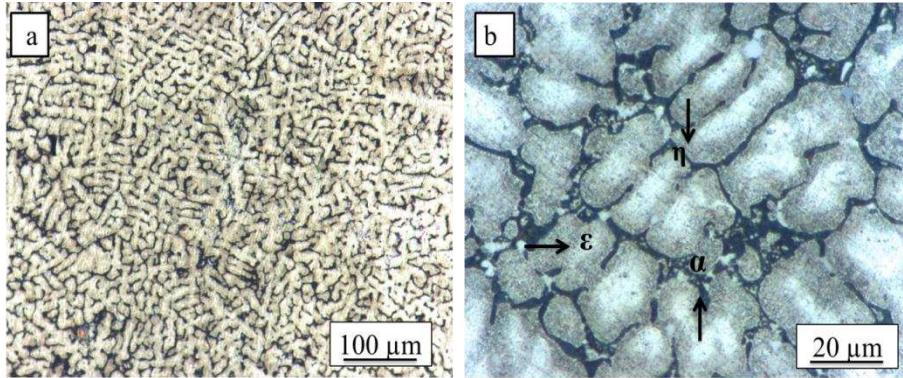


Figure 4.2: Optical microscopy images (a) Ascast ZA27 alloy at lower magnification (b) Ascast ZA27 alloy at higher magnification.

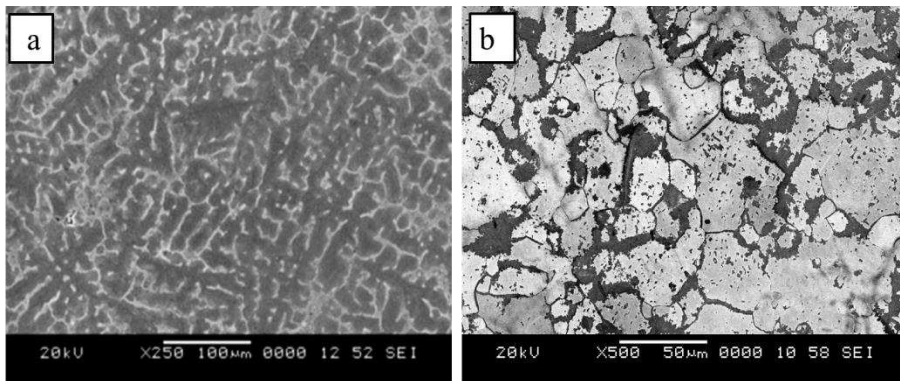


Figure 4.3: SEM images (a) Ascast ZA27 alloy (b) Solutionized ZA27 alloy

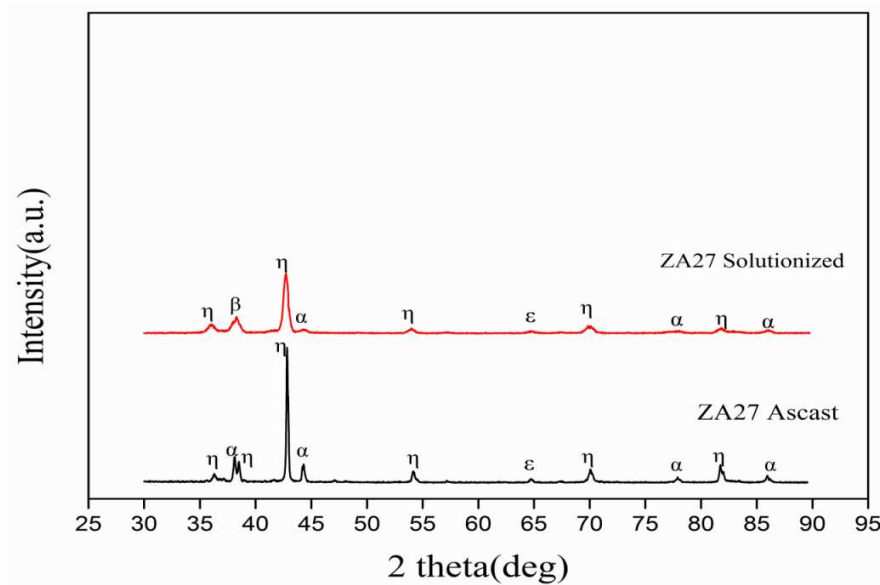


Figure 4.4: XRD patterns of ascast and solutionized ZA27 alloy

The average grain size measured was found to be approximately 25-30 μm for a solutionized sample. Also, the presence of α , η , ϵ (CuZn_4), and β phase in ZA27 alloys was confirmed in accordance with the XRD analysis shown in fig. 4.4. The XRD analysis on the solutionized sample indicated the presence β phase, it's Zn-rich fcc phase which is formed by solutionizing treatment at 365 $^\circ\text{C}$ for 5 hours followed by water quenching. This is confirmed by the SEM images present in fig. 4.3 (b).

Table 4.2: Density and Hardness values of ZA27 alloy

Sl. No	Sample Name	Experimental Density g cm^{-3}	Theoretical Density g cm^{-3}	Porosity %	Rockwell Hardness HRB
1	Ascast	5.2189	5.314	1.78	40
2	Homo	5.2421	5.2975	1.04	51

Table 4.2 shows the physical and mechanical properties of ZA27 alloy. This alloy has the highest aluminum content, highest strength, highest melting point, and the lowest density of the Zinc aluminum group. There is a slight decrease in porosity percentage of ZA27 alloy after solutionizing treatment due to the removal of a small amount of interdendritic porosity present in the ascast condition. Results of hardness measurement are shown in table 4.2. The hardness of the alloy in ascast condition was 40 HRB and after solutionized treatment, it was 51 HRB. This improvement in hardness is attributed to the uniform distribution of different phases present in the alloy, during solutionizing treatment. Figure 4.5 shows the tensile test plot of engineering stress versus engineering strain for ascast and solutionized condition. Initially, the ascast sample shows 282 MPa of ultimate tensile strength with 3.8 % of elongation and on solutionizing the UTS of 324 MPa and elongation of 4.3% was achieved. The elimination of the dendritic structure by solutionizing treatment caused the formation of most of the equilibrium phases (Joes et al. 2014). Figure 4.6 (a, c) shows the SEM images of the fractured surface in the as-cast condition taken at different magnification, in which features of brittle fracture are discernible. As-cast structures are inherently brittle because of the presence of interdendritic porosity in the matrix. Further, the precipitation of non-equilibrium hard ϵ phases too contributes to the brittleness of as-cast materials. The dendritic type structure contains interdendritic porosity during solidification due to incomplete filling of liquid melt

and this is the reason for the brittle fracture in the as-cast alloy. In the case of the solutionized fractured sample surface, some dimples are seen in few regions in fig. 4.6 (d) which shows the transformation of brittle mode to a ductile mode of fracture has been initiated.

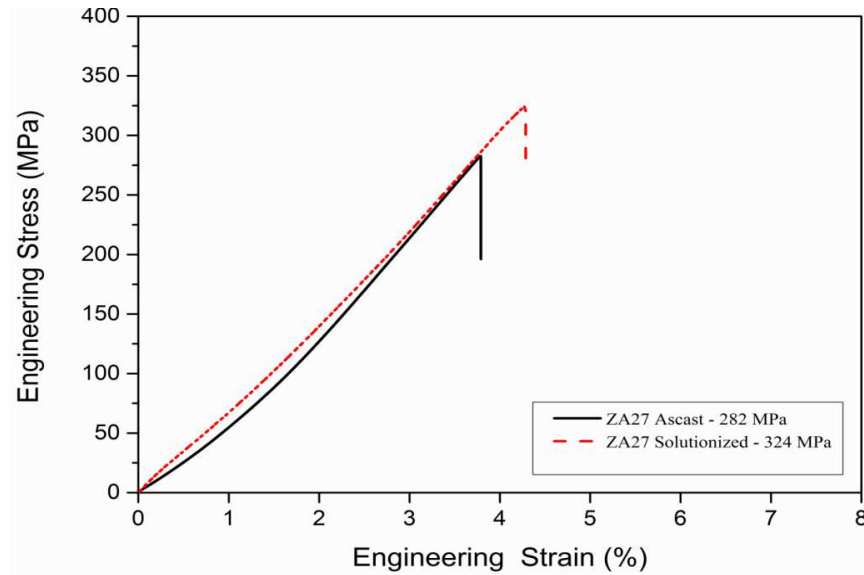


Figure 4.5: Engineering stress versus engineering strain graph of tensile test for ascast ZA27 alloy and solutionized ZA27 alloy.

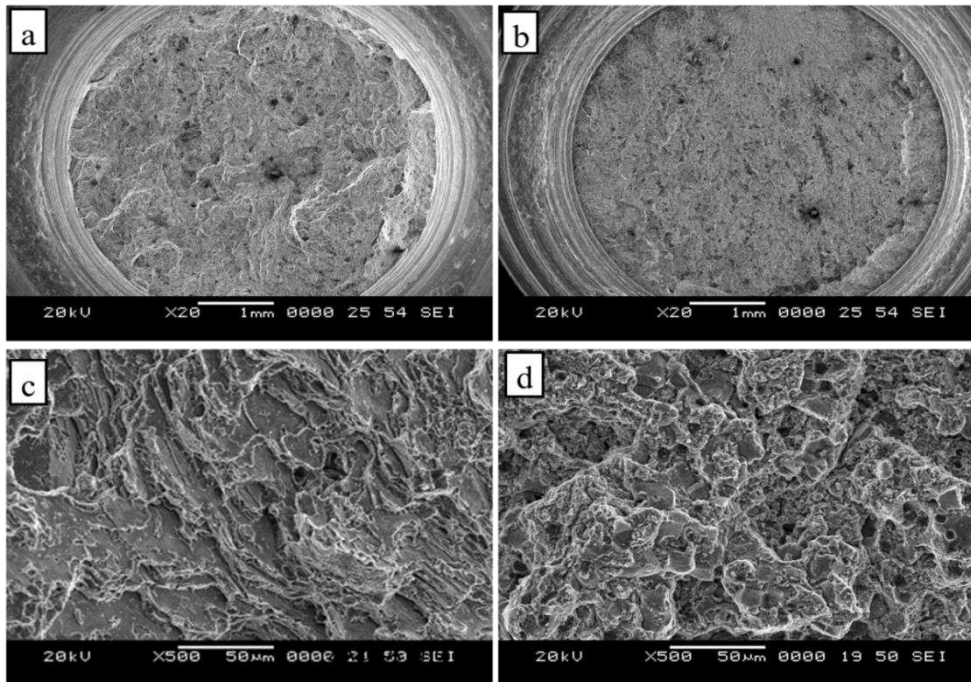


Figure 4.6: SEM images of the tensile fracture surfaces of ZA27 alloy (a,c) Ascast ZA27 alloy (b,d) ZA27 alloy in solutionized condition.

4.2 MDF Processing Temperature

ZA27/SiC 5 wt% composite was cast and solutionized at 365 °C for 5 hours. This material is successfully processed by MDF at 100 °C upto three passes and at 200 °C upto six passes as shown in fig. 4.7. However material failed when processed at room temperature as Zn is the main alloying content with a hexagonal close-packed structure, which possesses limited slip systems (Purcek, 2005) and the presence of brittle and hard SiC particles further limits the plastic deformation of Zn based material at room temperature. Lower strain hardening and more number of slip systems are active for ZA27/SiC 5% composite at higher temperatures. These are the factors responsible for successful processing of ZA27 based composites at higher temperatures.

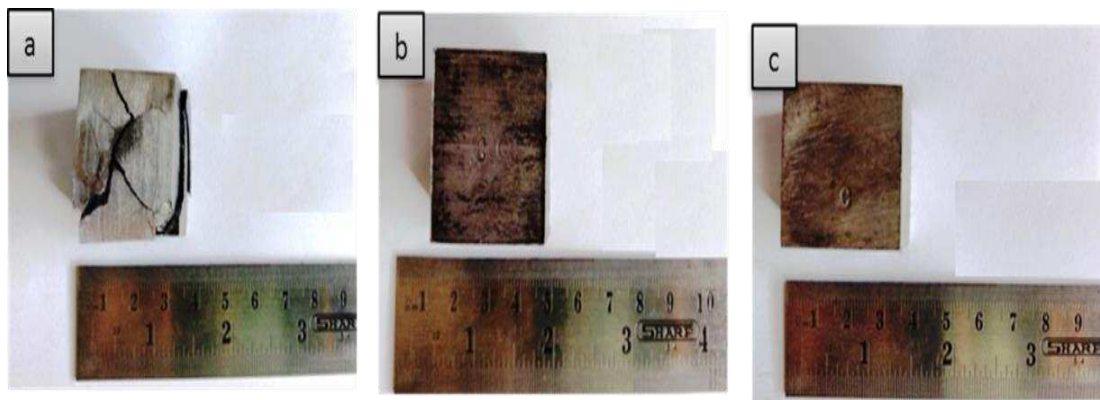


Figure 4.7: ZA27/SiC composite processed by MDF (a) At room temperature (b) Upto 3 passes at 100 °C (c) Upto 6 passes at 200 °C

4.3 ZA27 Reinforced with SiC Composites Properties Evaluation

4.3.1 Density

Physical properties depend on microstructure. In ZA-27 alloy the microstructure is a complex function of the casting process and subsequent cooling rates (Durman et al. 1997). Table 4.3 show the variations in theoretical and experimental density value with porosity percentage.

Table 4.3: Experimental and Theoretical density with porosity percentage of ZA27/SiC 5%

Sl. No	Sample Name	Experimental Density g cm^{-3}	Theoretical Density g cm^{-3}	Porosity %
1	Ascast SiC 5%	5.1454	5.1849	0.76
2	Homo SiC 5%	5.1583	5.1851	0.51
3	3P @ 100 SiC 5%	5.1644	5.1755	0.21
4	6P @ 200 SiC 5%	5.1678	5.1731	0.10
5	Ascast SiC 10%	5.1101	5.1372	0.52
6	Homo SiC 10%	5.1234	5.1475	0.46
7	3P @ 100 SiC 10%	5.1323	5.1414	0.17
8	6P @ 200 SiC 10%	5.1463	5.1525	0.12

Presence of voids or porosity in the cast sample leads to a considerable difference in experimental and theoretical density values. According to the rule of mixture incorporation of lower density SiC particle (3.21 g/cm^3) in higher density ZA27 alloy, ensures the density decrease in final composite. 10% of SiC reinforced composites showed less density as compared with 5% SiC reinforced composites. The discrepancy between theoretical and experimental density values were less in the case of MDF processed samples, as the number of passes increased. Mechanical working such as MDF processing reduces porosity level in cast materials. The difference in the density of ascast and solutionized sample could be due to the dimensional change in ZA27 alloy during the solutionizing treatment, in addition to that conversion of metastable phases to stable phase, which is retained by non-equilibrium solidification and solid-state transformation.

4.3.2 Microstructure

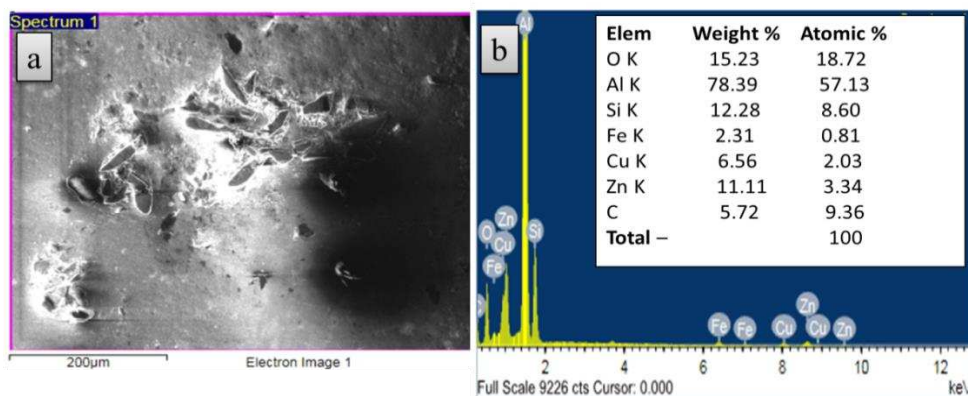


Figure 4.8: Energy dispersive spectroscopy images for alloy composition and presence of SiC particles confirmation

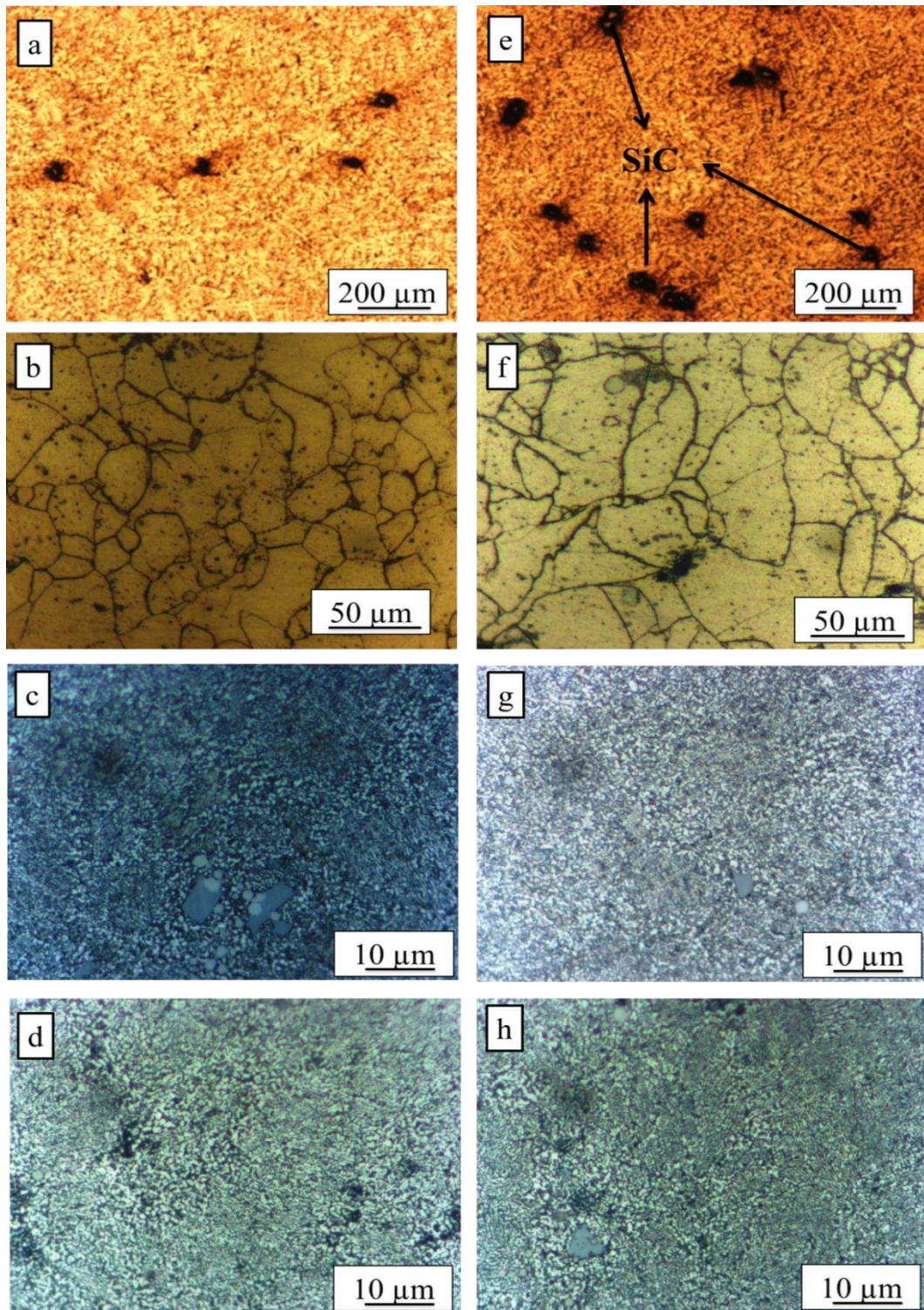


Figure 4.9: Optical microscopy images (a) Ascast ZA27/SiC 5% composite (b) Solutionized ZA27/SiC 5% composite (c) ZA27/SiC 5% MDF processed at 100 °C for 3 passes (d) ZA27/SiC 5% MDF processed at 200 °C for 6 passes (e) Ascast ZA27/SiC 10% composite (f) Solutionized ZA27/SiC 10% composite (g) ZA27/SiC 10% MDF processed at 100 °C for 3 passes (h) ZA27/SiC 10% MDF processed at 200 °C for 6 passes.

Microstructure plays a prominent role in the overall performance of the composites and alloys. The optical microstructure of ZA27 alloy and its composite in ascast condition shows the presence of dendritic structure with smaller in size because of squeezing pressure 120 MPa. Dendrite size in ZA-27 alloy is comparatively larger than that of the composite (Rafael et al. 2004). This refinement may be caused by the accumulation of the particles in the liquid between the growing dendrites, which seems to inhibit continued dendritic growth. Composition of ZA27 alloy and distribution of SiC particles is confirmed by the EDX analysis, which is shown in fig. 4.8. Some micro-constituents in the OM and SEM correspond mainly to the phases α -Al-rich fcc phase, β -Zn rich fcc phases, ϵ -CuZn₄ hexagonal close-packed phase, η -Zn rich hcp Phase, τ' -distorted bcc structure are shown in fig. 4.9 and 4.10. Samples after the solutionizing treatment dendritic structure will break and forms the grain structure as shown in fig. 4.9 (b, f). Dendrites grow away from the particle, due to the restriction caused by the particle to solute enrichment (Shanta et al. 2001). At 365 °C, the dissolution of Zn and Al takes place. Supersaturated β phase in as-quenched specimen later transformed to α , ϵ and η phases in both the composites reinforced with 5 and 10 wt% of SiC. Figure 4.9 (a, e) indicates some cluster and fair uniform distribution of SiC particles in ZA27/SiC composite material. It is clear from the optical microstructure of fig. 4.9 (c, g) that there is a substantial grain refinement due to the multidirectional forging process. Fine grains were seen in MDF processed samples for 3 passes at 100 °C and slightly less fine grain size observed in the MDF process sample for 6 passes at 200 °C. The SiC particle is completely surrounded by matrix material after the MDF process as compared with unprocessed composites and it is shown in fig. 4.9 (c, h). Porosity associated with particle clusters reduced after the MDF process. When ZA27 alloy is cooled from the melt condition to room temperature, it undergoes several phase transformations, like (α +L), β , (α + β), and finally (α + η) (Yao et al. 2004). The incorporation of low Cu in the Zinc aluminum alloy will lead to the development of an inter-metallic compound CuZn₄ (ϵ) at 377 °C (Fatih et al. 2005). With the SEM images, it is very much clear that dendritic structure can be seen in initial as-cast material, after solution heat treatment and MDF processing, dendritic structure converts almost into agglomerates of Zn-rich and Al-rich phase with lamellar structure.

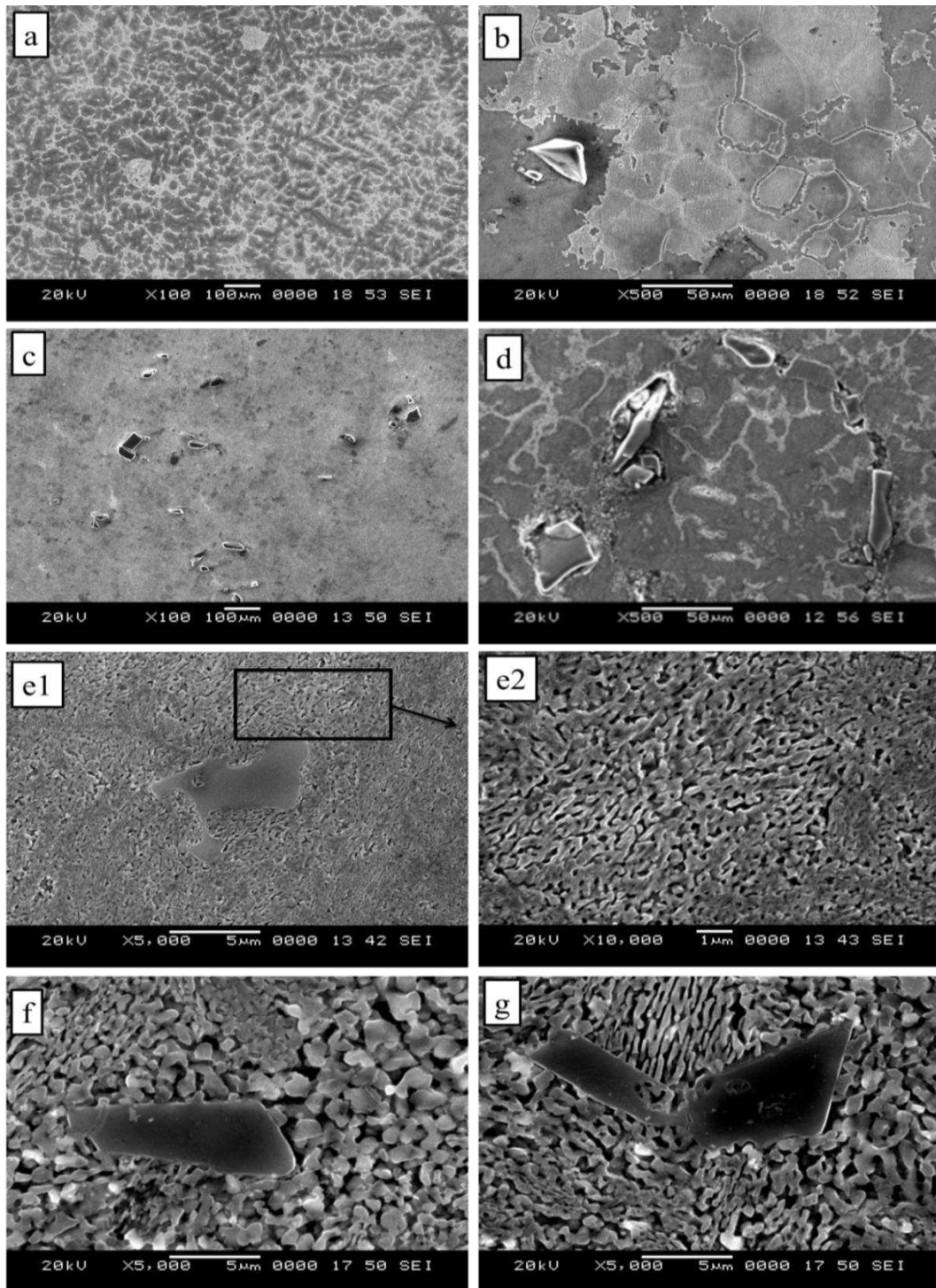


Figure 4.10: SEM images (a) Ascast ZA27/SiC 5% composite (b) Solutionized ZA27/SiC 5% composite (c, d) SiC Particle distribution in ZA27/SiC 5% composite (e1) ZA27/SiC 5% - MDF processed at 100 °C for 3 passes (e2) ZA27/SiC 5% - MDF processed at 100 °C for 3 passes (higher magnification x10,000) (f) ZA27/SiC 5% MDF processed at 200 °C for 6 passes showing cellular type of grains (g) ZA27/SiC 5% MDF processed at 200 °C for 6 passes showing mixture of cellular and lamellar type of grains structure.

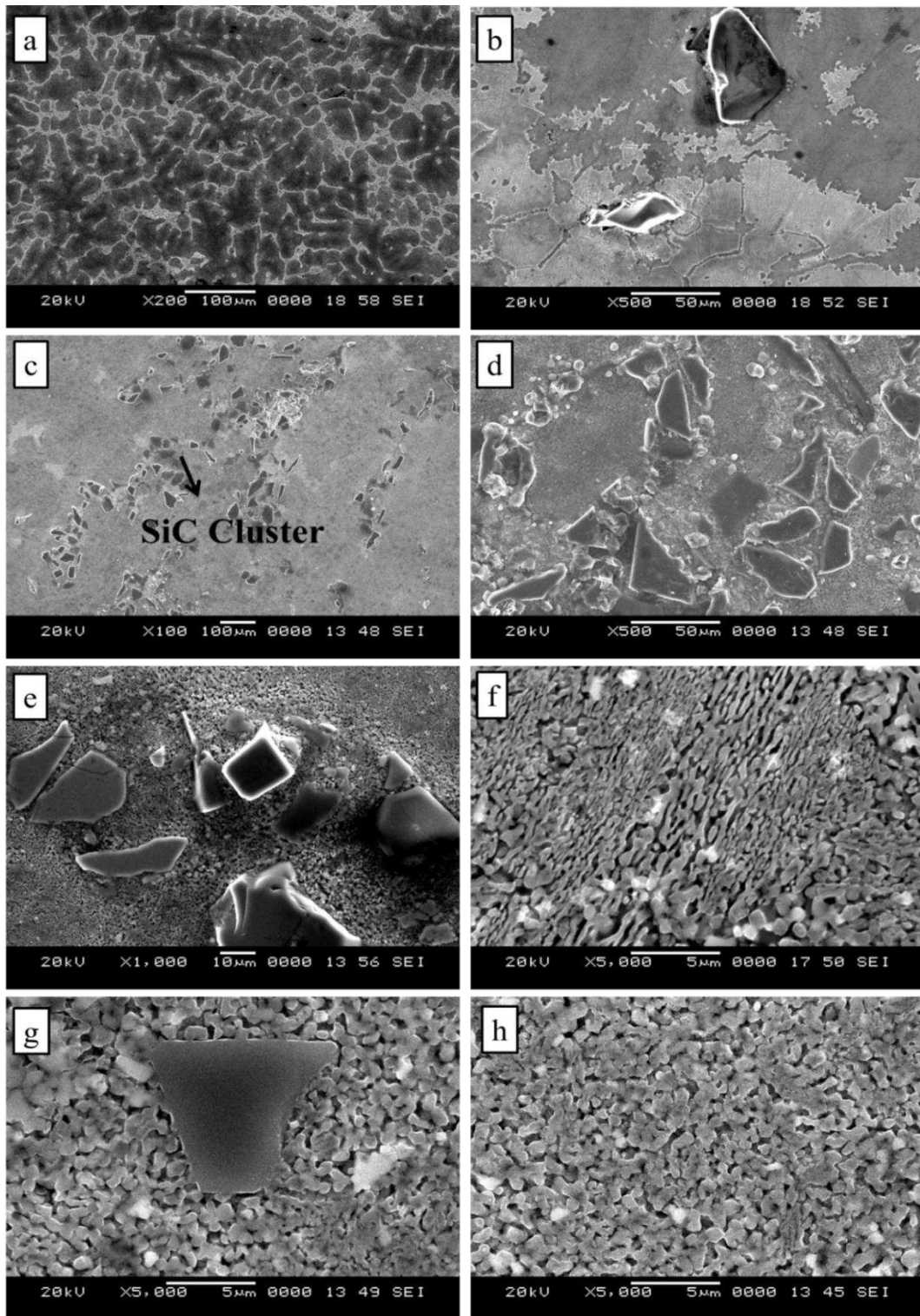


Figure 4.11: SEM images (a) Ascast ZA27/SiC 10% composite (b) Solutionized ZA27/SiC 10% composite (c, d) SiC Particle distribution in ZA27/SiC 10% composite (e) ZA27/SiC 10% - MDF processed at 100 °C for 3 passes (f) ZA27/SiC 10% - MDF processed at 100 °C for 3 passes (higher magnification x5,000) (g,h) ZA27/SiC 10% MDF processed at 200 °C for 6 passes showing cellular type of grain structure

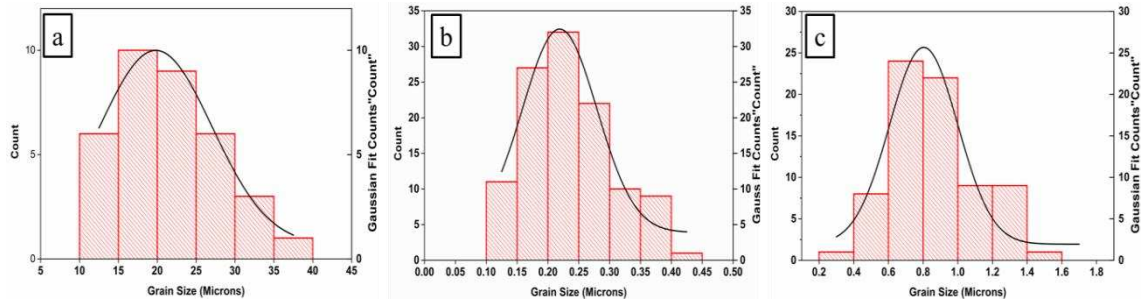


Figure 4.12: Grain size distribution curve a) Solutionized ZA27/SiC 5% composite b) ZA27/SiC 5% - MDF processed at 100 °C for 3 passes c) ZA27/SiC 5% - MDF processed at 200 °C for 6 passes

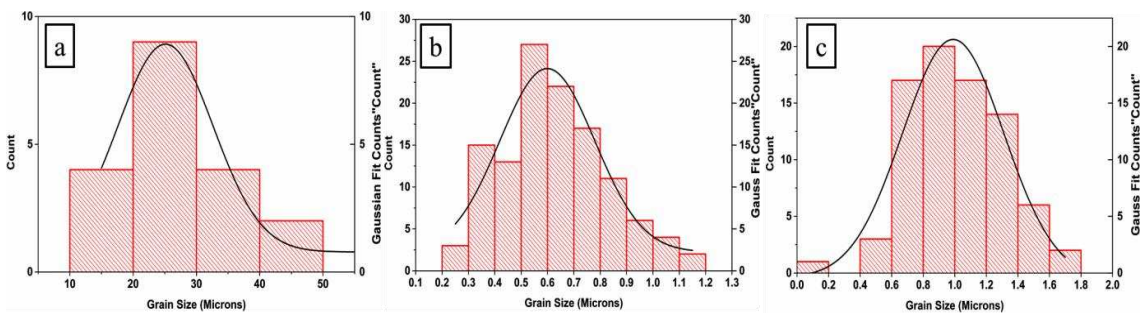


Figure 4.13: Grain size distribution curve a) Solutionized ZA27/SiC 10% composite b) ZA27/SiC 10% - MDF processed at 100 °C for 3 passes c) ZA27/SiC 10% - MDF processed at 200 °C for 6 passes

Similar kind of observation were made by many researchers on Zn base alloys (Fatih et al. 2005). Figure 4.10 shows the SEM images of (a) Ascast ZA27/SiC 5% composite (b) Solutionized ZA27/SiC 5% composite (c, d) SiC Particle distribution in ZA27/SiC 5% composite (e1) ZA27/SiC 5% - MDF processed at 100 °C for 3 passes (e2) ZA27/SiC 5% - MDF processed at 100 °C for 3 passes (higher magnification x10,000) (f) ZA27/SiC 5% MDF processed at 200 °C for 6 passes showing cellular type of grains (g) ZA27/SiC 5% MDF processed at 200 °C for 6 passes showing mixture of cellular and lamellar grain structure, and similar naming is also done to ZA27/SiC 10% reinforced. A coarse-grained structure in the unprocessed sample can be observed with the grain size of 20-25 μ m after solutionizing treatment of ZA27/SiC composites reinforced with SiC in 5 and 10 weight percentage which is as shown in fig. 4.10 (b) and fig. 4.11 (b) respectively. Fair distribution of SiC particles observed ZA27/SiC with 5wt % and few clusters were observed in 10wt % SiC reinforced composite (fig. 4.10 (c) and fig. 4.11 (c)). ZA27/SiC 5% composites processed with Multi-direction forging upto 3 passes at 100

°C shows ultrafine grain structure with an average grain size of 0.2-0.25 μm as shown in fig 4.10 (e₁,e₂) and ZA27/ SiC 10% composites processed with MDF upto 3 passes at 100 °C shows a UFG structure with a range of average grain size 0.4 -0.45 μm as shown in fig. 4.11 (e, f). After six passes of MDF at 200 °C, a homogeneous grain structure with a range of average grain size approximately 0.8-1 μm and 0.9-1.2 μm was achieved for ZA/SiC 5 and 10wt % composites respectively. Image J software was used to find the average grain size and corresponding grain size histogram was plotted for the confirmation of uniform grain size distribution, for convenience these plots were smoothed using gauss fit as shown in fig. 4.12 and 4.13. At 200 °C upto 6 passes MDF processed sample showed a larger grain size as compared with MDF processed samples at 100 °C upto 3 passes. This is due to grain growth in composite material processed at a higher temperature (Sharath et al. 2016). Figure 4.10 (f, g) shows ZA27/SiC 5% MDF processed at 200 °C for 6 passes having the mixture of cellular and lamellar grain structure. Either the eutectic or peritectic β phase transforms into lamellar α and η phases in the form of cellular decomposition (Li et al. 2006). In the case of ZA27/SiC 10% MDF processed at 200 °C for 6 passes showed uniformly distributed cellular structure, this indicates the transformation of lamellar to cellular is complete which is as shown in fig. 4.11 (g, h) and its appearance also confirms better bonding between the SiC particles and ZA27 matrix. Formation of ultrafine grain structure was attributed to very large strain deformation.

Transmission electron microscopy can be used to observe nano level grain size, twins, dislocations and some additional features within the microstructure of the material. Thin samples were prepared to render them transparent to the electron beam of the microscope. The electron beam undergoes diffraction by the regular crystal lattice planes into a diffraction pattern and contrast is generated in the image by this diffraction. Dislocations have different local atomic structures and produce a strain field, and therefore will cause the electrons in the microscope to scatter in different ways. Transmission electron microscope investigation results of ZA27 based SiC 5 wt% and 10 wt% reinforced composites are presented on fig. 4.14. Bright field TEM micrograph of ZA27/SiC 5% MDF processed at 100 °C for three passes (a), the width of the grains was around 200 to 250 nm. Further MDF processing upto 6 passes at 200 °C of composite lead to grain growth with an average grain size of 0.8 to 1 μm .

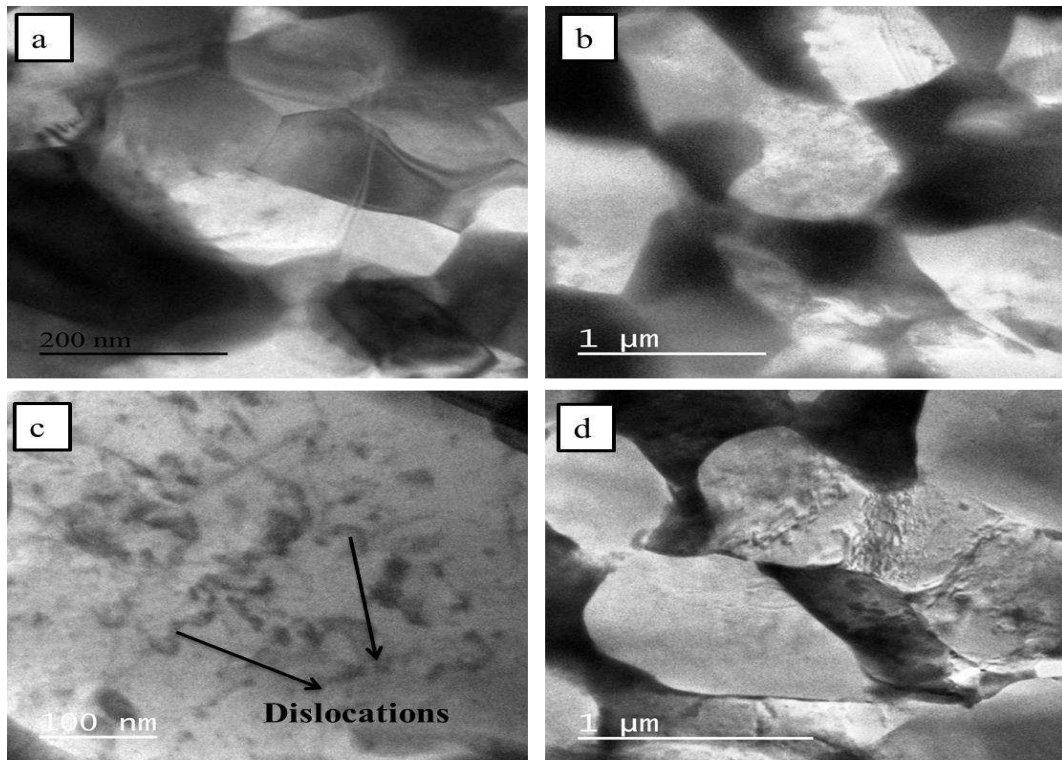


Figure 4.14: Bright-field TEM micrograph a) ZA27/SiC 5% MDF processed at 100 °C for three passes b) ZA27/SiC 5% MDF processed at 200 °C for six passes c) ZA27/SiC 10% MDF at 100 °C for three passes reveals a large number of dislocations d) ZA27/SiC 10% MDF processed at 200 °C for six passes.

Processing of ZA27/SiC composite material by multi directional forging at 100 °C and 200 °C temperatures introduces dislocation substructure in the grain interiors. During the early stages of deformation, high densities of dislocations are introduced into the material. Dislocations were observed with in the α phase which we can see in fig. 4.14 (c) and (d) gives a clear picture of grain boundaries and shape of grain which is almost equiaxed. The contrast mechanism in TEM images of multi-phase structures is different from that in SEM images and depends on preferential thinning, mean atomic number, crystal orientation and structure of the different phases present. In general, for ZA27 material aluminium-rich phases were light in tone, copper and zinc-rich phases and its precipitated phases were dark in the transmission electron micrographs. Figure 4.15 shows the EDS analysis of the TEM image of ZA27/SiC 10% MDF at 100 °C upto three passes for the identification of Al-rich phase and fig. 4.16 shows the EDS analysis of the TEM image of ZA27/SiC 10% MDF at 100 °C upto three passes for the identification of Zn rich phase.

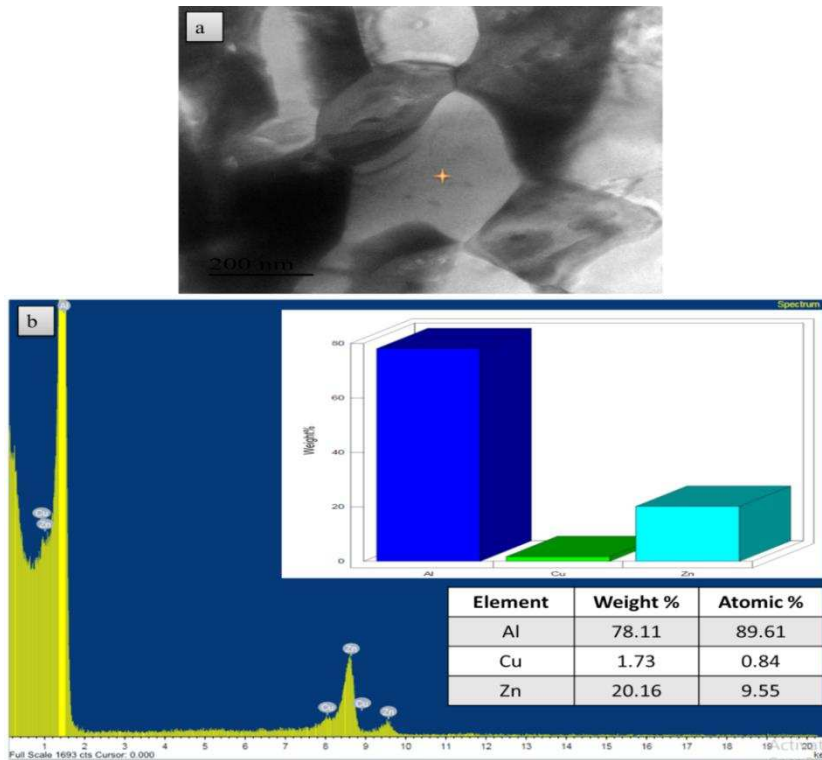


Figure 4.15: EDS analysis of the TEM image of ZA27/SiC 10% MDF at 100 °C upto three passes for the identification of Al-rich phase

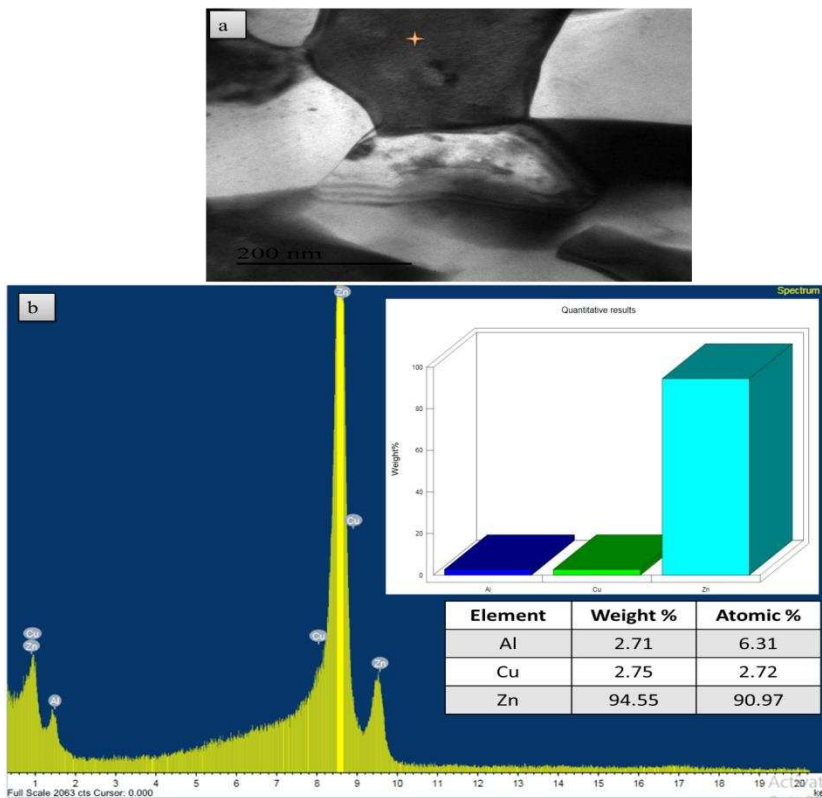


Fig. 4.16: EDS analysis of the TEM image of ZA27/SiC 10% MDF at 100 °C upto three passes for the identification of Zn rich phase

4.3.3 XRD Analysis

In ZA27 alloy and its composite system reinforced with SiC 5 and 10m wt%, α (Al-rich fcc), η (Zn rich hcp), ϵ (CuZn_4 hcp) phases are present and along with these, β (Zn rich fcc) phase is also present in solutionized condition as shown in fig. 4.17 and fig. 4.18. Presence of SiC is confirmed by matching peaks with JCPDS files of SiC - (00-019-0628) (00-031-1232) (00-037-0922) and it is shown in appendix AI-1.3. It is clear from the above XRD graphs that SiC particles did not react with the molten ZA27, nor carbide formed at the interface. This may be due to the low melting point of ZA27 alloy, which means that the temperature is insufficient to reach the free energies for interfacial reactions. Another possible reason is that SiC particles are thermodynamically stable in the ZA27 melt (Ablu et al. 2011). The intensity of α and η decreased after solutionizing in both the composites reinforced with 5 and 10wt % of SiC particles but 10% reinforced is very less as compared with 5% reinforced material. High-temperature solution heat treatment leads to a large extent of dissolution of η and α phases. This is due to natural aging at room temperature (Liu et al. 2013). Presence of SiC particles in ZA27 matrix facilitates the transformation of SiC neighbored matrix by accelerating Zn and Cu diffusion (Li et al. 2006). Plastic deformation due to subsequent MDF process has initiated the decomposition of β phase.

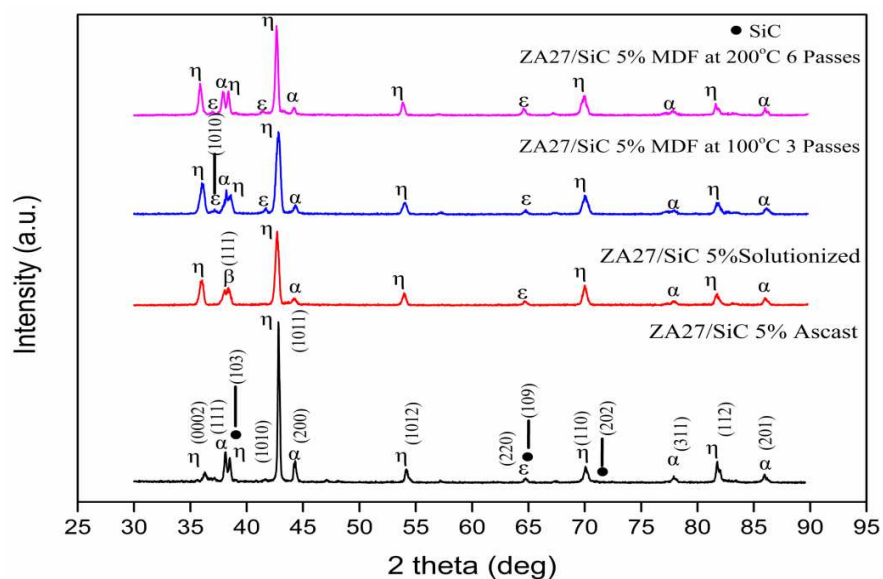


Figure 4.17: XRD patterns of ZA27 /SiC 5% ascast, solutionized and MDF processed at different temperature.

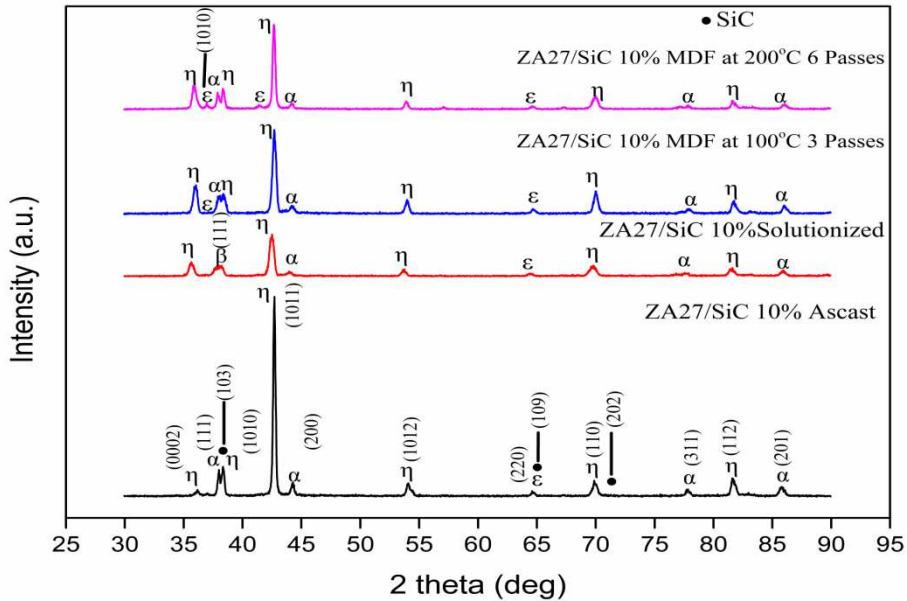


Figure 4.18: XRD patterns of ZA27/SiC 10% ascast, solutionized and MDF processed at different temperature.

Therefore, peak intensities for the β phase in the XRD profile decreased while those of α and η phases intensity increased after MDF processing at higher temperatures. MDF processing led to an increase in the intensity of η and α phases by replacing β phase. Presence of the ε phase can be observed in a sample of MDF processed at 100 °C for 3 passes and by further processing, at the higher temperature, the intensity of ε phase decreased. The intensity of α and η phase was the same after processing by MDF process at 200 °C upto 6 passes. The same type of trend was observed in both the composite materials reinforced with SiC at different weight percentage. Higher temperature improved the ability of diffusion and this initiated the diffusion of elements from a metastable state to a stable state (Yao et al. 2004).

4.3.4 Mechanical properties

Hardness measured on the plane perpendicular to the axis of the last forging axis of the MDF processed samples. Results of hardness value of ZA27/SiC 5% and ZA27/SiC 10% are shown in fig. 4.19 (a & b). The hardness value of ascast, solutionized MDF processed for 3 passes at 100 °C and 6 passes at 200 °C of ZA27/SiC 5% composite increased from 53 to 64, 79 and 76 HRB respectively and base alloy in ascast and solutionized condition showed lower hardness values of 40 and 51 respectively, when compared with composites and processed sample. Hardness

value of ZA27/SiC 10% composite shows a similar trend with increasing nature as illustrated in fig. 4.19 (b). In unprocessed condition SiC 10% reinforced material performs better when compared with 5 % reinforced material. But after processing SiC 5% reinforced composite performs better when compared with 10% this is due to small grain structure present in 5% reinforced material. Presence of hard SiC particles in soft matrix contributed to improvement in the hardness of composites. This improvement in hardness is also attributed to thermal strain mismatch between the SiC particle and ZA27 matrix during the casting process. These thermal strains value decreases as the distance between reinforcement and matrix interface increases. These thermal strains are primarily located near the reinforcement-matrix interface (Shanta et al. 2001).

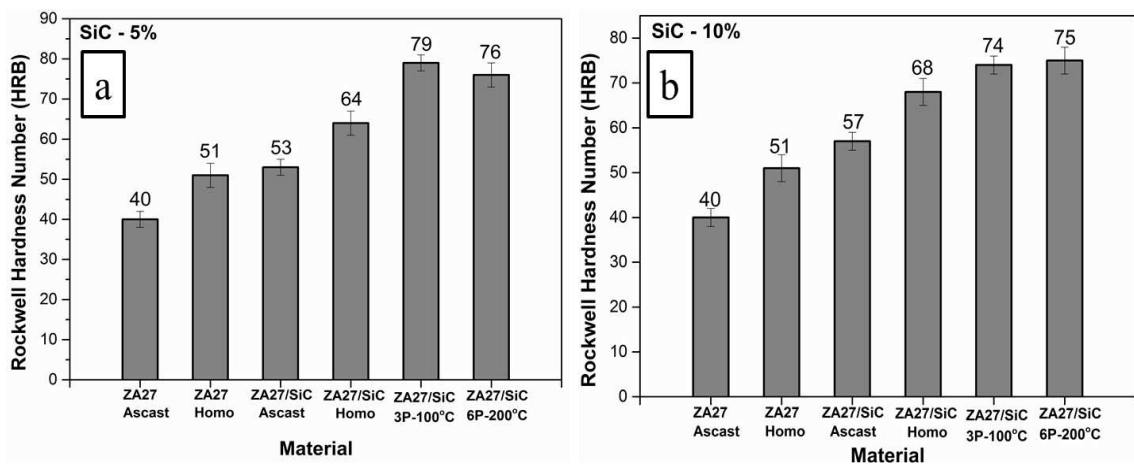


Figure 4.19: Rockwell hardness values of ascast and solutionized ZA27 alloy and ZA27/SiC composites MDF processed up to three passes at 100 °C and up to six passes at 200 °C. a) ZA27/SiC 5% b) ZA27/SiC 10%

Increase in the hardness of processed material due to the grain refinement with increased volume of grain boundaries which occur during plastic deformation. Figure 4.20 and 4.21 illustrates the engineering stress versus engineering strain for tensile test results of ZA27 ascast alloy and its SiC particles reinforced composite after solutionizing, MDF processing up to three passes at 100 °C and up to six passes at 200 °C. The elongation to fracture is a quantifiable measure of ductility and is taken as the strain at which the sample breaks. Initially ascast and solutionized ZA27/SiC 5wt % reinforced composite sample show a lower percentage of elongation with an increment in ultimate tensile strength from 312 to 363 MPa respectively.

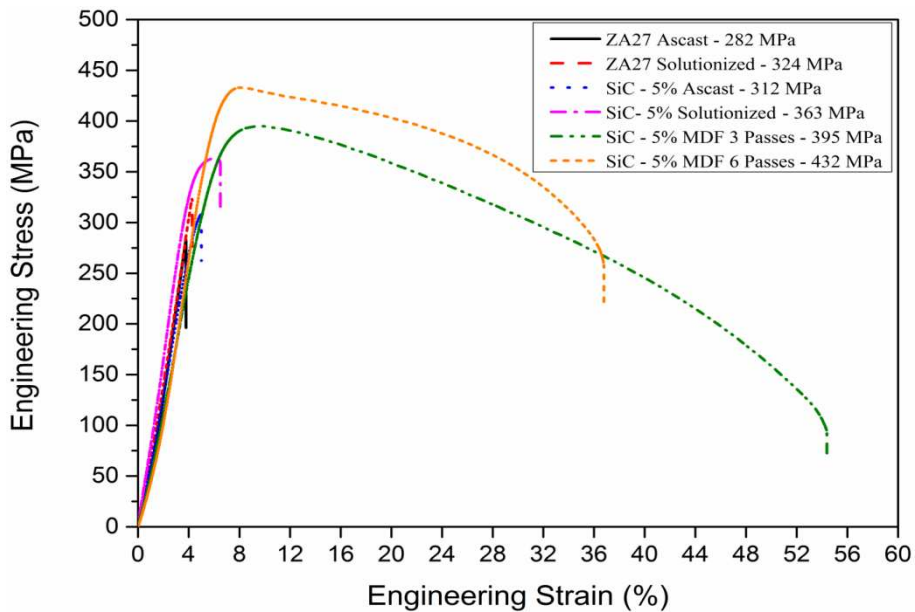


Figure 4.20: Engineering stress versus engineering strain for the tensile test of ZA27 ascast alloy and ZA27/SiC 5% composite after solutionized, MDF processed up to three passes at 100 °C and up to six passes 200 °C

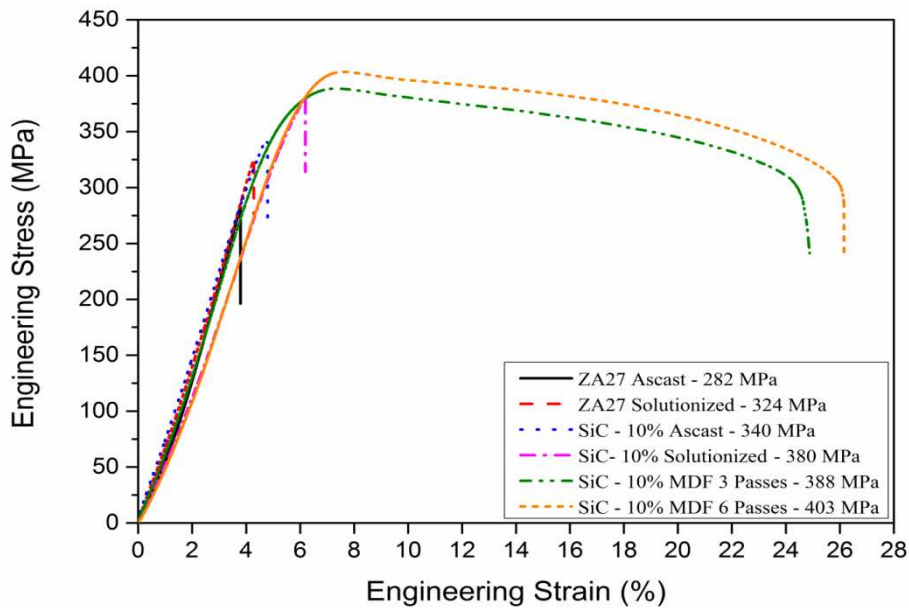


Figure 4.21: Engineering stress versus engineering strain for the tensile test of ZA27 ascast alloy and ZA27/SiC 10% composite after solutionized, MDF processed up to three passes at 100 °C and up to six passes 200 °C

However, after being processed by the MDF technique, the strength and ductility were improved simultaneously. Ultimate tensile strength and percentage of elongation for ZA27/SiC 5wt % sample processed at 100 °C up to 3 passes is 395 MPa and 54%,

respectively. ZA27/SiC 5wt % sample processed at 200 °C upto 6 passes showed the ultimate tensile strength of 432 MPa and 37% of elongation. But in the case of ZA27/SiC 10wt % composites showed better UTS in ascast and solutionized condition when compared with ZA27/SiC 5wt % composites ie., (340 and 380 MPa respectively). Furthermore, MDF processing of this composites leads to increase in UTS and percentage of elongation to 388 and 403 MPa, 25 and 26 % respectively. Repetitive pressing resulted in strain hardening which is the cause of dislocation multiplication. However, it is possible that the lamellae may block the sliding of equiaxed grains, leading to higher strength in the processed sample. Spherical and well spread Al-rich and Zn-rich phase obtained provides more equiaxed grains as seen in SEM micrographs presented in fig. 4.10 and 4.11. If the ultrafine grains are reasonably stable at elevated temperatures, there is a potential for achieving excellent superplastic properties (Roberto et al. 2009).

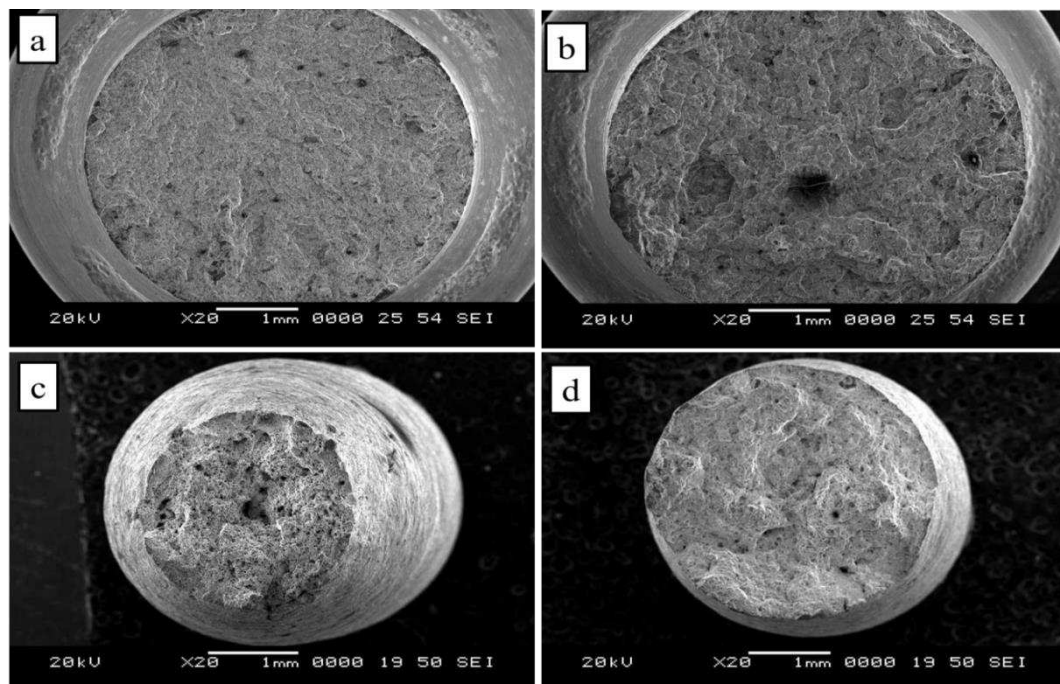


Figure 4.22: SEM images of the fracture surfaces of after tensile tests of ZA27/SiC 5% composite in macroscopic scale (a) Ascast ZA27/SiC 5% (b) Solutionized ZA27/SiC 5% (c) ZA27/SiC 5% MDF at 100 °C up to 3 passes (d) ZA27/SiC 5% MDF at 200 °C up to 6 passes

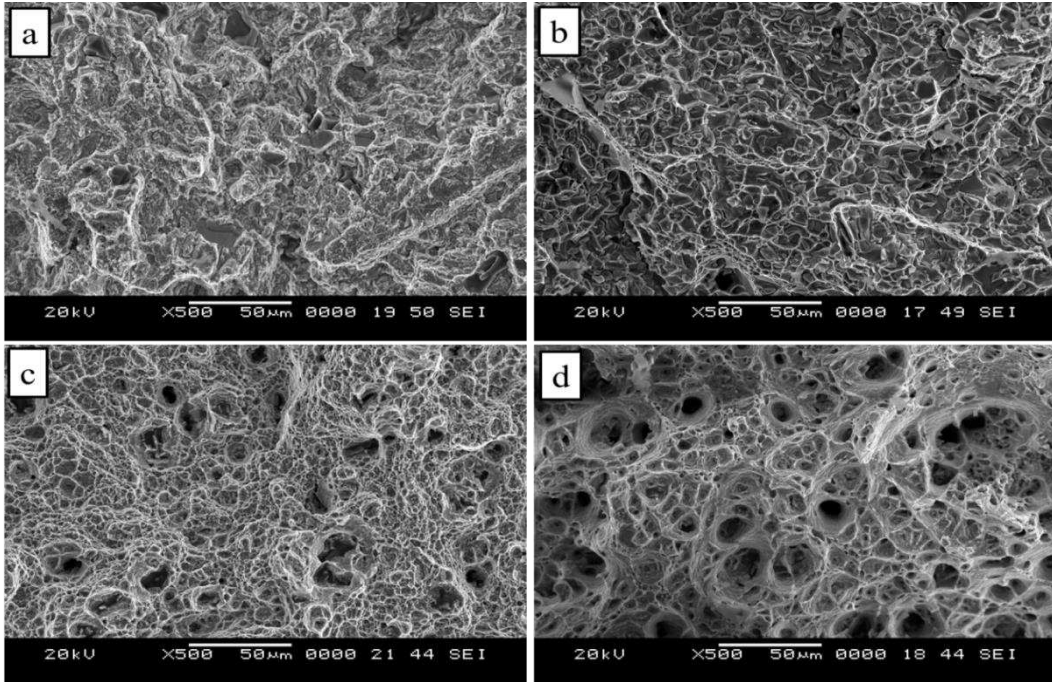


Figure 4.23: SEM images of the fracture surfaces of after tensile tests of ZA27/SiC 5% composite (a) Ascast ZA27/SiC 5% (b) Solutionized ZA27/SiC 5% (c) ZA27/SiC 5% MDF at 100 °C up to 3 passes (d) ZA27/SiC 5% MDF at 200 °C up to 6 passes

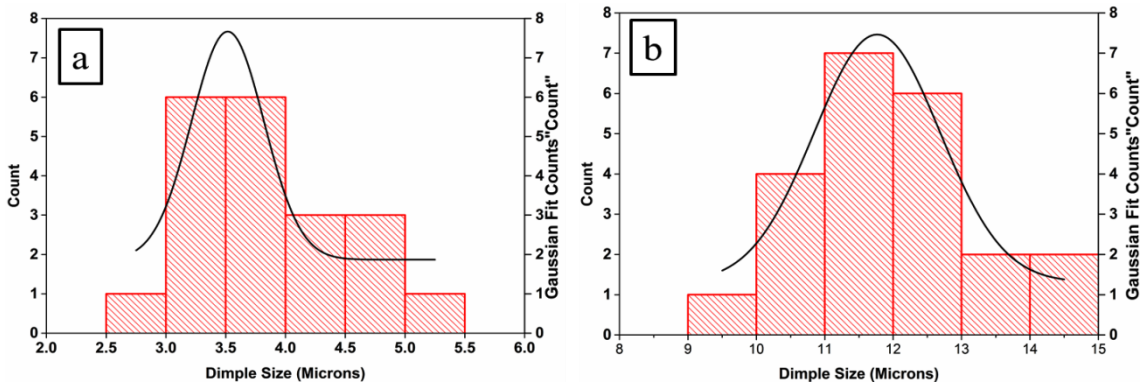


Figure 4.24: Dimple size distribution curve a) ZA27/SiC 5% - MDF processed at 100 °C for 3 passes b) ZA27/SiC 5% - MDF processed at 200 °C for 6 passes

Figure 4.22, 4.23, 4.25 and 4.26 shows the SEM micrographs of tensile fractured sample surface of ZA27 alloy and its SiC (5% and 10%) reinforced composite in both forged and unforged conditions. Fracture of particle reinforced metal matrix composites is very much dependent on particle strength and reinforcement/matrix interfacial bond strength. If the strength of the interface bonding between reinforcement and matrix is greater than the particle strength, then it leads to the fracture of particles before the interface. Matrix void growth and shear localization

between fractured particles resulted in the failure of the composites. When interfacial bonding strength between the reinforcement and matrix is much lower than particle strength lead to void nucleation and growth at the interface, due to decohesion of the matrix from the particle (Ranjit et al. 2007) (Williams et al. 2002). In SiC 5, 10 weight percentage reinforced composites in the ascast condition of both reinforced and unreinforced samples followed brittle mode fracture because of its dendritic structure, as a consequence of higher tendency of crack nucleation and propagation. Precipitation of non-equilibrium hard ϵ phase also contributes to the brittleness of as-cast materials. Dendritic structure contains interdendritic porosity during solidification process due to incomplete filling of the liquid melt is the cause for the brittle fracture in the as-cast materials. A similar result was observed by other researches in SiC and B₄C reinforced composite materials (Jian et al. 2016) (Tham et al. 2001) (Hamidreza et al. 2017) (Teng et al. 2016). In solution heat treated samples a small amount of dimples were seen in few regions and it is shown in fig. 4.23 (b) and 4.26 (b).

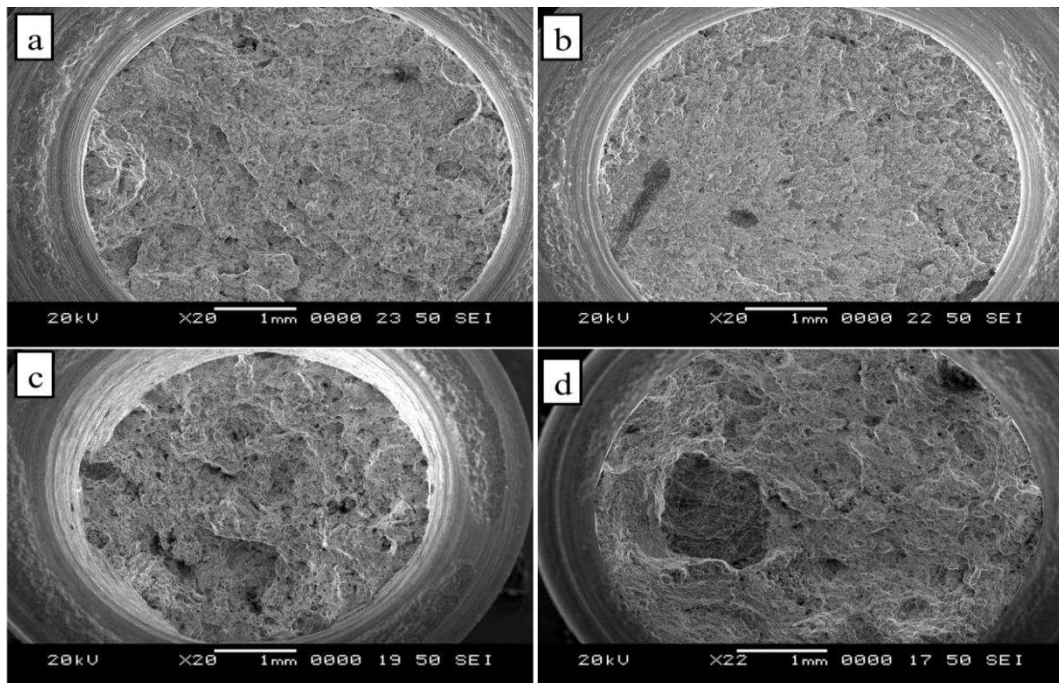


Figure 4.25: SEM images of the fracture surfaces of after tensile tests of ZA27/SiC 10 % composites in macroscopic scale (a) Ascast ZA27/SiC 10 % (b) Solutionized ZA27/SiC 10% (c) ZA27/SiC 10% MDF at 100 °C up to 3 passes (d) ZA27/SiC 10% MDF at 200 °C up to 6 passes.

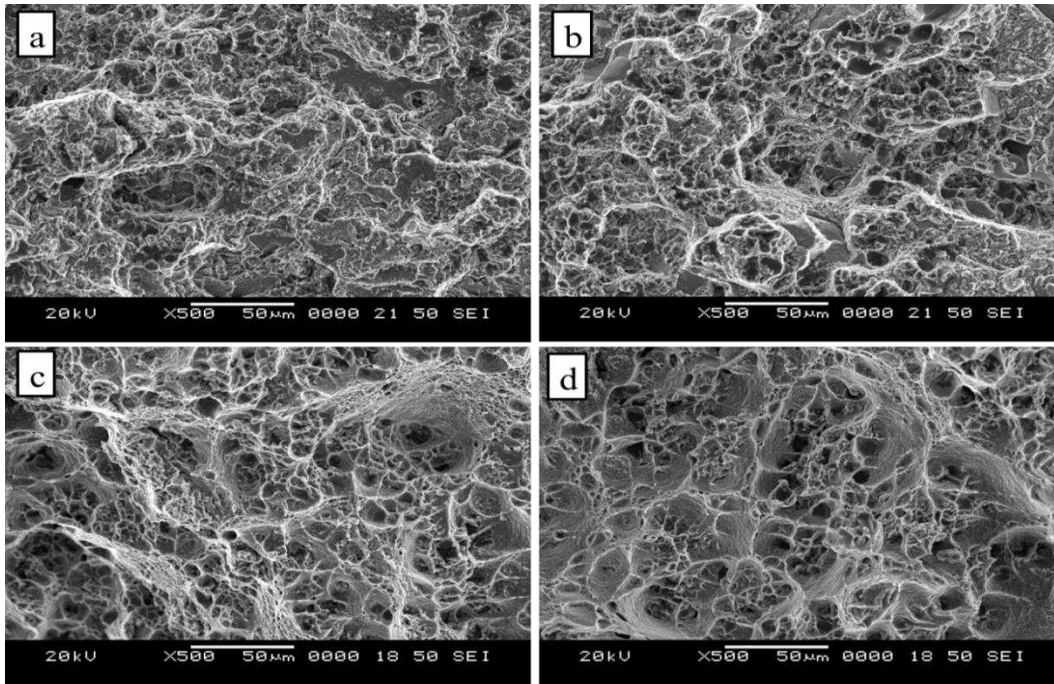


Figure 4.26: SEM images of the fracture surfaces of after tensile tests of ZA27/SiC 10 % composite (a) Ascast ZA27/SiC 10 % (b) Solutionized ZA27/SiC 10% (b) ZA27/SiC 10% MDF at 100 °C up to 3 passes (d) ZA27/SiC 10% MDF at 200 °C up to 6 passes

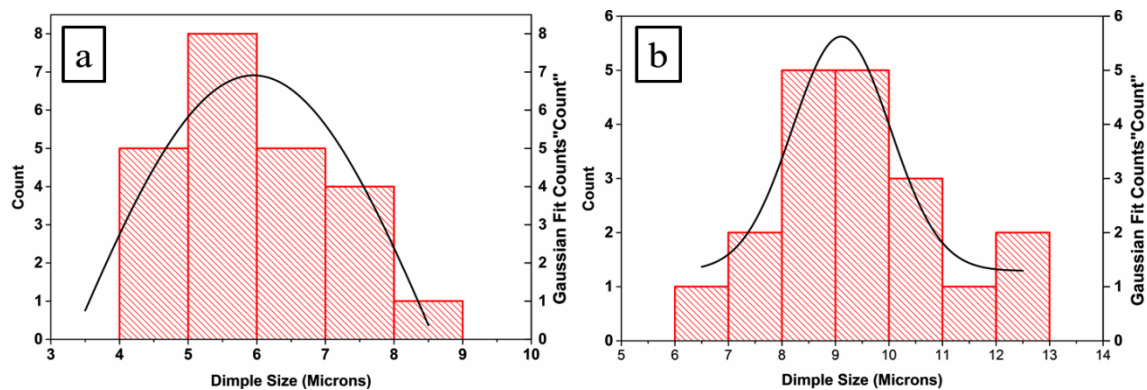


Figure 4.27: Dimple size distribution curve a) ZA27/SiC 10% - MDF processed at 100 °C for 3 passes b) ZA27/SiC 10% - MDF processed at 200 °C for 6 passes

For solutionized condition, fracture surface was composed of microporosities and dimples were larger in size with low ductility. The presence of dimples shows that the mode of fracture is changing from brittle to ductile. And there is no much significant difference between fig. 4.22 and 4.25 it has almost the same trend as that of ascast condition showing brittle, solutionized condition little ductile and in MDF processed condition shows completely ductile nature. Micrographs of the fractured surface at lower magnification is also taken at the equidistance to show the mode of fracture

which is shown in fig. 4.22 and 4.25 for 5 wt % and 10 wt % reinforced composites respectively. For 5 wt % SiC reinforced composites processed by MDF at 100 °C upto 3 passes is having finer grain size as well as dimple size (3-4 μm) as compared with samples of MDF processed at 200 °C upto 6 passes(11-13 μm). For 10wt % SiC reinforced composites processed by MDF at 100 °C upto 3 passes is having finer dimple size of 5-6 μm as compared with samples of MDF processed at 200 °C upto 6 passes 8-9 μm . The dimple size distribution curves are fitted with guess fit and is shown in fig. 4.24 and 4.27. Material is completely converted from brittle mode to ductile mode of fracture and formed cup and cone type of failure which is clearly indicated in the macroscopic scale as shown in fig. 4.22 and 4.25. After MDF processing dimples size decreased and showed a homogeneous distribution across the fracture surfaces. This shows improved ductility compared to solutionized material.

4.3.5 Wear Properties Evaluation of ZA27/SiC reinforced composites

Composite materials usually demonstrate enhanced tribological behavior such as lower wear rate, higher wear resistance than that of alloys, due to the strength improvement of the composites achieved by adding the particles as reinforcement into the matrix. Wear behaviour of the ZA27 alloy and its composites have been tested with varying applied load (39.24N, 49.05N & 58.86N) and sliding distance (2000m and 4000m) at a constant sliding velocity of 1 ms^{-1} . Wear rate increased for samples tested with 4000m of sliding distance as compared with 2000m and is as shown in fig. 4.28 and fig. 4.30. Both 5 wt% and 10 wt% reinforced composites showed better wear resistance than that of base alloy. Improvement of wear resistance was observed by addition of SiC particles from 5 wt% to 10 wt%. The presence of SiC particles improved the wear resistance of ZA27 alloy as it is correlated with hardness by Archard equation (Purcek et al. 2010). Applied load has a major influence on wear rate than that of sliding distance. Wear resistance of the material decreased with increase in applied load and sliding distance. The positive effect of SiC towards enhancement of the wear behaviour of the ZA27 material was confirmed by Mitrovic et al. 2012. MDF processed sample showed better wear resistance as compared with unprocessed composite and it is shown in fig. 4.29 and fig. 4.31.

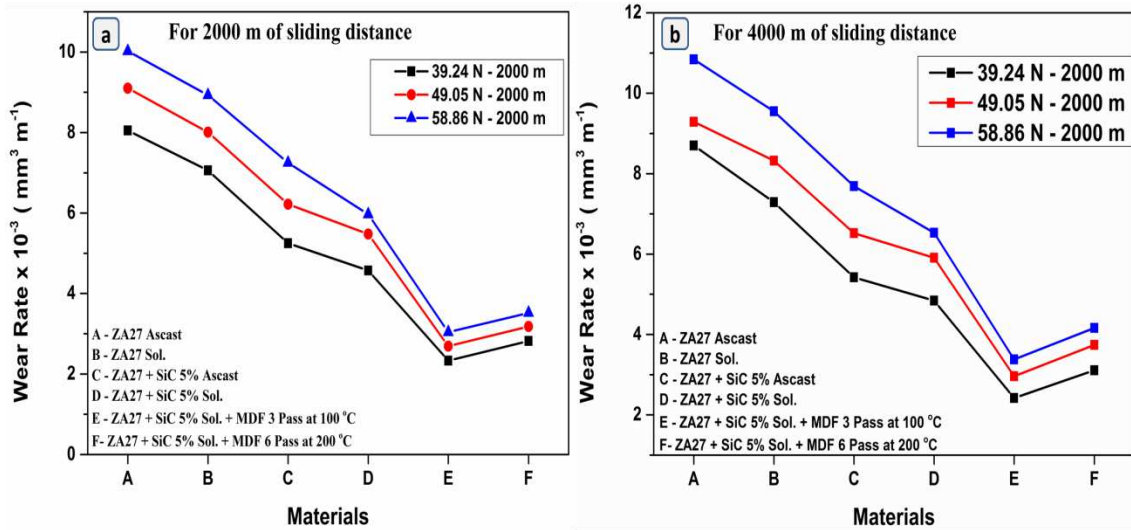


Figure 4.28: Wear rate of ZA27/ SiC 5 wt% composite in different condition (a) For 2000m of sliding distance (b) For 4000m of sliding distance.

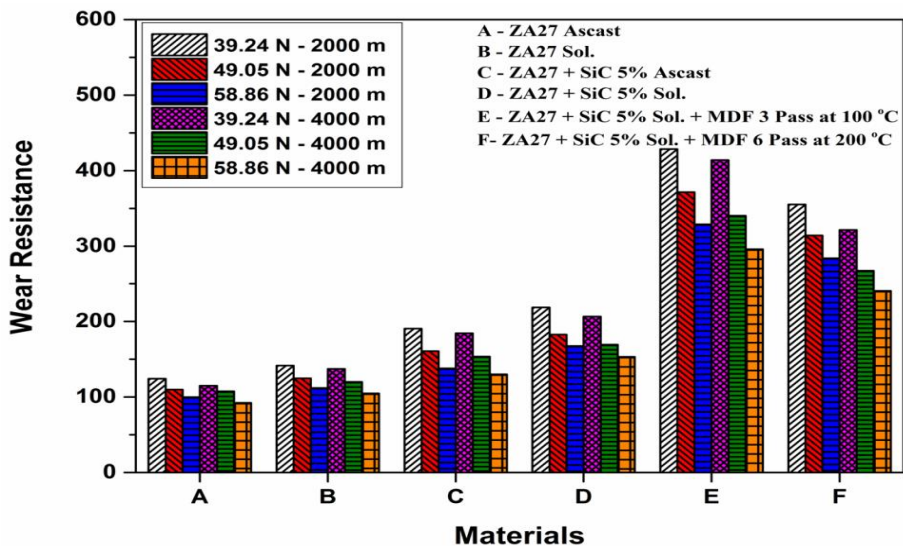


Figure 4.29: Wear Resistance of ZA27/ SiC 5wt% composite in different condition

The improvement in wear behavior of processed samples was due to the enhanced mechanical properties of the ZA27/SiC 5 wt% and 10 wt% composite materials. In both the case MDF processed upto 3 and 6 passes at 100 °C and 200 °C performed better than that of unprocessed composite materials. But MDF processed upto 3 passes at 100 °C have maximum wear resistance due to the presence of micro constituents and by formation of ultrafine grain structure.

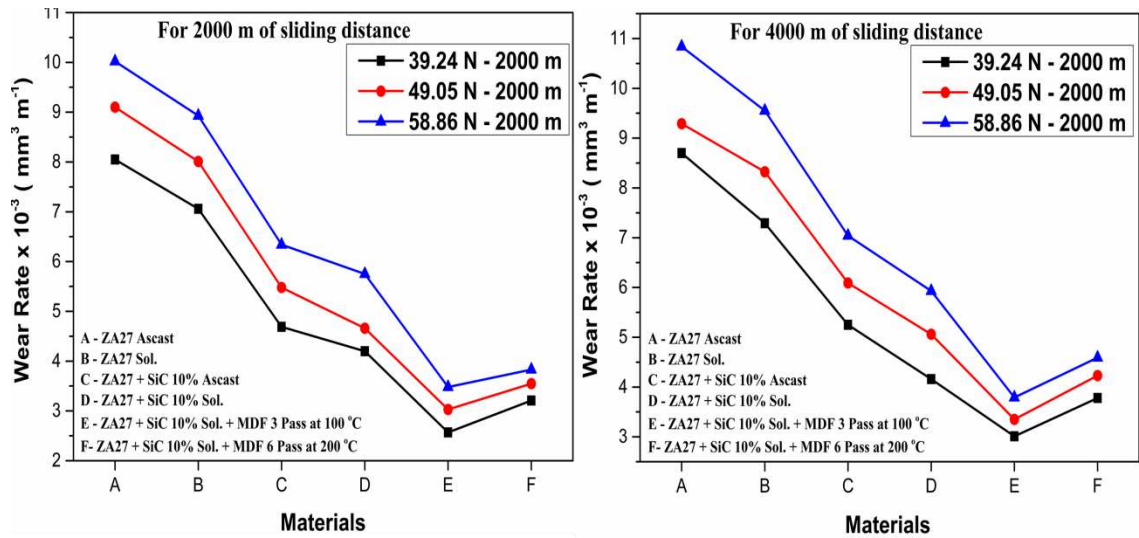


Figure 4.30: Wear rate of ZA27/ SiC 10 wt% composite in different conditions (a) For 2000m of sliding distance (b) For 4000m of sliding distance.

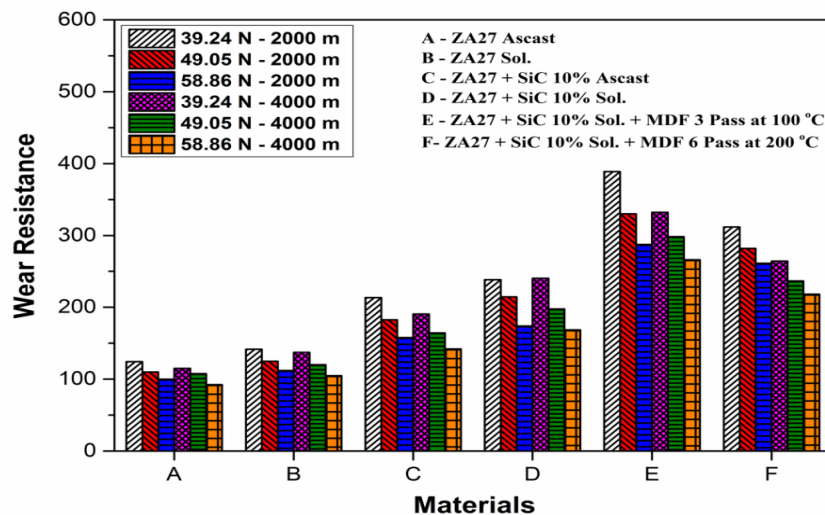


Figure 4.31: Wear Resistance of ZA27/SiC 10wt% composite in different conditions.

For brevity and convenience, only few micrographs have been presented in fig. 4.33 which shows the worn surface morphology of ZA27 alloy and ZA27 reinforced with 5 wt% and 10 wt% of SiC particles. The white color arrow mark in all the images indicates sliding direction. Wear surface of ZA27/SiC_p samples tested at 39.24N and 2000m with a constant sliding velocity of 1 ms⁻¹ revealed some scratches and grooves caused by abrasive action of hard ϵ particle in the form of debris removed from the sample surface and these particles caught in between the mating surface causing abrasion which shows that the main wear mechanism is abrasive type for lower load

and shorter sliding distance condition. Presence of SiC_P and debris of the base matrix material shown in fig. 4.33 (c) has a major influence on wear behaviour of material. Some micro cracks were observed in fig. 4.33 (d).

At higher applied load and sliding distance the debris gets smeared and adhered to surface of pin which in turn increases the temperature between the pin and disc causing lower wear resistance with an adhesive type of wear mechanism (fig. 4.33 (f)). In mentioned research (Abou El-khair et al. 2004) the observations indicated that severe adhesive wear took place by material transfer from the pin to the steel ring and detachment of long arc shaped metallic debris from the pin material was seen. A similar type of observation was made by other researchers showing particle reinforced composites perform better as compared with unreinforced ones with dual type of wear mechanism (Aleksandar et al. 2014). Figure 4.32 shows the energy dispersive X-Ray spectroscopy analysis of the worn surfaces after wear tests, carried out at 39.24 N load with 2000 m of sliding distance and at 1 m/s sliding speed, for ZA27/ SiC 5 wt% ascast condition. The scanned region confirms the presence of Al-31.31, Zn-66.62, Cu-2.52, Fe- 2.51 and any type of oxide layer was not found.

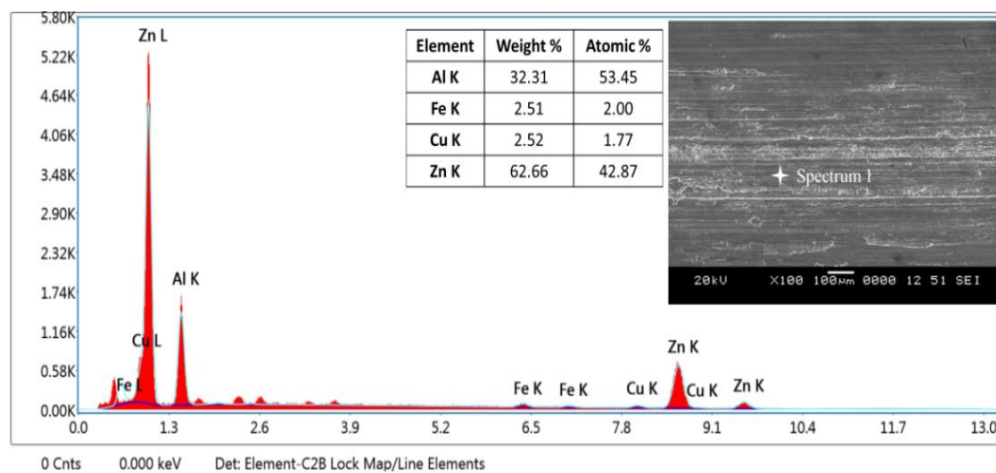


Figure 4.32: EDS analysis of the worn surfaces of composite material (ZA27/SiC 5% ascast - 39.24N - 2000m

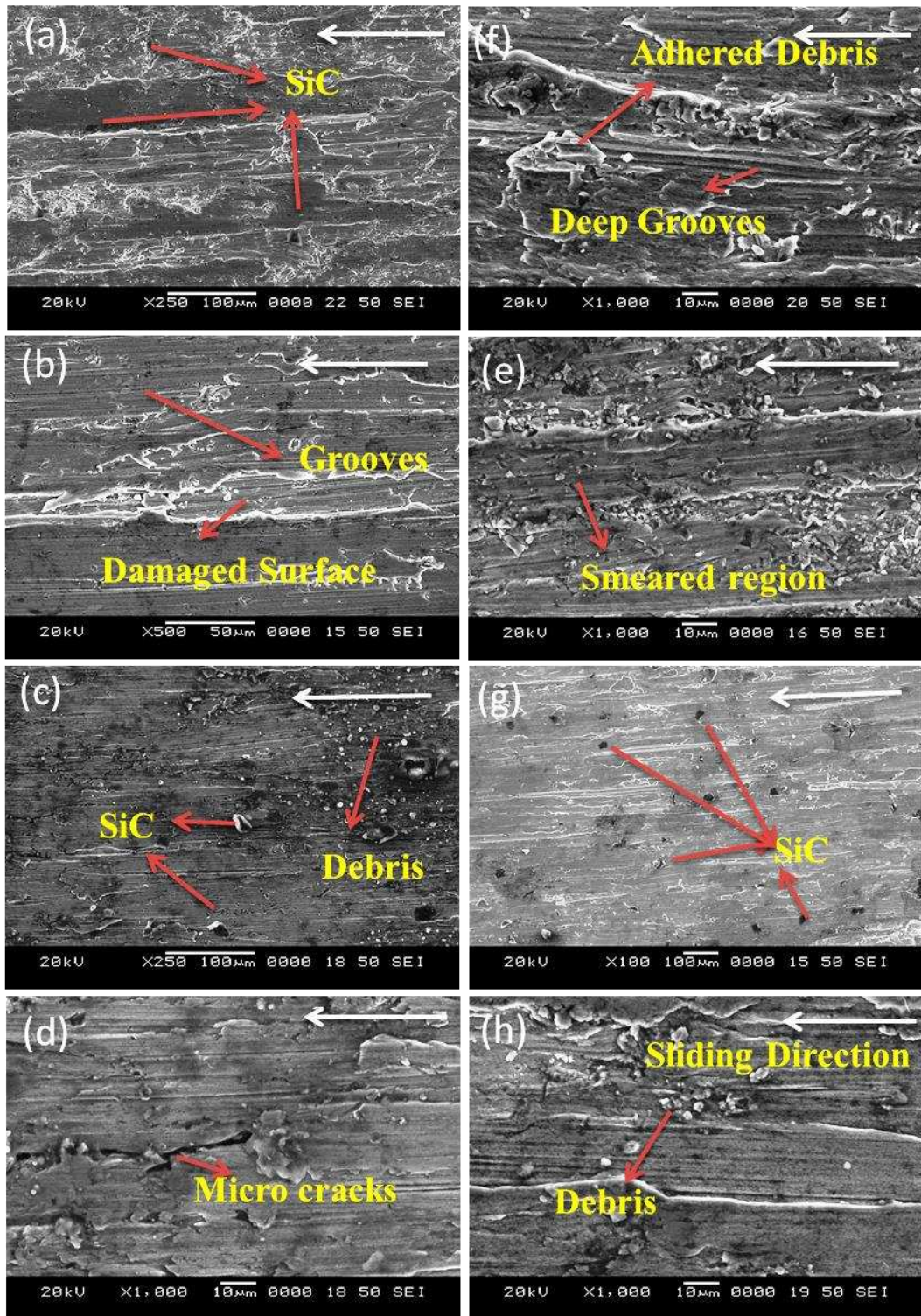


Figure 4.33: SEM micrographs of the worn surfaces of ZA27/SiC in 5 & 10 wt%. (a) ZA27/SiC 5% sol - 39.24N - 2000m (b) ZA27/SiC 5% -MDF 3 Pass 49.05N - 2000m (c) ZA27/SiC 5%-MDF 6 pass 58.86N - 2000m (d) ZA27/SiC 5% sol-39.24N - 4000m (e) ZA27/SiC 5%-MDF 3 pass- 49.05N - 4000m (f) ZA27/SiC 5%- MDF 6 Pass- 58.86N - 4000m (g) ZA27/SiC 10%- ascact 39.24N – 2000 (h) ZA27/SiC 10%- MDF 3 pass- 49.05N - 4000m

4.4 ZA27 REINFORCED WITH Al₂O₃ COMPOSITES PROPERTIES EVALUATION

4.4.1 Density

The porosity and density of the ZA27 alloy and its composites reinforced with Al₂O₃ particles in various weight percentage (5 and 10 wt %) are given in table 4.4. The results show that incorporation of Al₂O₃ leads to the reduction in the density of the composites in comparison to that of the ZA27 alloy because of the lower density value 3.91 g cm⁻³ of Al₂O₃ particles as compared to that of ZA27 alloy. The density of 10% Al₂O₃ reinforced material is less when compared to 5% Al₂O₃ reinforced composite and unreinforced ZA27 alloy. It has been found that the porosity percent in 10% Al₂O₃ reinforced composite is higher than that of composite reinforced with 5% Al₂O₃, this is due to a higher amount of gas entrapment during the stirring processing.

Table. 4.4: Experimental and Theoretical density with porosity percentage of ZA27/Al₂O₃ 5% and 10%

Sl. No	Sample Name Al ₂ O ₃ 5% and 10%	Experimental Density g cm ⁻³	Theoretical Density g cm ⁻³	Porosity %
1	Ascast Al ₂ O ₃ 5%	5.1658	5.1932	0.52
2	Homo Al ₂ O ₃ 5%	5.1714	5.1899	0.35
3	3P @ 100 Al ₂ O ₃ 5%	5.1786	5.1897	0.21
4	6P @ 200 Al ₂ O ₃ 5%	5.179	5.1886	0.18
5	Ascast Al ₂ O ₃ 10%	5.1499	5.2112	1.17
6	Homo Al ₂ O ₃ 10%	5.1536	5.1901	0.70
7	3P @ 100 Al ₂ O ₃ 10%	5.1641	5.1736	0.18
8	6P @ 200 Al ₂ O ₃ 10%	5.169	5.1764	0.14

In both the cases after solutionizing heat treatment, the density value increased in small amount because of homogeneous distribution of phases during the solutionizing process. Composites reinforced with 5 and 10 wt% of Al₂O₃ particles were MDF processed at 100 °C upto 3 passes and at 200 °C upto 6 passes increased the density of the composite by reducing the porosity percentage. As the number of passes increases the density value also increased. During MDF processing the material is forced to fill into the voids related defects to produce a dense material.

4.4.2 Microstructure

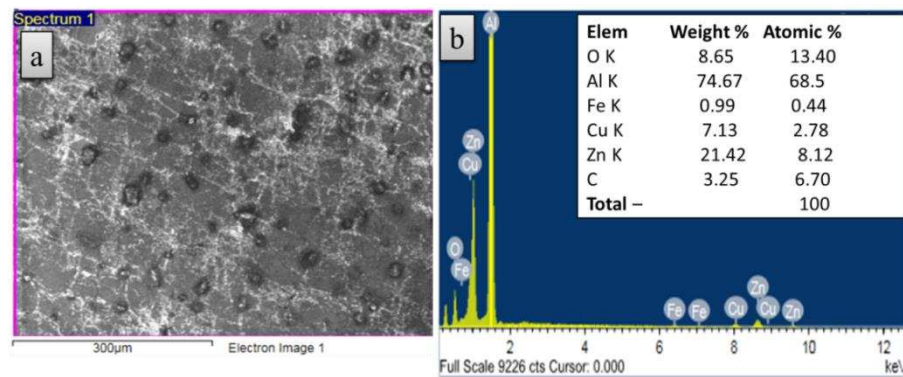


Figure 4.34: Energy dispersive spectroscopy images for alloy composition and presence of particles confirmation

The specimens for metallographic examination were prepared using standard polishing technique and then etched with 3% nital. The microstructural features were examined before and after the MDF process. For the MDF processed composites, metallographic specimens were machined from the centre area of the billet and which is perpendicular the final forged axis. Figure 4.34 (a, b) shows the distribution of Al_2O_3 particles in ZA27 matrix and composition of the ZA27/ Al_2O_3 composite material.

The microstructure of ZA27 as-cast alloy contains aluminum-rich matrix (α -fcc) and an interdendritic zinc-rich phase (η -hcp), (ϵ - CuZn_4), (τ' -distorted bcc structure - $\text{Zn}_{10}\text{Al}_{35}\text{Cu}_{55}$). Figure 4.35 (a, b, e, f) shows the optical micrographs of ascast and solutionized ZA27/ Al_2O_3 5% and 10% composite. The distribution of Al_2O_3 particles are nearly uniform in the ZA27 matrix. However, there are clusters of Al_2O_3 within some areas of the matrix, while other areas are entirely depleted from Al_2O_3 particles. Particle size of Al_2O_3 is around 20-40 microns with an irregular shape. Microstructure changed significantly after the MDF process and this process led to a substantial refinement and equiaxed microstructure with fragmented microconstituents were observed in fig. 4.35 (c, d, g, h). whereas composites of ZA27/ Al_2O_3 5% and 10% MDF processed at 100°C for 3 passes, ZA27/ Al_2O_3 5% and 10% MDF processed at 200°C for 6 passes respectively were processed. In few areas of particle located region showed sound bonding between the particles and matrix by the application of external load during MDF processing.

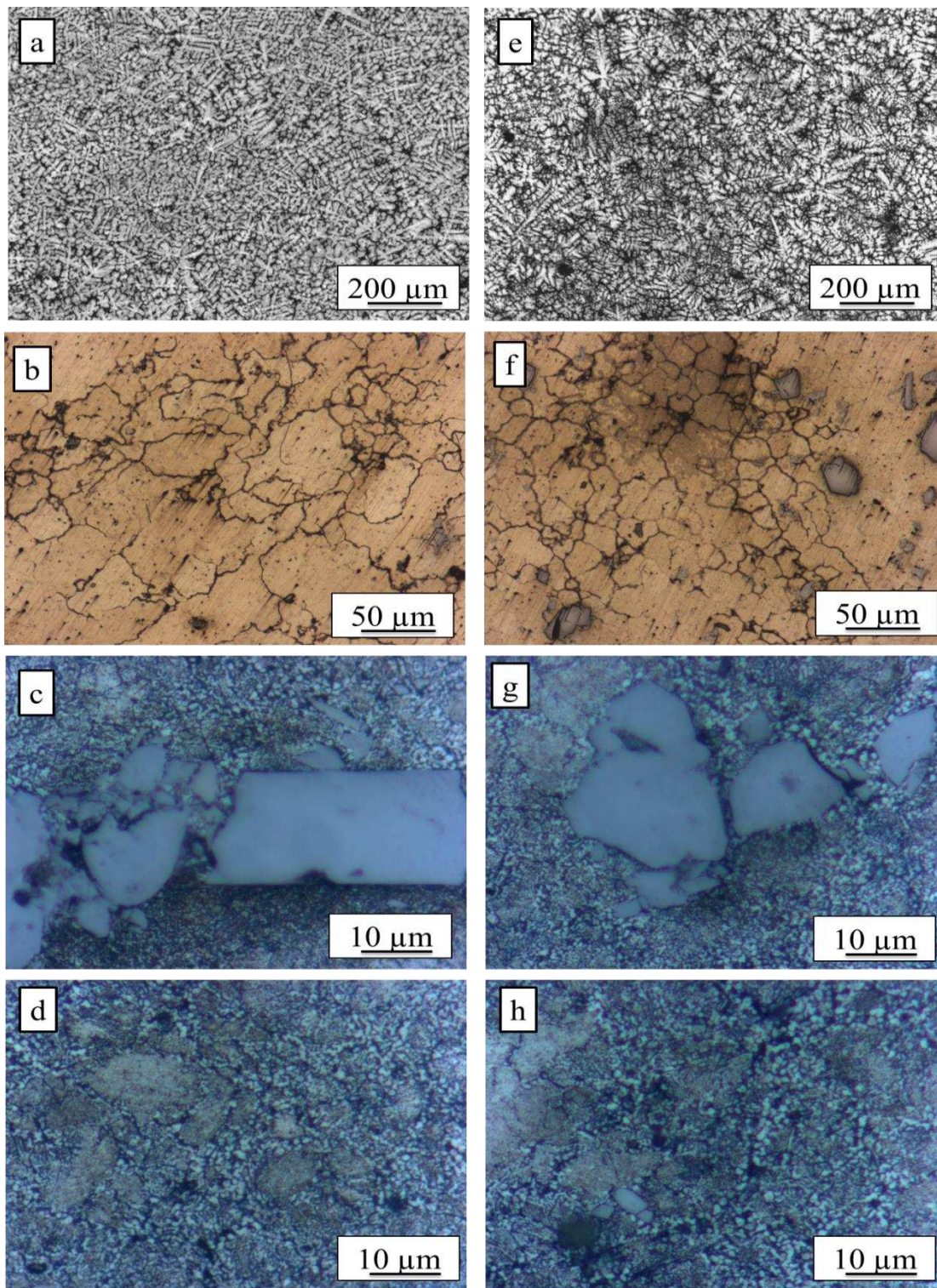


Figure 4.35: Optical microscopy images (a) Ascast ZA27/Al₂O₃ 5% composite (b) Solutionized ZA27/Al₂O₃ 5% composite (c) ZA27/Al₂O₃ 5% MDF processed at 100 °C for 3 passes (d) ZA27/Al₂O₃ 5% MDF processed at 200 °C for 6 passes (e) Ascast ZA27/Al₂O₃ 10% composite (f) Solutionized ZA27/Al₂O₃ 10% composite (g) ZA27/Al₂O₃ 10% MDF processed at 100 °C for 3 passes (h) ZA27/Al₂O₃ 10% MDF processed at 200 °C for 6 passes

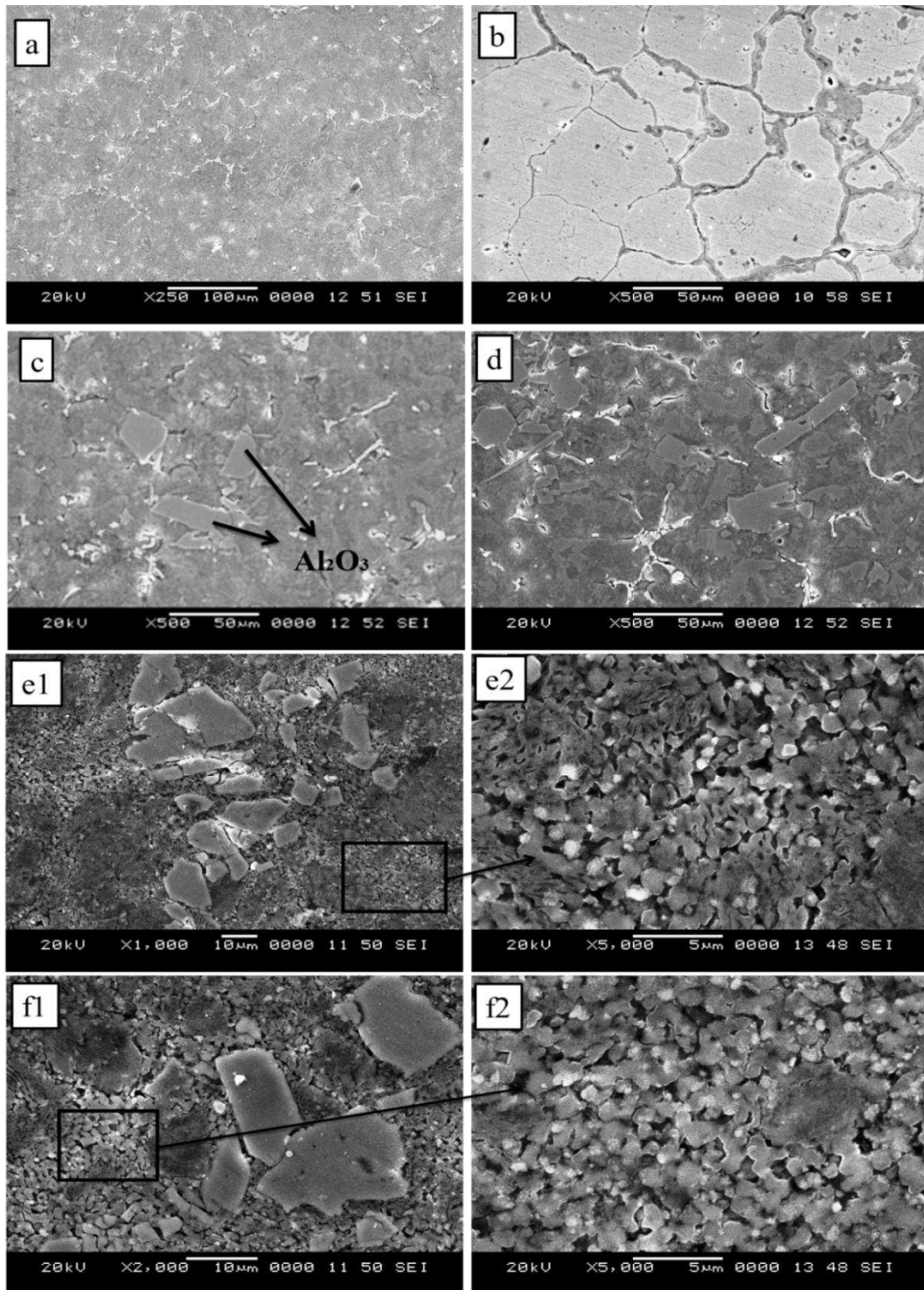


Figure 4.36: SEM images (a) Ascast ZA27/Al₂O₃ 5% composite (b) Solutionized ZA27/ Al₂O₃ 5% composite (c, d) Al₂O₃ Particle distribution in ZA27/ Al₂O₃ 5% composite (e1) ZA27/ Al₂O₃ 5% - MDF processed at 100 °C for 3 passes (e2) ZA27/ Al₂O₃ 5% - MDF processed at 100 °C for 3 passes (higher magnification x 5,000) (f1) ZA27/ Al₂O₃ 5% MDF processed at 200 °C for 6 passes showing cellular type of grains (f2) ZA27/ Al₂O₃ 5% MDF processed at 200 °C for 6 passes (higher magnification x 5,000)

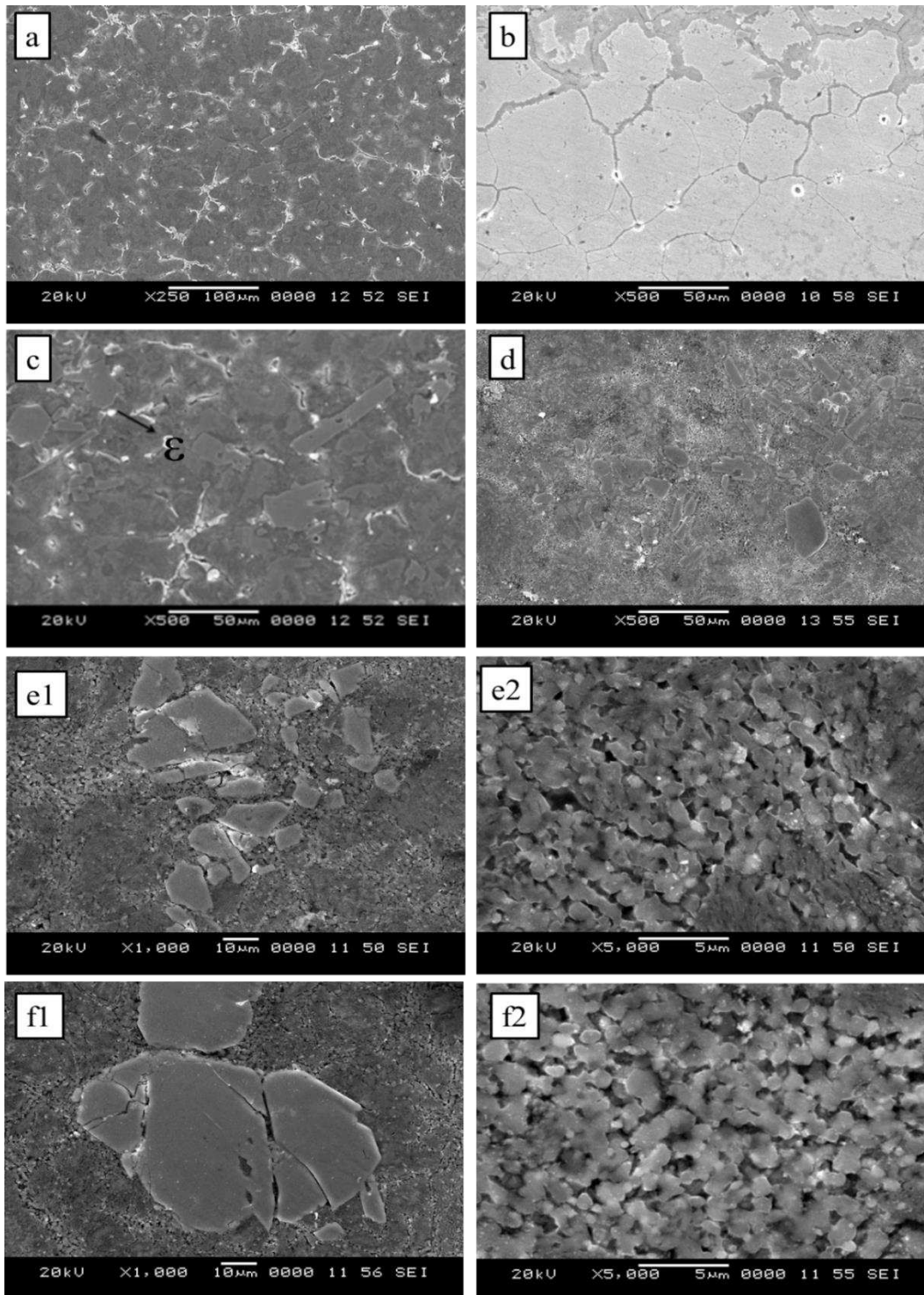


Figure 4.37: SEM images (a) Ascast ZA27/Al₂O₃ 10% composite (b) Solutionized ZA27/ Al₂O₃ 10% composite (c, d) Al₂O₃ Particle distribution in ZA27/ Al₂O₃ 10% composite (e1) ZA27/ Al₂O₃ 10% - MDF processed at 100 °C for 3 passes (e2) ZA27/ Al₂O₃ 10% - MDF processed at 100 °C for 3 passes (higher magnification x 5,000) (f1) ZA27/ Al₂O₃ 10% MDF processed at 200 °C for 6 passes showing cellular type of grains (f2) ZA27/ Al₂O₃ 10% MDF processed at 200 °C for 6 passes (higher magnification x 5,000).

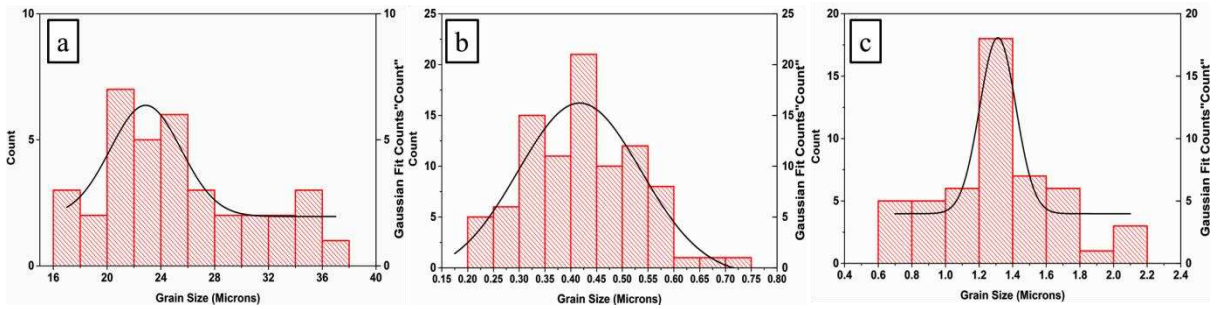


Figure 4.38: Grain size distribution curve a) Solutionized ZA27/ Al_2O_3 5% composite b) ZA27/ Al_2O_3 5% - MDF processed at 100 °C for 3 passes c) ZA27/ Al_2O_3 5% - MDF processed at 200 °C for 6 passes

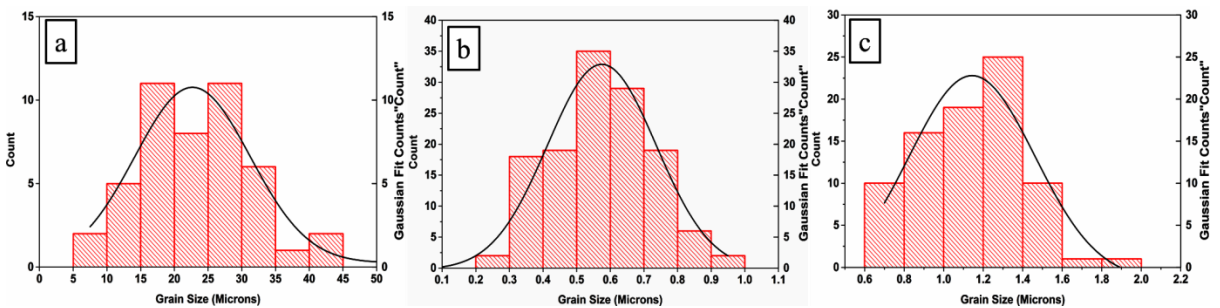


Figure 4.39: Grain size distribution curve a) Solutionized ZA27/ Al_2O_3 10% composite b) ZA27/ Al_2O_3 10% - MDF processed at 100 °C for 3 passes c) ZA27/ Al_2O_3 10% - MDF processed at 200 °C for 6 passes

There is a refinement in grain structure upto certain level but at the cost of particle crack. Small grain structure was observed with ZA27/ Al_2O_3 which are MDF processed at 100 °C for 3 passes as compared with MDF processed at 200 °C for 6 passes. The SEM micrographs of ZA27/ Al_2O_3 5% (fig. 4.36 (a,b)) in ascast and solutionized condition showed dendritic and grain structure respectively. Figure 4.36 (c, d) shows the distribution of Al_2O_3 . It can be noted that the Al_2O_3 particles are located at the interdendritic regions. The reason could be lower thermal conductivity of ceramic particles than those of ZA27 alloy. Therefore, the particles are not able to cool down as fast as the ZA27 melt. As a result, the temperature of the particles is slightly higher than that of the liquid alloy. The hotter particles may heat up the liquid in their immediate surroundings and thus delay solidification of the surrounding liquid. Moreover, the latent heat of fusion released during solidification of the matrix will reduce the cooling rate of the particles, resulting in temperature gradients such that the particles and melt in its vicinity will continue to be hotter than the melt away

from the particles. Thus, the nucleation and growth of different phases occur away from the particles, pushing the particles to the last freezing regions (interdendritic regions). It is worth noting that the presence of the particles in the ZA27 affected the matrix microstructure of the resultant composites. The measured grain size in solutionized was 25-30 μm . ZA27/ Al_2O_3 5% composites after MDF process upto 3 passes at 100 °C shows the grain size reduced from 25-30 μm to 0.4-0.45 μm with the dual type of microstructure having both lamellar to the cellular structure. On further MDF processing at 200 °C upto 6 passes showed the grain size of 1.2-1.4 microns with equiaxed grain structure, this increase in grain size is due to the rise in temperature of processing condition (grain growth process). Small cracks were seen at the edges of the Al_2O_3 particle because of load applied during MDF process upto 3 passes at 100 °C and with a higher number of passes the Al_2O_3 particle broken into several pieces and form a cluster of Al_2O_3 particle as shown in fig. 4.36 (f1) and 4.37 (f1). Grain size distribution curve was plotted with the help of Image J software and the curve is fitted using guess fit as shown in fig 4.38. The same type of structure was seen in ZA27/ Al_2O_3 10% composites in ascast and solutionized condition when compared with ZA27/ Al_2O_3 5%. The initial grain size in the solutionized condition is 25-30 μm . Figure 4.37 (c,d) shows the uniform distribution of Al_2O_3 particles in ZA27 matrix and the presence of ϵ is also clearly visible. A similar type of grain reduction trend was seen i.e., ZA27/ Al_2O_3 10% reinforced composites when MDF processed at 100 °C upto 3 passes showed refined grain structure with a grain size of 0.5-0.6 microns. on further processing upto 6 passes at 200 °C leads to grain growth (1.2-1.5 μm) as shown in fig. 4.37 (e1, f1). The lower magnification images were taken to show the distribution and interfacial bonding between the particles and matrix. The enlarged view of fig. 4.37 (e1 and f1) is 4.37 (e2 and f2) which gives a noticeable change in grain refinement at different processing condition. Formation of ultrafine grain structure was attributed to very large deformation strain. The grain size of ZA27/ Al_2O_3 10% composite is slightly larger than that of ZA27/ Al_2O_3 5%, this is due to the presence of a larger amount of Al_2O_3 particles which restrict the further grain size reduction. Figure 4.39 shows the grain size distribution curve which is smoothed by Gauss function. Microstructures of the ZA27/ Al_2O_3 composites using the bright field technique are as shown in fig. 4.40. Application of huge amount of total

equivalent strain into the material one can achieve smaller grain structure by subdivision of original coarse grains with heavily misoriented fractions. The lamellar grain can be observed in fig. 4.40 (a) which is an alternate layer of α & η . On further processing this lamellar structure will break and form an equiaxed structure with an average grain size of 300 to 400 nm shown in fig. 4.40 (b) for MDF processed ZA27/ Al_2O_3 10wt% reinforced composite material at 200 °C up to six passes with total equivalent strain of 1.08.

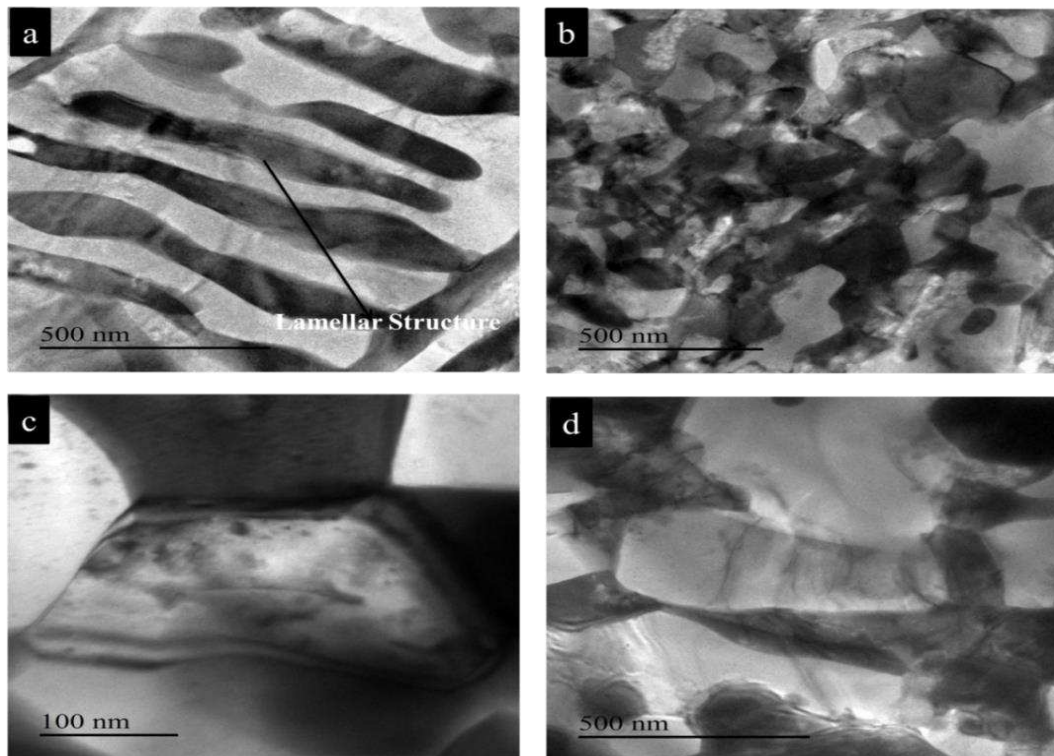


Figure 4.40: Bright-field TEM micrograph a) ZA27/ Al_2O_3 5% MDF processed at 100 °C for three passes showing lamellar structure b) ZA27/ Al_2O_3 5% MDF processed at 200 °C for six passes showing equiaxed structure c) ZA27/ Al_2O_3 10% MDF at 100 °C for three passes d) ZA27/ Al_2O_3 10% MDF processed at 100 °C for three passes showing dislocation.

Figure 4.40 (c) TEM micrograph of MDF processed material at 100 °C up to three passes with 10 wt % reinforcement clearly showing grain boundaries with an average grain size of 300 to 350 nm. Figure 4.40 (d) it shows that dense dislocations are entangled with each other inside the Al rich phase. In fig. 4.40 (b) ZA27/ Al_2O_3 5% MDF processed at 200 °C for six passes showed some small amount of precipitates at the right bottom corner of the image. EDX analysis was performed to know the concentration of precipitate which is shown in fig. 4.41.

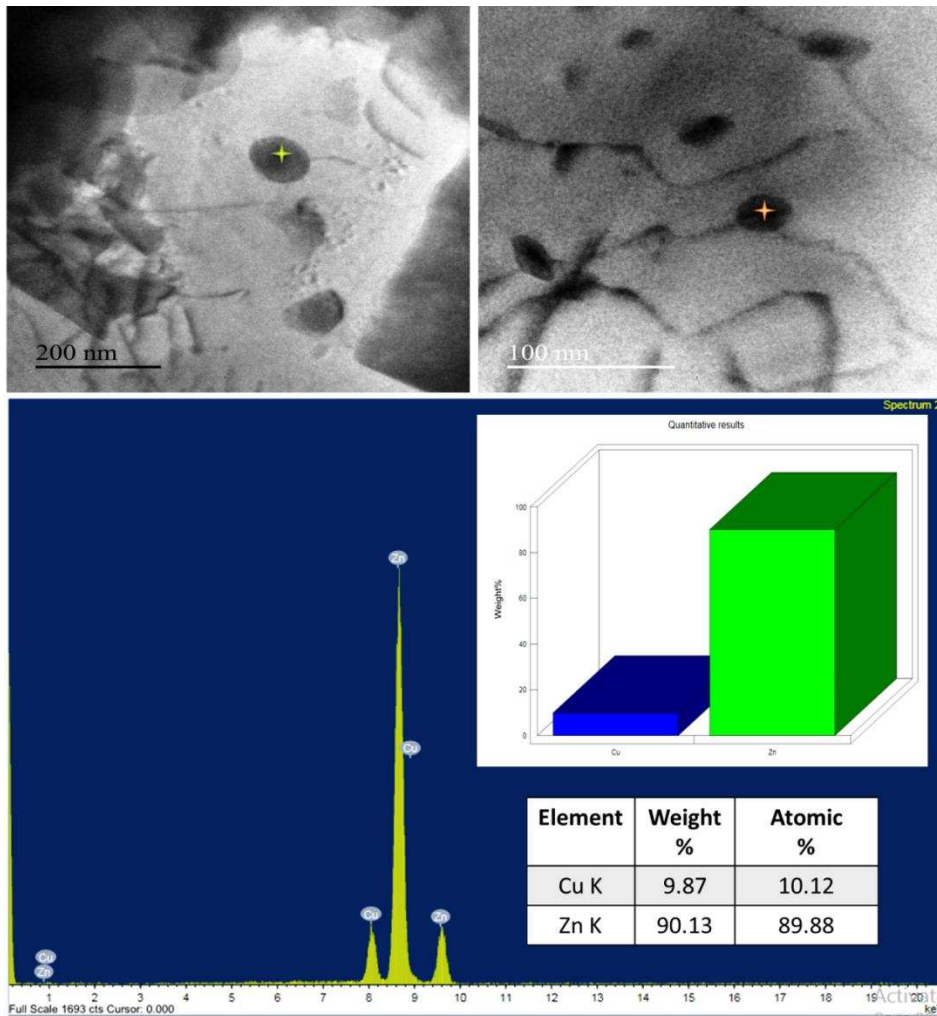


Figure 4.41: EDS analysis of the TEM image of ZA27/ Al₂O₃ 5% MDF processed at 200 °C for six passes for identification nano-crystalline particles inside the α phase

Precipitation of η phase in α phase - The α phase at 268 °C contains more zinc in the Zn-Al based alloys compared with the composition of the α phase at 100 and 170 °C, according to the phase diagrams of Zn-Al binary, Zn-Al-Cu ternary and Zn-Al-Cu-Si alloy systems. There must be Zn-rich η phase precipitated from the unstable α phase at 100 and 170 °C (Zhu et al. 2003). After deformation by MDF a high density of defects (dislocation and vacancies) are introduced, which enhance the diffusion and accelerate the decomposition. This is one of the reason for acceleration of the metastable phase in the material.

4.4.3 XRD Analysis

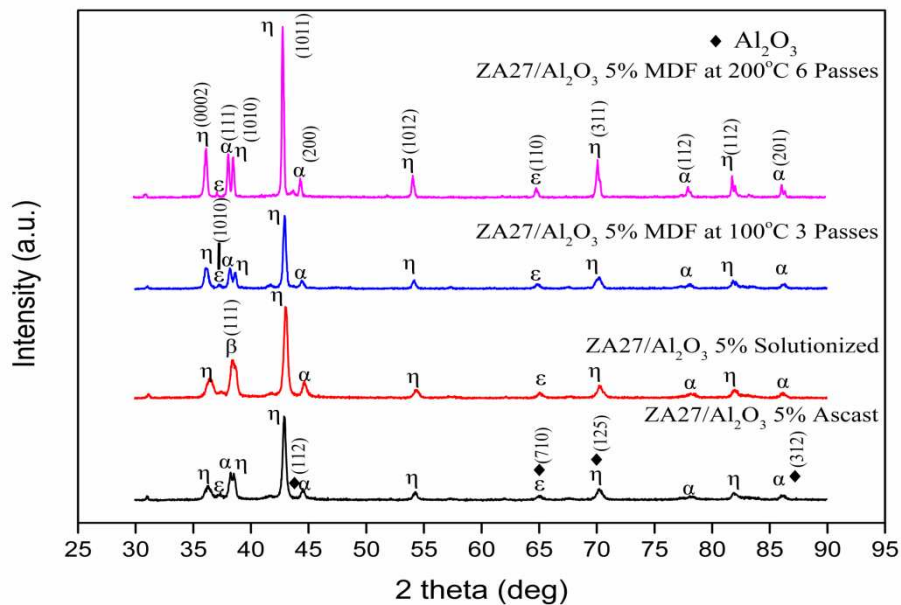


Figure 4.42: XRD patterns of ZA27/Al₂O₃ 5% ascast, solutionized and MDF processed at different temperature.

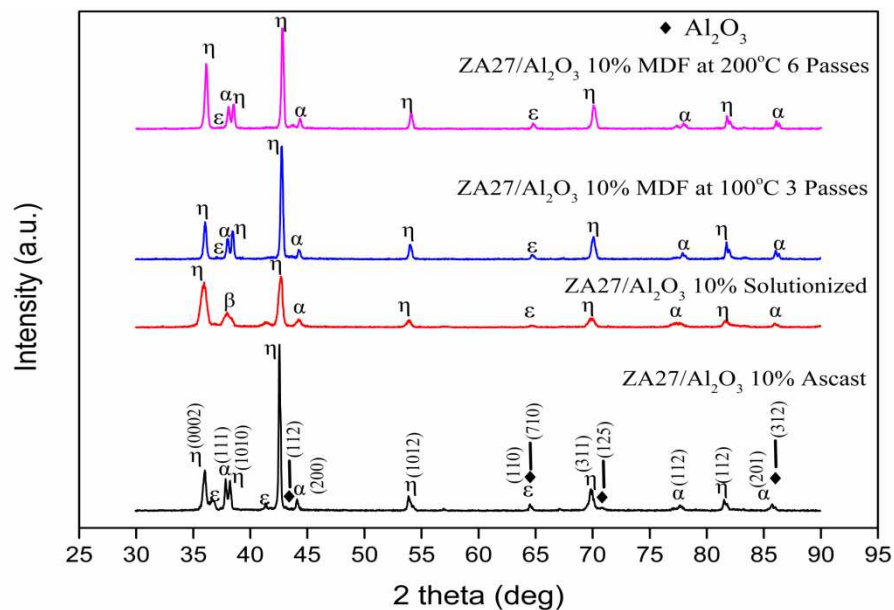


Figure 4.43: XRD patterns of ZA27/Al₂O₃ 10% ascast, solutionized and MDF processed at different temperature.

Figure 4.42 and 4.43 shows the XRD patterns of ZA27 based composites reinforced with Al₂O₃ particles in varying weight percentage. Presence of Al₂O₃ is confirmed by matching peaks with JCPDS files of alumina - ((00-010-0173) (00-023-1009) (00-026-0031)) and it is shown in appendix AI-1.4. It is reported that the η phase and α

phase dissolved to a larger extent when the alloy was solution treated at a higher temperature (Liu et al. 2013). In the case of sample MDF processed at 200 °C up to six passes, η phase peak intensity increased due to increase in volume fraction. It is a known fact that dislocations support the diffusion process leading to fast dissociation of β phase into α and η phases. This type of behavior was observed earlier for cold working of Zn-Al alloy (Zhu 2004).

4.4.4 Mechanical properties

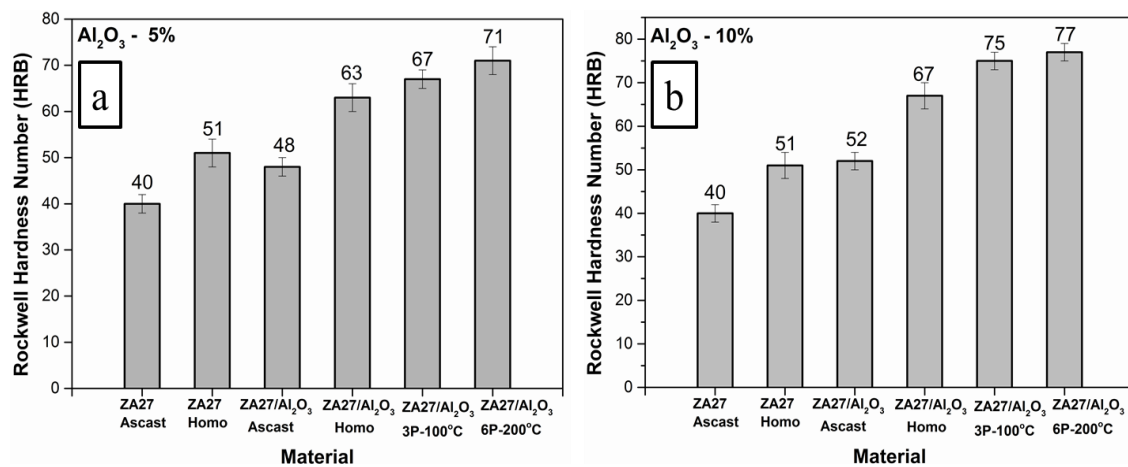


Figure 4.44: Rockwell hardness values of ascast and solutionized ZA27 alloy and ZA27/Al₂O₃ composites MDF processed up to three passes at 100°C and up to six passes at 200°C. a) ZA27/ Al₂O₃ 5% b) ZA27/ Al₂O₃ 10 %.

The hardness of the investigated alloy and composites reinforced with are Al₂O₃ in two different weight percentages are shown in fig. 4.44. Generally, hardness increased with the addition of Al₂O₃ particles, as the particle content increased the hardness value also increased, the presence of the particle will resist the deformation. There is a small increase in hardness value of base alloy after solutionizing heat treatment (Jovanovic et al. 2007). MDF process led to a gradual improvement in hardness with the increasing number of passes. Both the composites reinforced with Al₂O₃ showed a similar type of increasing trend. This is due to microstructural changes and decreased porosity level.

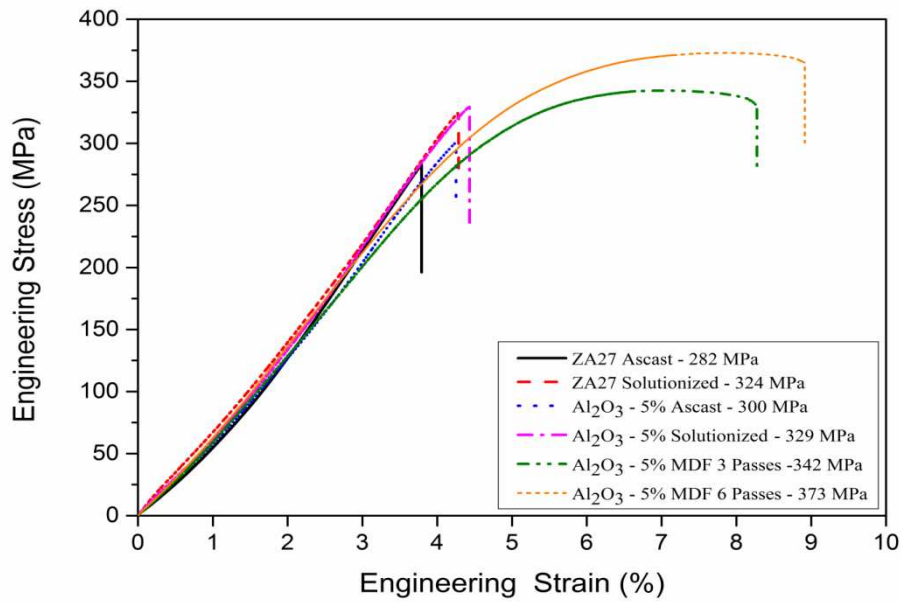


Fig. 4.45: Engineering stress versus engineering strain for the tensile test of ZA27 ascast alloy and ZA27/Al₂O₃ 5% composite after solutionized, MDF processed up to three passes at 100 °C and up to six passes 200 °C.

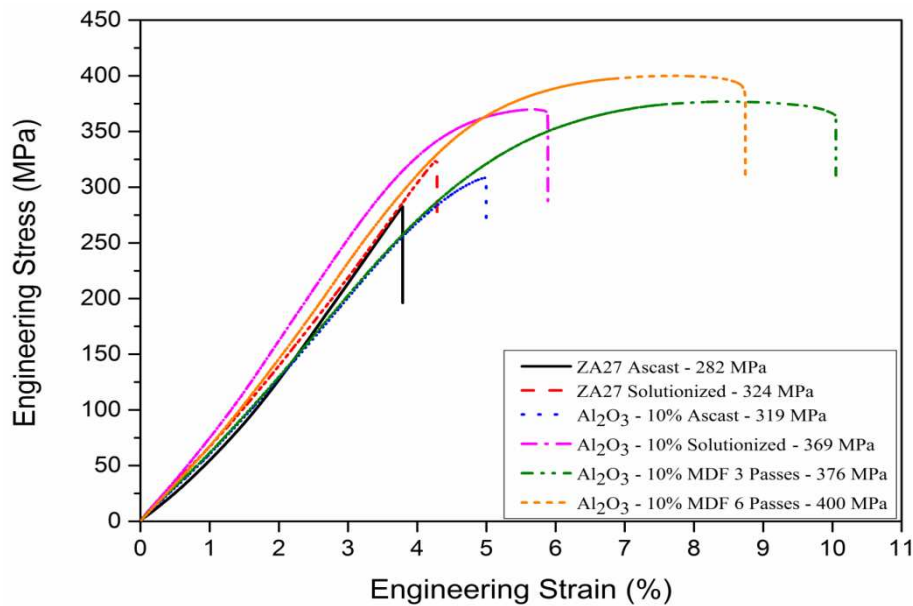


Fig. 4.46: Engineering stress versus engineering strain for the tensile test of ZA27 ascast alloy and ZA27/Al₂O₃ 10% composite after solutionized, MDF processed up to three passes at 100 °C and up to six passes 200 °C.

Figure 4.45 and 4.46 show the tensile stress-strain curves of the ZA27/Al₂O₃ 5 and 10 wt% composites. It is worth noting that the ultimate tensile strength of the composite samples is slightly higher than that of ZA27 base matrix alloy. Moreover, the lower ultimate tensile strength of ZA27 alloy may be due to the lower ductility

and presence of porosity. Inter dendritic porosity can serve as an effective stress concentration site, which promotes crack initiation and results in decreasing the strength and ductility. The structures and properties of the interface between the particles and matrix alloys play a significant role in controlling the tensile properties of the composites. Increased strength can be achieved only by developing a strong interface between the particles and matrix, which permits transfer and distribution of the load from the matrix to the particles. In the present work, the microstructures of the composites reinforced with Al_2O_3 particles indicate that these composites exhibit good evidence of significant interfacial bonding occurred between the particles and matrix alloy during the fabrication of the composites. This means that the interfacial bonding strength between the matrix and particles is sufficient for load transfer. As a result, the tensile strength of the composites is better than that of the matrix. Initial ultimate tensile of the base material was 282 MPa and after solutionizing the UTS value increased to 324 MPa with a small improvement in ductility. Addition of Al_2O_3 particles improved the UTS in both ascast and solutionized condition, 10 wt% Al_2O_3 particles reinforced composites shows good results as compared with base alloy with 5 wt % Al_2O_3 particles. On further processing, the composites by MDF process at 100 °C and 200 °C for a different number of passes enhances the UTS and ductility upto 373 MPa and 400 MPa, (8.7 and 11%) for 5 and 10 wt% Al_2O_3 reinforced composites respectively. The lower ductility of the composites in unprocessed condition may be related to the higher amount of porosity in the composites when compared with MDF processed materials. The improvement in strength after processing can be attributed to the elimination of dendritic structure, strain hardening, presence of reinforcing particles and the reduction in as cast porosity. SEM micrographs of tensile fracture surfaces of the ZA27/ Al_2O_3 5% and Al_2O_3 10% reinforced composites are shown in fig. 4.47 to 4.50. In general, the ZA27 alloy shows clearly a macroscopic brittle fracture nature. The fracture surface is even and nearly perpendicular to the tensile direction. This indicates that the fracture surface of ZA27 alloy exhibits a brittle fracture. The fracture surfaces of the composites exhibit limited ductility on a macroscopic scale with fracture essentially normal to the loading axis. Larger differences in the coefficient of thermal expansion values between ZA27 alloy and the Al_2O_3 particles led to a thermal mismatch. The stresses generated due to

this thermal mismatch put the particles into compression and the matrix into tension. These residual stresses would probably contribute to the brittle nature of composites. Fracture of metal matrix composites depends on particle cracking, particle–matrix debonding or grain boundary fracture, which are influenced by the local stress field, the presence of the interface inhomogeneities, structural alterations in the matrix close to the interface or flaws around particles area. Due to MDF processing, the smaller cracks were formed in the edge of the particles and some cracks were bisecting the Al_2O_3 particles, which we can observe in SEM images of ZA27/ Al_2O_3 reinforced composites (fig. 4.48 (d)). In the present ZA27/ Al_2O_3 reinforced composites, fracture of the particles is common; signifying that particle-matrix interface debonding due to the weak interfacial bond between the particles and matrix is favoured during fracture after MDF processing. Strain localization at the sharp corners of particles may also lead to debonding between the particle and matrix, which is a possible source of the failure of the present composites. Moreover, if the contact area between particles increases, the particles are no longer isolated by the ZA27 matrix alloy.

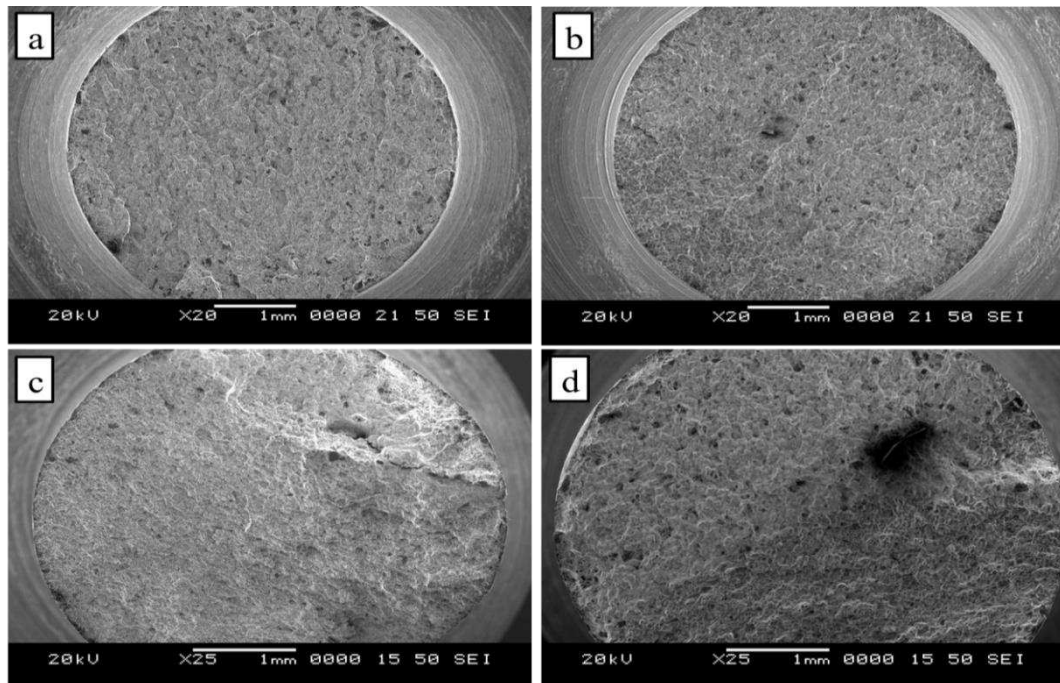


Figure 4.47: SEM images of the fracture surfaces of after tensile tests of ZA27/ Al_2O_3 5% composites in macroscopic scale (a) Ascast ZA27/ Al_2O_3 5% (b) Solutionized ZA27/ Al_2O_3 5% (c) ZA27/ Al_2O_3 5% MDF at 100 °C up to 3 passes (d) ZA27/ Al_2O_3 5% MDF at 200 °C up to 6 passes

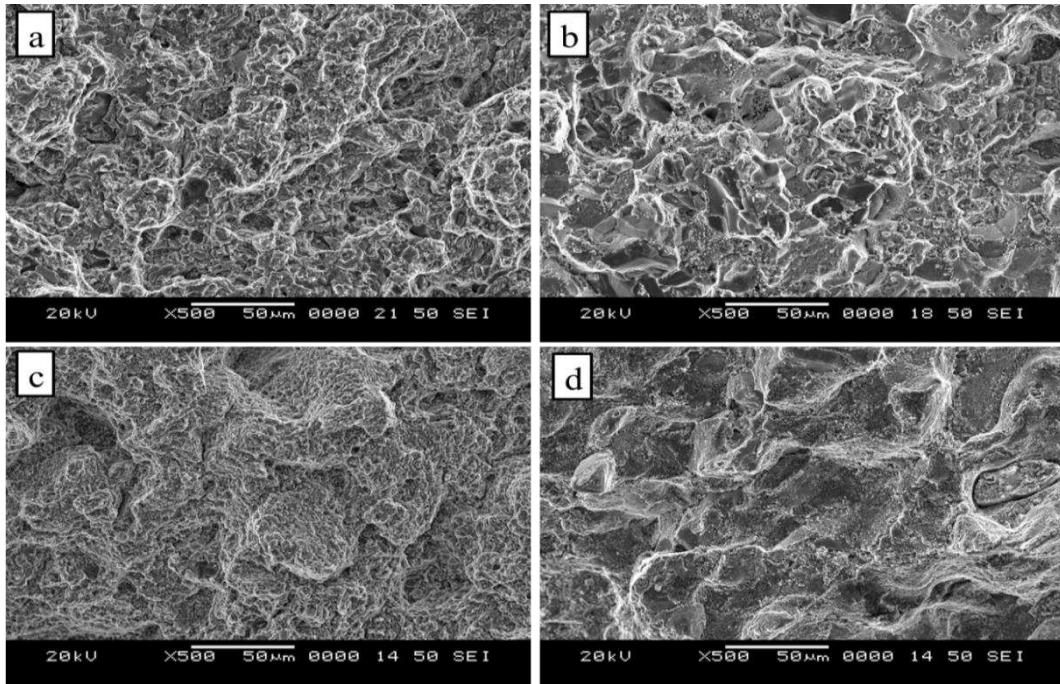


Figure 4.48: SEM images of the fracture surfaces of after tensile tests of ZA27/Al₂O₃ 5% composite (a) Ascast ZA27/Al₂O₃ 5% (b) Solutionized ZA27/Al₂O₃ 5% (b) ZA27/Al₂O₃ 5% MDF at 100 °C up to 3 passes (d) ZA27/Al₂O₃ 5% MDF at 200 °C up to 6 passes

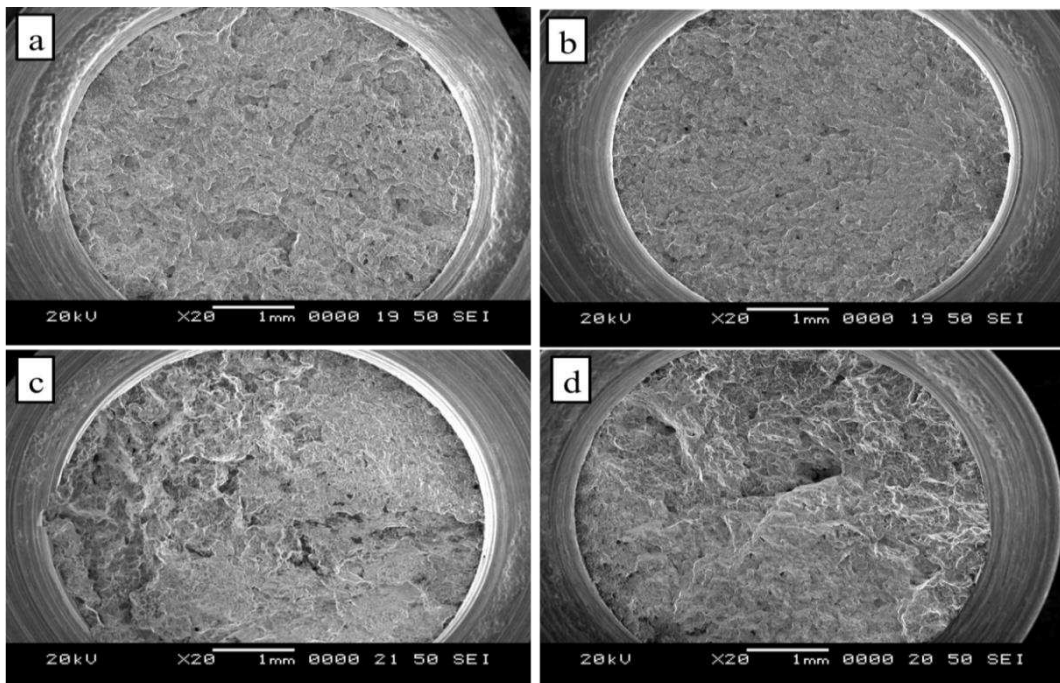


Figure 4.49: SEM images of the fracture surfaces of after tensile tests of ZA27/Al₂O₃ 10% composites in macroscopic scale (a) Ascast ZA27/Al₂O₃ 10% (b) Solutionized ZA27/Al₂O₃ 10% (b) ZA27/Al₂O₃ 10% MDF at 100 °C up to 3 passes (d) ZA27/Al₂O₃ 10% MDF at 200 °C up to 6 passes

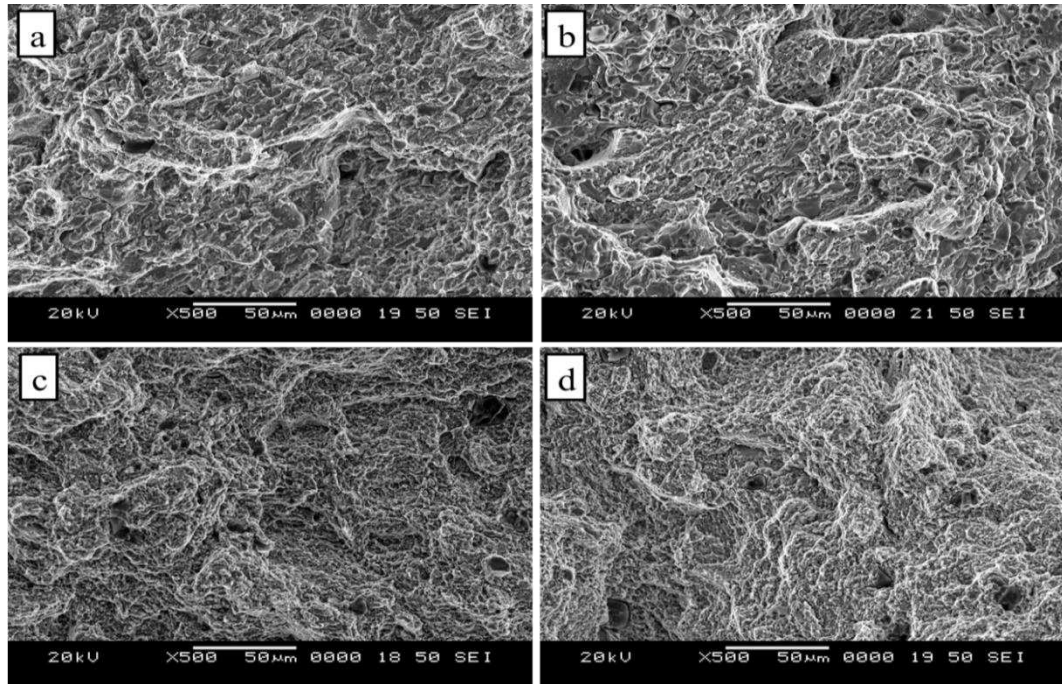


Figure 4.50: SEM images of the fracture surfaces of after tensile tests of ZA27/Al₂O₃ 10% composite (a) Ascast ZA27/Al₂O₃ 10% (b) Solutionized ZA27/Al₂O₃ 10% (c) ZA27/Al₂O₃ 10% MDF at 100 °C up to 3 passes (d) ZA27/Al₂O₃ 10% MDF at 200 °C up to 6 passes

4.4.5 Wear Properties Evaluation

Therefore, cracks will not get arrested by the ZA27 matrix and propagate between the particles. All of the above-mentioned reason confirmed the notably lower level of ductility by the composite in comparison to those of the ZA27/SiC reinforced composite. In summary, it is thought that cracks mainly initiate at the particle-matrix interface, propagate through the matrix and link up with other cracks leading to failure of the composites. The scenario is similar in both the composites reinforced with a different weight percentage of Al₂O₃ particles.

4.4.5 Wear Properties Evaluation of Al₂O₃ reinforced composites

On the other hand, wear is sensitive to the change of various wear test parameters such as mass, shape, stiffness, material properties, and environment. Because of such multi parameter sensitivity of wear, quantitative prediction of wear rate in practice is still far from reality. It becomes important to recognize the major wear type and its typical wear mechanism in relation to wear test parameters.

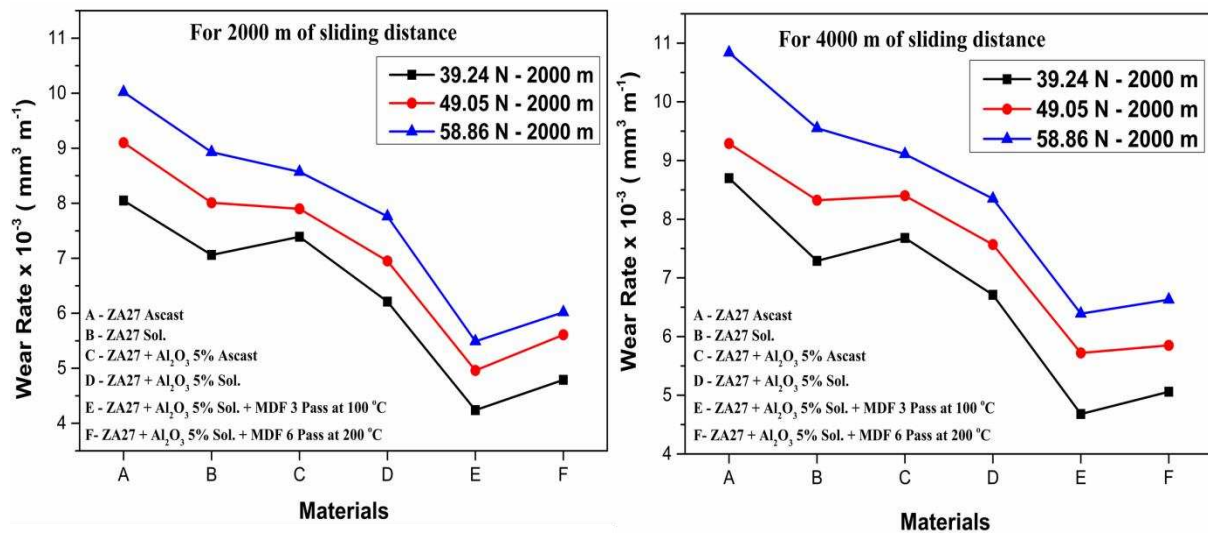


Figure 4.51: Wear rate of ZA27/Al₂O₃ 5 wt% composite in different conditions (a) For 2000m of sliding distance (b) For 4000m of sliding distance.

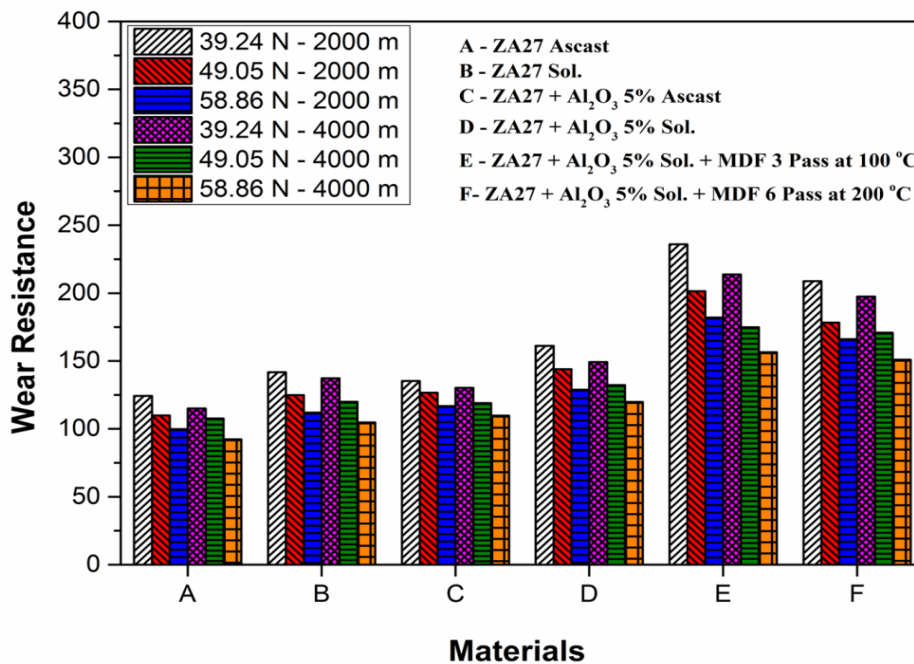


Figure 4.52: Wear Resistance of ZA27/Al₂O₃ 5wt% composite in different conditions

Tribological behaviour of the ZA27 alloy and its composites reinforced with Al_2O_3 particles have been tested with varying applied load 39.24N, 49.05N & 58.86N and sliding distance 2000m and 4000m at a constant sliding velocity of 1 ms^{-1} . Wear rate of ZA27 alloy and its composites expressed for various material types which is shown in fig. 4.51 (a, b) and fig. 4.53 (a, b) for two different sliding distances. The effect of applied load and sliding distance is evident from these diagrams, i.e., the wear rate increased with increase in applied load and sliding distance. Addition of Al_2O_3 particles leads to the improvement of wear resistance, also anti-wear improvement of ZA27 increases with increase of the percentage content of the Al_2O_3 particles, which is shown in fig. 4.51 and 4.53. Generally, the hard phase provides protection of the alloy matrix and offers increased load bearing capacity that can lead to less wear in composites as compared to the matrix alloy. Superior wear characteristics of ceramic particle reinforced MMCs based on ZA27 alloys especially at higher sliding speed and pressures, have also reported by various investigators (Prasad et al. 2007) (Modi et al. 2007) (Sharma et al. 1999) (Ranganath et al. 2001).

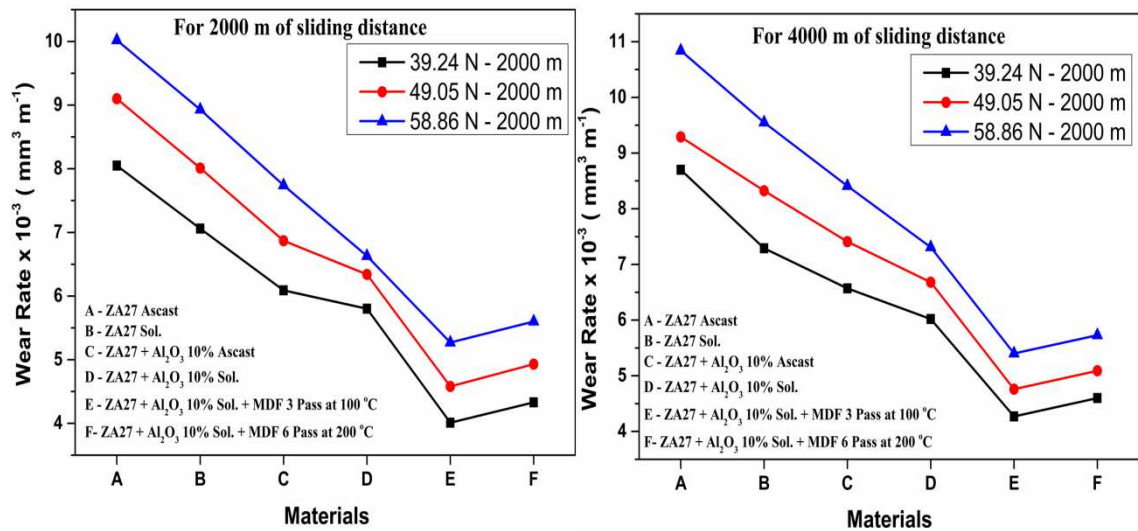


Figure 4.53: Wear rate of ZA27/ Al_2O_3 10 wt% composite in different conditions (a) For 2000m of sliding distance (b) For 4000m of sliding distance.

Ascast conditions showed a very higher wear rate in both reinforced and unreinforced conditions. Composite material processed at 100°C upto 3 passes showed the least wear rate when compared with composite processed at 200°C upto 6 passes and unreinforced once. After solutionizing heat treatment the wear property was improved

in unreinforced ZA27 alloy and its reinforced composites. Variation of the slope of the curve suggests clearly that the degree of the wear rate reduction was large after the MDF process at different temperatures upto to 3 and 6 passes, respectively. Figure 4.52 and 4.54 clearly show the improvement in wear resistance after MDF process and this can be attributed to its ultrafine grain structure. But when compared with SiC reinforced material, Al₂O₃ reinforced material showed lower wear resistance this is because, from Archard equation for brittle material k becomes very large due to enhanced material removal via brittle fracture during wear, leading to reduced wear resistance (Purcek et al. 2010) and in addition to that formation of cracks in Al₂O₃ particles during the multi directional forging process also affects. At the higher applied load and sliding distance composites with large number of crack within the Al₂O₃ particles and interfacial regions act as potential sites for nucleation and propagation of new micro cracks (Babic et al. 2010). The worn surface of the ZA27/Al₂O₃ 5 wt % and 10 wt% reinforced composite specimens tested for 2000m and 4000m at different material condition are shown in fig. 4.55 (a-h).

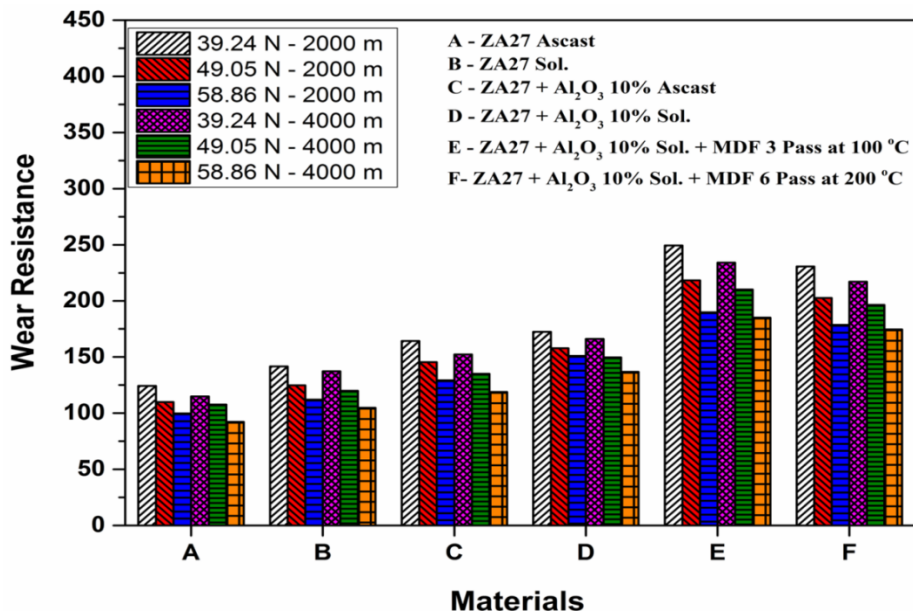


Figure 4.54: Wear Resistance of ZA27/Al₂O₃ 10 wt% composite in different condition

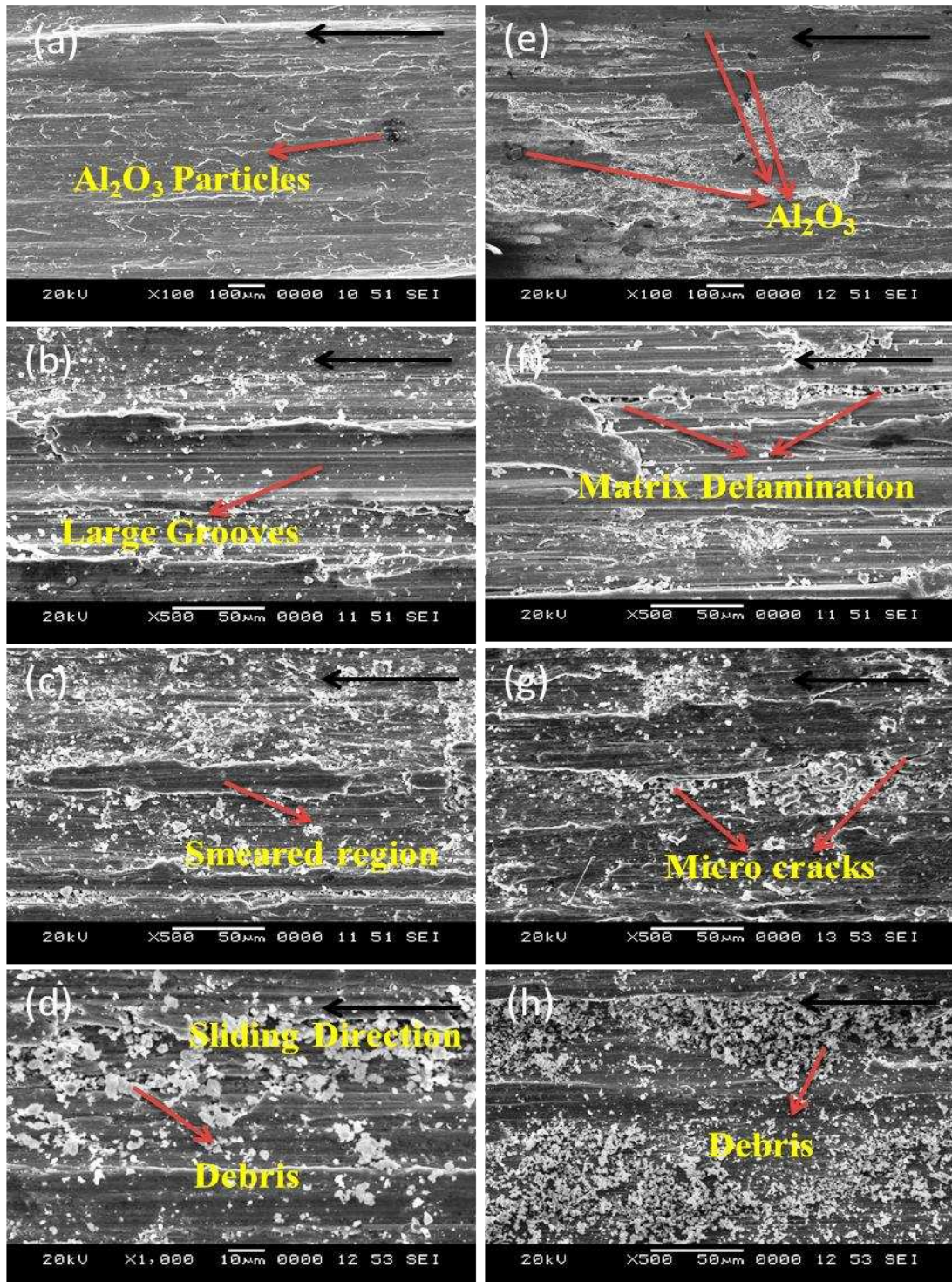


Figure 4.55: SEM micrographs of the worn surfaces of ZA27/Al₂O₃ in 5 & 10 wt%. (a) ZA27/Al₂O₃ 5% ascast - 39.24N - 2000m (b) ZA27/Al₂O₃ 5% - MDF 6 Pass - 49.05N - 2000m (c) ZA27/Al₂O₃ 5% - MDF 3 pass - 58.86N - 2000m (d) ZA27/Al₂O₃ 5% MDF 6 Pass - 58.86N - 4000m (e) ZA27/Al₂O₃ 5% - ascast - 39.24N - 4000m (f) ZA27/Al₂O₃ 5% - MDF 3 Pass - 58.86N - 4000m (g) ZA27/Al₂O₃ 10% - MDF 3 Pass 49.05N - 2000m (h) ZA27/Al₂O₃ 10%- MDF 6 pass- 58.86N - 4000m.

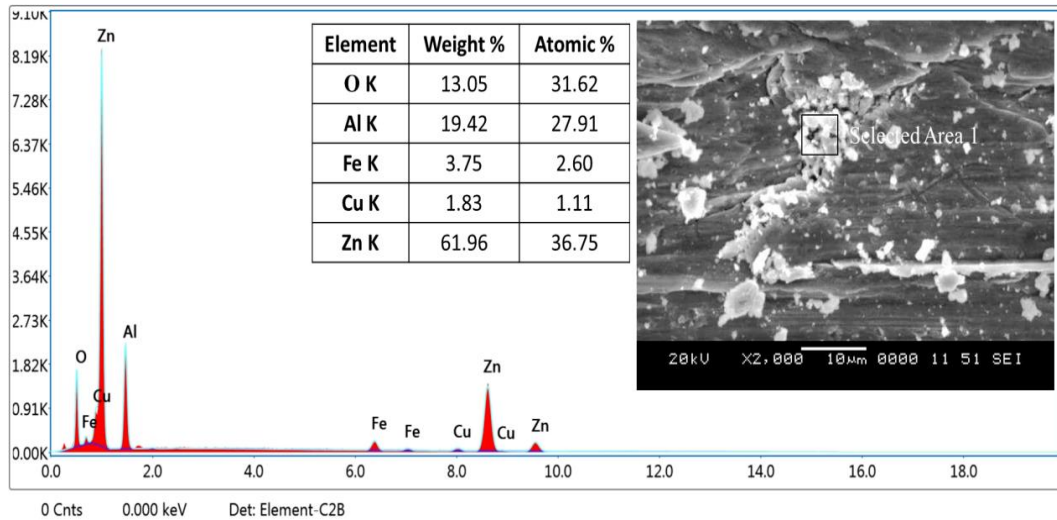


Figure 4.56: EDS analysis of the worn surfaces of composite material (ZA27/Al₂O₃ 10% - MDF 3 Pass 49.05N)

Wear surface of ZA27/Al₂O₃ samples tested at 39.24N and 2000m with a constant sliding velocity of 1 ms⁻¹ revealed some scratches and grooves which is shown in fig. 4.55 (a) and presence of Al₂O₃ was clearly observed in figure 4.55 (e). Increasing the applied load to 49.05N the groove size enlarged which can be observed in fig. 4.55 (b). Due to the detachment of Al₂O₃ particles and large amount of debris lead to formation of micro cracks and delamination of matrix can be observed in fig. 4.55 (f & g) and in addition to this fragmented debris entrapped in the delaminated region. Figure 4.55 (d & h) worn surface of ZA27/Al₂O₃ 5% MDF 6 Pass with a load 58.86N for a sliding distance of 4000m and ZA27/Al₂O₃ 10%-MDF 6 pass with a load 58.86N for a sliding distance of 4000m shows abrasive action of hard ε particle in the form of debris removed from the sample surface and these particles caught in between the mating surface causing abrasion which indicates the main wear mechanism. Figure 4.56 shows the energy dispersive X-Ray spectroscopy analysis of the worn surfaces after wear tests, carried out at 49.05 N load with 2000 m of sliding distance and at 1 m/s sliding speed, for ZA27/Al₂O₃ 5 wt% MDF processed at 100°C upto 3 passes. The scanned region confirms the presence of O-13.05, Al-19.42, Zn-61.96, Cu-1.80, Fe-3.75, the observed small traces of oxygen does not form oxide layer as seen in SEM micrograph.

4.5 ZA27 REINFORCED WITH SiC+Al₂O₃ COMPOSITES PROPERTIES EVALUATION

4.5.1 Density

Density is a physical property which is of prime importance in several weight sensitive applications. It depends on the relative proportion of the matrix and the reinforcing materials in the composite. There is always a difference between the experimental and the theoretical density values of a composite due to the presence of voids and pores. These voids significantly affect some of the mechanical properties and even the performance of composites. The experimental densities and volume fraction of voids (porosities) of all ZA27/SiC+ Al₂O₃ in varying wt percentage of composites are presented in table 4.5.

Table 4.5: Experimental and Theoretical density with porosity percentage of ZA27/ SiC+Al₂O₃ 5% and 10%

Sl. No	Sample Name	Experimental Density g cm ⁻³	Theoretical Density g cm ⁻³	Error %
1	Ascast SiC+Al ₂ O ₃ 5%	5.1569	5.2149	1.11
2	Homo SiC+Al ₂ O ₃ 5%	5.1591	5.1893	0.58
3	3P @ 100 SiC+Al ₂ O ₃ 5%	5.1699	5.1842	0.27
4	6P @ 200 SiC+Al ₂ O ₃ 5%	5.1763	5.1829	0.12
5	Ascast SiC+Al ₂ O ₃ 10%	5.1377	5.1982	1.16
6	Homo Ascast SiC+Al ₂ O ₃ 10%	5.1474	5.1633	0.30
7	3P @ 100 Ascast SiC+Al ₂ O ₃ 10%	5.1597	5.1688	0.17
8	6P @ 200 Ascast SiC+Al ₂ O ₃ 10%	5.1618	5.1663	0.08

It is observed that by the addition of SiC+Al₂O₃ particles, the density of the composites is gradually decreased. It also noted that the increment in the wt% of filler in the matrix led to an increase in porosity percentage. The difference between the experimental and theoretical density values gradually decreased with an increase in a number of MDF Passes, this is due to the elimination of porosity.

4.5.2 Microstructure

Typical optical microstructure of ZA27 based composites in the squeeze cast condition is shown in fig. 4.57. This microstructure of ZA27 composites revealed a

dendritic structure of primary Al-rich dendrites, Zn-rich in the interdendritic regions along with metastable (Cu-rich) phase. After solutionization heat treatment dendrite structure will break and form grain type of microstructure shown in fig. 4.57 (b, f). further MDF processing of this composite materials led to a refinement in grain size with respect to the number of MDF passes and condition of MDF processing. MDF processed sample at 100 °C up to three passes have a higher level of refinement as compared with MDF sample processed at 200 °C for six passes.

SEM images of composites reinforced by a mixture of SiC+Al₂O₃ particles in varying weight percentage upto 10% in a step of 5 is shown in figure 4.58 and 4.59. Conversion of ascast composites to solutionized composites provides a microstructural change in the composites, ie., the dendritic structure was converted into grain type structure which one can observe in fig. 4.58 (a, b) and 4.59 (a, b). Figure 4.58 (c) confirms the uniform distribution of a mixture of SiC+Al₂O₃ particles, the back scattered image of fig. 4.59 (d) gives the clear vision with the difference in a color contract of particles which vary with atomic numbers. The interfacial bonding between the particles and matrix is of excellent type. ZA27/SiC+Al₂O₃ 5% and 10% composites have MDF processed at 100 °C up to three passes and at 200 °C up to six passes with an equivalent strain of 0.54 to each pass. Figure 4.58 (e1, e2) and 4.59 (e1,e2) shows the duplex type of microstructure with lamellar and equiaxed grains for MDF processed sample at 100 °C up to three passes with a grain size of 0.2-0.25 μm and 0.3-0.4 μm respectively. The microstructure of the MDF sample processed at 200 °C for six passes exhibited more uniformly distributed ε phase accompanied by breaking out of elongated grains into α and η phases with a grain size of 0.8-0.9 μm and 0.9-1.1 μm respectively as shown in fig. 4.58 (f1, f2) and 4.59 (f1, f2) respectively. After six passes of MDF processing at 200 °C coarse grains are seen due to recovery and recrystallization process at a higher temperature. It can be observed that as the number of passes increased the phase distribution was more uniform and grain size decreased considerably.

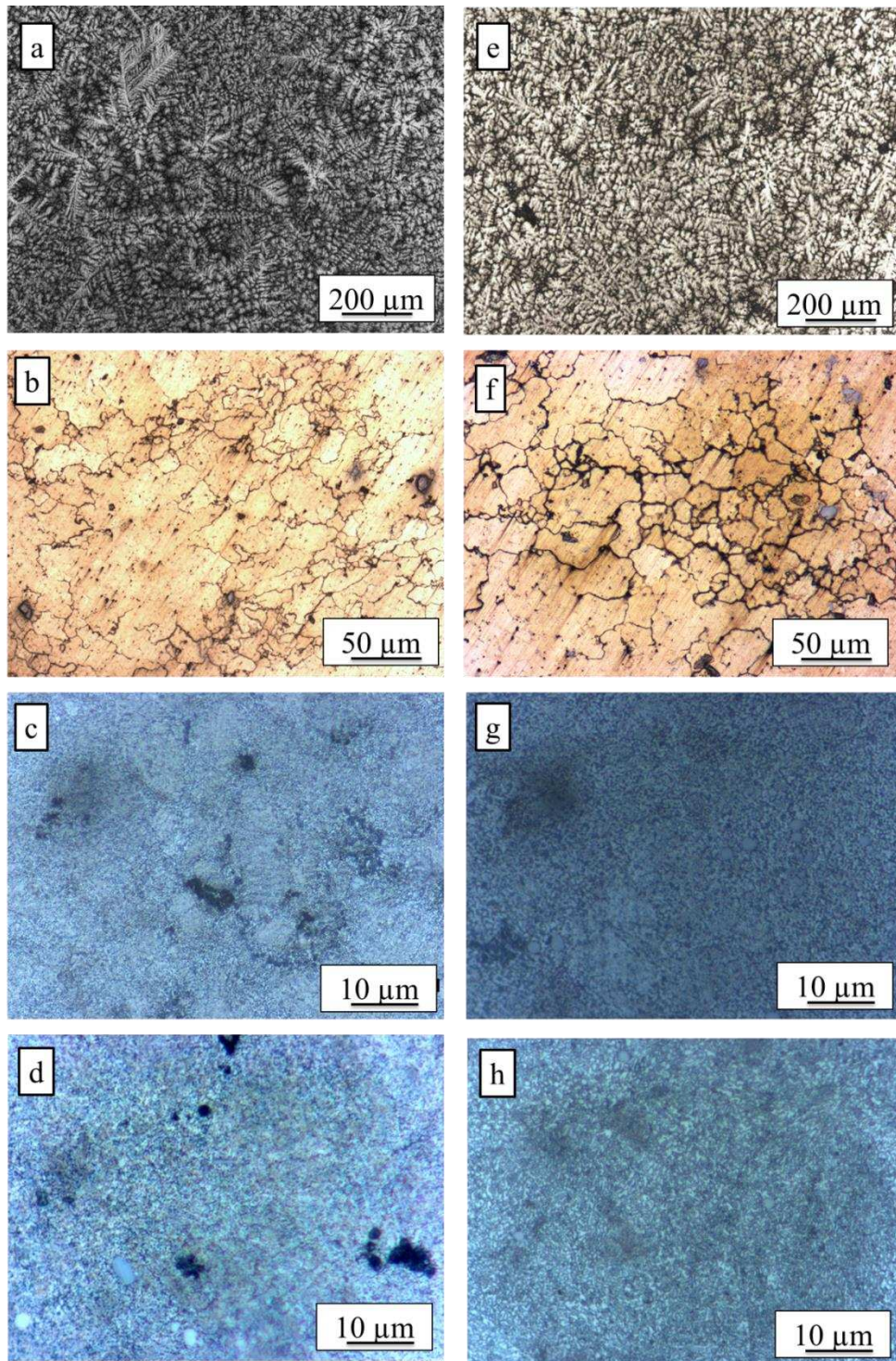


Figure 4.57: Optical microscopy images (a) Ascast ZA27/SiC+Al₂O₃ 5% composite (b) Solutionized ZA27/SiC+Al₂O₃ 5% composite (c) ZA27/SiC+Al₂O₃ 5% MDF processed at 100 °C for 3 passes (d) ZA27/SiC+Al₂O₃ 5% MDF processed at 200 °C for 6 passes (e) Ascast ZA27/SiC+Al₂O₃ 10% composite (f) Solutionized ZA27/SiC+Al₂O₃ 10% composite (g) ZA27/SiC+Al₂O₃ 10% MDF processed at 100 °C for 3 passes (h) ZA27/SiC+Al₂O₃ 10% MDF processed at 200 °C for 6 passes.

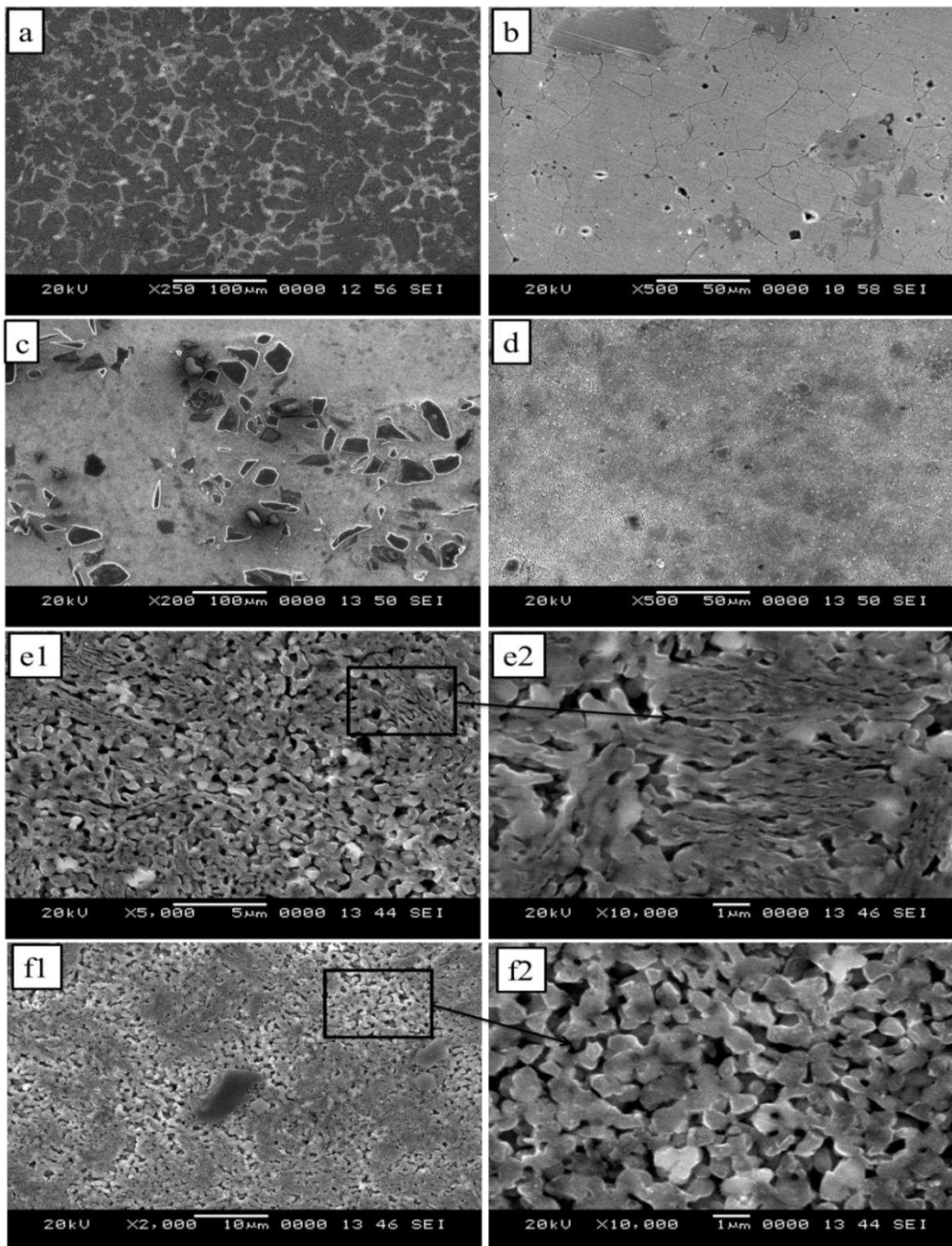


Figure 4.58: SEM images (a) Ascast ZA27/SiC+Al₂O₃ 5% composite (b) Solutionized ZA27/ SiC+Al₂O₃ 5% composite (c, d) SiC+Al₂O₃ Particle distribution in ZA27/SiC+Al₂O₃ 5% composite (e1) ZA27/SiC+Al₂O₃ 5% - MDF processed at 100 °C for 3 passes (e2) ZA27/ SiC+Al₂O₃ 5% - MDF processed at 100 °C for 3 passes (higher magnification x 10,000) (f1) ZA27/ SiC+Al₂O₃ 5% MDF processed at 200 °C for 6 passes (f2) ZA27/ SiC+Al₂O₃ 5% MDF processed at 200 °C for 6 passes (higher magnification x 10,000) showing cellular type of grains.

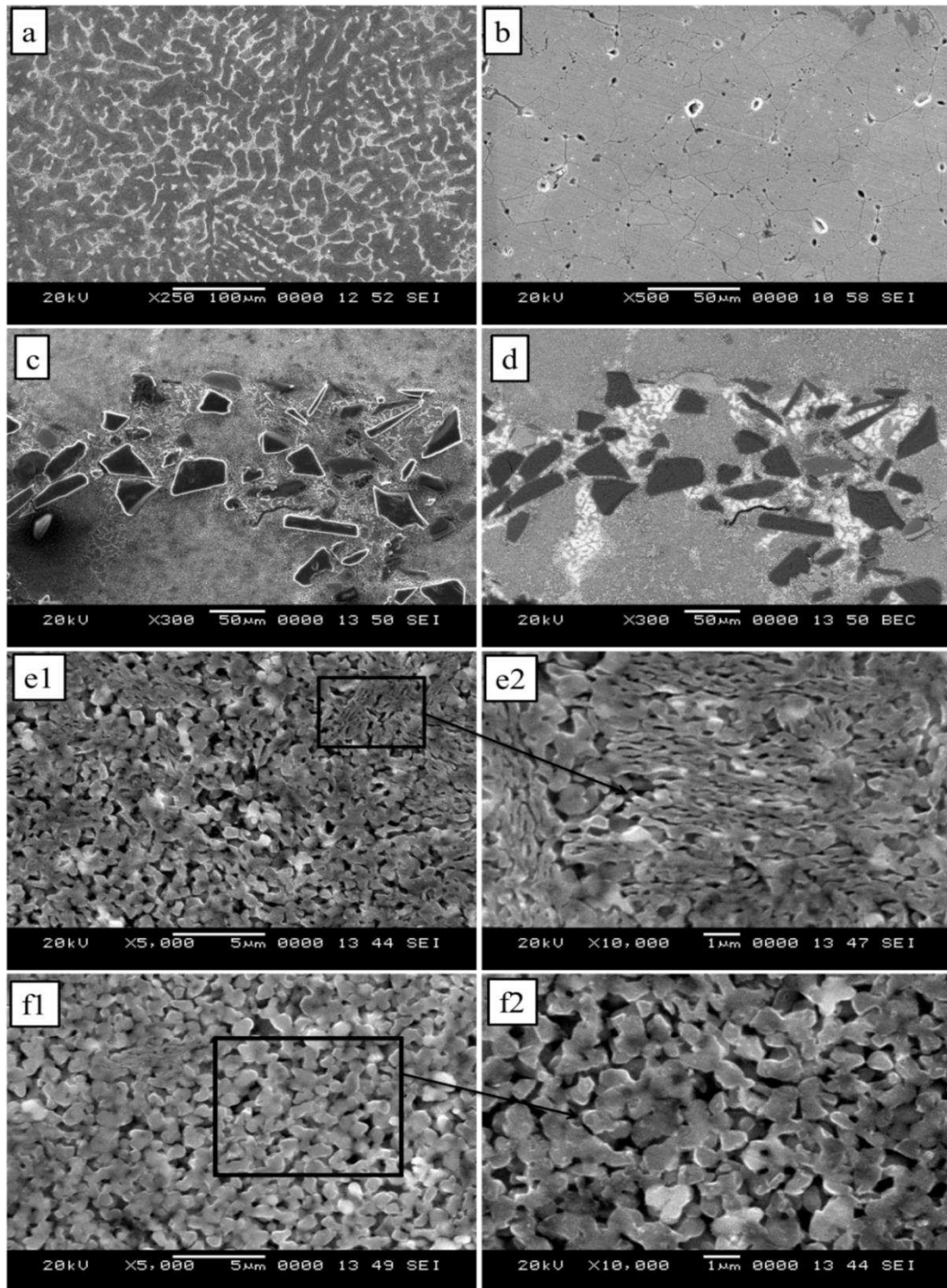


Figure 4.59: SEM images (a) Ascast ZA27/SiC+Al₂O₃ 10% composite (b) Solutionized ZA27/SiC+Al₂O₃ 10% composite (c, d)SiC+Al₂O₃ Particle distribution in ZA27/Al₂O₃ 10% composite (e1) ZA27/SiC+Al₂O₃ 10% - MDF processed at 100 °C for 3 passes (e2) ZA27/ ZA27/SiC+Al₂O₃ 10% - MDF processed at 100 °C for 3 passes (higher magnification x 10,000) (f1) ZA27/ SiC+Al₂O₃ 10% MDF processed at 200 °C for 6 passes (f2) ZA27/ SiC+Al₂O₃ 10% MDF processed at 200 °C for 6 passes (higher magnification x 10,000) showing cellular type of grains.

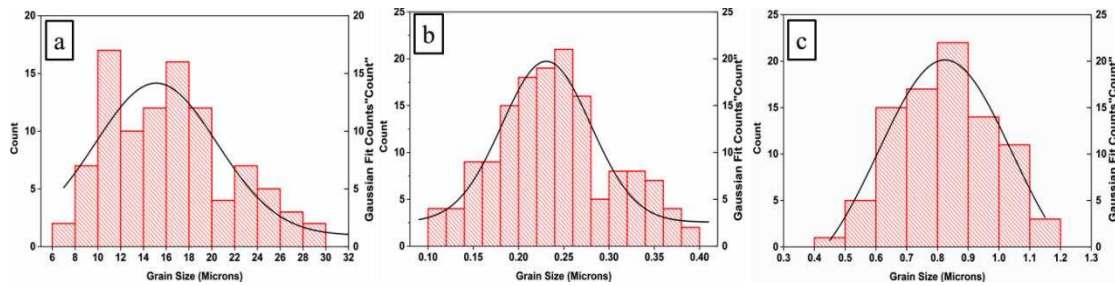


Figure 4.60: Grain size distribution curve a) Solutionized ZA27/SiC+Al₂O₃ 5% composite b) ZA27/SiC+Al₂O₃ 5% - MDF processed at 100 °C for 3 passes c) ZA27/SiC+ Al₂O₃ 5% - MDF processed at 200 °C for 6 passes.

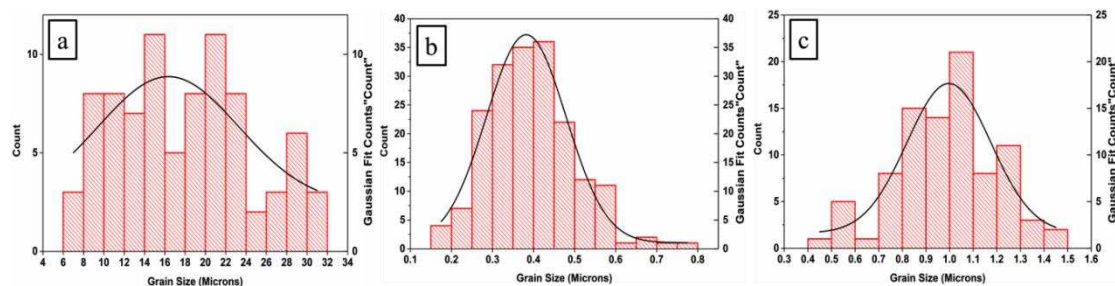


Figure 4.61: Grain size distribution curve a) Solutionized ZA27/SiC+Al₂O₃ 10% composite b) ZA27/SiC+Al₂O₃ 10% - MDF processed at 100 °C for 3 passes c) ZA27/SiC+ Al₂O₃ 10% - MDF processed at 200 °C for 6 passes.

10 wt % of SiC+Al₂O₃ reinforced composites performed better when compared with 5 wt% reinforced and base matrix alloy in both MDF processed and unprocessed condition. Grain size distribution curve was plotted and compared with the processing condition of composites materials in terms of grain size (fig. 4.60 and 4.61). The curve was smoothed by Gaussian fit. Initial grain size in solutionized material was 15-20 μm in both the ZA27/SiC+Al₂O₃ 5% and 10% composites. The ε phase greatly got refined when the MDF process was carried out at higher temperatures. However, it is possible that the lamellae may block the sliding of equiaxed grains, leading to higher strength in the processed sample. The spherical and well spread Al-rich and Zn-rich phase obtained provides more equiaxed grains as seen in fig. 4.58 and 4.59.

The TEM images of the microstructure of the MDF processed at 100 °C up to three pass sample and MDF at 200 °C up to six pass for ZA27/SiC+Al₂O₃ composite samples are shown in fig. 4.62. (a) Material reinforced with 5wt% of mixture processed at 100 °C for three passes showing lamellar structure with identification of

lamellar boundaries. Broken lamellar structure can be observed with an average grain size of 0.25 to 0.35 nm (fig. 4.62 (b)). Figure 4.62 (c) ZA27/ SiC+Al₂O₃ 10% MDF at 100 °C for three passes showing equiaxed grain structure 300 to 400 nm. Dense dislocations were observed with in the α phase, similar type of identification of dislocation was done by (Zhang et al., 2012) for Zn-Al alloy (fig. 4.62 (d)).

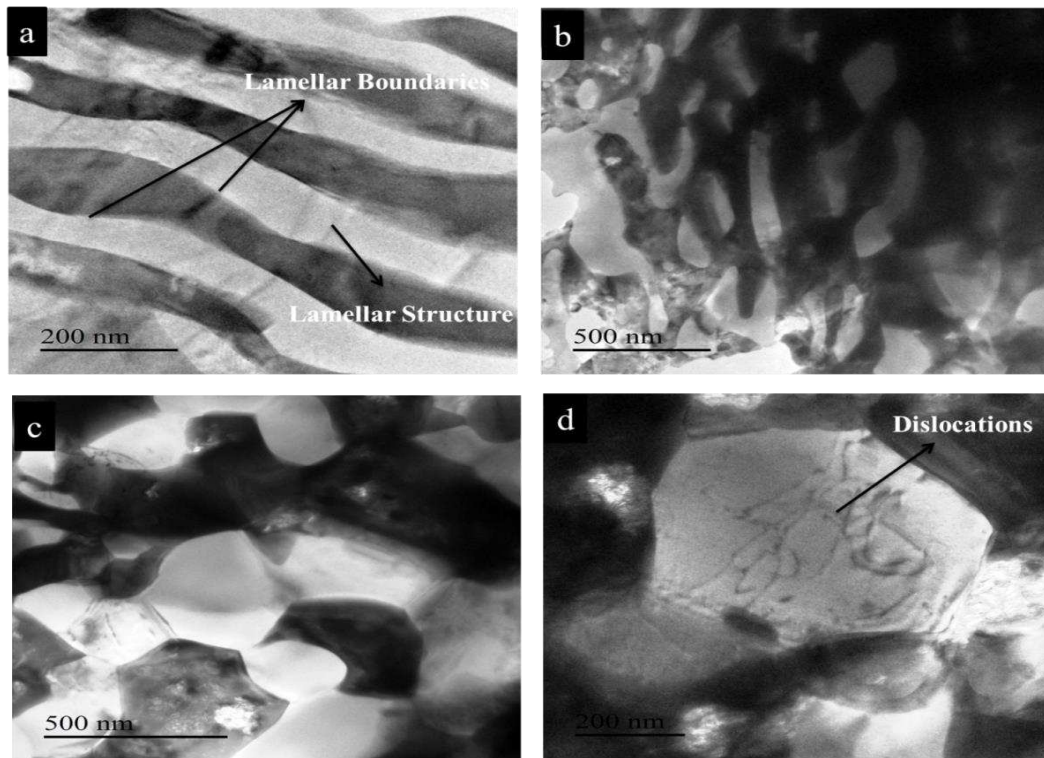


Figure 4.62: Bright-field TEM micrograph a) ZA27/SiC+Al₂O₃ 5% MDF processed at 100 °C for three passes showing lamellar boundaries b) ZA27/SiC+Al₂O₃ 5% MDF processed at 100 °C for three passes showing equiaxed structure or broken lamellar structure c) ZA27/ SiC+Al₂O₃ 10% MDF at 100 °C for three passes d) ZA27/ SiC+Al₂O₃ 5% MDF processed at 100 °C for three passes showing dislocation.

4.5.3 XRD Analysis

It was observed that the β phase decomposed at the stage of MDF processing. It is confirmed by the fact that the XRD intensity of the β phase decreased, accompanying the formation of three phases α , ϵ , and η , i.e., $\beta \rightarrow \alpha + \epsilon + \eta$, after MDF processing. A similar type of results was observed by Zhu (2004).

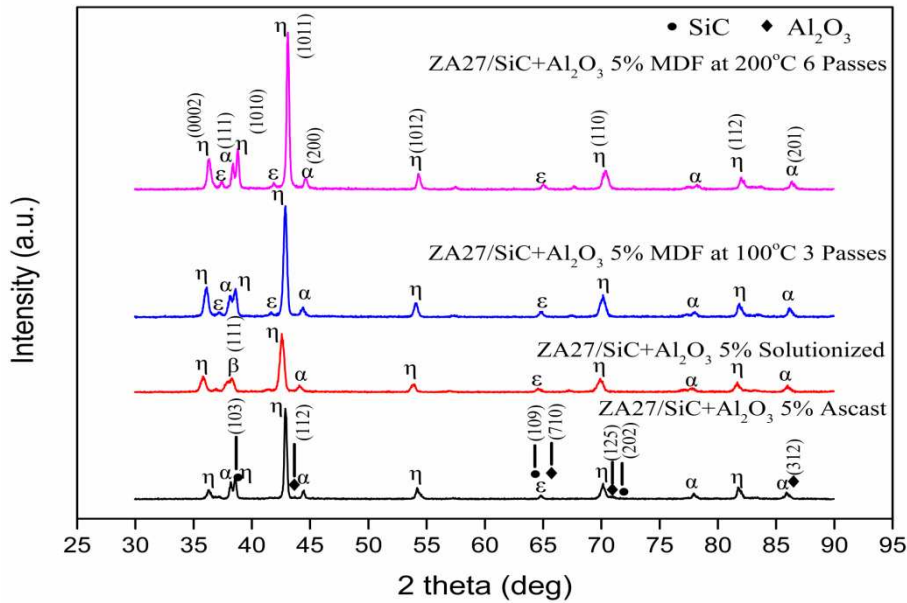


Figure 4.63: XRD patterns of ZA27/SiC+Al₂O₃ 5% ascast, solutionized and MDF processed at different temperature.

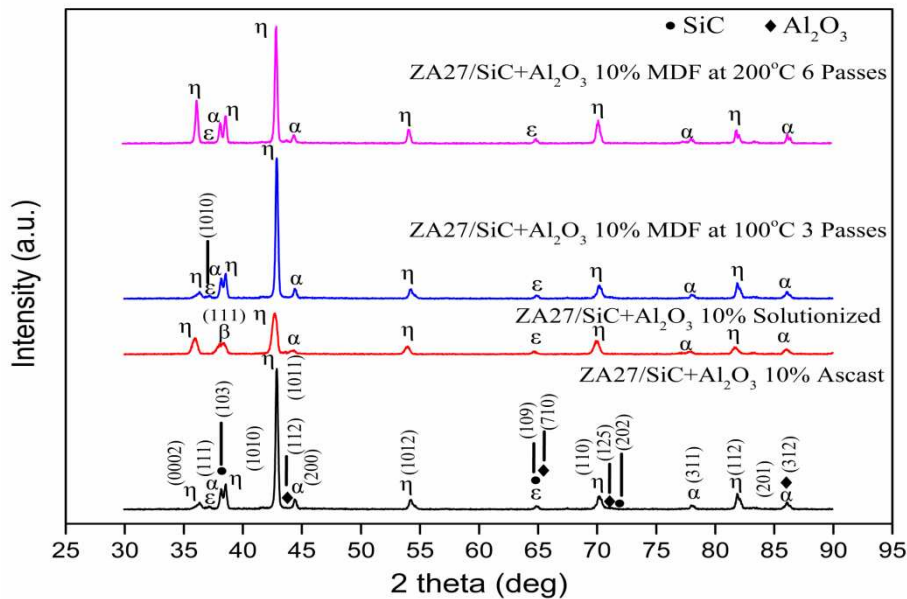


Figure 4.64: XRD patterns of ZA27 /SiC + Al₂O₃ 10% ascast, solutionized and MDF processed at different temperature.

From the XRD results, it can be suggested that MDF processed sample will enhance the formation of α, η phase during processing. As it was shown from XRD analysis in fig. 4.63 that formation of ε phase with higher intensity is possible only after six number of passes. Because of the external stress, the specimens are already deformed, a high density of dislocations are introduced both at grain boundaries and inside the

grains that provide effective nucleation sites for the formation of the new phases and enhance the diffusion. Uniform distribution of η was observed with increasing intensity of η phase in composite material processed at 200 °C upto six number of passes. A similar type of trend was observed in ZA27/SiC+Al₂O₃ 5% composite.

4.5.4 Mechanical properties

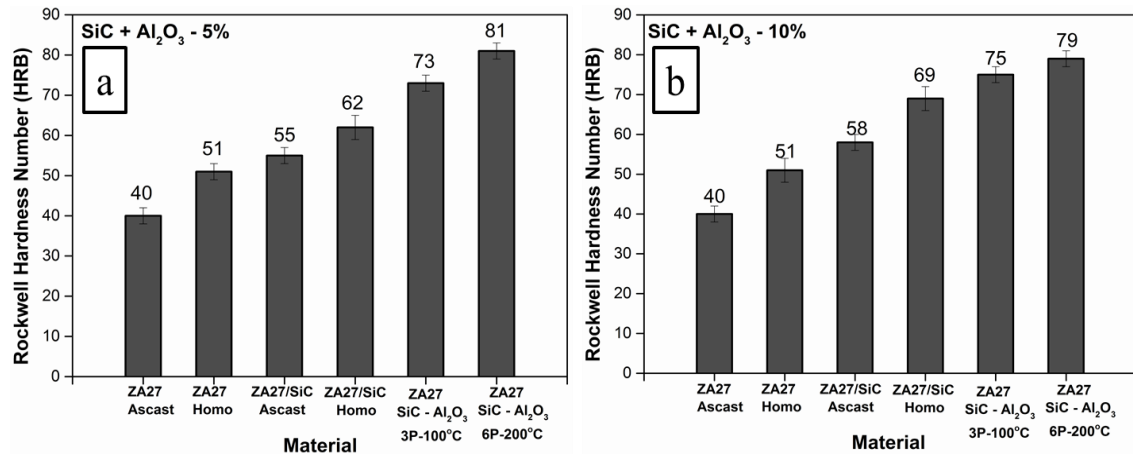


Figure 4.65: Rockwell hardness values of ascast and solutionized ZA27 alloy and ZA27/SiC+Al₂O₃ composites MDF processed up to three passes at 100 °C and up to six passes at 200 °C. a) ZA27/ SiC + Al₂O₃ 5% b) ZA27/ SiC + Al₂O₃ 10 %

Figure 4.65 shows the variation in the hardness with processing at a different number of passes at different temperature of ZA27/SiC+Al₂O₃ 5% and 10% MDF processed composites. The incorporation of particle mixture with 5% showed better hardness in both ascast and solutionized sample with a hardness value of 55 and 62 HRB respectively. Composites with 10% reinforced samples shows the higher value of hardness when compared with 5% and base alloy (58 and 69 ascast and solutionized condition). Both the ZA27/SiC + Al₂O₃ 5% and 10% MDF processed samples shows the hardness values of 73, 75 and 81, 79 HRB at 100 °C up to three passes, 200 °C up to six passes respectively. The increase in hardness can be attributed to the particle presence, grain refinement and increased grain boundaries which occurs during intensive plastic deformation. The large improvement in strength and ductility of MDF processed material may be attributed to many metallurgical factors like grain refinement, reduction in the amount of porosity and reduced heterogeneity by way of improved uniform distribution of phase (α) in the matrix of Zn-rich phase.

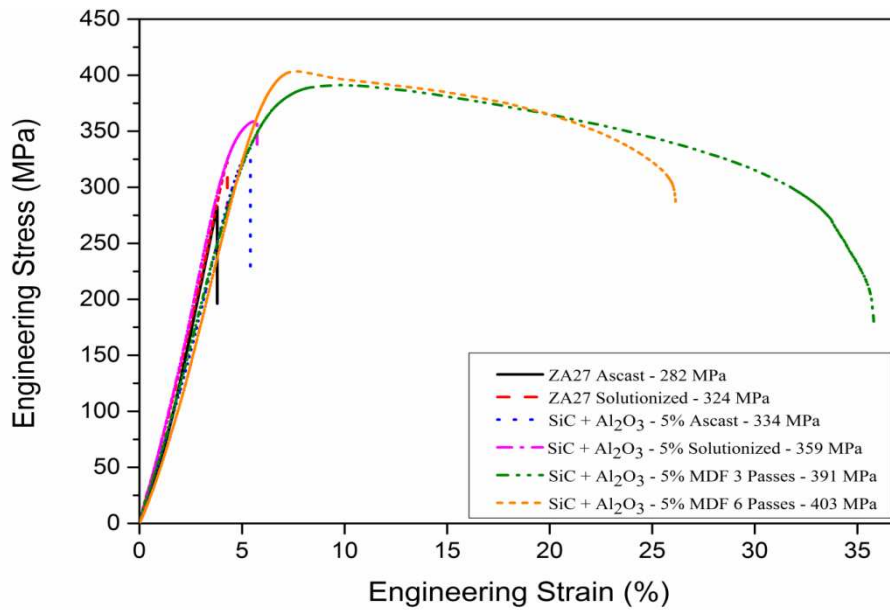


Figure 4.66: Engineering stress versus engineering strain for the tensile test of ZA27 ascast alloy and ZA27/SiC+Al₂O₃ 5% composite after solutionized, MDF processed up to three passes at 100 °C and up to six passes 200 °C.

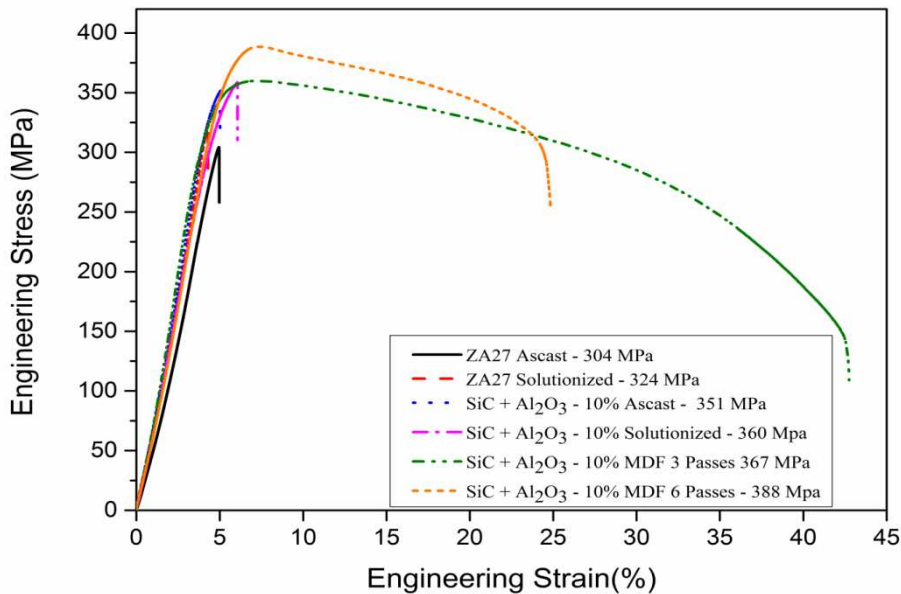


Figure 4.67: Engineering stress versus engineering strain for the tensile test of ZA27 as-cast alloy and ZA27/SiC+Al₂O₃ 10% composite after solutionized, MDF processed up to three passes at 100 °C and up to six passes 200 °C.

ZA27/SiC+Al₂O₃ with 5% and 10% reinforced composites showed lower strength and ductility in ascast condition with 334 and 351 MPa. After solutionizing the strength of the composites increased to 359 and 362 MPa. When ZA27/SiC+Al₂O₃ with 5% and 10% composites MDF processed at 100 °C at up to three passes and up to six

passes at 200 °C enhanced the strength to 367, 391 and 388, 407 MPa respectively. Ductility of these composite materials improved after the MDF process for a different number of passes. Greater plastic deformation by conventional techniques such as rolling, drawing or extrusion introduces greater strain hardening, which in turn increases strength but decreases the ductility of the metal (Yamashita et al. 2001). In other words, an increase in the strength of a material is accompanied by a loss of ductility. This simultaneous increase in strength and ductility of the alloy may be explained by the microstructural changes and more dislocations generated by severe plastic deformation during ECAP. Valiev et al. (2002) attribute the increase in ductility during ECAP to the refinement of microstructure and to an increase in the fraction of high-angle grain boundaries, which results in the activation of boundary sliding and grain rotation deformation mechanisms. Refined structures with high-angle grain boundaries may impede the motion of dislocations and consequently enhance strength. At the same time, these refined grains may also facilitate other deformation mechanisms such as grain boundary sliding and enhanced grain rotation, which improves ductility. They also claimed that (Valiev et al. 2002) the grain boundaries generated by SPD are not usually in a state of equilibrium with many dislocations that are not geometrically necessary to form the grain boundary. These dislocations could move to facilitate grain boundary sliding and grain rotation which improves the ductility. On the other hand, commercially used Zn–Al alloys in eutectic (Zn–5%Al) and eutectoid (Zn–22%Al) compositions have a dendritic network within individual grains in which porosity exists during solidification in the as-cast state structure has to be considered in the explanation of this simultaneous increase in strength and ductility. As can be seen in fig. 4.69 and 4.70, the MDF processing of the ZA27/SiC+Al₂O₃ composite led to finer and equiaxed microstructure. A number of studies have pointed out the effect of the MDF processing on mechanical properties of Zn–Al alloys (Ungar et al. 2000) (Osorio et al. 2002) (Turhal et al. 2003). It has been shown that the strength of the Zn–Al alloys having dendritic structures increased significantly with microstructural changes and decreasing grain size. MDF processing substantially increased the ductility of the ascast ZA27 based composites. The samples subjected to MDF process at 100 °C at up to three passes and up to six passes at 200 °C showed the total elongation of 42.78%, 35.81% and 24.82%,

25.74% respectively as against only 5.01, 5.4% elongation of the as-cast sample indicating more than one order of magnitude increase in elongation after several passes of MDF. Also, visible necking was observed with the uniform elongation up to failure was seen to be almost in a uniform manner. The similar results were also observed for other Zn–Al-based alloys processed by SPD (Savaskan et al. 2003) (Murphy et al. 2003) (Turhal et al. 2003).

The as-cast structure of Zn–Al based composites has dendritic structure and including interdendritic microporosities that occur due to incomplete filling of the liquid melt during solidification. Therefore, the as-cast Zn–Al-based composites generally exhibit very limited ductility. The morphological changes in these composites may cause a further increase in ductility of the material. Furthermore, the microporosities (microvoids) in the as-cast microstructure were mostly eliminated by the effect of severe plastic deformation. Which decreased the stress riser points and led to improvements in ductility. The influence of microporosity on the tensile properties has also been the matter of several studies (C.D. Lee et al. 2007) and it has been suggested that the shape and distribution aspect of reinforcing particles, as well as their interfacial bonding with matrix, contribute significantly to the tensile properties of the materials. It has been shown from these studies that a reduction in the amount of porosity significantly improves the ductility of the materials. Some recent studies also showed porosity reduction during SPD and found that the porosity in the as-cast structure significantly decreased after processing the material by SPD, resulting in improved ductility (T. Savaskan et al. 2003). There is also a deformation-induced homogenization process during ECAP due to the relatively high processing temperature as explained above. This homogenization may lead to compensate for the strengthening effect due to high-temperature deformation but cause a further increase in ductility properties of the alloy. The MDF process also increased the ductility of the present alloy as shown in fig. 4.69. The as-cast structure of the composites as a dendritic structure with some cast defects like as cast porosity. Therefore the composites exhibit very limited ductility. The total elongation to fracture as a measure of the ductility of the composites increased dramatically with an increasing number of MDF passes and the samples subjected to larger passes showed the largest elongation.

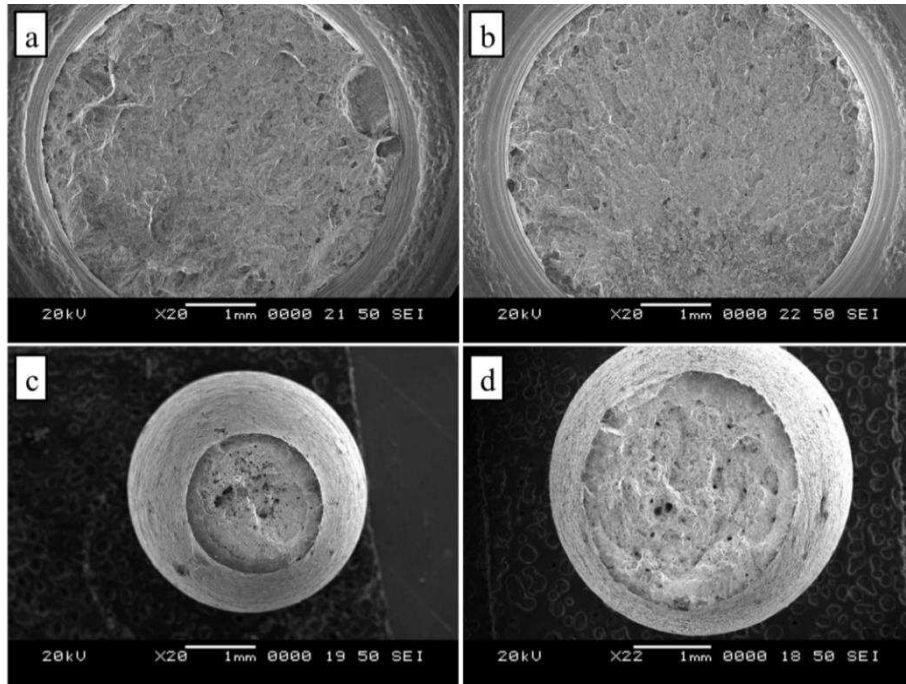


Figure 4.68: SEM images of the fracture surfaces of after tensile tests of ZA27/SiC+Al₂O₃ 5% composites in macroscopic scale (a) Ascast ZA27/SiC+Al₂O₃ 5% (b) Solutionized ZA27/SiC+Al₂O₃ 5% (b) ZA27/SiC+Al₂O₃ 5% MDF at 100 °C up to 3 passes (d) ZA27/SiC+Al₂O₃ 5% MDF at 200 °C up to 6 passes.

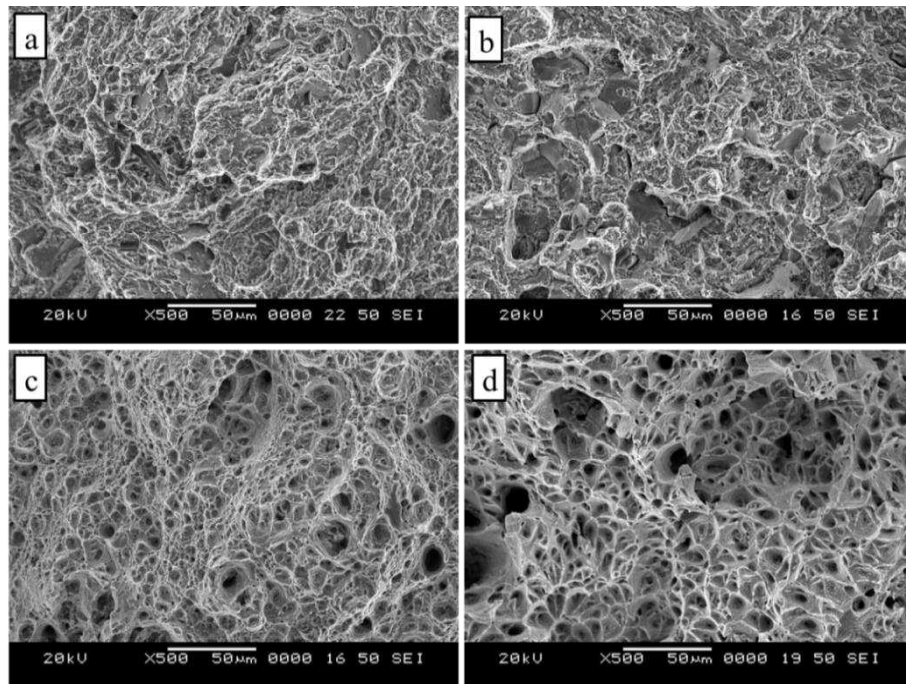


Figure 4.69: SEM images of the fracture surfaces of after tensile tests of ZA27/SiC+Al₂O₃ 5% composite (a) Ascast ZA27/SiC+Al₂O₃ 5% (b) Solutionized ZA27/SiC+Al₂O₃ 5% (b) ZA27/SiC+Al₂O₃ 5% MDF at 100 °C up to 3 passes (d) ZA27/SiC+Al₂O₃ 5% MDF at 200 °C up to 6 passes

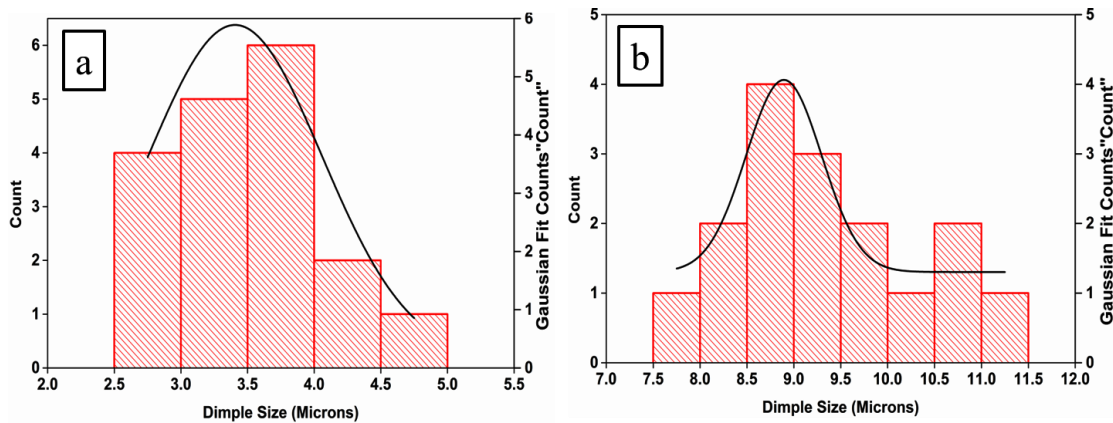


Figure 4.70: Dimple size distribution curve a) ZA27/SiC+Al₂O₃ 5% - MDF processed at 100 °C for 3 passes b) ZA27/SiC+Al₂O₃ 5% - MDF processed at 200 °C for 6 passes

This may be attributed to the elimination of cast morphology as well as grain refinement, reduction in porosity. Macroscopic appearance of the failed tensile samples is as shown in fig. 4.68. It is apparent that there is no necking in the as-cast and solutionized sample, furthermore demonstrates brittle fracture without any notable plastic strain. The fracture surface of the as-cast sample is basically normal to the tensile axis. After the MDF process, the sample showed necking near the fracture section. Figure 4.69 (a-d) shows the SEM micrographs of the fracture surfaces. In the as-cast condition, the fracture mode is mainly brittle fracture after solutionizing treatment composites shows very small contribution toward ductile mode. Dendritic type structures comprise of interdendritic porosity due to incomplete filling of liquid melt during solidification and this is the main reason for the brittle fracture mode in this composite material. The micrographs clearly show that the fracture mechanism of this material changed by MDF process, while the as-cast composites exhibit mainly a brittle fracture mode, with the fracture transforming into a ductile mode after the MDF processing. In addition, there are large dimples connected by a lot of small dimples on the fracture surface as shown in fig. 4.69 and 4.71. ZA27/SiC+Al₂O₃ 5 wt % reinforced composites processed by MDF process at 100 °C upto three passes and upto six passes at 200 °C shows a dimple size of 0.4 and 1 μm respectively but as the percentage of reinforcement increased to 10 wt % the dimple size increases with respect to grain size. This may indicate a failure mechanism resulting from ductile void growth, coalescence, and failure.

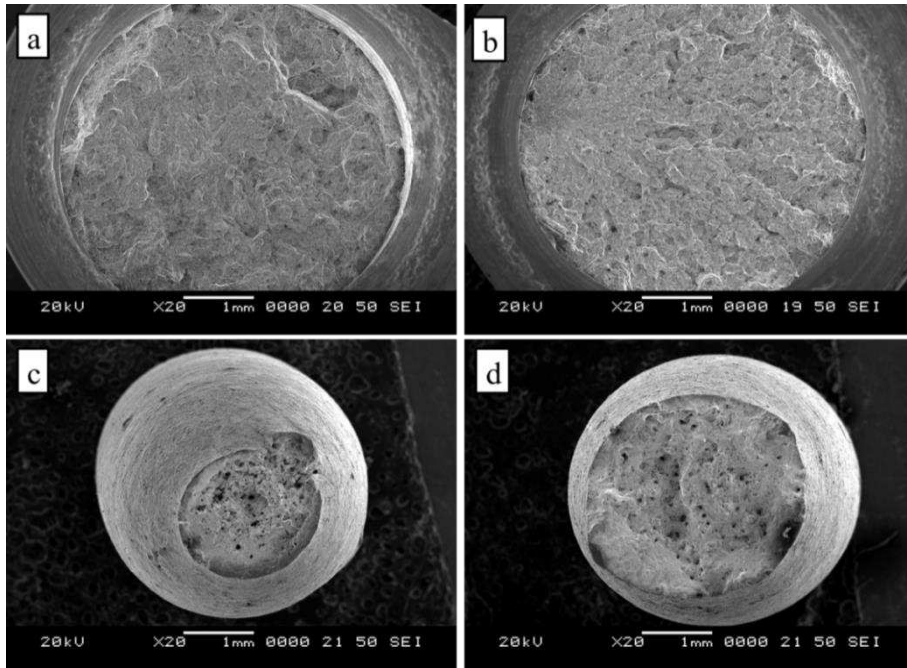


Figure 4.71: SEM images of the fracture surfaces of after tensile tests of ZA27/SiC+Al₂O₃ 10% composites in macroscopic scale (a) Ascast ZA27/SiC+Al₂O₃ 10% (b) Solutionized ZA27/SiC+Al₂O₃ 10% (c) ZA27/SiC+Al₂O₃ 10% MDF at 100 °C up to 3 passes (d) MDF at 200 °C up to 6 passes.

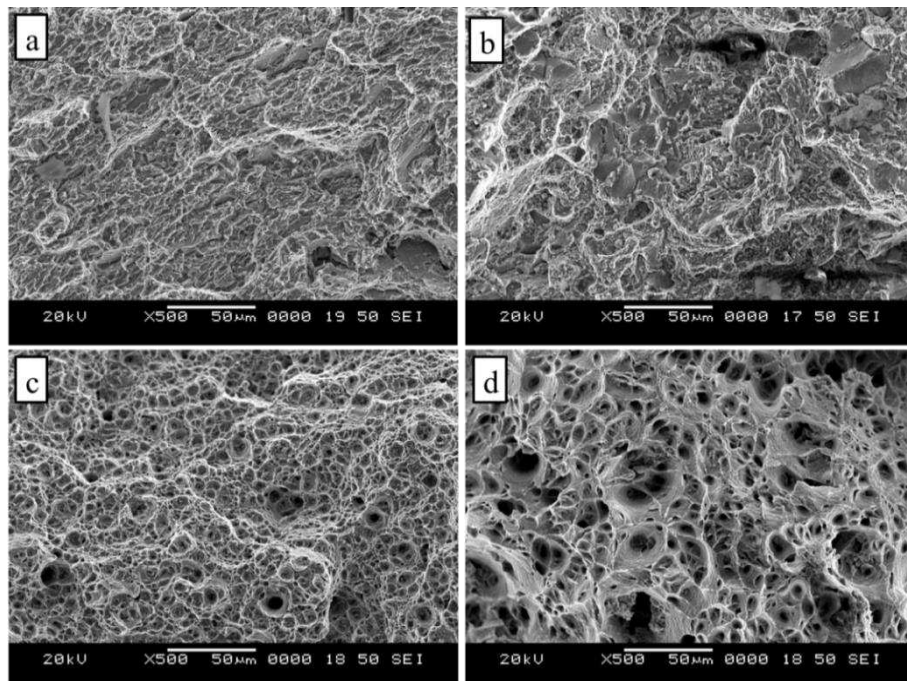


Figure 4.72: SEM images of the fracture surfaces of after tensile tests of ZA27/SiC+Al₂O₃ 10% composite (a) Ascast ZA27/SiC+Al₂O₃ 10% (b) Solutionized ZA27/SiC+Al₂O₃ 10% (c) ZA27/SiC+Al₂O₃ 10% MDF at 100 °C up to 3 passes (d) MDF at 200 °C up to 6 passes.

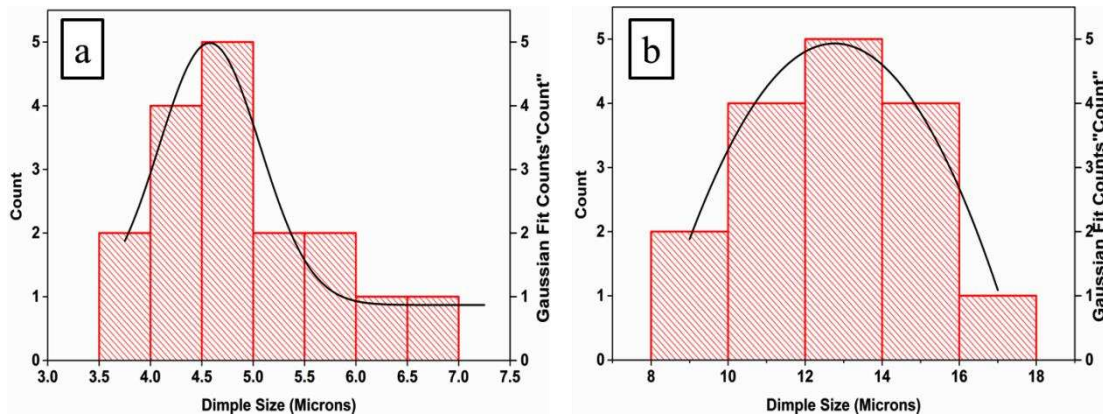


Figure 4.73: Dimple size distribution curve a) ZA27/SiC+Al₂O₃ 10% - MDF processed at 100 °C for 3 passes b) ZA27/SiC+Al₂O₃ 10% - MDF processed at 200 °C for 6 passes.

During MDF processing, the as-cast dendritic structure including porosity mostly gets eliminated, grain refinement and deformation-induced homogenization occur. These changes in structure result in improved ductility.

4.5.5 Wear Properties Evaluation of SiC+Al₂O₃ Reinforced composites

Wear is the progressive loss of material during relative motion between a surface and the contacting substance. The reinforcement has a significant effect on wear behavior of composites than other parameters such as the normal load and the sliding speed. The volume fraction, size, and shape of reinforcements are the material factors which affect the tribological behavior of the composites. The mixture of SiC+Al₂O₃ particles reinforced in ZA27 matrix exhibits better wear properties. Ascast material in both the condition of with and without reinforcement showed higher wear rate but after solutionizing heat treatment dendrites will break and grain structure will be formed with finer and well-distributed micro constituents are helpful to reduce the wear. In accordance with higher uniformity of distribution and decreased size of various micro constituents, positive tribological effects of heat treatment were slightly higher after solutionizing. 10 wt% reinforced composites showed better wear resistance than that of 5 wt% reinforced once. Ultrafine grain was achieved by MDF process at 100 °C and 200 °C upto 3 passes and 6 passes respectively, which affect the wear rate in significantly. Composite processed for 3 passes illustrates excellent performance which we can see in fig. 4.75 and 4.77.

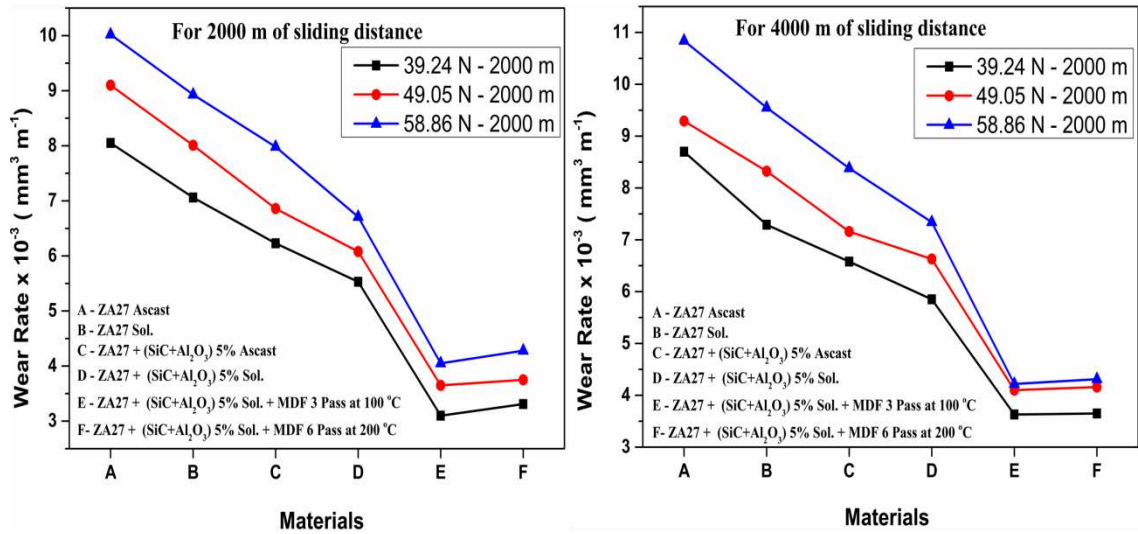


Figure 4.74: Wear rate of ZA27/SiC+Al₂O₃ 5 wt% composite in different conditions (a) For 2000m of sliding distance (b) For 4000m of sliding distance.

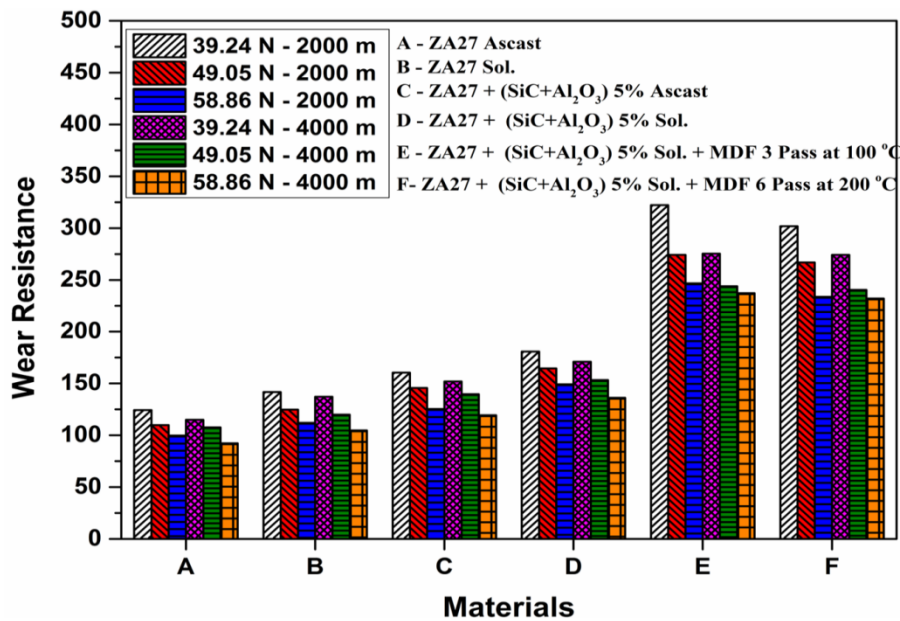


Figure 4.75: Wear Resistance of ZA27/SiC+Al₂O₃ 5 wt% composite in different conditions

Wear rate increased with sliding distance and applied load as that of previous composites reinforced with SiC and Al₂O₃ individually. Wear resistance of the ZA27/SiC+Al₂O₃ composite was higher than that of ZA27/Al₂O₃ composites but with respect to ZA27/SiC composite it was less. Abraded surfaces of the composites after testing at different applied loads and sliding distances are shown in fig. 4.78. The SEM micrographs of typical worn surfaces of the composites reinforced with

SiC+Al₂O₃ mixture in ZA27 matrix are presented in fig. 4.78. The worn surface was found similar to above two materials reinforced with SiC and Al₂O₃ individually in ZA27 alloy. SiC+Al₂O₃ particles were seen in fig. 4.78 (a & e), parallel grooves and scratches can be seen over the entire surface in the direction of sliding, these grooves and scratches resulted from the ploughing action.

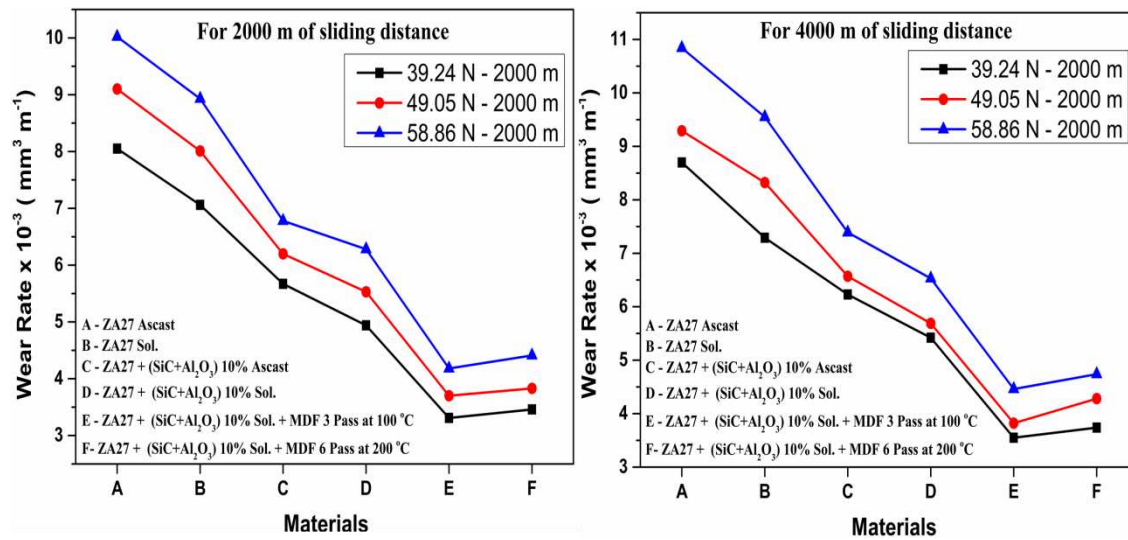


Figure 4.76: Wear rate of ZA27/ SiC+Al₂O₃ 10 wt% composite in different conditions (a) For 2000m of sliding distance (b) For 4000m of sliding distance.

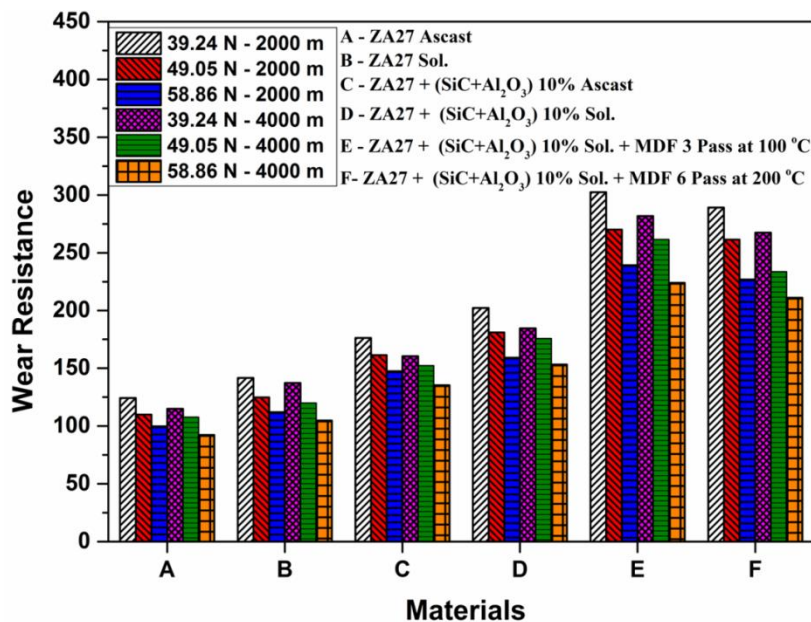


Figure 4.77: Wear Resistance of ZA27/SiC+Al₂O₃ 10 wt% composite in different condition

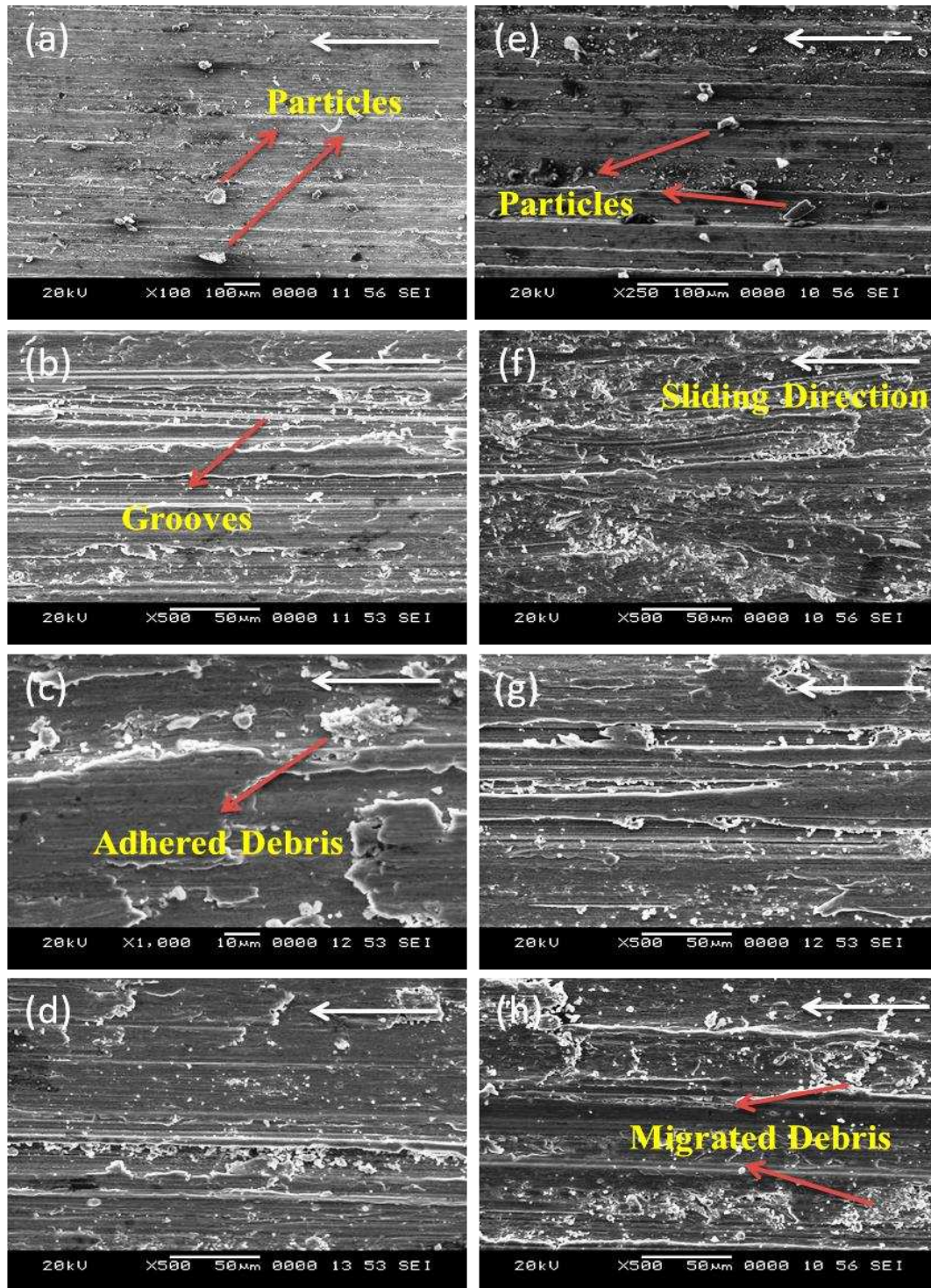


Figure 4.78: SEM micrographs of the worn surfaces of ZA27/ SiC+Al₂O₃ in 5 & 10 wt%.(a) ZA27/ SiC+Al₂O₃ 5% ascast - 39.24N - 2000m (b) ZA27/ SiC+Al₂O₃ 5% - sol - 49.05N - 2000m (c) ZA27/ SiC+Al₂O₃ 5% - MDF 3 pass - 58.86N - 2000m (d) ZA27/ SiC+Al₂O₃ 5% - MDF 6 Pass - 58.86N - 4000m (e) ZA27/ SiC+Al₂O₃ 5% - ascast- 39.24 - 2000m (f) ZA27/ SiC+Al₂O₃ 5% - sol- 58.86N - 4000m (g) ZA27/ SiC+Al₂O₃ 10% - Ascact 39.24N – 4000m (h) ZA27/ SiC+Al₂O₃ 10%- MDF 6 pass- 49.05N - 4000m.

Adhered and migrated debris were observed in fig.4.78 (c & h) which shows the dual type of wear mechanism, abrasive mechanism was observed in initial condition for lower load and shorter sliding distance but as we increase the distance and load the adhesive mechanism was seen. Thus, wear resistance is improved after the addition of particle and by MDF processing. Improvement in wear resistance can make these alloys very attractive compared to traditional bearing alloys. Also, the improvement in wear resistance is significant at high pressures and long range distances which provide competencies for these composites in different tribological applications, including low speed and high load.

CHAPTER 5

APPLICATIONS

5.1 ZA27/SiC/Al₂O₃ COMPOSITE MATERIAL FOR CYLINDER ROLLER BEARING

Cylindrical Roller Bearings are bearing in which cylinders are used as the rolling elements. As such, the rollers have a greater (linear) contact area with the outer ring and they distribute loads across a broader surface. Roller bearing has a high radial load capacity and is suitable for low speed and as well as high speeds.

Cylinder roller bearing features are it as high load carrying capacity, high stiffness, accommodate axial displacement, low friction, long service life- The roller profile reduces edge stresses at the roller/raceway contact and sensitivity to misalignment and shaft deflection, enhanced operational reliability- The surface finish on the contact surfaces of the rollers and raceways supports the formation of a hydrodynamic lubricant film, Separable and interchangeable- The separable components of cylindrical roller bearings are interchangeable. This facilitates mounting and dismounting, as well as maintenance inspections, and lower machining cost- they can be machined very accurately due to their structure. Having a separable inner or outer ring.

In the case of Roller bearings, the bearing has inner and outer races and a set of rollers. Outer race is a ring with a groove where the rollers rest. The groove is usually shaped so the rollers are a slightly loose fit in the groove. Thus, in principle, the roller's contacts are linear type. Inner ring is plane in design ie., it does not have any groove on the outer surface of it as shown in fig. 5.1. The pressure at the rolling contact area and the cyclic over rolling creates fatigue in the bearing rings when the bearing is in operation. The rolling element rollers transfer the load between inner and outer rings. Typically, the same material is used for fabrication of bearing rings and rolling elements.

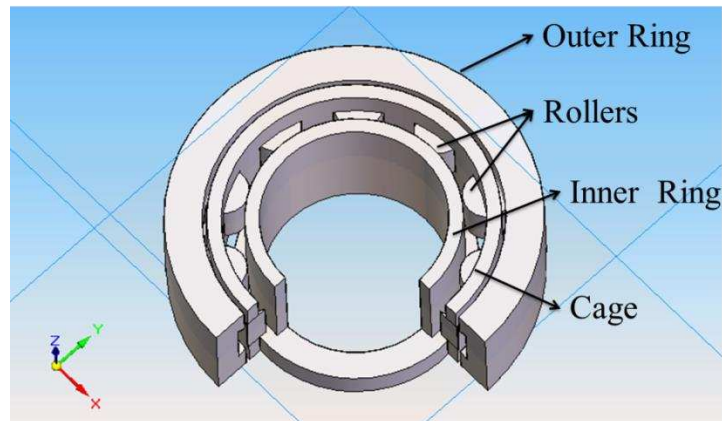


Figure 5.1: Representation of cylinder Roller Bearing Parts

Table 5.1: Bearing Weight and Cost Estimation (B1, B2, B3)

Sl.No	1	2	3
Name	B1 – Bearing 1	B2 – Bearing 2	B3 – Bearing 3
Cylinder Roller Bearing part Weight - g			
Inner Ring	6.001	12.80	15.91
Outer Ring	15.025	23.648	31.965
Roller	$0.724 \times 11 = 7.96$	$0.7241 \times 10 = 7.24$	$2.02 \times 11 = 22.22$
Cage	2	5	3
Total	31.014	48.688	73.095
Cylinder Roller Bearing Part Dimension - mm			
Outer Diameter	35	40	47
Inner Diameter	17.5	20	20
Width of the Bearing	11	12	14
Roller Diameter	5.5	5.5	7
Height of the Roller	5.5	5.5	10
Cost Estimation - ₹			
Machining and Material Cost	~ 450	~ 600	~ 650

The primary purposes of a cage is, it separating the rolling elements to reduce the frictional heat generated in the bearing, keeping the rolling elements evenly spaced to optimize load distribution, guiding the rolling elements in the unloaded zone of the bearing, retaining the rolling elements of separable bearings when one bearing ring is removed during mounting or dismounting and cages centre the rolling elements permit the lubricant to enter the bearing easily. Different types of cage materials are used in general are 1. **Stamped metal cages** - Stamped metal cages are lightweight and withstand high temperatures. 2. **Machined metal cages** -Machined metal cages

are made of brass or sometimes steel or light alloy. They permit high speeds, temperatures, accelerations and vibrations. 3. **Polymer cages** - Polymer cages are made of polyamide 66 (PA66), polyamide 46 (PA46) or sometimes polyetheretherketone (PEEK) or other polymer materials. The good sliding properties of polymer cages produce little friction and, therefore, permit high speeds. 4. **Pin-type cages**- Steel pin-type cages need pierced rollers and are only used together with large-sized roller bearings. These cages have relatively low weight and enable a large number of rollers to be incorporated.

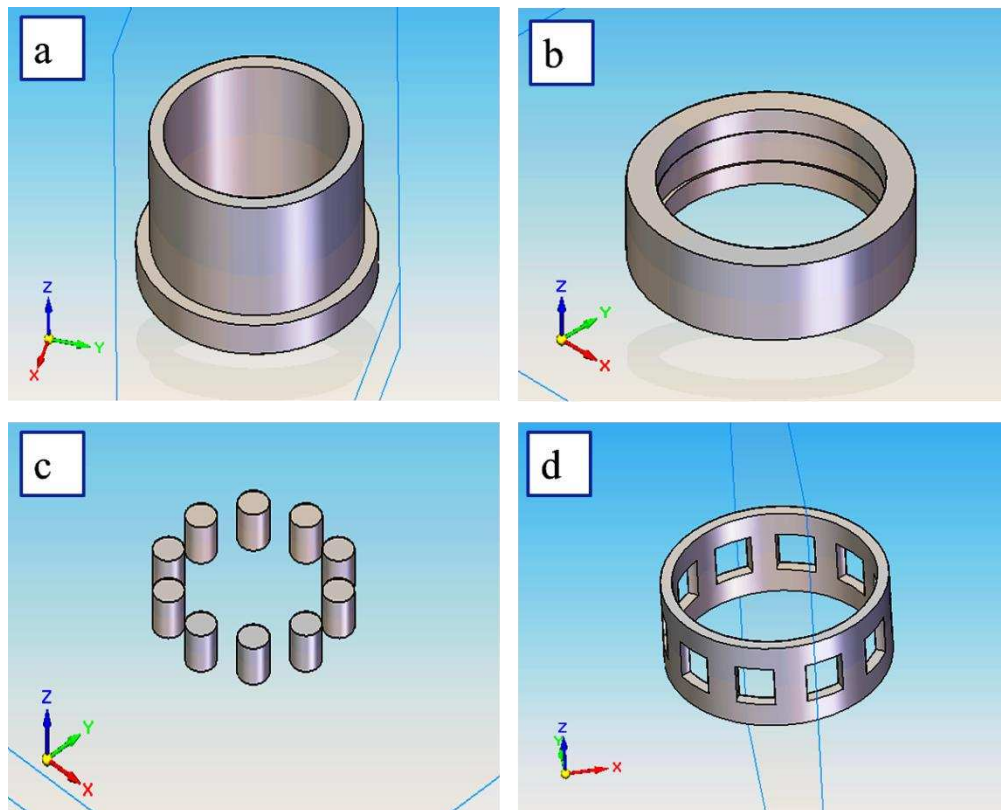


Figure 5.2: CAD model for different parts of Cylinder Roller Bearing
a) Inner Ring b) Outer Ring c) Rollers d) Cage

Figure 5.2 shows the CAD model of cylinder roller bearing parts designed using solid edge V19 software. Successfully multi directional forged ZA27 based composites reinforced with SiC and Al₂O₃ particles were tested for various mechanical and tribological properties, after summarizing the results of both mechanical and tribological test, the composite material with best performance was taken as a raw material for machining of cylinder roller bearing application. Design and dimension of cylinder roller bearing is shown in fig. 5.3. Machining of different parts of cylinder

roller bearing was done by CNC machine in three stages, foremost normal CNC machining was done with an allowance in dimension and rest of two stages in micron level for machining to achieve super grind finish. As a final step assembling of cylinder roller bearing parts was done manually, commercially available synthetic oil was used as a lubricate for trail runs of assembled cylinder roller bearing. In three different dimensions cylinder roller bearing was fabricated and it is shown in fig. 5.4.

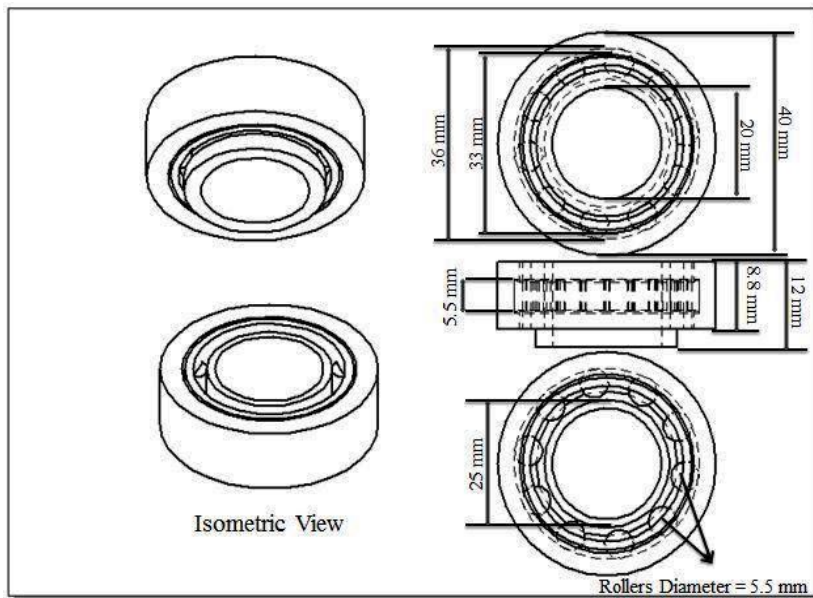


Figure 5.3: Schematic diagram of cylinder roller bearing design

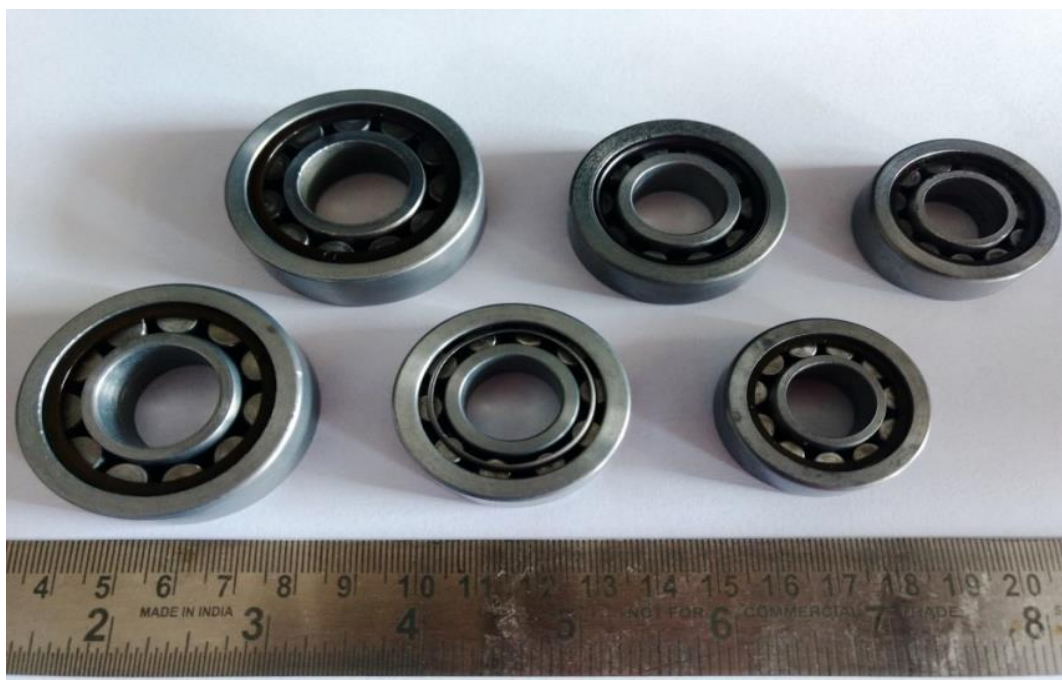


Figure 5.4: Photograph of Cylinder Roller Bearing

CHAPTER 6

CONCLUSIONS

In present research work, ZA27 alloy as base matrix and SiC and Al₂O₃ as reinforcement were used to prepare the metal matrix composites. The composites were fabricated using stir casting method followed by squeezing at a certain pressure. Microstructural aspects, mechanical and tribological properties of the base alloy, MDF processed and unprocessed composites were studied. Based on the experimental evaluation, the study is summarized.

1. Stir casting was successful in achieving fairly uniform distribution of SiC and Al₂O₃ particles in ZA27 matrix.
2. Reinforcement of SiC and Al₂O₃ particles in ZA27 matrix shows the improvement in mechanical and tribological properties as compared with the base material.
3. The density of ZA27 alloy decreased by incorporation of SiC and Al₂O₃ particles. Some Clusters and fair dispersion of SiC and Al₂O₃ particles in ZA27 matrix were observed in microstructure and confirmed by EDX.
4. SiC reinforced composites performs better when compared with Al₂O₃ reinforced, mixture of SiC and Al₂O₃ particles reinforced and ZA27 base matrix material. As the percentage of reinforcement increased from 5 wt% to 10 wt% the properties of the material also increased, this trend remains same in all the composites reinforced with different reinforcing particles.
5. The enhancement of tensile strength and hardness with the incorporation of particles fillers can be explained as follows. Presence of hard particles, the load on the matrix gets transferred to the reinforcing elements thereby increasing the load bearing capability of the composites. Increase in weight percentage of the filler material, more load gets transferred to reinforcement which leads to an increase in tensile strength. Moreover, Presence of hard ceramics like SiC and Al₂O₃, puts a restriction to the plastic flow as a result of

dispersion of these hard particles in the matrix, thereby providing enhanced mechanical properties in the composite.

6. Solutionizing heat treatment was carried out at 365 °C for 5 hours by using muffle furnace and quenched in water at room temperature. At 365 °C, the dissolution of Zn and Al takes place and the as-quenched specimen will be in supersaturated β phase. Later β phase get transformed to α , ϵ and η phases which gives homogenizes microstructure. Elimination of the dendritic structure during solutionizing treatment promoted the increase in hardness for the ZA27 alloy and its composites, this is due to the formation of equilibrium phases.
7. ZA27 based composites were successfully processed by the MDF at temperature of 100 °C up to three passes and 200 °C up to six passes with an equivalent strain of 0.54 and 1.08 respectively. Porosity level decreased with an increase in the number of MDF passes when compared with unreinforced material.
8. Composites reinforced with SiC particles in 5 and 10 wt % were MDF processed at different temperatures. The average grain size was reduced from 25-30 μm to 0.2-0.35 μm , 0.45-0.5 μm respectively in the case of samples MDF processed at 100°C up to three passes. Grain growth phenomena were observed in MDF processed composites at a higher temperature (200 °C) which leads to the formation of larger grains, even though composites were MDF processed for 6 passes (0.8-1 μm , 0.9-1.2 μm respectively) when compared with 3 passes at 100 °C. The initial lamellar Al-rich and Zn-rich phase was gradually refined to a spherical shape and distributed more uniformly with an increasing number of passes. Moreover, the process carried out at 200 °C for six passes showed more uniform microstructure.
9. Tensile strength of the composite material was increased with that addition of SiC particles. Further MDF process leads to an improvement in UTS. The highest ductility was obtained when the sample forged at 100 °C 3 passes. The excellent ductility attributed to its uniform distribution of secondary phase particles, reduction in inhomogeneity, porosity and fine grain structure. Initial ascast condition showed a brittle type of fracture. Brittle mode of fracture was

transformed into ductility mode by MDF processing at 100 °C upto 3 passes and at 200 °C upto 6 passes. Dimple type of fracture reveals the ductile behavior. After MDF processing for higher number of passes dimples size decreased and showed a homogeneous distribution across the fracture surfaces.

10. Composites reinforced with Al₂O₃ particles in 5 and 10 wt % were MDF processed at 100 °C up to three passes reduces the grain size from 20-30 μm to 0.4-0.45 μm, 0.5-0.6 μm respectively with the dual type of microstructure having both lamellar to the cellular structure. On further MDF processing at 200 °C upto 6 passes showed the grain size of 1.2-1.4, 1.5 μm with equiaxed grain structure, this increase in grain size is due to the rise in temperature of processing condition. Small cracks were seen at the edges of the Al₂O₃ particle because of load applied during MDF process upto 3 passes at 100 °C and with a higher number of passes the Al₂O₃ particle broken into several pieces and forms a cluster of Al₂O₃ particle.
11. Addition of Al₂O₃ particle increased the UTS and hardness values in both 5 and 10 wt % reinforced composites and further improvement in UTS and hardness value is due to MDF process upto three passes at 100 °C and upto six passes at 200 °C. The ductility of Al₂O₃ particle reinforced composites were low when compared with other composites reinforced with SiC and mixture of SiC+ Al₂O₃ particle.
12. A mixture of SiC +Al₂O₃ with 5 and 10 wt % reinforced composites were also MDF processed at varying temperature for a different number of passes. The average grain size reduced from 15-20 μm to 0.2-0.25 μm, 0.3-0.4 μm when processed at 100 °C upto three passes and 0.8-0.9 μm, 0.9-1.1 μm when processed at 200 °C upto Six passes. Hardness, ultimate tensile strength and ductility of the composites were improved by MDF processing.
13. Zinc Aluminum based composites reinforced with SiC, Al₂O₃ and mixture of SiC +Al₂O₃ showed a remarkable improvement in UTS and ductility after SPD process as a function of a number of passes, i.e. the higher the number of passes leads to achieving higher the elongation to failure. This substantial improvement in ductility of the present composites after several MDF passes

can be attributed to the elimination of as-cast morphology as well as grain refinement, reduction in microporosity (or micro-voids), redistribution of reinforcing particles, and also the change in the composition of the phases.

14. Composites reinforced with SiC particles in 5 and 10 wt% were MDF processed at 100 °C and 200 °C, these composite materials were tested for wear behaviour with three different loads and for two sliding distance at constant sliding speed. As applied load and sliding distance increased the wear rate of the material also increased.
15. Samples tested with lower load and sliding distance were showing abrasive type of wear mechanism but as the applied load and sliding distance increased, mechanism changed to adhesion type. This is due to the rise in temperature between the interface of pin and disc, material detached from the pin as debris get adhered to the surface of pin which influences the mode of mechanism to switch from abrasion to adhesion. MDF processed ZA27/SiC_p for 3 passes at 100 °C showed better wear resistance with ultra-fine grains and higher hardness. Temperature is an important parameter that affects the tribological behavior of composites.
16. Wear rate of Al₂O₃ reinforced composite was more when compared with SiC reinforced ones. Results of wear test showed that Al₂O₃ reinforced composites MDF processed for 3 passes at 100 °C gives higher wear resistance than the other condition in Al₂O₃ reinforced materials. Increased wear rate due to higher applied load and sliding distance resulting in abrasive type of wear mechanism with more amount of matrix debris formation.
17. In an overall the results of wear test shows, SiC reinforced composite performed better as compared with Al₂O₃ reinforced and Mixture of SiC + Al₂O₃ reinforced materials. Applied load plays a major role followed by sliding distance in concluding the wear resistance of the composite materials.
18. Wear study of composites indicated that the specific wear rate was highly influenced by applied load and sliding distance. Ascast and solutionized samples show relatively higher wear rate as compared to MDF processed samples when tested with higher applied load, long sliding distance and constant speed, due to the redistribution of particles after MDF process and

lower grain size achieved by MDF process. Both abrasive type and adhesive type of wear mechanism has been proposed as revealed by SEM investigation on worn surfaces of processed samples.

19. Grain size reduction from micron level to nano level was observed by the SEM micrograph and it is confirmed by TEM analysis. Presence of large number of dislocations was observed which influence the enhancement of mechanical properties. Different phases were confirmed with the help of EDX analysis.
20. As an application, a Cylinder Roller Bearing is fabricated by best mechanical properties and wear resistant ZA27/SiC/Al₂O₃/SiC+Al₂O₃ composite material.

6.1 Scope for future work

After successful fabrication of ZA27/SiC/Al₂O₃/SiC+Al₂O₃ composites in different composition with varying weight percentage, further composites were processed through multidirectional forging upto three passes at 100 °C and upto six passes at 200 °C temperature. Fairly uniform distribution of SiC and Al₂O₃ were confirmed by optical microscopy and electron microscopy. Density, Ultimate tensile strength, percentage of elongation, hardness and wear resistance were enhanced by the multidirectional forging process. X-Ray diffraction analysis was done to know the phase transformation in composites after solutionizing and multidirectional forging process. Apart from these features, to meet the real time application in tough environment the following different approaches can also be considered for future work.

1. Tribological and mechanical properties can be improved by the incorporation of many other reinforcing materials but one should consider the density of opt reinforcing materials as an important factor.
2. Various reinforcing materials behavior can be analyzed with zinc aluminum based alloy after multidirectional forging process for higher end application.
3. Orientation of grains plays a major role in defining the material properties, so texture analysis using pole figures can be study with Electron back scattered diffraction (EBSD).

4. Corrosion is a significant challenge to most of the industries in the present scenario, so it is very important to understand the corrosion behavior of ZA27 based composites, before proposing the material to any real time applications.
5. Wear behavior of the material under high temperature and lubricated conditions can be considered for practical usage of this material in bearings.
6. Prolonged Aging studies can be conducted for multidirectional forged samples to know the behavior of composites processed material after aging.
7. Fatigue behavior of multidirectional forged samples can be examined to determine the behavior of composite material under fluctuating loads.
8. Evaluation of mechanical performance and efficiency of the designed and fabricated cylinder roller bearing.

REFERENCE

Aashuri, H., (2005). "Globular structure of ZA27 alloy by thermomechanical and semi solid treatment", *Materials Science and Engineering A*, 391, 77-85.

Ahmet, T., Can, K., Huseyin, S. (2007). "Comparison on the wear properties of modified ZA-08 alloys and conventional bearing bronze", *Materials and Design*, 28, 1889-1897.S

Al-maharbi, M., Karaman, I., & Purcek, G. (2010). "Flow response of a severe plastically deformed two-phase zinc-aluminum alloy". *Tribology in Industry*, 527, 518–525. <http://doi.org/10.1016/j.msea.2009.09.053>.

Aleksandar, V., Ilija, B., filip, V., Biljana, B., Jovan, R., (2014). "Structural, mechanical and tribological characterization of Zn25Al alloys with Si and Sr addition", *Materials and Design*, 64, 381-382.

Alicia, E. Ares., and Carlos, E. Schvezov. (2013). "Columnar to equiaxed transition in metal matrix composite reinforced with silicon carbide particles", *Journal of Metallurgy*, Vol 2013, Article ID- 628495, 12 pages.

Altinkok, N., Oxsert, I., and Findik, F., (2013). "Dry sliding wear behavior of Al₂O₃/SiC particle reinforced aluminium based MMCs fabricated by stir casting method", *Acta Physica Polonica A*, Vol 124, pp 11-19.

Auras, R., and Schvezov, C. (2004). "Wear behavior, microstructure, and dimensional stability of as-cast zinc-aluminum/SiC (metal matrix composites) alloys", *Metallurgical and Materials Transactions*, Vol 35 A, 1579–1590.

Babic, M., S. Mitrovic and Bobic, I. (2007). "Tribological properties of composites with substrate made of the ZA-27 alloy reinforced by the graphite particles". *Tribology in Industry*, Vol 29 (3), 3–8.

Babic, M., Mitrovic, S., and Jeremic, B. (2010). "The influence of heat treatment on the sliding wear behavior of a ZA-27 alloy." *Tribology International*, 43(1-2), 16–21.

Babic, M., Slobodan, M., Fatima, Z., Ilija, B. (2010). "Wear behavior of composites based on ZA27 alloy reinforced by Al₂O₃ Particles under dry sliding condition" *Tribol Lett*, 38:337-346. DOI: 10.1007/s11249-010-9613-5.

Bansal, U., & Sharma, M. (2015). "Development of mechanical properties by severe plastic deformation methods", 2 (5), 38-45. <http://doi.org/10.17148/IARJSET.2015.2507>.

Biljana Bobić¹, Nikola Bajić, Milan T. Jovanović, I. B. (2009). "Microstructure and mechanical properties of Zn₂₅Al₃Cu based composites with large Al₂O₃ particles at room and elevated temperatures". *Association of Metallurgical Engineers of Serbia*, Vol 15 (4) p. 245-255.

Bobic, I., Ninkovic, R., & Babic, M. (2004). "Structural and mechanical characteristics of composites with base matrix of ZA27 alloy reinforced with Al₂O₃ and SiC particles". *Tribology in Industry*, Vol 26 (3), 27–29.

Babic, M., Aleksandar, V., Slobodan, M., Ilija, B. (2009). "Influence of T4 heat treatment on tribological behavior of ZA27 alloy under lubricated sliding condition", *Tribol Lett*, 36:125-134. Doi: 10.1007/s11249-009-9467-x.

Baskar, S., Sriram, G. (2014). " Tribological behaviour of journal bearing materials under different lubricants", *Tribology in Industry*, Vol 36, No. 2, 127-133.

Bozic, D., Stasic, J., Rajkovic, (2011). " Microstructures and mechanical properties of ZA27-Al₂O₃ composites obtained by powder metallurgy process", *Science of Sintering*, 43, pp 63-70. doi: 10.2298/SOS1101063B.

C. D. Lee, (2007). *Material science and Engineering A Structure* 464 2007 249-266.

Chen, F., Wang, T., Chen, Z., Mao, F., Han, Q., and Cao, Z. (2015). "Microstructure, mechanical properties and wear behavior of Zn – Al – Cu – TiB₂ in situ composites". *Trans. Nonferrous Met. Soc. China*, 25, 103–111.

Chen, Q., Shu, D., Hu, C., Zhao, Z., & Yuan, B. (2012). "Grain refinement in an as-cast AZ61 magnesium alloy processed by multi-axial forging under the multi-temperature processing procedure". *Materials Science and Engineering*, 541, 98–104.

Chengpeng, W., Fuguo, L., Bo, C., Zhanwei, Y., & Hongya, L. (2012). "Severe plastic deformation techniques for bulk ultrafine-grained materials". *Rare Metal Materials and Engineering*, 41(6), 941–946. [http://doi.org/10.1016/S1875-5372\(12\)60049-6](http://doi.org/10.1016/S1875-5372(12)60049-6).

Chih-Fu., Jiun-Hung Pan., Te-Hao Lee. (2009). "Work softening and anneal hardening behaviours in fine grained Zn-Al Alloys", *Journal of Alloys and Compounds*, 468, 230-236.

Chou, C.Y., Lee, S.L., Lin, J.C., and Hsu, C.M. (2007). "Effects of cross-channel extrusion on the microstructures and superplasticity of a Zn–22wt.% Al eutectoid alloy." *Scripta Materialia*, 57(10), 972–975.

Choudhary. P., Das. K., Das. S., (2005). "Evolution of cast and heat treated microstructure of a commercial bearing alloy". *Materials Science Engineering A*, 398 (1-2) : 332-43.

Chuan Ting Wang., Mong Gao., Robert, J. K., Wood., Terence G. Langdon. (2011). "Wear behavior of an aluminum alloy processed by equal channel angular pressing", *Journal of Materials Science*, 46: 123-130.

Dora siva prasa., Chintada Shoba., Nallu Ramanaiah. (2014). " Investigations on mechanical properties of aluminum hybrid composites" , *Jour of Materials Research and Tech*, , 3(1), 79-85.

Durman, M., S. Murphy. (1997). "An electronmetallographic study of pressure die-cast commercial zinc–aluminum-based alloy ZA27", *Journal of Materials Science*, 32 1603-1611.

El Aal, M. I. A., El Mahallawy, N., Shehata, F. A., El Hameed, M. A., Yoon, E. Y., and Kim, H. S. (2010). "Wear properties of ECAP processed ultrafine grained Al-Cu alloys", *Materials Science and Engineering: A*, 527(16), 3726-3732.

El-khair, M. T. A., Daoud, A., & Ismail, A. (2004). "Effect of different Al contents on the microstructure, tensile and wear properties of Zn-based alloy". *Materials Letters*, 58, 1754–1760.

El-khair, M. T. A., Lotfy, A., Daoud, A., & El-sheikh, A. M. (2011). "Microstructure, thermal behavior and mechanical properties of squeeze cast SiC, ZrO₂ or C reinforced ZA27 composites". *Materials Science & Engg A*, 528 (6), 2353–2362.

Estrin, Y., and Vinogradov, A. (2013). "Extreme grain refinement by severe plastic deformation: A wealth of challenging science." *Acta Materialia*, 61(3), 782–817.

Fatih, C., ay., S. Can, Kurnaz., (2005) "Hot tensile and fatigue behavior of zinc–aluminum alloys produced by gravity and squeeze casting". *Materials Design*. 26 479–485.

Fei Chen., Tong-min Wang., Zong-ning Chen., Feng Ao., Qiang Han., Ahi-qiang Cao. (2015). " Microstructure , Mechanical properties and wear behaviour of Zn-Al-Cu-TiB₂ in Situ composites", *Trans nonferrous Met. Soc. China*, 25, 103-111.

Fethma, M. Nor., Muhammad Amin Sidek., Daisman, P.B. Aji., Denni Kurniawan. (2020). "Finite element analysis of multidirectional forging dies for severe plastic deformation of magnesium alloy", *AIP conference proceedings*, 2262, 030019.

G. Salishchev, R. Zaripova, R. Galeev, O. V. (1995). "Nanocrystalline structure formation during severe plastic deformation in metals and their deformation behavior", *Nanostructured Materials*, 6, 913–916.

Gao, L. L., and Cheng, X. H. (2008). "Microstructure, phase transformation and wear behavior of Cu–10% Al–4% Fe alloy processed by ECAE." *Materials Science and Engineering: A*, 473(1), 259-265.

Gencaga Purcek., Temel, S., Tevfik, K., Samuel, Murphy. (2002). "Dry sliding friction and wear properties of zinc based alloys", *Wear*, 252, 894-901.

Gencaga Purcek. (2005). "Improvement of mechanical properties for Zn – Al alloys using equal-channel angular pressing", *J. of Materials Proc. Tech*, 169 169, 242–248.

Geng Haoran., Tian Xianfa, Cui Hongwei., Li, Cjengdong., Zhao Peng. (2001). "Antifriction and wear behaviour of ZAS35 zinc alloys: Influence of heat treatment and melting technique", *Materials Science and Engineering A* 316, 109-114.

Gencaga, Purcek., Burhanettin, S. Altan., Ibrahim Miskioglu., Pey H. Ooi. (2004). "Processing of eutectic Zn 5% Al alloy by equal channel angular pressing", *Journal of Materials Processing Technology*, 148, 279-287.

Guo, W., Wang, Q., Ye, B., and Zhou, H. (2013). "Enhanced microstructure homogeneity and mechanical properties of AZ31 – Si composite by cyclic closed-die forging". *Journal of Alloys and Compounds*, 552, 409–417.

Hall. E, O., and Sylwestrowicz. W. (1951). " The Deformation and Ageing of Mild Steel", *Proc. Phys. Soc. B* 64, 495.

Hamidreza Ghandvar., Mohd Hasbullah Idris., Norhayati Ahmad., Navid Moslemi. (2017). "Microstructure development mechanical and tribological properties of a

semisolid A356/xSiCp composite" *Journal of Applied Research and Technology*, 15 533–544.

Hashim, J., Looney, L., & Hashmi, M. S. J. (2002)A. "Particle distribution in cast metal matrix composites" *Journal of Materials Processing Technology*, 123 Part I, 251–257.

Hashim, J., Looney, L., & Hashmi, M. S. J. (2002)B. "Particle distribution in cast metal matrix composites". *Journal of Materials Processing Technology*, 123 Part II, 258–263.

Hector, J., Dorantes-Rosales., Victor M., Loopez-Hirata., Jose de Jesus Cruz-Rivera., Maribel L., Saucedo-Munoz. (2005). "Coarsening of t precipitates during aging in a Z2-22 wt.% Al-2wt% Cu alloy", *Materials letters*, 59, 2075-2078.

Hesham Elzanaty (2014). "Al- Addition influence on tribological properties of Zn based alloys", *International Journal of Research in Engineering and Technology*, Vol 2, issue 7, 63-68.

Hong, M., Wu. D., Chen, R.S., and Du. X.H. (2014). "Ductility enhancement of Ew75 alloy by multi directional forging", *Journal of Megnesium and Alloys* 2, 317-324.

Jayashree, P. K., C, G. S. M., Kini, A., Sharma, S. S., and Shetty, R. (2013). "Review on effect of silicon carbide (SiC) on stir cast aluminium metal matrix composites", *International Journal of Current Engineering and Technology*, ISSN 2277 - 4106, 1061–1071.

Jian-quan, T. A. O., Yuan-sheng, C., Shao-dong, H., Fei-fei, P., & Wen-xuan, Y. (2012). "Microstructural evolution and mechanical properties of ZK60 magnesium alloy prepared by multi-axial forging during partial remelting". *Transactions of Nonferrous Metals Society of China*, 22, s428–s434.

Jian Qin., Zhan Zhang and X-Grant Chen. (2016). "Mechanical properties and thermal stability of hot-rolled Al–15%B4C composite sheets containing Sc and Zr at Elevated Temperature" *Journal of composite materials Sage*, DOI: 10.1177/0021998316674351.

Jose D. Villegas-C., Maribel. L., Saucedo-M., Victor M. Lopez-H., Antonio D., Avila-Davila., and Jorge Luis Gonzalez-Velazquez. (2014). "Effect of homogenization process on the hardness of Zn–Al–Cu alloys", *International Journal of Minerals, Metallurgy, and Materials*, Vol 22, 1076.

Jose David Villegas-Cardenas., Maribel Leticia Saucedo-Munoz., Victor Manuel Lopez-Hirata., (2014). "Effect of phase transformation on hardness in Zn-Al-Cu alloys". *Materials Research*, DOI:<http://dx.doi.org/10.1590/1516-1439.228913>.

Jovanovic, M. T., & Ilic, N. (2003). "Microstructure and strength of ZA-27-based composites reinforced with Al₂O₃ particles". *Materials Letters*, 57, 1683–1688.

Jyothi. P. N., Jagath. M.C., Channakeshavalu. (2015). "Wear characteristics of Za27/Al2O3 composites processed by centrifugal casting", *International Journal of Materials Science and Engineering*, Vol 3, no 4.

Kaibyshev, O. A. (2001). "Grain refinement in commercial alloys due to high plastic deformations and phase transformations", *Journal of Materials Processing Technology*, 117, 300–306.

Kai-bo NIE., Zhi-Hao Zhu., Paul Munroe., and Kun-kun Deng., Ya-chao Guo. (2020). " Microstructure and mechanical properties of Tic nano particle- reinforced Mg-Zn-Ca matrix nano composites processed by combining multidirectional forging and extrusion", *Trans. Non ferrous Met. Soc. China*, 30, 2394-2412.

Kavosi, J., Saei, M., Kazeminezhad, M., & Dodangeh, A. (2014). "Modeling of dislocation density and strength on rheoforged A356 alloy during multi-directional

forging", *Computational Materials Science*, 81, 284–289. <http://doi.org/10.1016/j.commatsci.2013.08.029>.

Kenneth Kanayo Alaneme and Olusola Joseph Ajayi. (2015) "Microstructure and mechanical behaviour of stircast Zn27 Al vased compsites reinforced with rice huck ash, Silicon carbide and graphite", *Journal of Kind Saud University- Engineering Science*, <http://dx.doi.org/10.1016/j.jksues.2015.06.004>.

Khan Hasib Kaisar., Md. Nasrul Haque and Kazi Md. Shorowordi. (2011). "Processing and characterization of SiC reinforced zinc -aluminum metal matrix composites as bearing materials", *International Conference on Mechancial Engineering*, ICME 11-RT-046.

Kim, W. J., Kim, J. K., Kim, H. K., Park, J. W., and Jeong, Y. H. (2008). "Effect of post equal-channel-angular-pressing aging on the modified 7075 Al alloy containing Sc." *Journal of Alloys Compounds*, 450(1–2), 222–228.

Kiran, T.S., Prasanna Kumar., Basavarajappa, S., Vishwanatha, B. M., (2013). "Mechanical properties of Ascst ZA27-27/Gr/SiCp Hybrid compsoite for the application of Journal Bearing", *Journal of Engineering Science and Technology*, Vol. 8, No. 5, pp 557-565.

Kobayashi, C., Sakai, T., Belyakov, A., & Miura, H. (2007). "Ultrafine grain development in copper during multidirectional forging at 195 K". *Philosophical Magazine Letters*, Vol. 87, N (October), 751–766.

Kumar, S., Ramanathan, S., & Sundarrajan, S. (2015). "Synthesis, microstructural and mechanical properties of ex situ zircon particles ($ZrSiO_4$) reinforced Metal Matrix Composites (MMCs)". *Integrative Medicine Research*, 4(3), 333–347.

Kurnaz, S. C. (2005). "Materials & Design Hot tensile and fatigue behavior of zinc – aluminum alloys produced by gravity and squeeze casting", *Materials and Design*, 26, 479–485. <http://doi.org/10.1016/j.matdes.2004.07.023>.

Li, R., Li, R., & Bai, Y. (2010). "Effect of specific pressure on microstructure and mechanical properties of squeeze casting ZA27 alloy". *Transactions of Nonferrous Metals Society of China*, 20(1), 59–63.

LI Zi-quan, ZHOU Heng-zhi, LUO Xin-yi, WANG Tao, S. K. (2006). "Aging microstructural characteristics of ZA-27 alloy and SiC ZA-27 composite". *Trans. Nonferrous Met. Soc. China*, 98-104.

L. M. Tham., M. Gupta and L. Cheng. (2001). "Effect Of limited matrix–reinforcement interfacial reaction on enhancing the mechanical properties of aluminum–silicon carbide composites" *Acta materials*, 49 3243–3253.

Lubin, G., ed. (1982). "Handbook of composites", New York: van Nostrand Reinhold.

M. Babic, S. Mitrovic, R. N. (2009). "Tribological Potential of Zinc- Aluminium Alloys Improvement", *Tribology in Industry*, 31(1), 15–28.

M. T. Abou El-Khair., A.Lotfy., A. Daoud., and A.M. El-Sheikh. (2011). "Microsturcture, thermal behaviour and mechanical properties of squeeze cast SiC , ZrO₂ or C reinforced ZA27 composites", *Materials Science and Engineeing A*, 528, 2353-2362.

Mario, R. Rosenberger., Alicia E. Ares., Isaura P.Gatti., Carlos E.Schvezov. (2010). "Wear resistance of dilute Zn-Al alloys", *Wear*, 268,1533-1536.

Martinez-Flores, E., Negrete, J., Torres Villasenor, G. (2003). "Structure and properties of Zn-Al-Cu alloy reinforced with alumina particles", *Materials and Design*, 24 , 281-286.

Madhu, G., Manjunath, B. A., Manoj, K. A., Manoj Kumar, B., Manjunath, L. H., Manjunath G. K., (2020). "Design and Fabrication of Multi Directional Forging Die for processing of Aluminium materials". *Inter. Journal of Scientific and Engineering Research*, 11, 6, ISSN 2229-5518.

Miroslav, B., Slobodan, M., Branislav, J. (2010). "The influence of heat treatment on the sliding wear behavior of a ZA-27 alloy". *Tribology International*, 43(1–2), 16–21. <http://doi.org/10.1016/j.triboint.2009.04.016>.

Miroslav, B., Mitrovic, S., Zivic, F., and Bobic, I. (2010). "Wear behavior of composites based on ZA-27 Alloy Reinforced by Al₂O₃ particles under dry sliding condition". *Tribology Letters*, 337–346. <http://doi.org/10.1007/s11249-010-9613-5>.

Mishra, A., Kad, B. K., Gregori, F., and Meyers, M. A. (2007). "Microstructural evolution in copper subjected to severe plastic deformation: Experiments and analysis", *Acta Materialia* 55, 13–28. <http://doi.org/10.1016/j.actamat.2006.07.008>.

Mishra, S. K., & Biswas, S. (2012). "erosion wear analysis of Al₂O₃ particles reinforced ZA-27 alloy metal matrix composite using Ann", *Academic Research Journals (India)* 1(1), 65–76.

Mishra, S. K., Biswas, S., and Satapathy, A. (2014). "A study processing, characterization, and erosion wear behavior of silicon carbide particle filled ZA-27 metal matrix composites", *Materials and Design*, 55, 958–965.

Mitrovi, S., Babić, M., Miloradović, N., Bobi, I., Stojanović, B., Džunić, D., & Pantić, M. (2014). "Wear Characteristics of Hybrid Composites Based on Za27 Alloy Reinforced With Silicon Carbide and Graphite Particles", *Tribology in Industry*, 36(2), 204–210.

Mitrović, S., Babić, M., Stojanović, B., Miloradović, N., Pantić, M., & Džunić, D. (2012). "Tribology in industry tribological potential of hybrid composites based on

zinc and aluminium alloys reinforced with SiC and graphite particles", *Tribology in Industry*, 34(4), 177–185.

Modi, O. P., Rathod, S., Prasad, B. K., Jha, A. K., & Dixit, G. (2007). "The influence of alumina particle dispersion and test parameters on dry sliding wear behavior of zinc-based alloy", *Tribology International*, 40, 1137–1146. <http://doi.org/10.1016/j.triboint.2006.11.004>.

Mohamed Ibrahim., Abd El aal., M.M. Sadawy. (2015). "Influence of ECAP as grain refinement technique on microstructure evolution, mechanical properties and corrosion behaviour of pure aluminum", *Trans Non ferrous Met. Soc. China*, 25, 3865-3876.

Miura, H., Kobayashi, M., and Benjanarasuth, T. (2016). "Effects of strain rate during multi-directional forging on grain refinement and mechanical properties of AZ80Mg alloy." *Materials Transactions*, 57(9), 1418-1423.

M.S. Turhal., T.Savaskan. (2003). "Relationships between secondary dendrite arm spacing and mechanical properties of Zn40 AlCu alloys", *Journal of Material Science*, 38 2639-2646.

Murphy, S. (2002). "Dry sliding friction and wear properties of zinc-based alloys", *Wear*, 252, 894–901.

Miura, H., Maruoka, T., Yang, X., and Jonas, J. J. (2012). "Microstructure and mechanical properties of multi-directionally forged Mg–Al–Zn alloy." *Scripta Materialia*, 66(1), 49–51.

Mykura, N., Zhu, Y. H., Murphy, S., (1986). "Solid State Reactions in Zn-Al Based Alloys", *Canadian Metallurgical Quarterly*, Vol 25, No2, PP.151-159.

M. T. Jovanovic., I. Babic., B.Djuric., N. Grahovac., & N. Ilic (2007). "Microstructural and sliding wear behavior of heat treat zinc-based alloy", *Tribology Letters*, vol.25, No.3.

Ortiz-Cuellar, E., Hernandez-Rodriguez, M. A. L., and García-Sánchez, E. (2011). "Evaluation of the tribological properties of an Al–Mg–Si alloy processed by severe plastic deformation", *Wear*, 271(9), 1828-1832.

Petch, N. J. (1953). " The cleavage strength of polycrystals", *Journal of Iron steel Inst.* 174: 25-8.

Prabu, S. B., Karunamoorthy, L., Kathiresan, S., & Mohan, B. (2006). "Influence of stirring speed and stirring time on the distribution of particles in cast metal matrix composite", *Journal of Materials Processing Technology*, 171 171, 268–273.

Prasad, B. K. (2002). "Abrasive wear characteristics of a zinc-based alloy and zinc-alloy/SiC composite", *Wear*, 252, 250–263.

Prasad, B.K. (1998). "Tensile properties of some zinc based alloys comprising 27.5% Al: effects of alloys microstructure composition and test conditions", *Materials Science and Engineering A*, 245, 257-266.

Prasad, B.K., Modi, O.P., Yegneswaran, A.H. (2008). "Wear behaviour of zinc based alloys as influenced by alloy composition nature of the slurry and traversal distance", *Wear*, 264, 990-1001.

Prasad, B. K., Modi, O. P., & Khaira, H. K. (2004). "High-stress abrasive wear behavior of a zinc-based alloy and its composite compared with a cast iron under varying track radius and load conditions", *Wear* 381, 343–354.

Prasad, B. K., Patwardhan, A. K., & Yegneswaran, A. H. (2013). "Wear characteristics of a zinc-based alloy compared with a conventional bearing bronze

under mixed lubrication conditions: Effects of Material and Test Parameters, *Canadian Metallurgical Quarterly*, 4433.

Pruthviraj, R. D. (2011). "Wear characteristics of Chilled Zinc aluminium alloy reinforced with silicon carbide particulate composites", *Research Journal of Chemical Sciences*, Vol.1(2), pp 17-23.

Purcek, G. (2005). "Improvement of mechanical properties for Zn–Al alloys using equal-channel angular pressing", *Journal of Material Processing and Technology*. 169 242.

Purcek, G., Saray, O., & Karaman, I. (2008). "Effect of severe plastic deformation on tensile properties and impact toughness of two-phase Zn – 40Al alloy", *Materials Science and Engineering A*, 490, 403–410. <http://doi.org/10.1016/j.msea.2008.01.080>.

Purcek, G., Saray, O., Kucukomeroglu, T., Haouaoui, M., and Karaman, I. (2010). "Effect of equal-channel angular extrusion on the mechanical and tribological properties of as-cast Zn–40Al–2Cu–2Si alloy." *Materials Science and Engineering: A*, 527(15), 3480–3488.

Rafael, Auras., Carlos, Schvezov. (2004) "Wear behavior, microstructure, and dimensional stability of as-cast zinc-aluminum/SiC (Metal Matrix Composites)" *Alloys Metall. Mater. Trans.*, 35 A 1579-1590.

Rahul Gupta., Sanjay Srivastava., Preetham Kumar G. V., S. K. P. (2014). "Investigation of mechanical properties, microstructure and wear rate of high leaded tin bronze after multidirectional forging", *Procedia Materials Science*, 5, 1081–1089.

Ramesh. S., H. Shivananda Nayaka., Sandeep Sahu., K.R. Gopi., M.J. Shivaram., and Shashibhushan Arya.(2019), " Influence of Multiaxial Cryoforging onMicrostructural, Mechanical, and Corrosion Properties of Copper-Titanium Alloy", *JMEPEG- ASM International*, 1059-9495. <https://doi.org/10.1007/s11665-019-04454-9>.

Ranganath, G., Sharma, S. C., and Krishna, M. (2001). "Dry sliding wear of garnet reinforced zinc/aluminum metal matrix composites". *Wear*, 251, 1408–1413.

Ranjit Bauria., M. K. Surapp. (2007). "Processing and properties of Al-Li-SiCp composites", *Science and Technology of Advance. Materials*, 8 494–502.

Roberto B. Figueiredo., and Terence G. Langdon. (2009), "Using severe plastic deformation for the processing of advanced engineering materials" *Mater. Trans.* 50 7 1613- 1619.

S. Balasivanandha Prabu., L. Karunamoorthy., S. Kathiresan., B. Mohan. (2006). "Influence of stirring speed and stirring time on distribution of particles in cast metal matrix composite", *Journal of Materials Processing Technology*, 171, 268-273.

S. Mitrović, M. Babić, I. B. (2007). "ZA-27 alloy composites reinforced with Al₂O₃ particles", *Tribology in Industry*, 29(3), 35–41.

Sastry, S., Krishna, M., & Uchil, J. (2001). "A study on damping behavior of aluminite particulate reinforced ZA-27 alloy metal matrix composites". *Journal of Alloys and Compounds*, 314, 268–274.

Seah, K. H. W., Sharma, S. C., Krishna, M. (2003). "Mechanical properties and fracture mechanism of ZA27/TiO₂ particulate metal matrix composites", *Journal of Materials : Design and Applications*, Vol 217, pp 201-206.

Sharma, S. C., Girish, B. M., Somashekar, D. R., Satish, B. M., & Kamath, R. (1999). "Sliding wear behavior of zircon particles reinforced ZA-27 alloy composite materials" *Wear*, 89–94.

Sharath P. C. • K. R. U. • G. V. P. (2016). "Effect of Multi-Directional Forging on the Microstructure and Mechanical Properties of Zn-24 wt % Al-2 wt % Cu Alloy". *Trans. of the Indian Institute of Metals*, <http://doi.org/10.1007/s12666-016-0863-2>

Shanta Sastry., M. Krishna., Jayagopal Uchil. (2001). "A study on damping behavior of aluminite particulate reinforced ZA-27 alloy metal matrix composites", *Journal of Alloys Compounds*, 314 - 268–274.

Shengli Guo., Defu Li., Xiaoping Wu., Xiaoqing Xu., Peng Du., Jie Hu. (2012). "Characterization of hot deformation behavior of a Zn-10.2Al-2.1Cu alloy using processing maps", *Materials and Design*, 41, 158-166.

Shivakumar, Nagavelly., Vasu, Velagapudi., N. Narasaiah. (2017). "Mechanical properties and dry sliding wear behaviour of molybdenum disulphide reinforced zinc aluminium alloy composites", *Trans Indian Inst. Met*, 70(8), 2155-2163.

Shu-Qing Yan., Jing-pei Xie., Zhong-xia Liu., Ji-Wen Li., Wen-Yan Wang., Ai-qin Wang.(2009) " The effect of composition segregation on the friction and wear properties of Za48 alloys in dry sliding condition", *Journal of Material Science*, 44:4169-4173.

Shuqing Yan., Jingpei Xie., Zhongxia Liu., Wenyan Wang., Aiqin Qang., Jiwen Li. (2010). " Influence of different Al contents on Microstructure, Tensile and wear properties of Zn based alloy", *Journal of Materials. Science and Technology.*, 26(7), 664-652.

Srimant Kumar Mishra., Sandhyarani Biswas., Alok Satapathy. (2014). "A Study on processing characterization and erosion wear behavior of silicon carbide particles filled ZA27 metal matrix composites", *Materials and Design*, 55, 958-965.

Srimant Kumar Mishra., Sandhyarani Biswas., Alok Satapathy., Amar Patnaik. (2012). "Erosion wear analysis of Al₂O₃ particles reinforced ZA27 alloy metal matrix composite using ANN", *Academic Research Journals (India)*, pp 65-76.

Swati Gangwar., Amar Patnaik., I. K. Bhat. (2015). "Tribological and thermomechanical analysis of Cao (quick lime) particulates filled ZA-27 alloy

composites for bearing application", *Journal of Materials Design and Application*, pp1-15. DOI: 10.1177/146442071509196.

Swati Gangwar., Viresh Payak., Vimal Kumar Pathak., Anbesh Jamwal., Pallav Gupta. (2020). "Characterization of mechanical and tribological properties of graphite and alumina reinforced zinc alloy (ZA27) hybrid metal matrix composites", *Journal of composite materials*, 1-13.

Teng Liu., Qudong Wang., Yudong Sui., Qigui Wang. (2016). "Microstructure and mechanical properties of overcast 6101–6101 wrought Al alloy joint by squeeze casting", *Journal of Material Science & Technology*, 32 4 298-305.

T. Savaskan., G. Purcek., S. Murphy. (2002). "Sliding wear of cast zinc based bearing under static and dynamic loading conditions", *Wear*, 252,693-703.

T. Savaskan., G. Purcek., Hekimoglu, A. P. (2003). "Effect of copper content on the mechanical and tribological properties of ZnAl27-based alloys", *Tribology Letters*, Vol 15, No.3, 257-263.

T. A. Orhadahwe., O. O. Ajide., A. A. Adeleke and P. P. Ikubanni. (2020). " A review on primary synthesis and secondary treatment of aluminium matrix composites", *Arab Journal of Basic and Applied Sciences*, 27:1, 389-405.

Temel Savaşkan, R. A., & Maleki, H. O. T. (2015). "Tribological properties of Zn-25Al-3Cu-1Si alloy". *Tribology International*, 81, 105-111. <http://dx.doi.org/10.1016/j.triboint.2014.08.014>.

Temel Savaskan., and Ali Pasa Hekimoglu. (2014). "Microstructure and mechanical properties of Zn-15Al-based ternary and quaternary alloys", *Materials Science and Engineering A*,603, 52-57.

Temel Savaskan., Ali Pasa Hekimoglu and Gencaga Purcek. (2004). "Effect of copper content on the mechanical and sliding wear properties of monotectoid- based zinc aluminium copper alloys", *Tribology International*, 37, 45-50.

Temel Savaskan., Alev Aydiner. (2004). " Effects of silicon content on the mechanical and tribological properties of monotectoid based zinc aluminium silicon alloys", *Wear*, 257, 377-388.

Temel Savaskan and Reza Anvari Maleki. (2014). "Friction and wear properties of Zn-25Al-based bearing alloys", *Tribology Transactions*, 57:435-444, ISSN: 1040-2004/1547-397X.

T.J. Chen, Y. Hao. (2004). "The microstructural and constitutional evolution of cast dendritic ZA27 alloy during partial remelting", *Journal of Materials Processing Technology* 148, 8–14.

T.J. Chen., Y.Hao., J.Sun. (2002). "Microstructural evolution of previously deformed ZA27 alloy during partial remelting", *Materials Science and Engineering A337*,73-81.

T.J. Chen., X.W.Li., H. Y. Guo., and Y. Hao. (2014). "Effect of casting parameters on microstructure and dendrite morphology of ZA27 zinc based alloys", *International Journal of Cast Metal Research*, Doi- 10.1179/1743133614Y.0000000132.

T. Savaskan, M. S. Turhal, S. Murphy. (2003). "Effect of cooling rate on structure and mechanical properties of monotectoid zinc aluminum alloys ", *Materials Science and Technology*. 19 67-74.

T. Savaskan., G.Purcek., A.Hekimoglu. (2003). "Effect of copper content on the mechanical and tribological properties of ZnAl27 based alloys". *Tribology Letters*, 15(3) 257-263.

T. Savaskan, M.S Turhal. (2003). "Relationships between cooling rate, copper content and mechanical properties of monotectoid based Zn–Al–Cu alloys", *Materials Characterization*, 51, 259-270.

T. Ungar, I. Alexandrov, M. Zehetbauer. (2000). "Ultrafine grained microstructures evolving during severe plastic deformation", *Journal of Materials* 52 (4) 34-36.

Ujjwal Kumar., Ajay Kumar Mishra and Rajkumar Ohdar.(2014) "Hot Forging Lubricants", *Int. J. Mech. Eng. & Rob. Res.* Vol. 3, No. 4, ISSN 2278 – 0149.

Valiev, R., Islamgaliev, R., and Alexandrov, I. (2000). "Bulk nanostructured materials from severe plastic deformation". *Progress in Materials Science* (Vol. 45). [http://doi.org/10.1016/S0079-6425\(99\)00007-9](http://doi.org/10.1016/S0079-6425(99)00007-9).

Valiev, R. Z., Estrin, Y., Horita, Z., Langdon, T. G., Zehetbauer, M. J., & Zhu, Y. T. (2006). "Producing Bulk Ultrafine-Grained Materials by Severe Plastic Deformation", 33–39.

Valiev, R. Z., Alexandrov, I. V., Zhu, Y. T., and Lowe, T. C. (2002). "Paradox of strength and ductility in metals processed by severe plastic deformation", *J. Mater. Res.*, 17(1), 5–8.

Villegas-cardenas, J. D., Saucedo-muñoz, M. L., and Lopez-hirata, V. M. (2014). "Effect of Phase Transformations on Hardness in Zn – Al – Cu Alloys", *Materials Research*, 1–8.

W. R. Osorio., and A.Garcia. (2002). "Modelling dendritic structure and mechanical properties of Zn-Al alloys as a function of solidification condition", *Materials Science and Engineering A*, 325 103-111.

Wang, C. T., Gao, N., Wood, R. J., and Langdon, T. G. (2011). "Wear behavior of an aluminum alloy processed by equal-channel angular pressing." *Journal of Materials Science*, 46(1), 123-130.

Watanabe, C., R. Monzen., R. Ueji., and H. Miura. (2017). "Strain-Rate and temperature dependences of deformation behavior of AZ61Mg alloy processed by multi-directional forging under decreasing temperature conditions", *Metallurgical and Materials Transactions A*, vol 48A, 5368.

Wei Guo., Qudong wang., Bing ye., Hao Zhou. (2013). "Enhanced microstructure homogeneity and mechanical properties of ZA31-Si composite by cyclic closed die forging", *Journal of Alloys and Compounds*, 552, 409-417.

Williams, J.J., G. Piotrowski., R. Saha., and N. Chawla., (2002). "Effect of averaging and particle size on tensile deformation and fracture of particle-reinforced aluminum matrix composites", *Metallurgical and Materials Transaction*, A 33 - 3861.

Xia, X., Chen, M., Fan, F., & Zhu, C. (2013). "Microstructure and mechanical properties of isothermal multi-axial forging formed AZ61 Mg alloy". *Transactions of Nonferrous Metals Society of China*, 23(11), 3186–3192. [http://doi.org/10.1016/S1003-6326\(13\)62851-4](http://doi.org/10.1016/S1003-6326(13)62851-4).

Xu, F. M., Zhu, S. J., Zhao, J., Qi, M., Wang, F. G., Li, S. X., & Wang, Z. G. (2003). "Fatigue crack growth in SiC particulates reinforced Al matrix graded composite", *Materials Letters*, 360, 191–196.

Y. H. Zhu., W.B. Lee., S. To. (2003). "Ageing characteristics of cast Zn-Al based alloy (ZnAl7Cu3)", *Journal of Materials Science*, 38, 1945-1952.

Y. H. Zhu., S. To., X. M. Liu., W.B. Lee. (2006). "Microstructural changes inside the lamellar structures of alloy ZA27", *Materials Characterization*, 57, 326-332.

Yao Hua Zhu (2004). "General rule of phase decomposition in Zn-Al Based alloys (II), On Effects of External, Stresses on Phase Transformation". *Mater. Trans.* 45 11 3083-3097.

Yan, S., Xie, J., Liu, Z., Wang, W., Wang, A., & Li, J. (2010). "Influence of Different Al Contents on Microstructure, Tensile and Wear Properties of Zn-based Alloy", *Journal Of Material Science And Technology*, 26(7), 648–652.

Yang Liu., Hong-ying Li., hao-fan Jiang., Xiao-chao Lu. (2012). "Effects of heat treatment on microstructure and mechanical properties of ZA27 alloy", *Trans. Nonferrous Met. Soc. China* 23,642-649.

Yangming Zhang., Lijing Yang., Xuduo Zeng, Bizhang Zheng., Zhenlun Song. (2013). "The Mechanism of anneal- hardenign phenomenon in extruded Zn-Al alloys", *Materials and Design*, 50, 223-229.

Yeh, M. S., and Chang, C. B. (2002). "Microstructure effects on the forgeability of Zn-22Al eutectoid alloy", *Journal of Materials Engg and Performance*, 11, 71–74.

Yida Zeng., Yuhjin Chao., Zhen Luo., Yangchuan Cai., and Renfeng Song. (2017). " Effect of multi directional forging and heat treatment on mechanical properties of in situ ZrB_{2p}/ 6061Al composites", *High Temp. Mater. Proc*, aop.

Zhongliang, Shi., Mingyuan, Gu., Renjie, Wu., and Junyou, Liu. (1997). " Structure control of in situ silicon particles reinforced Zn-27Al composite materials", *Journal of Materials Processing Technology*, 63, 417- 420.

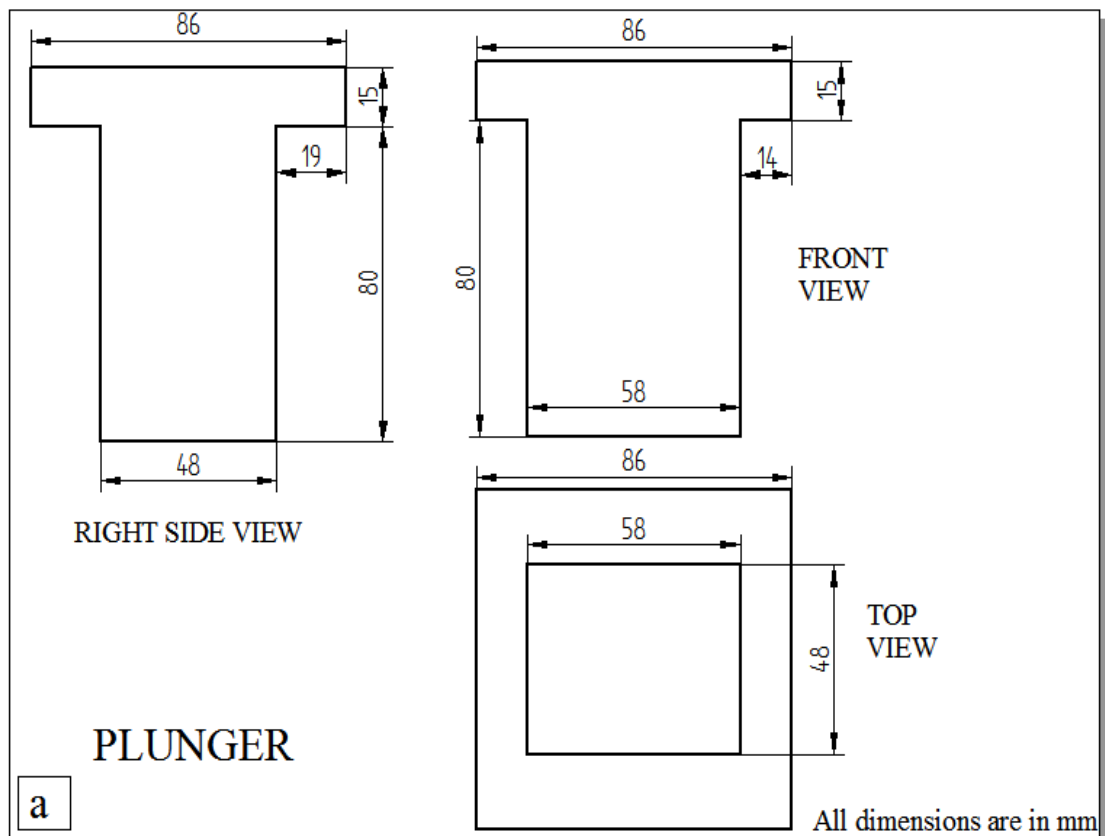
Zhu, Y. hua. (2004). "General Rule of Phase Decomposition in Zn-Al Based Alloys (II)On Effects of External Stresses on Phase Transformation", *Materials Transactions* 45(11), 3083–3097.

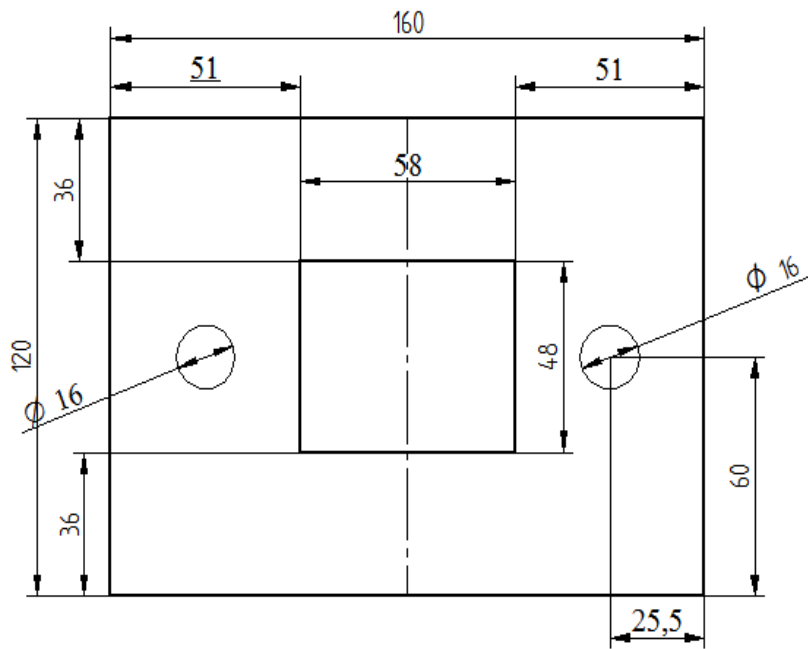
Zulkuf, B and Mehmet, K. (2007). " Investigation of the microstructure and wear properties of a cast ZA alloy", *International Journal of Science and Technology*, vol 2, No. 1, 75-81.

APPENDIX I

AI – 1.1 Squeeze Casting Die Design

Two dimensional representations of Squeeze casting die design in all different views (a) Plunger (b) Top view assembled (c) Right side view assembled (d) Front view assembled. Material used for squeeze casting die preparation was HDS steel, ie., H 13 tool steel which is usually used for aluminum extrusion dies, pipe manufacturing, casting die, hot and cold work tooling applications. Due to its excellent combination of high toughness and fatigue resistance H13 is used more than any other tool steel in tooling applications.

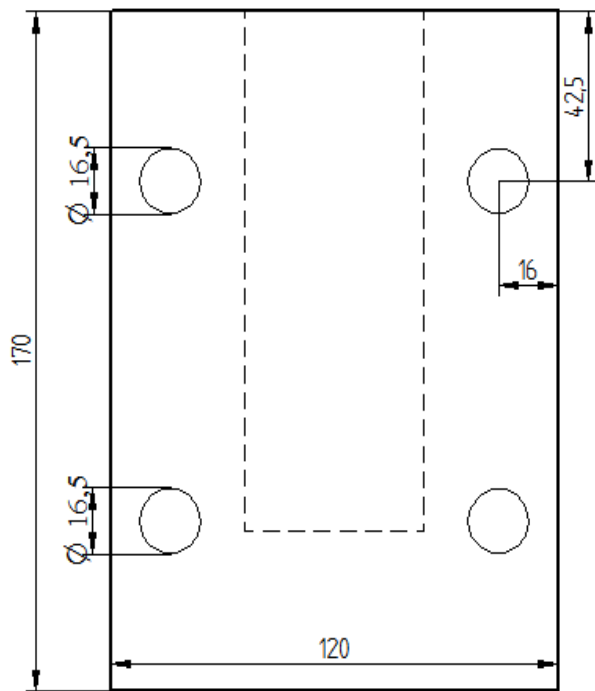




TOP VIEW (WITH BOTH PIECES ATTACHED)

b

All dimensions are in mm



RIGHT SIDE VIEW (WITH BOTH PIECES ATTACHED)

c

All dimensions are in mm

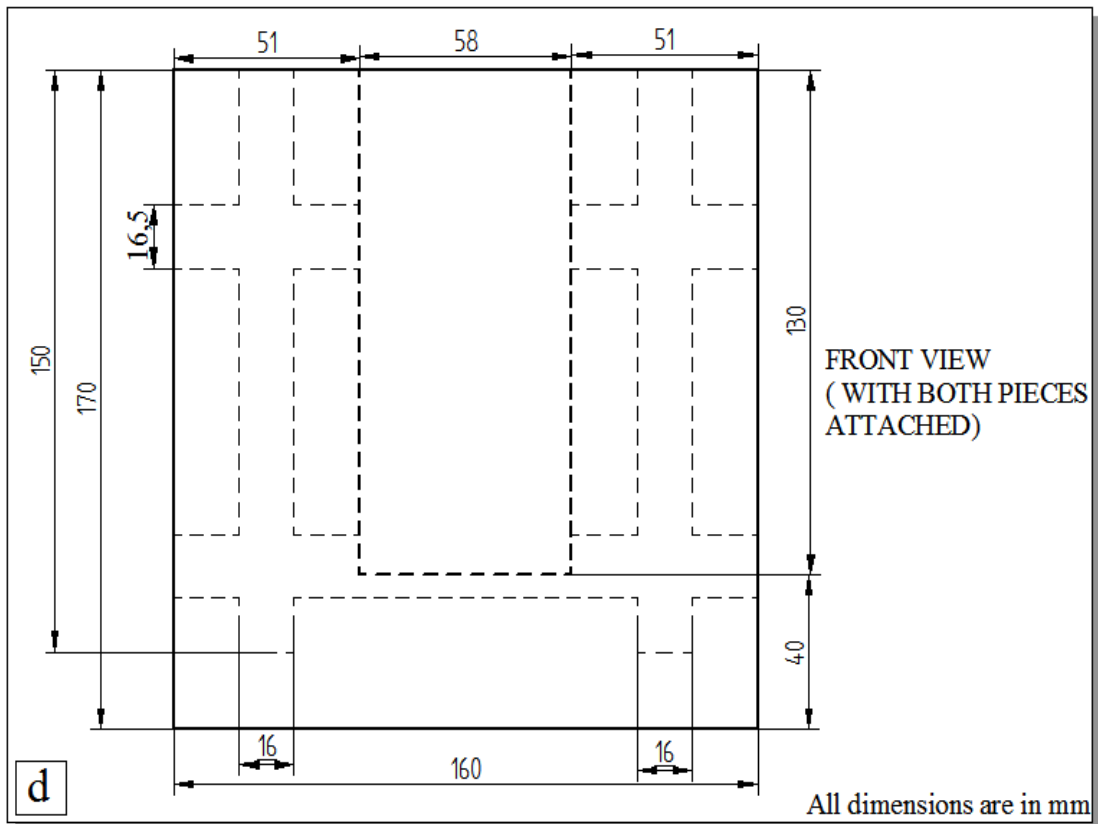
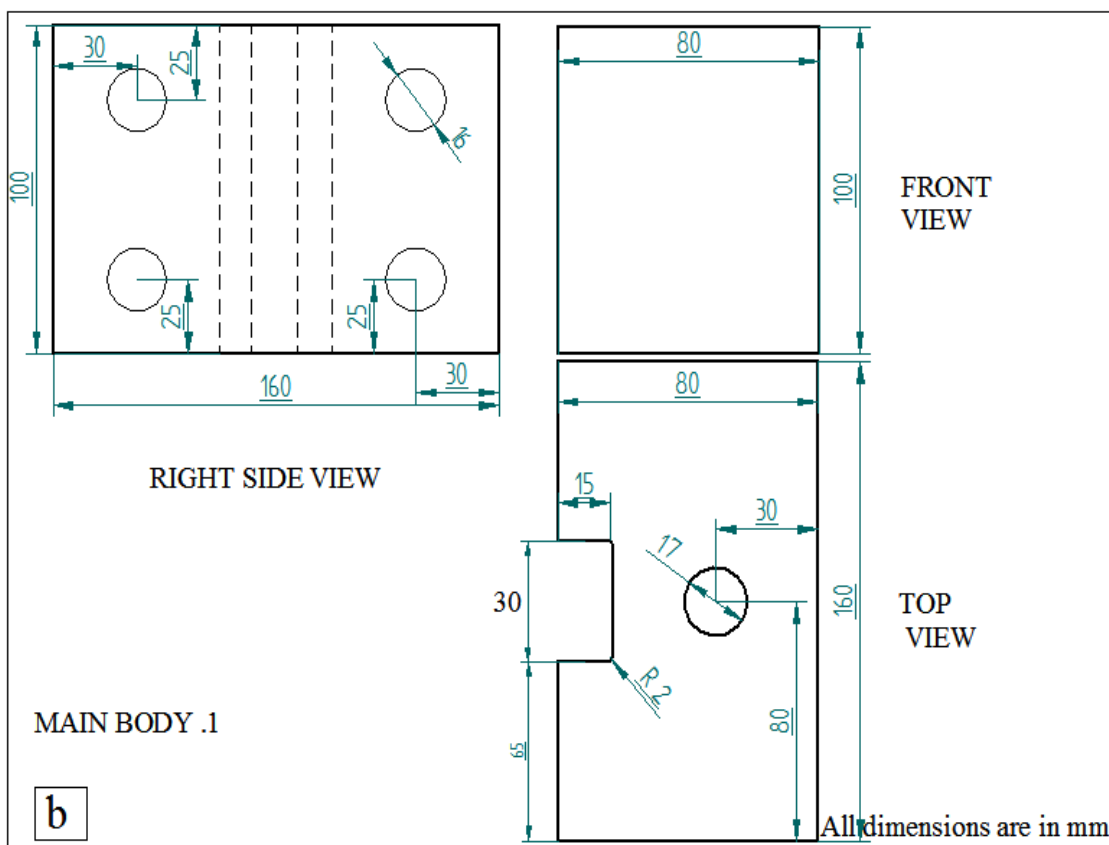
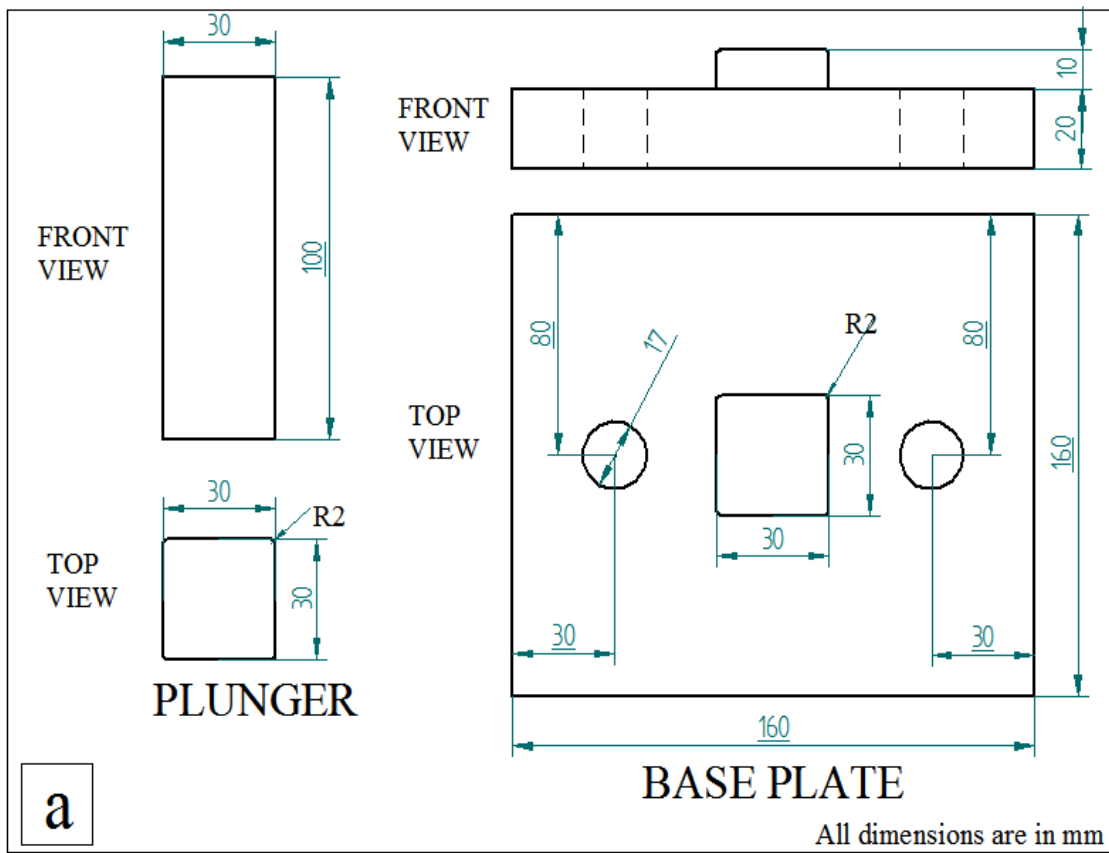


Figure AI-1.1: Two dimensional representations of Squeeze casting Die (a) Plunger (b) Top view assembled (c) Right side view assembled (d) Front view assembled

AI – 1.2 Multi Directional Die Design

Material used for MDF die was hot tool steel, ie., H-13 which as chromium, molybdenum, vanadium and characterized by high hardenability and excellent toughness. The molybdenum and vanadium act as strengthening agents in addition to that chromium content assists H-13 to resist softening when used at high temperatures.



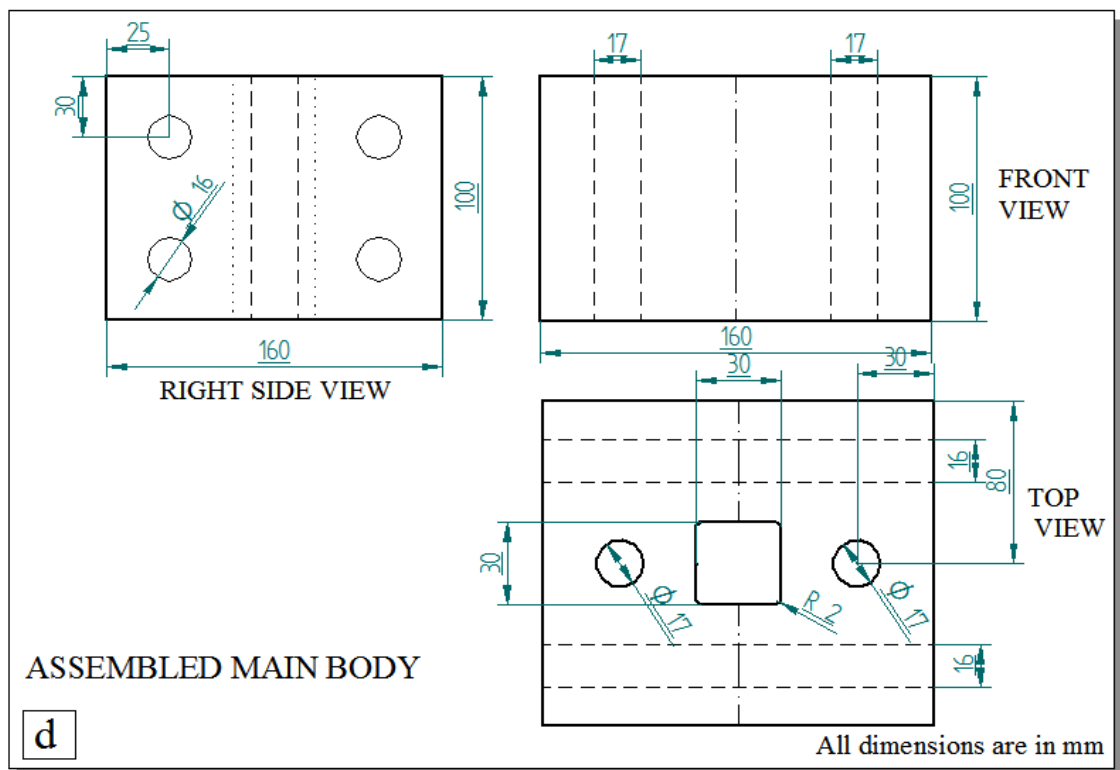
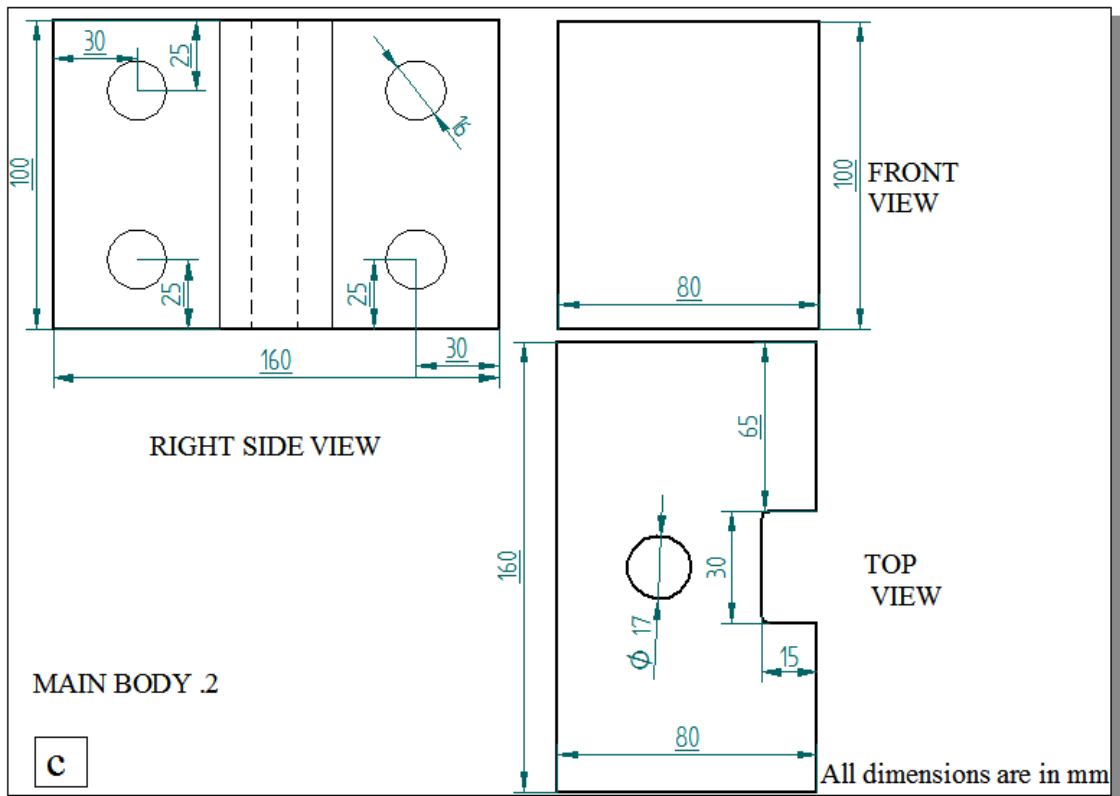


Figure AI-1.2 Two dimensional representations of MDF Processing die (a) Plunger and Base plate (b) Main body part one (c) Main body part two (d) Assembled main body

AI- 1.3: Supporting data for the confirmation of SiC particle’s presence in composite materials through XRD Analysis

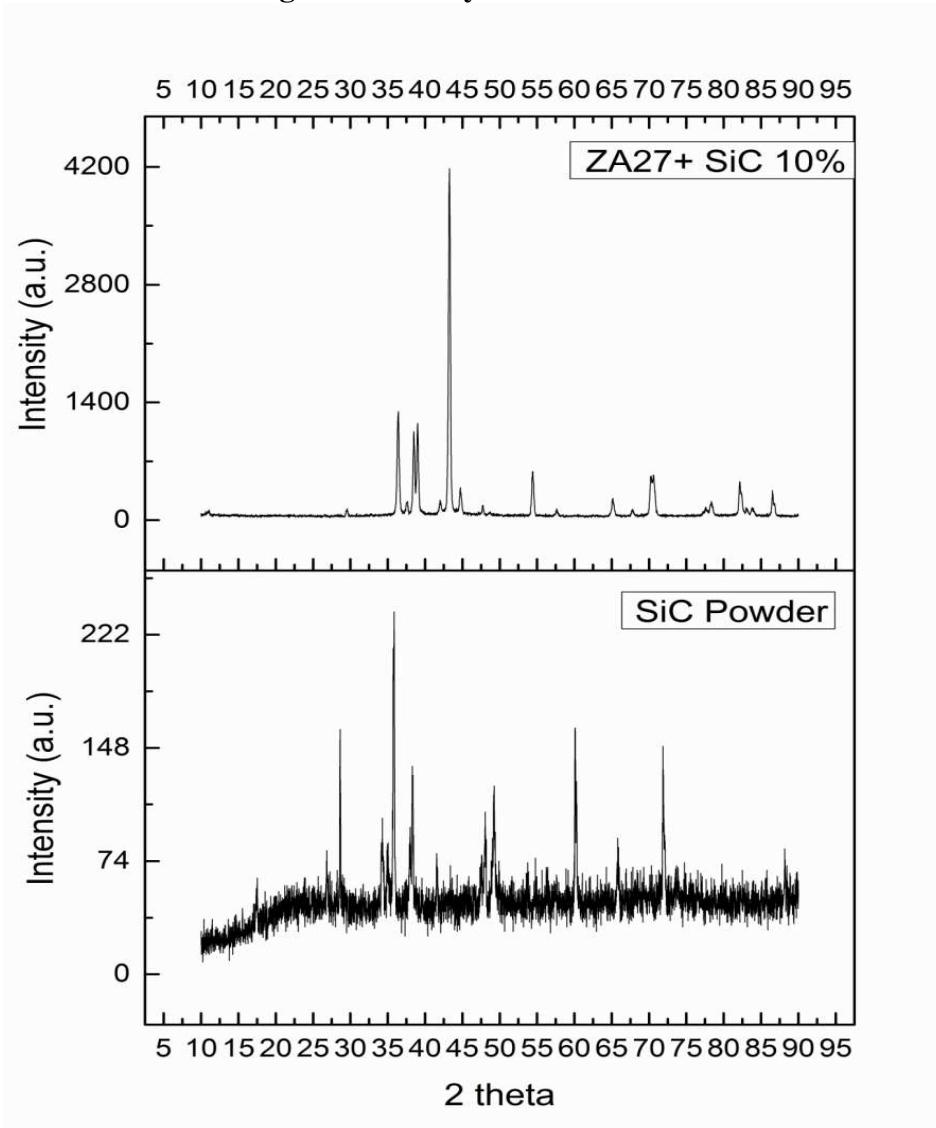


Figure AI-1.3 XRD patterns of ZA27/SiC 10% and SiC powder.

Table AI-1.1: Showing two theta values for ZA27 based composites reinforced with 10wt %/ SiC particles

Pos. [°2Th.]	Height [cts]	FWHM [°2Th.]	d-spacing [Å]
29.4998	64.22	0.3840	3.02789
36.3824	1213.18	0.3600	2.46934
38.4841	923.93	0.3120	2.33918
39.0122	1004.39	0.3360	2.30872
43.2518	3943.07	0.3360	2.09174
44.7224	271.14	0.2880	2.02632

54.3821	506.35	0.3360	1.68702
57.6312	42.90	1.1520	1.59940
65.1133	194.35	0.2880	1.43254
70.4991	426.96	0.2400	1.34070
71.2814	393.32	0.3840	1.33273
78.3352	141.83	0.4800	1.22057
82.1213	381.42	0.1920	1.17362
83.7964	93.62	0.4800	1.15437
86.5100	260.69	0.1920	1.12500

Table AI-1.2: Showing two theta value for SiC powder

Pos. [$^{\circ}2\theta$.]	Height [cts]	FWHM [$^{\circ}2\theta$.]	d-spacing [\AA]
17.2544	19.11	0.2880	5.13916
26.6576	17.96	0.5760	3.34391
28.4040	81.49	0.1920	3.14216
34.0508	39.14	0.2880	2.63290
34.7600	33.93	0.2880	2.58078
35.6062	171.36	0.2880	2.52137
38.1015	79.42	0.1920	2.36178
41.3817	23.67	0.2880	2.18184
47.8456	44.65	0.2880	1.90108
49.0337	63.62	0.2880	1.85777
59.8740	84.29	0.1920	1.54474
65.6409	22.40	0.3840	1.42230
71.4800	70.13	0.1920	1.31660

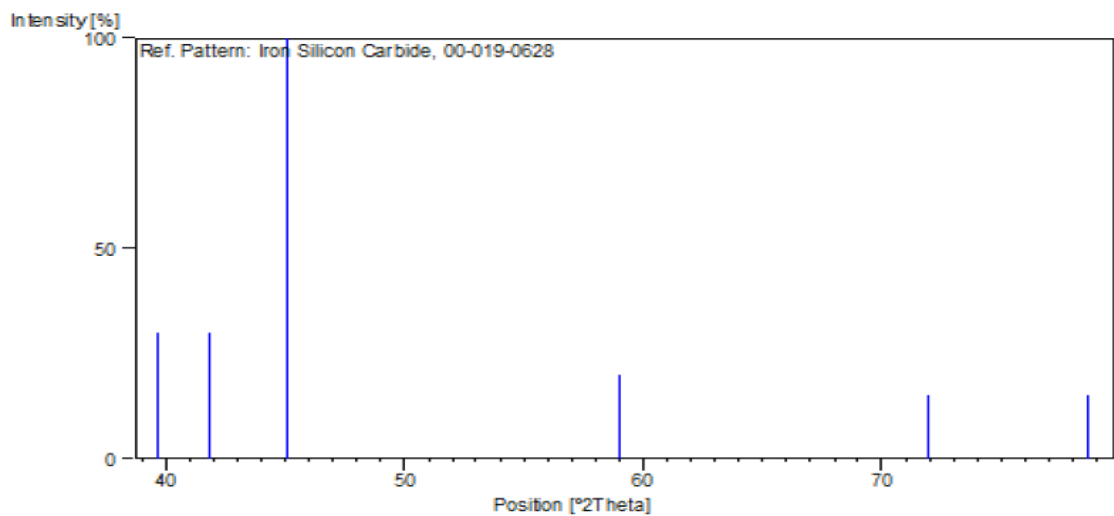


Figure AI-1.4: Standard stick file XRD patterns for Silicon Carbide (00-019-0628)

Table AI-1.3: Showing ‘hkl’ and 2 theta value for Silicon Carbide (00-019-0628)

Sl. No.	h	k	l	d [Å]	2 Theta [deg]
1	1	0	0	2.27300	39.651
2	0	0	2	2.15900	41.840
3	1	0	1	2.01200	45.258
4	1	0	2	1.56500	59.022
5	1	1	0	1.31300	71.907
6	1	0	3	1.21600	78.686

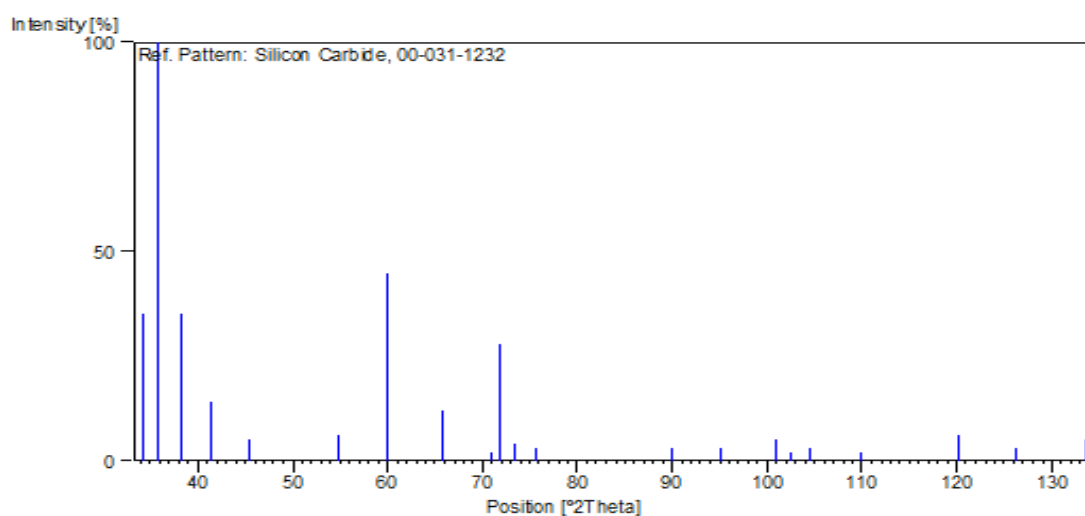


Figure AI-1.5 Standard stick file XRD patterns for Silicon Carbide (00-031-1232)

Table AI-1.4: Showing ‘hkl’ and 2 theta value for Silicon Carbide (00-031-1232)

Sl. No.	h	k	l	d [Å]	2 Theta [deg]
1	1	0	1	2.6800	34.116
2	1	0	2	2.51600	35.685
3	1	0	3	2.35700	38.182
4	1	0	4	2.17900	41.438
5	1	0	5	1.99930	45.360
6	1	0	7	1.67710	54.731
7	1	1	0	1.54070	60.047
8	1	0	9	1.41980	65.771
9	2	0	1	1.32910	70.903
10	2	0	2	1.31390	71.850
11	2	0	3	1.28970	73.416
12	2	0	4	1.25800	75.58
13	2	0	8	1.08940	90.086
14	2	0	9	1.04410	95.180
15	2	1	2	0.99980	100.897

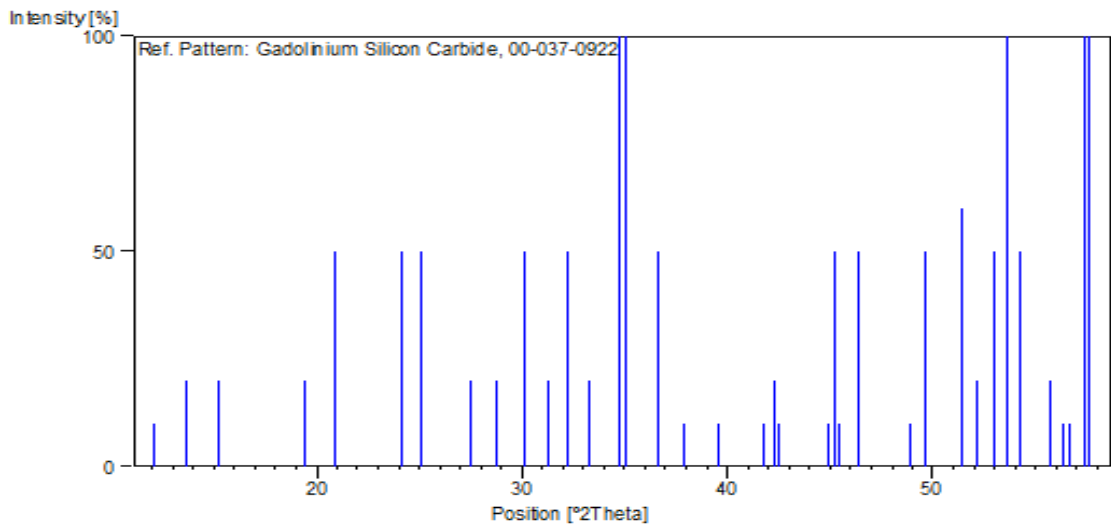


Figure AI-1.6 Standard stick file XRD patterns for Silicon Carbide (00-037-0922)

Table AI-1.5: Showing ‘hkl’ and 2 theta value for Silicon Carbide (00-037-0922)

Sl. No.	h	k	l	d [Å]	2 Theta [deg]
1	1	1	0	7.35000	12.041
2	0	0	1	6.50000	13.623
3	1	0	1	5.80000	15.276
4	2	0	1	4.56000	19.466
5	3	0	0	4.25000	20.901
6	2	2	0	3.68200	24.171
7	3	0	1	3.55800	25.027
8	0	0	2	3.24900	27.451
9	3	1	1	3.10600	28.742
10	1	1	2	2.96700	30.119
11	4	0	1	2.86100	31.263
12	4	1	0	2.78000	32.199
13	2	1	2	2.69100	33.294
14	3	0	2	2.57900	34.785
15	1	4	1	2.55500	35.122
16	3	3	0	2.45200	36.649
17	5	0	1	2.37300	37.915
18	4	0	2	2.27600	39.596
19	0	0	3	2.16400	41.739
20	1	0	3	2.13400	42.354
21	6	0	0	2.12400	42.563
22	6	0	1	2.01800	44.917
23	5	0	2	2.00600	45.200
24	4	3	1	1.99400	45.487
25	3	3	2	1.95700	46.397
26	6	1	1	1.86300	48.887

27	4	4	0	1.83900	49.568
28	6	0	2	1.77800	51.390
29	7	0	1	1.75300	52.177
30	5	2	2	1.72700	53.023
31	4	1	3	1.70800	53.660
32	7	1	0	1.68900	54.313
33	5	0	3	1.64900	55.744
34	7	1	1	1.63400	56.301
35	3	3	3	1.62300	56.717
36	6	3	0	1.60500	57.411
37	4	4	2	1.60000	57.608

AI- 1.4 Supporting data for the confirmation of Al₂O₃ particles presence in composite materials through XRD Analysis

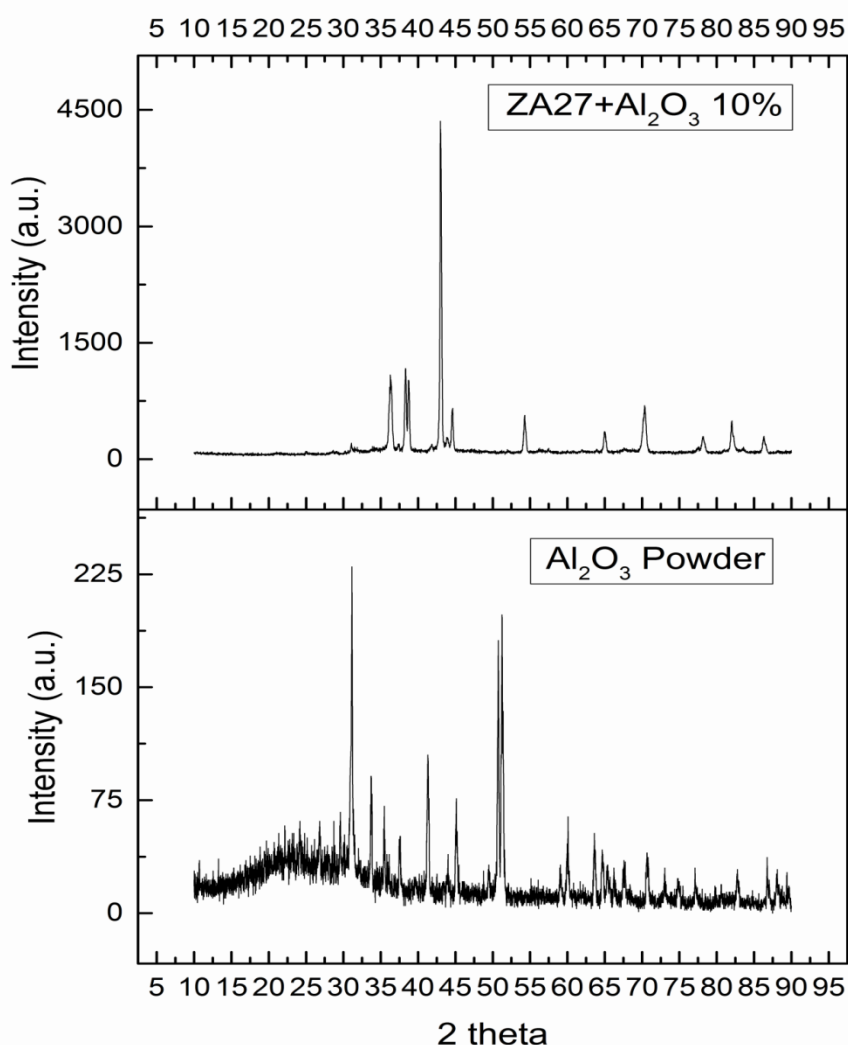


Figure AI- 1.7: XRD patterns of ZA27/ Al₂O₃ 10% and Al₂O₃ powder.

Table AI- 1.6: Showing two theta values for ZA27 based composites reinforced with 10wt %/ Al₂O₃ particles

Pos. [°2Th.]	Height [cts]	FWHM [°2Th.]	d-spacing [Å]
36.4299	788.90	0.5760	2.46623
38.3439	989.95	0.3120	2.34741
38.7653	878.22	0.2880	2.32286
43.0103	4057.33	0.3360	2.10292
44.5830	528.30	0.2880	2.03233
54.2740	445.65	0.3360	1.69013
65.0094	253.87	0.3360	1.43458
70.3670	570.16	0.6240	1.33791
78.1633	195.42	0.4800	1.22282

81.9904	361.45	0.2400	1.17516
86.2760	181.54	0.5760	1.12745

Table AI- 1.7: Showing two theta value for Al₂O₃ powder

Pos. [°2Th.]	Height [cts]	FWHM [°2Th.]	d-spacing [Å]
22.2562	10.73	0.2160	3.99424
24.3047	18.07	0.2880	3.66203
26.9939	24.47	0.2160	3.30301
29.6809	29.66	0.1920	3.00982
31.2819	225.07	0.2400	2.85934
33.8746	60.81	0.2640	2.64618
35.6109	36.67	0.2400	2.52104
37.6649	30.67	0.2400	2.38815
41.5064	73.60	0.3600	2.17558
44.0687	15.78	0.2160	2.05485
45.1706	45.96	0.2160	2.00725
49.5298	15.52	0.1920	1.84031
50.8323	134.20	0.2640	1.79618
51.3319	139.83	0.1440	1.77986
59.2955	13.46	0.2160	1.55842
60.2213	31.03	0.3360	1.53666
63.7335	33.10	0.3120	1.46019
64.7355	22.70	0.2400	1.43999
65.4445	19.37	0.2160	1.42610
66.3936	12.28	0.2880	1.40799
67.6840	18.58	0.4800	1.38426
70.7430	28.01	0.2880	1.33172
73.1931	10.98	0.2880	1.29307
74.9727	12.26	0.3840	1.26673
77.2534	14.77	0.1920	1.23493
80.7581	6.26	0.2880	1.18995
82.8921	15.58	0.4800	1.16465
84.8936	5.34	0.2880	1.14223
86.8652	20.14	0.1920	1.12131
88.1577	16.82	0.2160	1.10818
89.5327	12.42	0.2160	1.09469

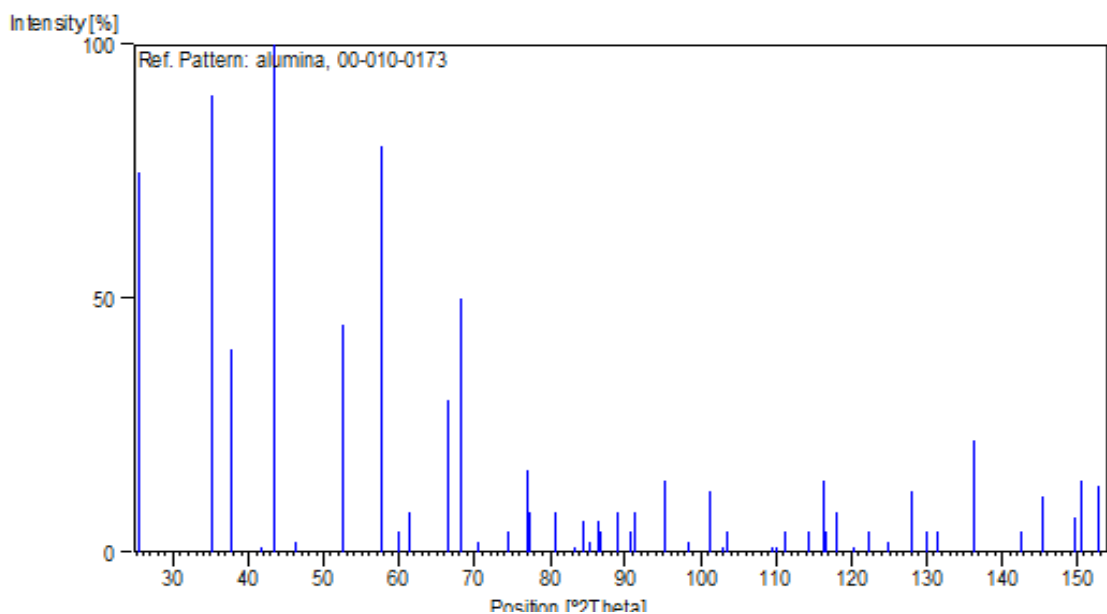


Figure AI-1.8: Standard stick file XRD patterns for Alumina (00-010-0173)

Table AI-1.8: Showing 'hkl' and 2 theta value for Alumina (00-010-0173)

Sl. No.	h	k	l	d [Å]	2 Theta [deg]
1	0	1	2	3.47900	25.604
2	1	0	4	2.55200	35.165
3	1	1	0	2.37900	37.815
4	0	0	6	2.16500	41.719
5	1	1	3	2.08500	43.399
6	2	0	2	1.96400	46.222
7	0	2	4	1.74000	52.597
8	1	1	6	1.60100	57.568
9	2	1	1	1.54600	59.820
10	1	2	2	1.51400	61.219
11	0	1	8	1.51000	61.398
12	2	1	4	1.40400	66.607
13	3	0	0	1.37400	68.259
14	1	2	5	1.33700	70.422
15	2	0	8	1.27600	74.336
16	1	0	10	1.23900	76.953
17	1	1	9	1.23430	77.300
18	2	2	0	1.18980	80.771
19	3	0	6	1.16000	83.299
20	2	2	3	1.14700	84.459
21	1	3	1	1.13820	85.266
22	3	1	2	1.12550	86.462
23	1	2	8	1.12460	86.548

24	0	2	10	1.09880	89.108
25	0	0	12	1.08310	90.756
26	2	2	4	1.07810	91.295
27	2	2	6	1.04260	95.361
28	0	4	2	1.01750	98.513
29	2	1	10	0.99760	101.204
30	1	1	12	0.98570	102.904
31	4	0	4	0.98190	103.462
32	3	2	1	0.94310	109.653
33	1	2	11	0.94130	109.964
34	3	1	8	0.93450	111.163
35	2	2	9	0.91780	114.268
36	3	2	4	0.90760	116.289
37	0	1	14	0.90520	116.780
38	4	1	0	0.89910	118.055
39	2	3	5	0.88840	120.394
0	4	1	3	0.88040	122.238
41	0	4	8	0.86980	124.823
42	1	3	10	0.85800	127.919
43	3	0	12	0.85020	130.114
44	2	0	14	0.84600	131.352
45	1	4	6	0.83030	136.392
46	1	1	15	0.81370	142.668
47	4	0	10	0.80720	145.504
48	0	5	4	0.79880	149.525
49	1	0	16	0.79700	150.593

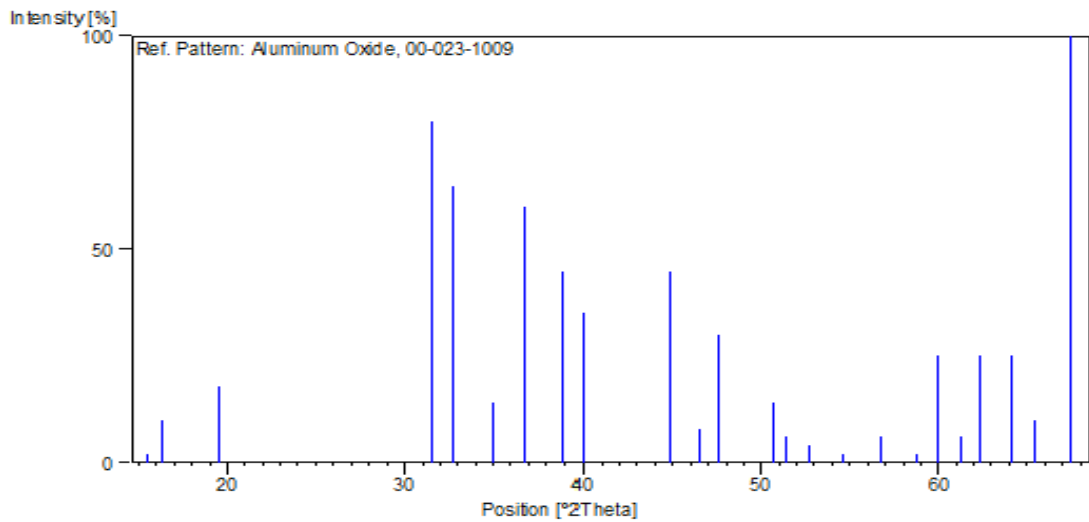


Figure AI-1.9 Standard stick file XRD patterns for Aluminum Oxide (00-023-1009)

Table AI-1.9: Showing ‘hkl’ and 2 theta value for Aluminum Oxide (00-023-1009)

Sl. No.	h	k	l	d [Å]	2 Theta [deg]
1	2	0	0	5.70000	15.546
2	0	0	1	5.54000	16.263
3	-2	0	1	4.54000	19.553
4	-4	0	1	2.83700	31.535
5	0	0	2	2.73000	32.805
6	-1	1	1	2.56600	34.967
7	1	1	1	2.44400	36.773
8	4	0	1	2.31500	38.902
9	2	0	2	2.25700	39.944
10	-1	1	2	2.01900	44.893
11	-6	0	1	1.95440	46.63
12	6	0	0	1.90940	47.624
13	5	1	0	1.79980	50.723
14	-6	0	2	1.77650	51.436
15	-4	0	3	1.73760	52.675
16	6	0	1	1.68070	54.604
17	2	0	3	1.62160	56.770
18	-1	1	3	1.57150	58.754
19	-3	1	3	1.54260	59.966
20	-6	0	3	1.51200	61.308
21	1	1	3	1.48830	62.106
22	0	2	0	1.45260	64.106
23	7	1	0	1.42640	65.429
24	4	0	3	1.38830	67.460

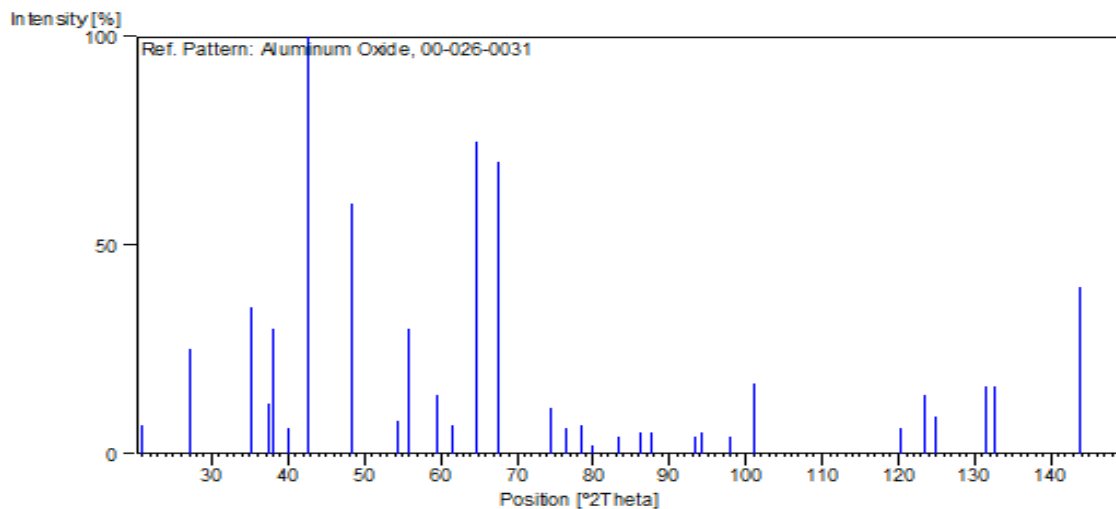


Figure AI-1.10 Standard stick file XRD patterns for Aluminum Oxide (00-026-0031)

Table AI-1.10: Showing ‘hkl’ and 2 theta value for Alumina (00-026-0031)

Sl. No.	h	k	l	d [Å]	2 Theta [deg]
1	1	0	1	4.23000	21.001
2	1	0	2	3.28000	27.187
3	1	0	3	2.54000	35.250
4	2	0	0	2.39000	37.488
5	1	1	2	2.36000	38.131
6	0	0	4	2.25500	39.981
7	2	0	2	2.11800	42.689
8	2	0	3	1.87600	48.526
9	2	1	2	1.68300	54.523
10	2	0	4	1.64300	55.965
11	2	1	3	1.55300	59.523
12	3	0	2	4.50700	61.534
13	2	0	5	1.44200	64.634
14	2	2	0	1.38600	67.587
15	2	0	6	1.27400	74.472
16	1	0	7	1.24500	76.515
17	3	1	3	1.21800	78.532
18	4	0	0	1.20000	79.945
19	4	0	2	1.16000	83.299
20	0	0	8	1.12800	86.223
21	4	0	3	1.11500	87.481
22	4	0	4	1.06000	93.315
23	2	1	7	1.05100	94.360

24	2	0	8	1.02100	98.058
25	4	0	5	0.99900	11.08
26	3	2	6	0.88900	20.259
27	2	2	8	0.87500	123.53
28	4	2	3	0.86900	25.025
29	2	0	10	0.84500	131.652
30	4	2	4	0.84200	132.570
31	4	2	5	0.81100	143.814
32	6	0	0	0.80000	148.998

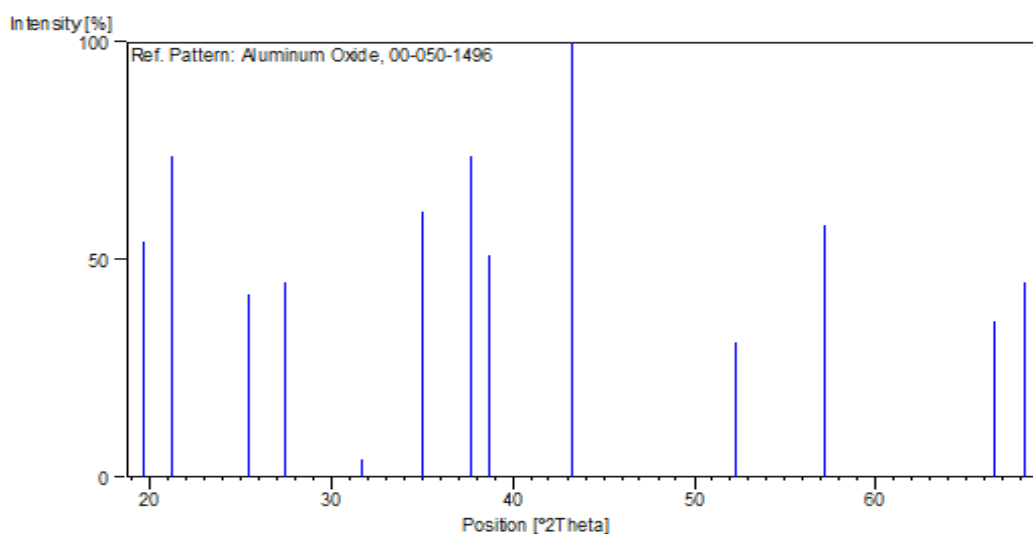


Figure AI-1.11 Standard stick file XRD patterns for Aluminum Oxide (00-050-1496)

Table AI-1.11: Showing ‘hkl’ and 2 theta value for Aluminum Oxide (00-050-1496)

Sl. No.	h	k	l	d [Å]	2 Theta [deg]
1	1	1	0	4.51999	19.640
2	1	0	-2	4.17909	21.260
3	2	1	0	3.49841	25.460
4	2	1	1	3.24451	27.490
5	2	1	-2	2.82605	31.660
6	0	2	0	2.56434	34.720
7	1	2	1	2.38479	37.720
8	2	1	-3	2.32894	38.660
9	4	0	2	2.09367	43.210
10	4	2	0	1.74948	52.220
11	3	0	-5	1.60909	57.220
12	4	2	-4	1.40506	66.550
13	4	2	4	1.37539	68.180

AI- 1.4: Additional Data - Ultimate Tensile Strength and Percentage Elongation

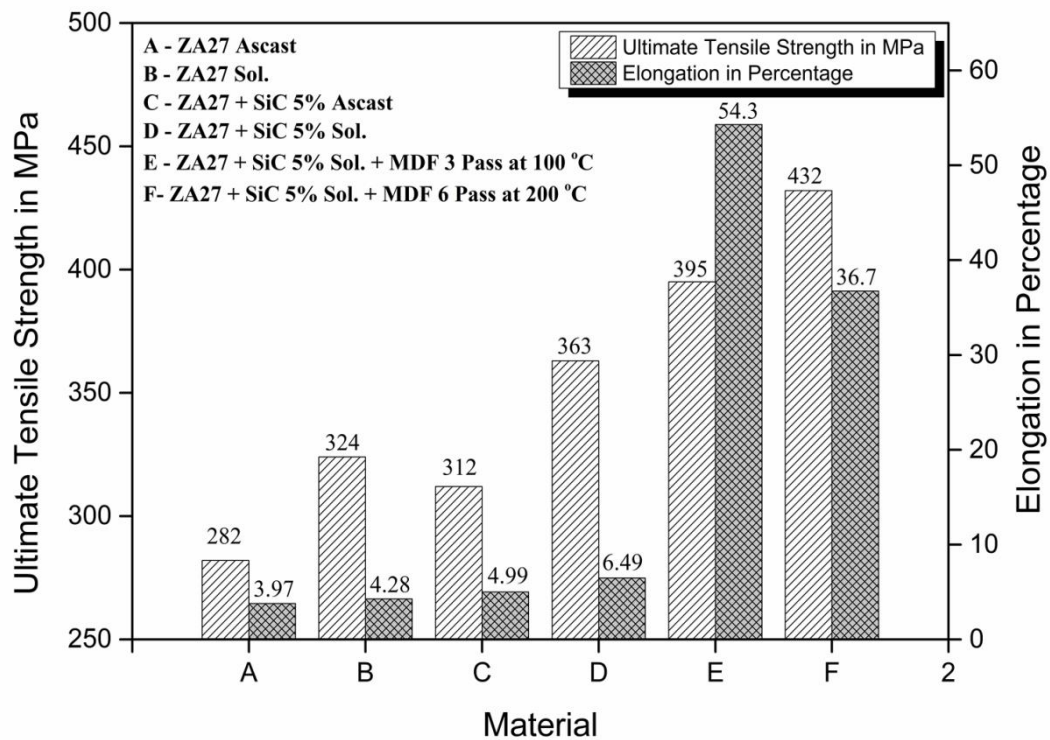


Figure AI- 1.12 Comparison bar chart for UTS and % Elongation of SiC 5 wt% reinforced composites under various materials condition

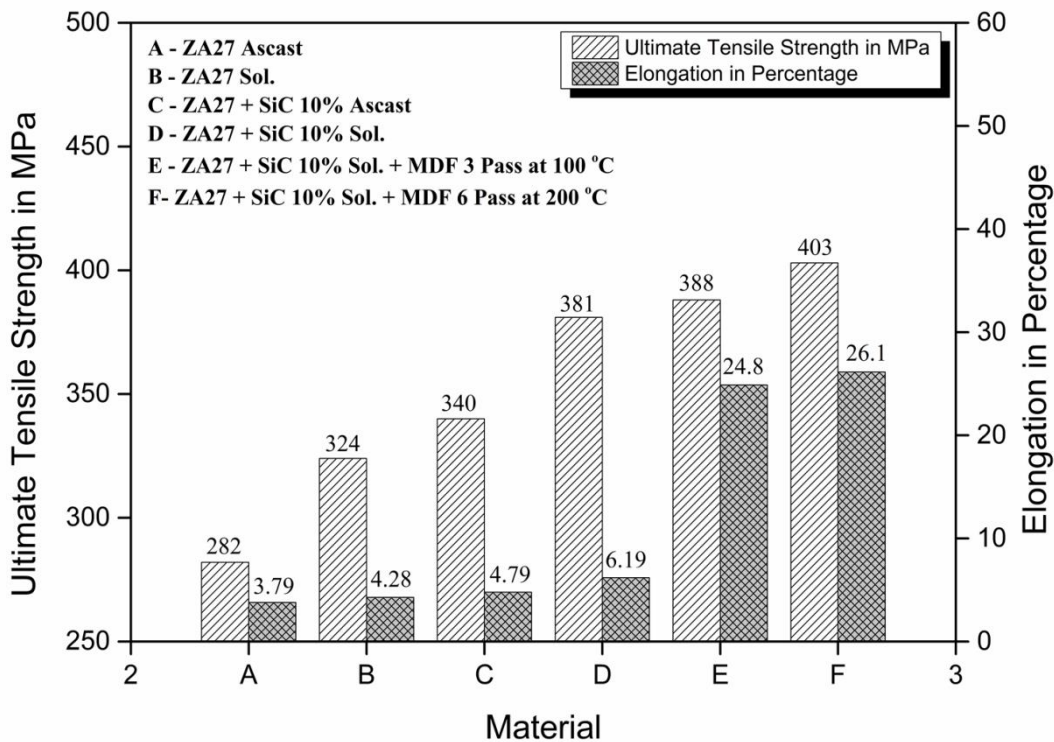


Figure AI- 1.13 Comparison bar chart for UTS and % Elongation of SiC 10 wt% reinforced composites under various materials condition

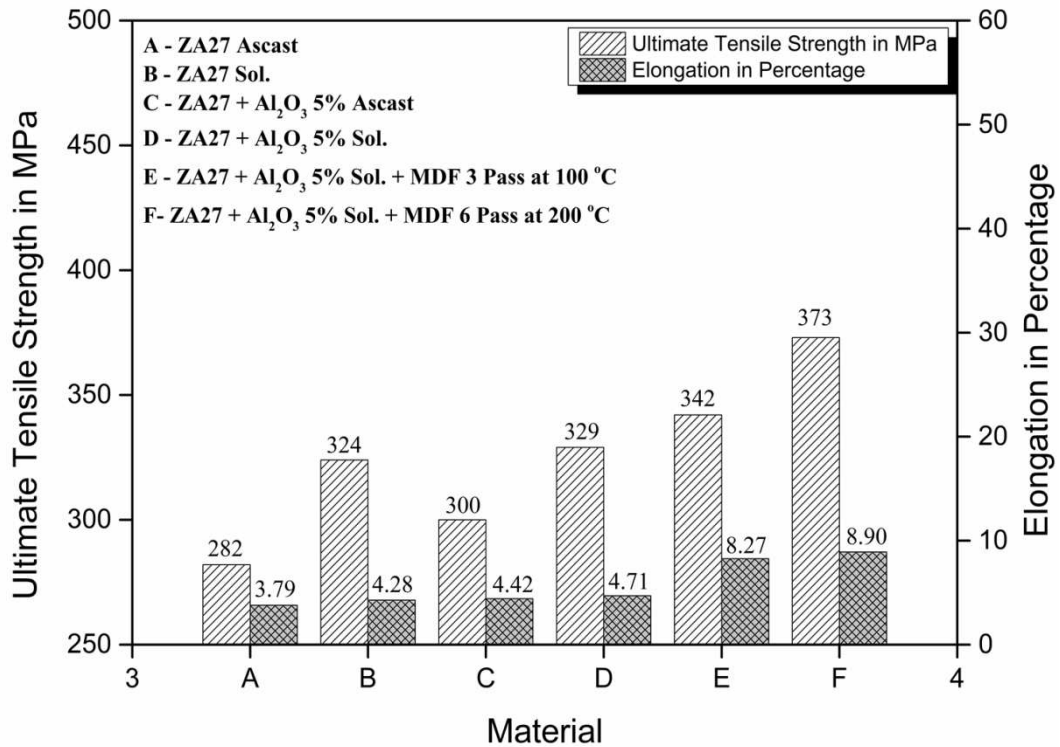


Figure AI- 1.14 Comparison bar chart for UTS and % Elongation of Al₂O₃ 5 wt% reinforced composites under various materials condition

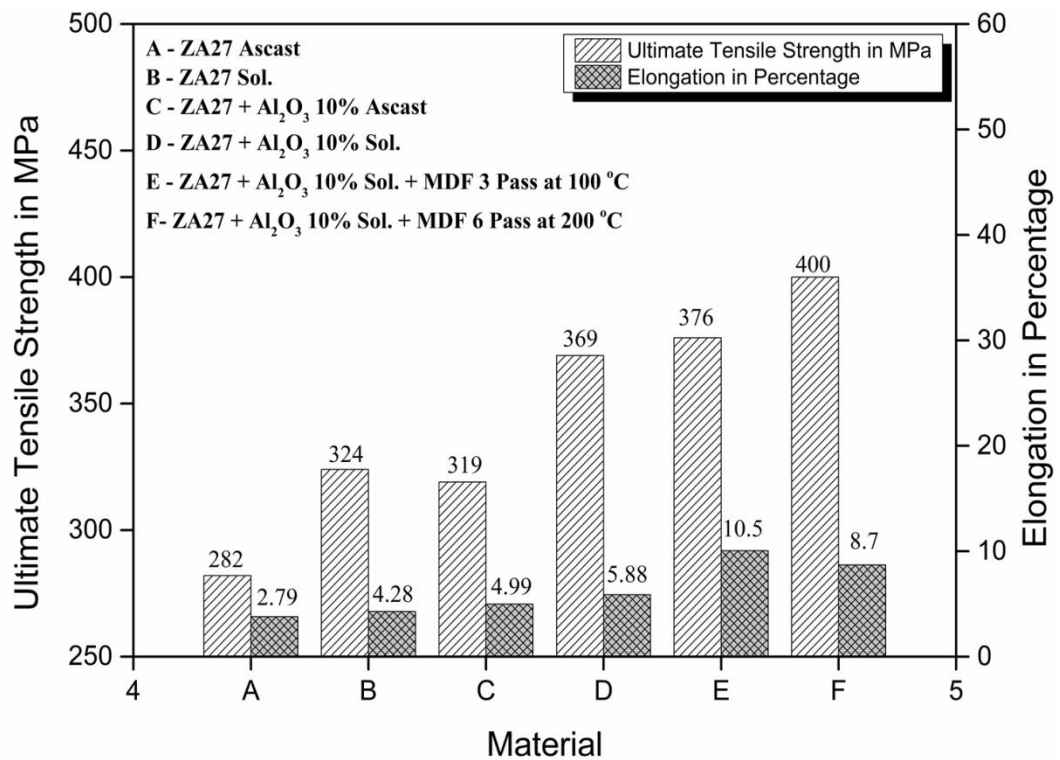


Figure AI- 1.15 Comparison bar chart for UTS and % Elongation of Al₂O₃ 10 wt% reinforced composites under various materials condition

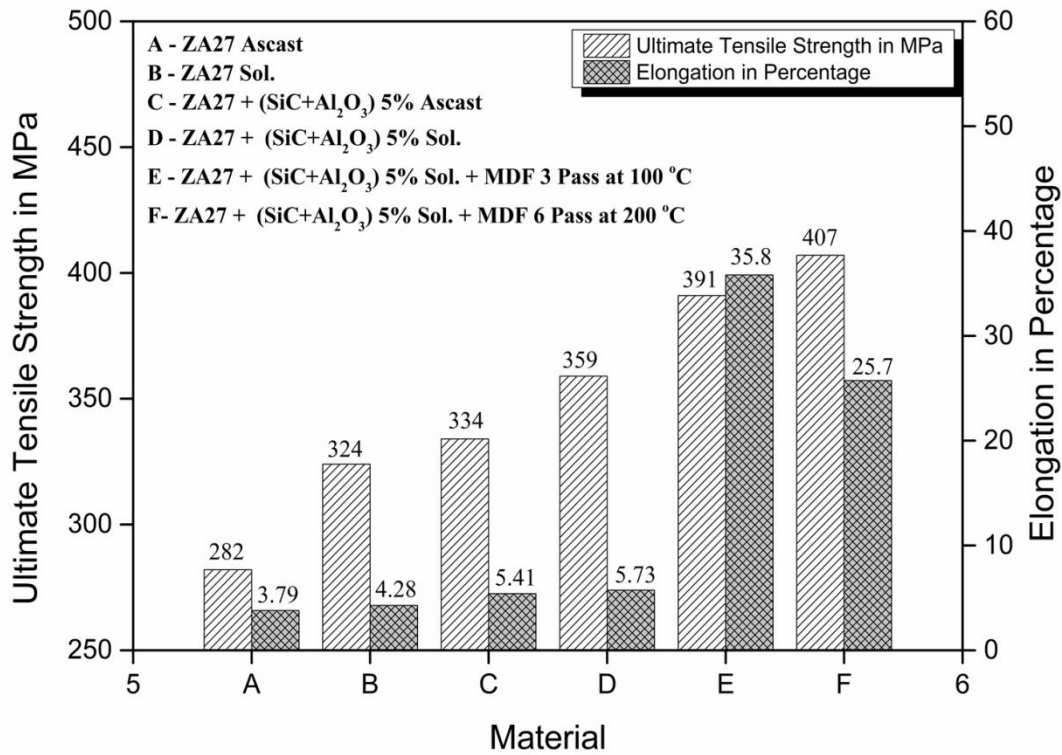


Figure AI- 1.16 Comparison bar chart for UTS and % Elongation of SiC+Al₂O₃ 5 wt% reinforced composites under various materials condition

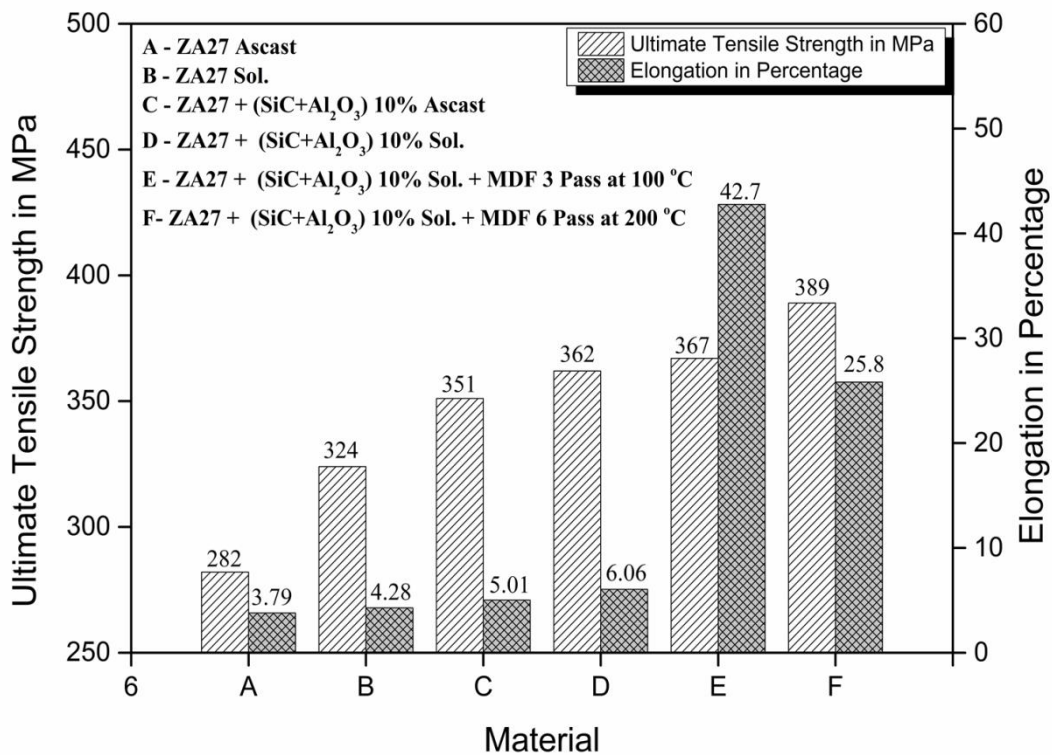


Figure AI- 1.17 Comparison bar chart for UTS and % Elongation of SiC+Al₂O₃ 10 wt% reinforced composites under various materials condition

APPENDIX II

Table AII-1.1: Mechanical properties and Grain size measurement values

Sl. No	Description	UTS in MPa	% Elongation	Density g/cm ³	Hardness	Grain size Range	Grain size in microns	Dimple Size in Range	Dimple size in microns
1	ZA27 Ascast	282	3.79	5.2189	40	-	-	-	-
2	ZA27 Solutionized	324	4.28	5.2421	51	30	28.56	-	-
3	ZA27 + SiC 5 % Ascast	312	4.99	5.1454	54	-	-	-	-
4	ZA27 + SiC 5 % Solutionized	363	6.49	5.1583	64	20-25	21.74		
5	ZA27 + SiC 5 % 3 Passes at 100 °C	395	54.3	5.1644	79	0.2-0.25	0.234	3-4	3.94
6	ZA27 + SiC 5 % 6 Passes at 200 °C	432	36.74	5.1678	76	0.8-1	0.866	10-12	10.98
7	ZA27 + SiC 10 % Ascast	340	4.79	5.1101	57	-	-	-	-
8	ZA27 + SiC 10 % Solutionized	381	6.19	5.1234	68	20-30	26.74	-	-
9	ZA27 + SiC 10 % 3 Passes at 100 °C	388	24.87	5.1323	74	0.45-0.5	0.483	5-6	5.63
10	ZA27 + SiC 10 % 6 Passes at 200 °C	403	26.14	5.1463	75	0.9-1.2	0.997	9-10	9.49
11	ZA27 + Al ₂ O ₃ 5 % Ascast	300	4.42	5.1658	48	-	-	-	-
12	ZA27 + Al ₂ O ₃ 5 % Solutionized	329	4.71	5.1714	63	25-30	28.52	-	-
13	ZA27 + Al ₂ O ₃ 5 % 3 Passes at 100 °C	342	8.27	5.1786	67	0.4-0.45	0.422	-	-
14	ZA27 + Al ₂ O ₃ 5 % 6 Passes at 200 °C	373	8.90	5.179	71	1-1.4	1.318	-	-
15	ZA27 + Al ₂ O ₃ 10 % Ascast	319	4.99	5.1499	52	-	-	-	-
16	ZA27 + Al ₂ O ₃ 10 % Solutionized	369	5.88	5.1536	67	25-30	25.15	-	-
17	ZA27 + Al ₂ O ₃ 10 % 3 Passes at 100 °C	376	10.05	5.1641	75	0.5-0.6	0.566	-	-
18	ZA27 + Al ₂ O ₃ 10 % 6 Passes at 200 °C	400	8.7	5.169	77	1-1.5	1.126	-	-
19	ZA27 + SiC + Al ₂ O ₃ 5 % Ascast	334	5.4	5.1569	55	-	-	-	-
20	ZA27 + SiC + Al ₂ O ₃ 5 % Solutionized	359	5.73	5.1591	62	15-20	17.73	-	-
21	ZA27 + SiC + Al ₂ O ₃ 5 % 3 Passes at 100 °C	391	35.81	5.1699	73	0.2-0.25	0.239	3-4	3.59
22	ZA27 + SiC + Al ₂ O ₃ 5 % 6 Passes at 200 °C	407	25.74	5.1763	81	0.8-0.9	0.824	9-10	9.15
23	ZA27 + SiC + Al ₂ O ₃ 10 % Ascast	351	5.01	5.1377	58	-	-	-	-
24	ZA27 + SiC + Al ₂ O ₃ 10 % Solutionized	362	6.06	5.1474	69	16-20	16.42	-	-
25	ZA27 + SiC + Al ₂ O ₃ 10 % 3 Passes at 100 °C	367	42.78	5.1597	75	0.3-0.4	0.395	5	4.95
26	ZA27 + SiC + Al ₂ O ₃ 10 % 6 Passes at 200 °C	389	25.82	5.1618	79	0.9-1.1	0.981	12-13	12.4

APPENDIX III: Wear Results

Table AIII-1.1: Wear results calculation for pin on disc wear test of MDF processed ZA27/SiC 5 wt% composites.

Sample Name	Sliding Distance m	Applied Load N	Time min	Initial Weight g	Final Weight g	Weight Loss g	Density (g cm ⁻³)	Volume Loss (mm ³)	Wear Rate (mm ³ m ⁻¹)	Specific Wear Rate (mm ³ N ⁻¹ m ⁻¹)	Wear Resistance
ZA27-SiC 5% Ascast	2000	39.24	33.33	5.0435	4.9895	0.054	5.1454	10.494	0.005247	0.000133726	190.570
	2000	49.05	33.33	4.3204	4.2564	0.064	5.1454	12.438	0.006219	0.000126792	160.793
	2000	58.86	33.33	4.5333	4.4587	0.0746	5.1454	14.498	0.007249	0.00012316	137.946
	4000	39.24	66.66	4.3429	4.2313	0.1116	5.1454	21.689	0.005422	0.000138183	184.422
	4000	49.05	66.66	4.4749	4.3408	0.1341	5.1454	26.062	0.006515	0.000132834	153.479
	4000	58.86	66.66	4.939	4.7808	0.1582	5.1454	30.745	0.007686	0.000130589	130.098
ZA27-SiC 5% Sol.	2000	39.24	33.33	4.2014	4.1542	0.0472	5.1585	9.149	0.004574	0.00011659	218.580
	2000	49.05	33.33	4.5612	4.5047	0.0565	5.1585	10.952	0.005476	0.000111649	182.601
	2000	58.86	33.33	4.0117	3.95011	0.0615	5.1585	11.939	0.005969	0.000101423	167.510
	4000	39.24	66.66	4.29	4.1901	0.0999	5.1585	19.366	0.004841	0.000123382	206.546
	4000	49.05	66.66	4.941	4.8191	0.1219	5.1585	23.630	0.005907	0.000120443	169.269
	4000	58.86	66.66	4.4308	4.2961	0.1347	5.1585	26.112	0.00652	0.000110908	153.184
ZA27-SiC 5%-MDF at 100 °C 3 Pass	2000	39.24	33.33	3.9595	3.9354	0.0241	5.1644	4.666	0.002333	5.94618E-05	428.580
	2000	49.05	33.33	4.0146	3.9868	0.0278	5.1644	5.383	0.002691	5.48726E-05	371.539
	2000	58.86	33.33	3.8766	3.8452	0.0314	5.1644	6.080	0.003040	5.16487E-05	328.942
	4000	39.24	66.66	3.689	3.6391	0.0499	5.1644	9.662	0.002415	6.1559E-05	413.979
	4000	49.05	66.66	3.9786	3.9179	0.0607	5.1644	11.753	0.002938	5.99059E-05	340.322
	4000	58.86	66.66	3.833	3.7632	0.0698	5.1644	13.515	0.003378	5.74057E-05	295.954
ZA27-SiC 5%-MDF at 200 °C 6 Pass	2000	39.24	33.33	3.777	3.7479	0.0291	5.1678	5.631	0.002815	7.17511E-05	355.175
	2000	49.05	33.33	3.9473	3.9144	0.0329	5.1678	6.366	0.003183	6.48965E-05	314.151
	2000	58.86	33.33	3.9501	3.9137	0.0364	5.1678	7.043	0.003521	5.98336E-05	283.945
	4000	39.24	66.66	3.9155	3.8512	0.0643	5.1678	12.442	0.003110	7.92714E-05	321.480
	4000	49.05	66.66	3.9222	3.8449	0.0773	5.1678	14.958	0.003739	7.62386E-05	267.415
	4000	58.86	66.66	3.6931	3.6072	0.0859	5.1678	16.622	0.004155	7.06004E-05	240.642

Note: Wear test was conducted at 1 m/s Velocity

Table AIII-1.2: Wear results calculation for pin on disc wear test of MDF processed ZA27/SiC 10 wt% composites.

Sample Name	Sliding Distance m	Applied Load N	Time min	Initial Weight g	Final Weight g	Weight Loss g	Density (g cm ⁻³)	Volume Loss (mm ³)	Wear Rate (mm ³ m ⁻¹)	Specific Wear Rate (mm ³ N ⁻¹ m ⁻¹)	Wear Resistance
ZA27-SiC 10% Ascast	2000	39.24	33.33	3.3061	3.2582	0.0479	5.1101	9.373	0.004686	0.000119439	213.365
	2000	49.05	33.33	3.4512	3.3952	0.056	5.1101	10.958	0.005479	0.000111709	182.503
	2000	58.86	33.33	3.6344	3.5696	0.0648	5.1101	12.680	0.006340	0.00010772	157.719
	4000	39.24	66.66	3.2342	3.1269	0.1073	5.1101	20.997	0.005249	0.000133777	190.497
	4000	49.05	66.66	3.3776	3.2532	0.1244	5.1101	24.343	0.006085	0.000124077	164.311
	4000	58.86	66.66	3.5352	3.3912	0.144	5.1101	28.179	0.007044	0.000119689	141.947
ZA27-SiC 10% Sol.	2000	39.24	33.33	3.0781	3.0351	0.043	5.1234	8.392	0.004196	0.000106943	238.297
	2000	49.05	33.33	3.1785	3.1307	0.0478	5.1234	9.329	0.004664	9.51044E-05	214.368
	2000	58.86	33.33	3.5845	3.5256	0.0589	5.1234	11.496	0.005748	9.76578E-05	173.969
	4000	39.24	66.66	3.0422	2.9569	0.0853	5.1234	16.649	0.004162	0.000106072	240.253
	4000	49.05	66.66	3.1285	3.0248	0.1037	5.1234	20.240	0.005060	0.000103162	197.623
	4000	58.86	66.66	3.5844	3.4628	0.1216	5.1234	23.734	0.005936	0.000100808	168.532
ZA27-SiC 10%-MDF at 100 °C 3 Pass	2000	39.24	33.33	4.5318	4.5054	0.0264	5.1323	5.143	0.002571	6.5544E-05	388.810
	2000	49.05	33.33	4.1242	4.0931	0.0311	5.1323	6.059	0.003029	6.17702E-05	330.051
	2000	58.86	33.33	4.3872	4.3515	0.0357	5.1323	6.955	0.003477	5.90889E-05	287.523
	4000	39.24	66.66	4.4921	4.4303	0.0618	5.1323	12.041	0.003010	7.67163E-05	332.187
	4000	49.05	66.66	4.0671	3.9983	0.0688	5.1323	13.405	0.003351	6.83246E-05	298.389
	4000	58.86	66.66	4.2835	4.2064	0.0771	5.1323	15.022	0.003755	6.38061E-05	266.267
ZA27-SiC 10%-MDF at 200 °C 6 Pass	2000	39.24	33.33	4.5892	4.5562	0.033	5.1463	6.412	0.003206	8.17071E-05	311.896
	2000	49.05	33.33	4.6275	4.591	0.0365	5.1463	7.092	0.003546	7.22984E-05	281.989
	2000	58.86	33.33	4.352	4.3126	0.0394	5.1463	7.655	0.003827	6.50356E-05	261.233
	4000	39.24	66.66	4.5627	4.4848	0.0779	5.1463	15.137	0.003784	9.64391E-05	264.251
	4000	49.05	66.66	4.0329	3.9459	0.087	5.1463	16.905	0.004226	8.61639E-05	236.611
	4000	58.86	66.66	4.3126	4.2182	0.0944	5.1463	18.343	0.004585	7.79106E-05	218.063

Note: Wear test was conducted at 1 m/s Velocity

Table AIII-1.3: Wear results calculation for pin on disc wear test of MDF processed ZA27/ Al₂O₃ 5 wt% composites.

Sample Name	Sliding Distance m	Applied Load N	Time min	Initial Weight g	Final Weight g	Weight Loss g	Density (g cm⁻³)	Volume Loss (mm³)	Wear Rate (mm³ m⁻¹)	Specific Wear Rate (mm³ N⁻¹ m⁻¹)	Wear Resistance
ZA27-5%-Ascast	2000	39.24	33.33	3.5361	3.4597	0.0764	5.1658	14.789	0.007394	0.00018845	135.230
	2000	49.05	33.33	3.7582	3.6766	0.0816	5.1658	15.796	0.007898	0.000161021	126.612
	2000	58.86	33.33	3.6533	3.5648	0.0885	5.1658	17.131	0.008565	0.000145531	116.741
	4000	39.24	66.66	3.4744	3.3157	0.1587	5.1658	30.721	0.007680	0.000195727	130.202
	4000	49.05	66.66	3.7035	3.5299	0.1736	5.1658	33.605	0.008401	0.000171283	119.027
	4000	58.86	66.66	3.6116	3.4233	0.1883	5.1658	36.451	0.009112	0.000154822	109.735
ZA27-Al₂O₃ 5%-Sol.	2000	39.24	33.33	3.9567	3.8925	0.0642	5.1714	12.414	0.006207	0.000158186	161.102
	2000	49.05	33.33	3.888	3.8161	0.0719	5.1714	13.903	0.006951	0.000141727	143.849
	2000	58.86	33.33	3.6228	3.5425	0.0803	5.1714	15.527	0.007763	0.000131904	128.801
	4000	39.24	66.66	3.7349	3.5962	0.1387	5.1714	26.820	0.006705	0.000170875	149.139
	4000	49.05	66.66	3.825	3.6685	0.1565	5.1714	30.262	0.007565	0.000154244	132.178
	4000	58.86	66.66	3.54	3.3673	0.1727	5.1714	33.395	0.008348	0.000141842	119.777
ZA27-Al₂O₃ 5%-MDF at 100 °C 3 Pass	2000	39.24	33.33	2.3351	2.2912	0.0439	5.1786	8.477	0.004238	0.000108017	235.927
	2000	49.05	33.33	4.2822	4.2308	0.0514	5.1786	9.925	0.004962	0.000101177	201.501
	2000	58.86	33.33	2.2713	2.2144	0.0569	5.1786	10.987	0.005493	9.33361E-05	182.024
	4000	39.24	66.66	4.3574	4.2605	0.0969	5.1786	18.711	0.004677	0.000119213	213.770
	4000	49.05	66.66	3.9075	3.7891	0.1184	5.1786	22.863	0.005715	0.000116531	174.952
	4000	58.86	66.66	3.7896	3.6572	0.1324	5.1786	25.566	0.006391	0.000108591	156.452
ZA27-Al₂O₃ 5%-MDF at 200 °C 6 Pass	2000	39.24	33.33	3.6878	3.6382	0.0496	5.179	9.577	0.004788	0.000122033	208.830
	2000	49.05	33.33	4.3256	4.2675	0.0581	5.179	11.218	0.005609	0.000114357	178.278
	2000	58.86	33.33	3.7519	3.6895	0.0624	5.179	12.048	0.006024	0.00010235	165.993
	4000	39.24	66.66	3.8512	3.7463	0.1049	5.179	20.254	0.005063	0.000129045	197.483
	4000	49.05	66.66	3.8936	3.7724	0.1212	5.179	23.402	0.005852	0.000119277	170.924
	4000	58.86	66.66	3.6958	3.5585	0.1373	5.179	26.510	0.006627	0.000112602	150.881

Note: Wear test was conducted at 1 m/s Velocity

Table AIII-1.4: Wear results calculation for pin on disc wear test of MDF processed ZA27/ Al₂O₃ 10 wt% composites.

Sample Name	Sliding Distance m	Applied Load N	Time min	Initial Weight g	Final Weight g	Weight Loss g	Density (g cm⁻³)	Volume Loss (mm³)	Wear Rate (mm³ m⁻¹)	Specific Wear Rate (mm³ N⁻¹ m⁻¹)	Wear Resistance
ZA27-Al₂O₃ 10%-Ascast	2000	39.24	33.33	3.5181	3.4554	0.0627	5.1499	12.174	0.006087	0.000155135	164.271
	2000	49.05	33.33	6.0472	5.9764	0.0708	5.1499	13.747	0.006872	0.000140141	145.477
	2000	58.86	33.33	6.0793	5.9996	0.0797	5.1499	15.476	0.007738	0.000131465	129.232
	4000	39.24	66.66	3.5634	3.4281	0.1353	5.1499	26.272	0.006568	0.000167382	152.251
	4000	49.05	66.66	6.1015	5.9489	0.1526	5.1499	29.631	0.007407	0.000151028	134.990
	4000	58.86	66.66	6.1426	5.9693	0.1733	5.1499	33.651	0.008412	0.000142929	118.866
ZA27-Al₂O₃ 10%-Sol.	2000	39.24	33.33	4.4997	4.4399	0.0598	5.1536	11.603	0.005807	0.000147853	172.361
	2000	49.05	33.33	4.3658	4.3005	0.0653	5.1536	12.670	0.006335	0.000129162	157.843
	2000	58.86	33.33	3.6539	3.5856	0.0683	5.1536	13.252	0.006626	0.00011258	150.910
	4000	39.24	66.66	4.5615	4.4374	0.1241	5.1536	24.080	0.006020	0.000153417	166.111
	4000	49.05	66.66	4.3332	4.1955	0.1377	5.1536	26.719	0.006679	0.000136183	149.705
	4000	58.86	66.66	3.6053	3.4546	0.1507	5.1536	29.241	0.007310	0.0001242	136.790
ZA27-Al₂O₃ 10%-MDF at 100 °C 3 Pass	2000	39.24	33.33	3.9145	3.8731	0.0414	5.1641	8.016	0.004008	0.000102152	249.473
	2000	49.05	33.33	4.0465	3.9992	0.0473	5.1641	9.159	0.004579	9.33679E-05	218.355
	2000	58.86	33.33	4.2976	4.2432	0.0544	5.1641	10.534	0.005267	8.94858E-05	189.856
	4000	39.24	66.66	3.9627	3.8745	0.0882	5.1641	17.079	0.004269	0.000108814	234.199
	4000	49.05	66.66	4.0548	3.9565	0.0983	5.1641	19.035	0.004758	9.70197E-05	210.136
	4000	58.86	66.66	4.359	4.2474	0.1116	5.1641	21.610	0.005402	9.17887E-05	185.093
ZA27-Al₂O₃ 10%-MDF at 200 °C 6 Pass	2000	39.24	33.33	3.8481	3.8033	0.0448	5.169	8.667	0.004333	0.000110436	230.758
	2000	49.05	33.33	4.1962	4.1452	0.051	5.169	9.866	0.004933	0.000100576	202.705
	2000	58.86	33.33	3.773	3.7151	0.0579	5.169	11.201	0.005600	9.51528E-05	178.549
	4000	39.24	66.66	3.9234	3.8282	0.0952	5.169	18.417	0.004604	0.000117339	217.184
	4000	49.05	66.66	4.2615	4.1563	0.1052	5.169	20.352	0.005088	0.000103731	196.539
	4000	58.86	66.66	3.7846	3.6661	0.1185	5.169	22.925	0.005731	9.73714E-05	174.481

Note: Wear test was conducted at 1 m/s Velocity

Table AIII-1.5: Wear results calculation for pin on disc wear test of MDF processed ZA27/ SiC+Al₂O₃ 5 wt% composites.

Sample Name	Sliding Distance m	Applied Load N	Time min	Initial Weight g	Final Weight g	Weight Loss g	Density (g cm⁻³)	Volume Loss (mm³)	Wear Rate (mm³ m⁻¹)	Specific Wear Rate (mm³ N⁻¹ m⁻¹)	Wear Resistance
ZA27-SiC+Al₂O₃-5% Ascast	2000	39.24	33.33	3.8041	3.7398	0.0643	5.1569	12.468	0.006234	0.000158878	160.401
	2000	49.05	33.33	4.6542	4.5834	0.0708	5.1569	13.729	0.006864	0.000139951	145.675
	2000	58.86	33.33	4.6133	4.531	0.0823	5.1569	15.959	0.007979	0.000135569	125.319
	4000	39.24	66.66	3.8244	3.6887	0.1357	5.1569	26.314	0.006578	0.000167649	152.008
	4000	49.05	66.66	6.3865	6.2388	0.1477	5.1569	28.641	0.007160	0.00014598	139.658
	4000	58.86	66.66	6.3286	6.1558	0.1728	5.1569	33.508	0.008377	0.000142323	119.372
ZA27-SiC+Al₂O₃-5% Sol.	2000	39.24	33.33	5.0917	5.0346	0.0571	5.1591	11.067	0.005533	0.000141027	180.704
	2000	49.05	33.33	3.8228	3.7601	0.0627	5.1591	12.153	0.006076	0.000123887	164.564
	2000	58.86	33.33	3.9493	3.8801	0.0692	5.1591	13.413	0.006706	0.000113941	149.106
	4000	39.24	66.66	5.1321	5.0114	0.1207	5.1591	23.395	0.005848	0.000149054	170.972
	4000	49.05	66.66	3.8472	3.7125	0.1347	5.1591	26.109	0.006527	0.000133074	153.202
	4000	58.86	66.66	3.9693	3.8178	0.1515	5.1591	29.365	0.007341	0.000124726	136.213
ZA27-SiC+Al₂O₃-10% MDF at 100 °C 3 Pass	2000	39.24	33.33	4.4651	4.433	0.0321	5.1699	6.209	0.003104	7.91159E-05	322.112
	2000	49.05	33.33	4.1142	4.0765	0.0377	5.1699	7.292	0.003646	7.43345E-05	274.265
	2000	58.86	33.33	4.4413	4.3994	0.0419	5.1699	8.104	0.004052	6.88465E-05	246.773
	4000	39.24	66.66	4.4295	4.3544	0.0751	5.1699	14.526	0.003631	9.25484E-05	275.360
	4000	49.05	66.66	4.0156	3.9308	0.0848	5.1699	16.402	0.004106	8.36016E-05	243.863
	4000	58.86	66.66	4.2358	4.1486	0.0872	5.1699	16.866	0.004216	7.16398E-05	237.151
ZA27-SiC+Al₂O₃-5% MDF at 200 °C 6 Pass	2000	39.24	33.33	4.4655	4.4312	0.0343	5.1763	6.626	0.003313	8.44337E-05	301.825
	2000	49.05	33.33	4.6516	4.6128	0.0388	5.1763	7.495	0.003747	7.64088E-05	266.819
	2000	58.86	33.33	4.5784	4.5341	0.0443	5.1763	8.558	0.004279	7.26999E-05	233.693
	4000	39.24	66.66	4.4551	4.3796	0.0755	5.1763	14.585	0.003646	9.29263E-05	274.241
	4000	49.05	66.66	4.5985	4.5124	0.0861	5.1763	16.633	0.004158	8.47783E-05	240.478
	4000	58.86	66.66	4.5193	4.4301	0.0892	5.1763	17.232	0.004308	7.31923E-05	232.121

Note: Wear test was conducted at 1 m/s Velocity

Table AIII-1.6: Wear results calculation for pin on disc wear test of MDF processed ZA27/ SiC+Al₂O₃ 10 wt% composites.

Sample Name	Sliding Distance m	Applied Load N	Time min	Initial Weight g	Final Weight g	Weight Loss g	Density (g cm ⁻³)	Volume Loss (mm ³)	Wear Rate (mm ³ m ⁻¹)	Specific Wear Rate (mm ³ N ⁻¹ m ⁻¹)	Wear Resistance
ZA27-SiC+Al₂O₃-10% Ascast	2000	39.24	33.33	3.4771	3.4188	0.0583	5.1377	11.347	0.005673	0.000144591	176.250
	2000	49.05	33.33	3.1223	3.0586	0.0637	5.1377	12.398	0.006199	0.000126387	161.309
	2000	58.86	33.33	3.3034	3.2337	0.0697	5.1377	13.566	0.006783	0.000115243	147.423
	4000	39.24	66.66	3.4455	3.3174	0.1281	5.1377	24.933	0.006233	0.000158852	160.427
	4000	49.05	66.66	3.1416	3.0066	0.135	5.1377	26.276	0.006567	0.000133926	152.228
	4000	58.86	66.66	3.2757	3.1238	0.1519	5.1377	29.565	0.007398	0.000125577	135.291
ZA27-SiC+Al₂O₃-10% Sol.	2000	39.24	33.33	3.1141	3.0632	0.0509	5.1474	9.888	0.004944	0.000126	202.255
	2000	49.05	33.33	3.2748	3.2179	0.0569	5.1474	11.054	0.005527	0.000112682	180.927
	2000	58.86	33.33	3.2929	3.2282	0.0647	5.1474	12.569	0.006284	0.000106774	159.115
	4000	39.24	66.66	3.1123	3.0007	0.1116	5.1474	21.680	0.005420	0.00013813	184.494
	4000	49.05	66.66	3.2495	3.1323	0.1172	5.1474	22.768	0.005692	0.000116049	175.679
	4000	58.86	66.66	3.2616	3.1272	0.1344	5.1474	26.110	0.006527	0.0001109	153.196
ZA27-SiC+Al₂O₃-10% MDF at 100 °C 3 Pass	2000	39.24	33.33	4.3961	4.362	0.0341	5.1579	6.611	0.003305	8.42408E-05	302.516
	2000	49.05	33.33	4.6323	4.5941	0.0382	5.1579	7.406	0.003703	7.54956E-05	270.047
	2000	58.86	33.33	4.3467	4.3036	0.0431	5.1579	8.356	0.004178	7.0983E-05	239.345
	4000	39.24	66.66	4.3298	4.2566	0.0732	5.1579	14.191	0.003547	9.04168E-05	281.852
	4000	49.05	66.66	4.5963	4.5174	0.0789	5.1579	15.296	0.003824	7.7966E-05	261.490
	4000	58.86	66.66	4.2662	4.1741	0.0921	5.1579	17.856	0.004464	7.58414E-05	224.013
ZA27-SiC+Al₂O₃-10% MDF at 200 °C 6 Pass	2000	39.24	33.33	4.1358	4.1001	0.0357	5.1618	6.916	0.003458	8.81268E-05	289.176
	2000	49.05	33.33	4.0649	4.0254	0.0395	5.1618	7.652	0.003826	7.80058E-05	261.356
	2000	58.86	33.33	4.356	4.3105	0.0455	5.1618	8.814	0.004407	7.4879E-05	226.892
	4000	39.24	66.66	4.2031	4.1259	0.0772	5.1618	14.956	0.003739	9.52856E-05	267.450
	4000	49.05	66.66	4.6362	4.5478	0.0884	5.1618	17.125	0.004281	8.72875E-05	233.565
	4000	58.86	66.66	4.3475	4.2497	0.0978	5.1618	18.946	0.004736	8.04743E-05	211.116

Note: Wear test was conducted at 1 m/s Velocity

List of Publications based on PhD Research Work

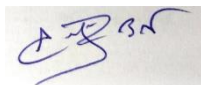
[to be filled-in by the Research Scholar and to be enclosed with Synopsis submission Form]

Sl. No	Title of the paper	Authors (in the same order as in the paper. Underline the Research Scholar's name)	Name of the Journal/ Conference/ Symposium, Vol., No., Pages	Month and Year of Publications	Category *
1	Mechanical and Microstructural characterization of ZA based SiC reinforced composites	<u>Anjan B N</u> , Preetham Kumar G V	(NMD ATM IIM 2017), 11th to 14th Nov 2017, BITS Pilani, Goa.	2017	4
2	Microstructure and mechanical properties of ZA27 based SiC reinforced composite processed by multi directional forging	<u>Anjan B N</u> , Preetham Kumar G V	<i>Mater. Res. Express</i> , 5 (2018) 106523. https://doi.org/10.1088/2053-1591/aadb02 .	2018	1
3	Microstructure and Mechanical properties of Multi-Directional Forged ZA-27 based composites reinforced with 5 wt% of Al ₂ O ₃ .	<u>Anjan B N</u> , Preetham Kumar G V	(NMD ATM IIM 2018), 14th to 16th Nov 2018, Kolkata.	2018	4
4	Investigation on Wear Behavior of Multi-Directional Forged Zn-24Al-2Cu Alloy	Sharath P C, <u>Anjan B N</u> , Preetham Kumar G V, Rajendra Udupa K	<i>International Conference on Advanced Materials and Manufacturing Process for Strategic Sector (ICAMPS 2018)</i> October 25-27, 2018, Kerala.	2018	4
5	Wear Behaviour of ZA27 Based Composite Reinforced with 5 wt % of SiC Particles and Processed by Multi-Directional Forging	<u>Anjan B N</u> , Preetham Kumar G V	<i>Transactions of The Indian Institute of Metals</i> . https://doi.org/10.1007/s12666-019-01705-0	2019	1
6	Influence of SiC and Al ₂ O ₃ Particulate Reinforcement on the Mechanical Properties of ZA27 Metal Matrix Composites	<u>Anjan B N</u> , Preetham Kumar G V	Material Science Forum. Trans Tech Publications Ltd, Switzerland, ISSN: 1662-9752, Vol. 969, pp 122-127	2019	1

- Category : 1: Journal paper, Full paper reviewed
- 2: Journal paper, Abstract reviewed
- 3: Conference/Symposium paper, Full paper reviewed
- 4: Conference/Symposium paper, Abstract reviewed
- 5: Others (including papers in workshop, NITK Research Bulletins, Short notes etc.

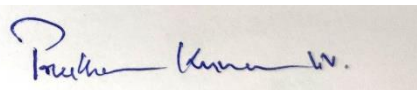
(If the paper has been accepted for publication but yet to be published, he supporting documents must be attached.)

Research Scholar



Signature, with Date

Research Guide



Name & Signature, with Date

BIO-DATA

Name: ANJAN B N

Father's Name: Narasimha Murthy B R

Date of Birth: 22-11-1989

Nationality: Indian

Marital Status: Married

Permanent Address: Door No 890 II D, Nekar Street,

Near KSRTC Bus Stand,

Chikmagalur - 577101

Mobile: +91-8123782423

E-mail: anjanbn89@gmail.com

Academic Qualification:

Bachelor of Engineering (B.E.): Industrial Production Engineer, Department of Industrial and Production Engineering, Adhichuchanagiri Institute of Technology, Chikmagalur, V.T.U University, Batch: 2007-2011.

Master of Technology (M.Tech): Production Engineering and System Technology, Industrial and Production Engineering Department, National Institute of Engineering, Mysore, Batch: 2011-2013.

Work Experience:

Two years of teaching experience as an Assistant Professor in the Mechanical Engineering Department. at Prasanna college of Engineering, Ujire and Alva's Institute of Engineering and Technology, Moodbidri, V.T.U University.